THE RUSSIAN ACADEMY OF SCIENCES

SCIENTIFIC COUNCIL ON COMPLEX PROBLEM
«METHODS OF DIRECT ENERGY CONVERSION»

SECTION «MAGNETOHYDRODYNAMICS ENERGY CONVERSION»

PERSPECTIVES OF MHD AND PLASMA TECHNOLOGIES IN AEROSPACE APPLICATIONS

March 24-25, 1999

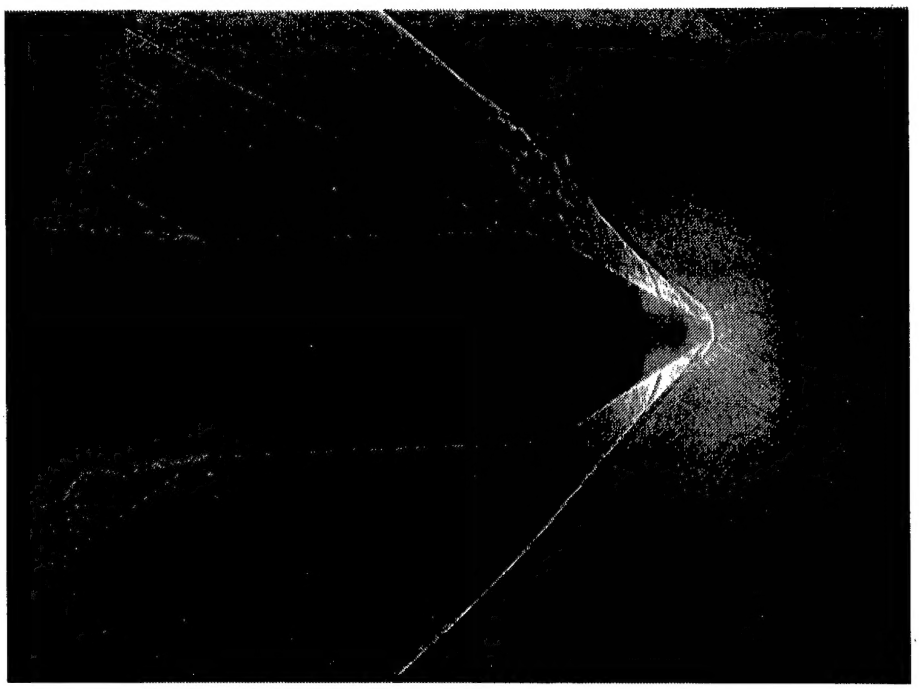

Moscow
IVTAN

REPORT DOCUMENTATION PAGE

Form Approved OMB No. 0704-0188

1. AGENCY USE ONLY (Leave blank)	2. REPORT DATE	3. REPORT TYPE AND DATES COVERED
	1999	Conference Proceedings

4. TITLE AND SUBTITLE

Perspectives of MHD and Plasma Technologies in Aerospace Applications

5. FUNDING NUMBERS

F61775-99-WF070

6. AUTHOR(S)

Conference Committee

7. PERFORMING ORGANIZATION NAME(S) AND ADDRESS(ES)

Russian Academy of Sciences
IVTAN, Izhorskaya str., 13/19
Moscow 127412
Russia

8. PERFORMING ORGANIZATION REPORT NUMBER

N/A

9. SPONSORING/MONITORING AGENCY NAME(S) AND ADDRESS(ES)

EOARD
PSC 802 BOX 14
FPO 09499-0200

10. SPONSORING/MONITORING AGENCY REPORT NUMBER

CSP 99-5070

11. SUPPLEMENTARY NOTES

12a. DISTRIBUTION/AVAILABILITY STATEMENT

Approved for public release; distribution is unlimited.

12b. DISTRIBUTION CODE

A

13. ABSTRACT (Maximum 200 words)

The Final Proceedings for Perspectives of MHD and Plasma Technologies in Aerospace Applications, 24 March 1999 - 25 March 1999

This is an interdisciplinary conference. Topics include MHD Super- and Hypersonic Flow Control; Plasma Aerodynamics (Drag and Flow/Flight Control); Shock Wave Structure and Propagation in Gas-Plasma Mixture; On-board MHD Systems and Plasma Generators; MHD/EM Accelerators and Thrusters, etc...

14. SUBJECT TERMS

EOARD

15. NUMBER OF PAGES

168

16. PRICE CODE

N/A

17. SECURITY CLASSIFICATION OF REPORT	18. SECURITY CLASSIFICATION OF THIS PAGE	19. SECURITY CLASSIFICATION OF ABSTRACT	20. LIMITATION OF ABSTRACT
UNCLASSIFIED	UNCLASSIFIED	UNCLASSIFIED	UL

NSN 7540-01-280-5500

Standard Form 298 (Rev. 2-89)
Prescribed by ANSI Std. 239-18
298-102

PREFACE

The Workshop «Perspectives of MHD and Plasma Technologies in Aerospace Applications» was organized by the Section «MHD Method of Energy Conversion» of the Scientific Council of the Russian Academy of Sciences «Direct Conversion of Heat into Electricity» with support of Institute of High Temperature of the Russian Academy of Sciences (IVTAN), MTC, the private company «Chance», and EOARD.

The Workshop was attended by more than 100 registered participants and more than 50 observers from approximately 30 institutions of Moscow, Moscow region, St.-Petersburg, Nizhny Novgorod, Novosibirsk, Krasnoyarsk, Samara, and Kiev. The Boeing Company and EOARD were also represented at the Workshop.

At four Sections of the Workshop: MHD methods and systems, Plasma Aerodynamics, Shock Waves in Gas Discharge Plasma, and Non-Equilibrium Plasma Flows, 41 papers were presented. The Workshop results were formulated at the Round Table Discussion with 12 speakers.

Basing on the Workshop discussions the possible applications area for MHD and Plasma technologies can be formulated as following:

1. New methods of the control of internal and external air flow;
2. New methods of the control of aerodynamics characteristics of bodies and aircraft;
3. New methods of the mixing, ignition and combustion control in airbreathing engines;
4. Reduction of drag and improving of aerodynamics quality of aircraft in wide range of flight Mach number by means, in particular, of modification of shock waves pattern, modification of the separation zones, of influencing on the momentum and energy transfer to the aircraft surface;
5. Heat flux management;
6. On-board power generation and conversion;
7. Marching and correcting MHD and plasma thrusters of low and moderate low thrust;

and others.

New results on theoretical analysis of MHD processes in external and internal flows in aircraft elements and in laboratory rigs were presented at the Workshop. It was defined the range of the governing parameters values where the MHD interaction can be effective and significant. New schemes of on-board MHD generators for hypersonic aircraft were proposed and discussed. The existing and industrial produced marching and correcting plasma thrusters of low and moderate low thrust were described.

In the field of plasma aerodynamics new experimental and theoretical results on the investigation of the integral and local characteristics of aerodynamics models in supersonic air-plasma flows were presented. New data on drag reduction with various gas discharge types created in flow (in particular, HF and MW discharges created in front of bow shock in some cases with laser initiation) were reported. The rather high effectiveness (the ratio of the gain of drag force work to the energy input) up to several units were obtained for some gas discharge types. It was demonstrated that high enthalpy plasma jets upstream directed could reduce the drag in supersonic flows for several tens of percents. New methods of analytical and numerical for adequate description and prediction of plasma aerodynamics effects were discussed.

The significant progress in experimental and the theoretical studies of the structure and propagation of shock waves in gas-plasma systems was demonstrated. It was shown, in particular, that the plasma non-uniformity and non-steady state nature of plasma formation and the plasma parameters may play an important role in the processes of interaction of shock waves with gas discharge plasma.

The importance and perspectives of the study of various aspects of non-equilibrium weakly ionized, multi-temperature plasma flow were outlined. It was shown, in particular, that the vibration non-equilibrium can result in a significant modification of shock wave configuration and drag in supersonic flows.

The Round table discussion besides of aforementioned positive trends in the area and confirmation of the new activity – Magnetic and Plasma Aerodynamics, revealed a list of actual problems. The mains are:

- The formulation and realization of the key experiments under well control conditions providing the maximal reliable experimental data treatment and the corresponding analytical support on the following topics:
  - High velocity flows of non-equilibrium gas-discharge plasma around a body;
  - Structure and propagation of shock waves in gas discharge plasma;
  - Ballistic experiments on high speed flight through gas discharge plasma with and without externally applied magnetic field;
  - Effects of gas discharge of various type on boundary layer flows;
  - MHD control of internal flows;
  - Plasma chemistry and control of ignition and combustion in high velocity flows;
  - Interaction of multi-temperature, strong non-equilibrium plasma with shock waves and walls;
  - Acoustics effects of gas discharge plasma in high speed turbulence jets;

- The improving in accuracy and reliability of plasma diagnostics with emphasizing of temporal and spatial resolution;
- Further improvement and optimization of special types of plasma generators, in particular, for creating of electrical conductivity sufficient for MHD applications;
- The development of adequate analytical and numerical models;
- System analysis and comparison with alternative approaches.

At the same time it was stated that the practical importance of the MHD and plasma technologies being developed for control of internal and external flows and aerodynamics characteristics of aircraft by means the directed changes of energy, momentum and state of a gas flow element is evident today.
The expedience of the efforts on experimental and theoretical researches and development of new methods of high speed flow control can be confirmed by the positive example of the productive developments of plasma and MHD thrusters of low thrust and small mass projectile presented at the Workshop as well.

During the Workshop the urgent necessity of co-ordination on current and especially planning activities was agreed. The format and scope of such a co-ordination would be prepared in several months for approval by the Workshop participants and by the others interested specialists.

The workshop attendance supported unanimous the idea of regular (annual) status of such a meeting. The official announcement of the Second Workshop on Magnetic and Plasma Aerodynamics is expected on the fall of this year.

The Organizing and Local Committee is highly satisfied with the positive estimation of the Workshop by the participants.

Valentin Bityurin
Chairman
Organizing and Program Committee

ACKNOWLEDGMENTS

The Organizing Committee of the Workshop «Perspectives of MHD and Plasma technologies in Aerospace Applications» express their application to the participants who have contributed to the success of the Workshop. The Committee gratefully acknowledges the collaboration and the financial support provided by the following organizations:

The Institute of High Temperatures of the Russian Academy of Sciences (IVTANs)
Moscow Technical Company (MTC)
The private company «Chance»
European Office of Aerospace research and development (EOARD)

CONTENTS

USE OF MHD SYSTEMS IN HYPERSONIC FLIGHT VEHICLES

D.I.Brichkin, A.L.Kuranov, E.G.Sheikin
Hypersonic System Research Institute, St. Petersburg, Russia

Hypersonic atmospheric flight is accompanied with extreme power and thermal loads on airframe of hypersonic flight vehicle. At high flight speeds, it is possible to change radically properties of the medium around the vehicle, because of the occurrence of so-called plasma envelope. It is clear that the creation of flight vehicle, which is capable to execute long-time hypersonic flight in such conditions, requires using the ways that are beyond the frameworks of conventional aerodynamics. The presence of high-speed ionized flow gives possibility to use electromagnetic methods of control over the flow parameters. Various uses of MHD systems aboard the hypersonic flight vehicles are under investigation in the Hypersonic System Research Institute within the framework of the concept "Ajax". The MHD effect allows executing adjustable energetic and power influence on the flow. It can be used for creating the driving moments, for reduction of heat flows on surface of the vehicle, for change of the flow pattern, and accordingly the aerodynamic characteristics of the vehicle, for control over scramjet characteristics and, at last, conventionally, for the producing of electric power.

Let's consider in more detail the potentialities of MHD systems for the control over the scramjet characteristics. The schematic diagram of scramjet with MHD systems is given in Fig.1. Such type of engine was named as the Magneto-Plasma-Chemical Engine (MPCE). The external MHD generator of MPCE allows to manage the flow pattern and to regulate the air flow through a channel of MPCE. The degree of flow contraction in MHD controlled air intake is determined by combined action of gas-dynamical contraction in shock waves and extra contraction at MHD influence on the flow. The internal MHD generator is used for additional compression, prevention of growing of separated flows and transformation of a part of enthalpy of airflow to the electric power with its subsequent use in the MHD accelerator located behind the combustor. The ionizer is used for creating necessary conductance of the flow in that case, when the natural flow conductance does not provide required degree of MHD effect. The electric power produced by MHD generators is spent for power supply of the ionizer and onboard equipment, and for creation of additional acceleration of products of combustion in the MHD accelerator.

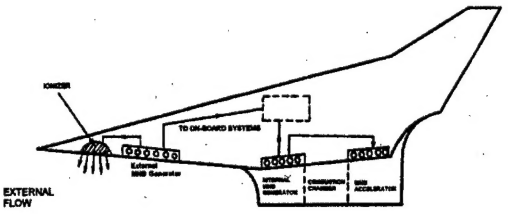

Fig.1. Simplified schematic diagram of MPCE

In article [1] the scheme of MPCE with internal MHD generator and MHD accelerator is in detail analysed in quasi-1D approximation under the assumption that the flow is initially ionized. Before inlet of channel of the MHD generator, the calculation was conducted in Eulerian 2-D approximation. At the inlet of the MHD generator, the parameters of the current were averaged on the flow cross-section and further, down to nozzle output, the calculation of parameters of the flow was conducted with use of quasi-1D approximation. Based on the analysis, the functional relation was arrived. It allows determine such range of parameters of MPCE subsystems that the use of MHD influence on the flow permits to increase specific impulse of propulsion system; in this case the key restriction is imposed on the operational mode of the MHD generator. There is demonstrated the specific impulse for this scheme of MPCE can be increased only if the MHD generator works in mode with increase of compression along length of the channel. The relationships between the specific impulse of MPCE I_{sp} and the enthalpy extraction rate η at the speed of incoming flow M_∞=6 for various values of load factor of the MHD generator k_1 and for two different values of the nozzle non-ideality coefficient φ (for ideal nozzle φ=1) are shown in Fig.2. In the calculations, the two-shock air intake with total angle of flow turn θ_N=0,2 radians was considered. It is obvious from Fig.2 that the specific impulse of MPCE grows with growth η. And for MPCE with non-ideal nozzle the relative increment of specific impulse is higher than with an ideal nozzle. The relations between the specific impulse of MPCE and load factor of the MHD

generator for various values θ_N are submitted in Fig.3. It is clear that with decrease θ_N the positive effect of use of MHD influence on flow grows. The results, shown in Fig.2, 3, are normalized on specific impulse of scramjet.

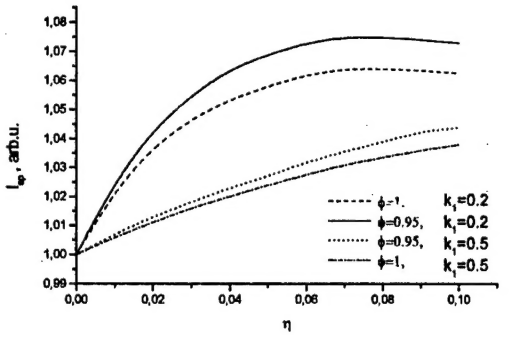

Fig.2. Relationship between the specific impulse of MPCE and the enthalpy extraction rate at various values k_1 and φ

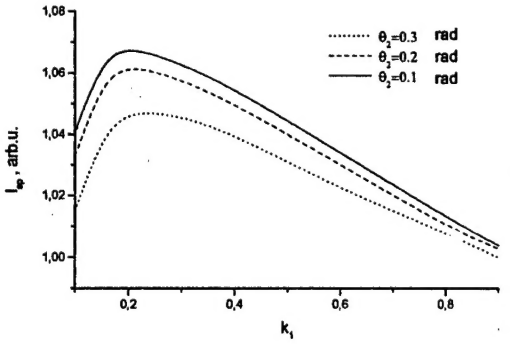

Fig.3. Relationship between the specific impulse of MPCE and load coefficient of MHD generator at various θ_N

In that case, when the natural ionization of airflow is insufficient for MHD influence, it is necessary to apply special efforts to ionize flow. It will need inputting the additional energy into the flow. As the methods of energy supply it is possible to consider the electrical discharge, microwave radiation, beams of high-energy charged particles. In deciding on ionization method, a major criterion is energy efficiency. At the conditions of flight vehicle it is expedient to consider only independent systems, for which the energy spent on the flow ionization does not exceed the energy produced by the MHD generator.

To estimate energy efficiency of the ionizer, we shall introduce the general energy characteristic of the ionizer q_i, the energy spent on ionization of single volume of air in unit of time. Simultaneously with q_i we shall consider quantity q_g, determining the energy extracted from a volume unit of the MHD generator in a unit time. The self-sustaining operational mode of the MHD generator and ionizer corresponds to a requirement $q_g > q_i$. Let's estimate boundaries of existence of self-sustaining mode in one-dimensional local approximation. In this case q_g is determined by a known relation: $q_g = k_1(1-k_1)\sigma B^2 v^2$, where σ is the flow conductivity, B the magnetic induction, v the flow velocity. If to consider electronic beam an ionizer, then $q_i = (j_b/e)\rho Y(E_b)$, where j_b is the current density in the beam, E_b the energy of electrons, ρ the flow density, Y the stopping power of electrons. We shall restrict our description of gas ionization by e-beam to the account of two processes only: birth of secondary electrons at the direct electronic shock and destruction during the dissociative recombination. Thus, the electron concentration n_e, generated in the flow in the field of action of e-beam (see Ref.2, for example) is determined by a following relationship: $n_e = \sqrt{j_b Y\rho/(eW_i k_{dr})}$, where W_i is the ionization cost k_{dr} the constant of dissociative recombination rate. If to express the conductivity via electron concentration and to use given relations, it is an easy to check, that the self-sustaining operational mode of the MHD generator and ionizer is can be realized at $0 < q_i < q_{cr}$. Thus, the quantity of critical energy supply in the field of ionization q_{cr} is determined by following relationship:

$$q_{cr} = \frac{1}{W_i k_{dr}} \left(k_1(1-k_1) B^2 v^2 \frac{e^2}{mnk_c} \right)^2, \qquad (1)$$

where m is the mass of an electron, k_c the rate constant of elastic collisions of electrons, n the concentration of neutral component. From the received relationship follows, that the range of existence of self-sustaining mode for the MHD generator and ionizer grows with increase of flow speed and decrease of gas concentration. Thus, the faster and higher the flight of hypersonic vehicle, the wider opportunities for application of MHD systems aboard the vehicle. The increase of a magnetic induction also leads to expansion of the range of existence of self-sustaining operational mode of MHD generator and ionizer. If to use for an estimation the values of constants given in Ref.2 k_{dr}=1,5·10^{-7}cm^3/s, k_c=5,8·10^{-9}cm^3/s, W_i=34eV, then for a flow with parameters v=200m/s, T=300K at B=1Tesla, k_1=0,5 from (1) follows q_{cr}=4,8W/cm^3.

Let us consider the effect of MHD influence on flow-field in flat air intake and on the characteristics of MPCE, working in self-sustaining mode. The considered air intake at the absence of MHD interaction is characterized by value of design Mach number M_d=10. The characteristics of MHD controlled air intake are explored and the parameters of MPCE are estimated under conditions which are strongly different from design, for M_∞=6.

Let's view the approximations used by us. To describe the parameters of flow we use 2D Eulerian approximation. The stationary mode is considered, such as:

$$\begin{aligned}
&\frac{\partial \rho v_x}{\partial x}+\frac{\partial \rho v_y}{\partial y}=0,\\
&\frac{\partial\left(\rho v_x^2+p\right)}{\partial x}+\frac{\partial \rho v_x v_y}{\partial y}=f_x,\\
&\frac{\partial\left(\rho v_y^2+p\right)}{\partial y}+\frac{\partial \rho v_x v_y}{\partial x}=f_y,\\
&\frac{\partial(e+p)v_x}{\partial x}+\frac{\partial(e+p)v_y}{\partial y}=q+q_r,
\end{aligned} \qquad (2)$$

where $e=\rho\left(c_v T+\left(v_x^2+v_y^2\right)/2\right)$., $p=R\rho T$.

It is supposed, that the vector of magnetic induction is located in the plane of figure $\vec{B}=\{B_x,B_y,0\}$. Density of induced current $\vec{j}$ is related to vector of magnetic induction $\vec{B}$ and electric field $\vec{E}$ by generalized Ohm's law: $\vec{j}=\sigma\left(\vec{E}+\vec{v}\times\vec{B}\right)$. The conductivity σ included in this relation depends from q_i, and calculates with use of results of Ref.3. The expressions for the right parts of Eq.(2) have following view: $\vec{f}=\{f_x,f_y,0\}$, $\vec{f}=\vec{j}\times\vec{B}$, $q=\vec{j}\cdot\vec{E}$. The quantity q_r included in the right part of Eq.(2) determines the energy released in unit of volume in unit of time at the expense of processes of recombination of charged particles. When the rate of recombination processes is high, it is possible to suppose approximately $q_r=q_i$.

The results of calculations of flow-fields in the MHD controlled air intake at various values of energy put into the flow ionization are demonstrated in Fig.4. The transverse distributions of density in the channel before the combustor inlet are presented in Fig.5. From Fig.4,5 it follows that the MHD influence allows to restructure the flow essentially. In particular, it follows from Fig.5 that MHD interaction leads to increase of the flow density and makes the transverse density distribution more saturated.

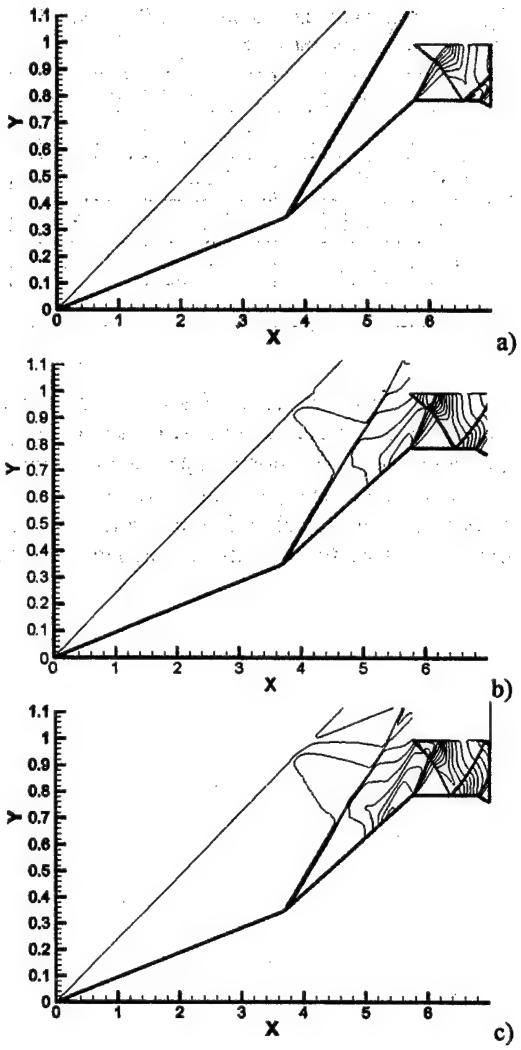

Fig.4. Density isolines for MHD controlled air intake at M_∞=6, velocity pressure 3,7·10^{4}Pa, B=3Tesla a) q_i/q_{cr}=0; b) q_i/q_{cr}=0,02; c) q_i/q_{cr}=1,0;

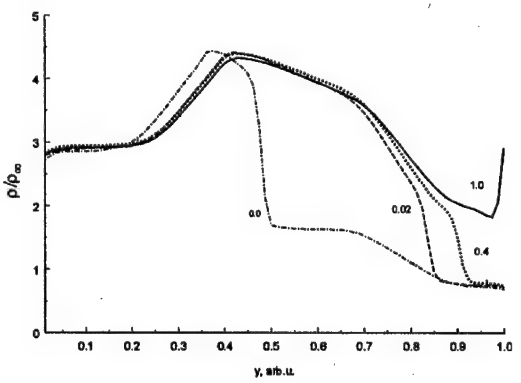

Fig.5. Density distribution in cross section of channel before the combustor of MPCE, M_∞=6, velocity pressure 3,7·10^{4}Pa; values for q_i/q_{cr} are indicated near the curves.

Table 1. Relative characteristics of MPCE with MHD controlled air intake

$\frac{q_i}{q_{cr}}$	$\frac{\dot{m}_{MPCE}}{\dot{m}_{scramjet}}$	$\frac{I_{MPCE}}{I_{scramjet}}$	$\frac{R_{MPCE}}{R_{scramjet}}$
0.02	1.19	1.04	1.24
0.4	1.25	1.07	1.34
0.8	1.27	1.07	1.36
1.0	1.3	1.06	1.38

The characteristics of MPCE with MHD controlled air intake for various values of energy put in the flow ionization are specified in Table.1. Here, $\dot{m}$ is the air mass flow-rate, R the thrust determined via specific impulse and air mass flow-rate. The results are represented as the relationship between the calculated characteristics of MPCE and the relevant characteristics for scramjet. These results show that the MHD influence on flow allows to increase significantly the air mass flow-rate up to 30% and the thrust up to 38%. The maximum increase of specific impulse in considered version reaches 7%.

References

1. *V.L.Fraishtadt, A.L.Kuranov, E.G.Sheikin//* The Journal of Technical Physics, 1998, vol.68, No.11, p.43-47 (in Russian).
2. *S.O.Macheret, R.B.Miles and G.L.Nelson //* AIAA 97-2429.
3. Calculation of electrokinetic characteristics of air and nitrogen plasmas excited by e-beam. The Report of Hypersonic System Research Institute. 1995, St.Petersburg (in Russian)

NUMERICAL INVESTIGATION OF HYPERSONIC INVISCID AND VISCOUS FLOW DECELERATION BY MAGNETIC FIELD

A.B. Vatazhin, O.V. Gouskov, V.I. Kopchenov (Central Institute of Aviation Motors, Moscow, Russia)

Abstract. The present article is devoted to the analysis of various aspects of magnetohydrodynamic (MHD) control over supersonic and hypersonic flow deceleration. The complicated flow structure (shock waves, boundary layer separation, recirculation zones) is simulated with the aid of numerical solution of axisymmetric Navier-Stokes equations for laminar and turbulent flows. Along with the flow field analysis, the deceleration process characteristics are estimated for the wide range of MHD interaction parameter. The special attention is focused on the question concerned with irreversible losses. The MHD effects and boundary layer interaction give rise to the unusual effects concerned with MHD interaction parameter influence on the deceleration process efficiency.

Recently some proposals [1-8] to use the MHD-devices for flow control in hypersonic vehicle-propulsion system are discussed. Promising suggestions exist concerning MHD effects use for the improvement of hypersonic propulsion system efficiency. These suggestions have their bases on the possibility to develop the special devices (using modern technologies) for flow pre-ionization before the vehicle or at the entrance to the propulsion system. The flow pre-ionization is complex technical problem. The large technical efforts are directed on its solution. One way to create the air stream conductivity by apparatus on the vehicle board has been studied in detail previously [5]. However the following development of technical work applied to hypersonic propulsion system requires precise understanding of possible advantageous of MHD control in itself. In spite of study undertaken, the clarity in this question is not yet conclusively established. Therefore these aspects of MHD control efficiency are of primary importance. It is necessary to estimate the existing proposals of MHD control not only qualitatively, but quantitatively as well. The flow field in the hypersonic propulsion system is too complex. The new physical models must be developed and included into the existing computational models of the flow in hypersonic propulsion system to study the efficiency of MHD control applied to hypersonic propulsion. Furthermore, it seems to be appropriate to solve some simplified model problems to understand main flow features and to estimate the efficiency of the supersonic and hypersonic flow control by MHD methods in the range of parameters typical for hypersonic propulsion systems.

The possibility of MHD flow control in the duct of hypersonic propulsion system and flow structure are investigated now in CIAM on the base of the combined mathematical model [9]. This combined model includes as constituents the gasdynamics, turbulence and supersonic combustion models. This model is supplemented by the physical models for the description of MHD flow. The existing preceding experience in MHD flow investigation [10] is used and adapted to new applications. The present article is devoted to the analysis of various aspects of MHD control over supersonic and hypersonic flow deceleration. The following schemes of the MHD control will be discussed. The first of them is concerned with supersonic flow deceleration by axisymmetric magnetic field. The structure of the flow in axisymmetric duct at the supersonic flow deceleration by magnetic field, generated by current loop or solenoid, is investigated. The complicated flow structure (shock waves, boundary layer separation, recirculation zones) is simulated with the aid of numerical solution of axisymmetric Navier-Stokes equations for laminar and turbulent flows. Another scheme of MHD control is also investigated. This scheme provides the supersonic flow deceleration in 2-D channel when magnetic field is perpendicular to the flow plane and, depending on wall electric properties, electric energy may be extracted from the duct. The exact problem including coupled system of 2-D electromagnetic field equations and 2-D gasdynamic equations with MHD terms is solved. Along with exact model, the simplified flow model based on local quasi 1-D electrodynamics and 2-D gasdynamics with MHD terms is used. The applicability of simplified model is analyzed by comparison with exact model solution.

It is necessary to note that corroboration of positive influence of MHD effects on the hypersonic propulsion system performances was made in the first stage, as a rule, on the base of simplified flow models and this was justified in the stage of effects revealing. The 1-D inviscid MHD approach was used in this analysis in many cases [6]. Some results [4,5,7] concerning both flow over aerodynamic body [4] and inlet flow [5,7] were obtained within 2-D Euler equations for inviscid gas. However, it was shown in previous investigations that viscous effects are very important in typical MHD systems [11]. Therefore it is necessary to estimate the role of

viscous effects at the hypersonic flow deceleration. It is supposed in this stage of our study that the adequate level of electric conductivity is available.

Short description of mathematical and physical models

The governing equations in the present analysis are the unsteady compressible two-dimensional or axisymmetric full Navier-Stokes equations. The time relaxation procedure permits to obtain the steady state solution starting from an arbitrary initial approximation. The volume densities of MHD force **f** and electric power q supplied to the gas must be included into the right side of equations written in divergent form as follows $\mathbf{f}=\mathbf{j}\times\mathbf{B}$, $q=\mathbf{j}\mathbf{E}$. Here **B**, **E** and **j** are vectors of magnetic field, electric field and electric current density. The volume electric charge density is neglected. When induced magnetic field is also neglected in comparison with the applied external magnetic field, the equations for **E**, **j** and **B** determination are following [10]

$$\mathbf{j}=\sigma(-\nabla\varphi+\mathbf{v}\times\mathbf{B})-\frac{\beta}{|\mathbf{B}|}\mathbf{j}\times\mathbf{B},$$

$$div\ \mathbf{j}=0,\ rot\mathbf{B}=0,\ \mathbf{E}=-\nabla\varphi$$

Here φ is electric potential, σ is electric conductivity, β is the Hall parameter, and β, σ are known function of thermodynamic parameters. In these equations **B** is applied magnetic field. The equations for **B** are supposed to be satisfied in the regions where external electric circuits are assumed to be absent. It is suggested that transport coefficients (viscosity, conductivity) do not dependent upon the magnetic field **B**.

In turbulent case, the averaged full Navier-Stokes equations are used. The one equation differential model "ν_t-91" [13] for turbulent viscosity is employed in the code FNAS2D [9].

Flow deceleration in cylindrical duct by magnetic field of single current loop or solenoid

The axisymmetric flow in the circular tube with nonperforated and electrically nonconductive walls is investigated. For simplicity, it is assumed that the electric conductivity is isotropic and constant and Hall effects are negligible. It is supposed that external magnetic field is generated by circular current loop or by axisymmetric solenoid. Therefore external magnetic field is assumed to be axisymmetric. In this case, the MHD source terms f and q in accordance with the velocity, magnetic and electric fields structure are following:

$$f_x=-\sigma B_y\left(uB_y-vB_x\right),\ f_y=\sigma B_x\left(uB_y-vB_x\right),$$
$$q=0.$$

Here x and y are axial and radial coordinates, u and v are axial and radial velocities. The axisymmetric magnetic field is presented according to [10,12].

The flow at the duct entry is supposed to be supersonic and uniform. All parameters distributions must be given for supersonic flow at the duct entry. The slip velocity conditions are posed on tube walls in inviscid case and no-slip conditions - in viscous case. For viscous and heat conducting gas, the wall temperature is supposed to be equal to free stream temperature in the entry cross-section. In supersonic inviscid flow on the exit computational boundary, the additional boundary conditions are not required. In viscous case, the so called drift boundary conditions with normal derivatives of all parameters being determined inside computational region are posed both in supersonic core region and in subsonic part of wall boundary layer.

The system of equations is used in dimensionless form. The main values used for reference are following: the duct radius R, the free stream velocity V_0, density ρ_0, gas constant $\mathcal{R}$, dynamic viscosity μ_0, characteristic magnetic field B_* and electric conductivity σ_0. Then the following dimensionless parameters appear in the system of equations

$$\mathrm{Re}=\rho_0V_0R/\mu_0,\ S=\sigma_0B_*^2R/\rho_0V_0^2,\ \mathrm{Pr},\ \mathrm{Pr}_t,\ \gamma,$$

where Re is Reynolds number and S is MHD interaction parameter.

As the first example, the inviscid, laminar and turbulent flows in the cylindrical duct with magnetic field generated by current loop were investigated for the entry Mach number equal to 5. The cross-section $x=0$ correspond to the position of electric current loop. The radius H of current loop is equal to two duct radius. The exit duct section is located in position $x=5$.

During these calculations influence of MHD interaction parameter on the flow field was estimated. In order to investigate the viscosity influence on the deceleration process some cases were considered. The calculations were performed for laminar viscous flow with $\mathrm{Re}=2\times10^5$ and $\mathrm{Re}=2\times10^4$. In order to provide the development of boundary layer in flow, the entry section of 15 radius length is positioned before cross-section where current loop is posed. For the turbulent flow, the Reynolds number is supposed

to be equal to 2×10^6. The Mach number fields for the current loop are presented in Fig.1.

Further, the data for flow in cylindrical duct when the magnetic field is generated by solenoid are presented. The solenoid entry is located in the cross-section x=0. The solenoid exit cross-section is located at x=10 and the right boundary of calculation region is posed at x=15. The length of the duct from entry cross-section to entrance to solenoid is equal to 5 and 15 duct radius correspondingly in the cases of inviscid and viscous flows. The solenoid radius is twice greater than channel radius.

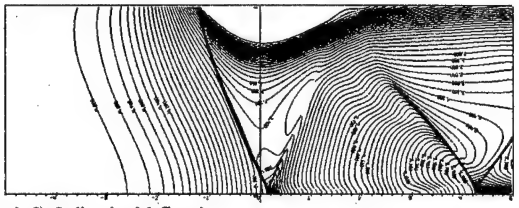

a) S=3 (inviscid flow)

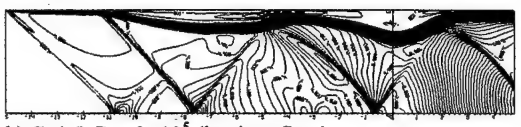

b) S=1.5, Re=2×10^5 (laminar flow)

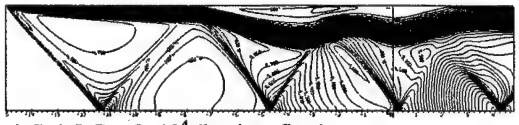

c) S=1.5, Re=2×10^4 (laminar flow)

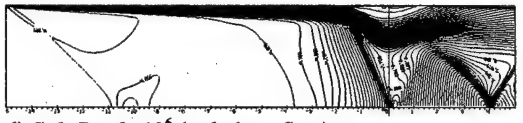

d) S=3, Re=2×10^6 (turbulent flow)

Fig.1. Mach number fields. Magnetic field generated by current loop

MHD interaction for inviscid flow (Euler equations) and for laminar and turbulent viscous flows at different Reynolds numbers (full Navier-Stokes equations) was analyzed. The Mach number contours for the solenoid are shown in Fig.2. For turbulent case, it is necessary to note that visible turbulent boundary layer exists already at the solenoid inlet. The boundary layer thickness is increased appreciably at the entry to solenoid as the result of magnetic field influence. Then in solenoid the boundary layer thickness is almost constant up to exit from solenoid. The flow in this case did not contain the separation region.

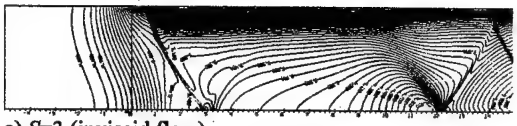

a) S=3 (inviscid flow)

b) S=1.5, Re=2×10^5 (laminar flow)

c) S=3, Re=2×10^6, (turbulent flow)

Fig.2. Mach number fields. Magnetic field of solenoid

Flow deceleration in 2-D channel in the regime of electric power generation

The 2-D flow in the tube of constant height with nonperforated walls is investigated. It is supposed that magnetic field **B** is directed normally to the plane of the flow. The magnetic field is averaged over lateral coordinate z in the channel. The component B_z of the magnetic field is designated as B and it is the only nonzero component **B**=(0, 0, $B(x)$). The 2-D electrodynamic equations can be formulated as follows:

$$j_x=\sigma_\beta\left[-\frac{\partial\varphi}{\partial x}+vB+\beta\left(\frac{\partial\varphi}{\partial y}+uB\right)\right],$$

$$j_y=\sigma_\beta\left[-\frac{\partial\varphi}{\partial y}+uB+\beta\left(-\frac{\partial\varphi}{\partial x}+vB\right)\right],$$

$$\frac{\partial j_x}{\partial x}+\frac{\partial j_y}{\partial y}=0\,,\ \sigma_\beta=\frac{\sigma}{1+\beta^2}\,,\ \beta=\alpha B\,.$$

Here α is supposed to be the known function of thermodynamic parameters. The components of MHD force f_x ,f_y and electric power q supplied to gas are defined as

$$f_x=j_yB\,,\ f_y=-j_xB\,,\ q=-j_x\frac{\partial\varphi}{\partial x}-j_y\frac{\partial\varphi}{\partial y}$$

In the considered approximation [10], B is function of x only and is supposed to be given. The presented equations can be used for the determination of electric potential distribution if velocity components u and v are known. The solution of these equations requires the formulation of the boundary conditions on the duct wall and at the entry and exit duct cross-sections. The formulation of these boundary conditions depends upon the physical problem (see, for example, [10]). The following wall

boundary conditions were considered in this article.

Walls are ideally sectioned electrodes. In this case, the electric potential distribution along the upper and lower walls is supposed to be known. Some analytical solutions [10] can be used. The wall potential distribution of some real devices obtained from experiments can also be used [14]. Thus, it is given that $\varphi=\varphi_-(s)$ along the lower wall and $\varphi=\varphi_+(s)$ along the upper wall. Here s is coordinate along the wall.

It is necessary to note that the solution of the whole gasdynamic - electrodynamic problem can be obtained with the aid of iterative procedure, when the electrodynamic subsystem is solved using known gasdynamic parameters and gasdynamic subsystem is solved taking into account known characteristics of electromagnetic field.

Simplified electrodynamic models are widely used in technical applications instead of 2-D models. Exact solution of electrodynamic equations exists, if to suppose that the channel height h, magnetic field B and electric boundary conditions do not vary with x, but velocity components u, v, electric conductivity σ and value α are dependent on transverse coordinate only. It is possible to suppose that these solutions can be used also, if the dependence of all aforementioned values upon the longitudinal coordinate is week. Then the quasi 1-D approach is described by equations [10,11]:

$$E_y=-\frac{\partial\varphi}{\partial y}=\frac{j_y}{\sigma_\beta}+B(u-\beta v),$$

$$j_y=-\frac{B\langle u-\beta v\rangle-(\delta\varphi/h)}{\langle\sigma_\beta^{-1}\rangle},$$

$$j_x=\sigma vB-\beta j_y,\ f_x=j_yB,\ f_y=-j_xB,\ q=j_yE_y.$$

Here $\delta\varphi=\varphi_--\varphi_+$, and $\langle\xi\rangle=h^{-1}\int\xi(x,y)dy$.

The system of equations is written in dimensionless form. The main values used for reference are following: the duct height D_0 at the entry, the free stream velocity V_0, density ρ_0, gas constant $\Re$, dynamic viscosity μ_0, characteristic magnetic field B_*, the reference difference $\delta\varphi=(\varphi_--\varphi_+)_0$ of electric potential on the duct walls, electric conductivity σ_0 and value α_0. Then the following dimensionless parameters appear in the system of equations

$$\mathrm{Re}=\rho_0V_0D_0/\mu_0,\ S=\sigma_0B_*^2D_0/\rho_0V_0,$$

$$K_0=\frac{\delta\varphi_0}{V_0B_*D_0},\ \mathrm{Pr},\ \mathrm{Pr}_t,\ \gamma,\ \beta_0=\alpha_0B_*,$$

where Re is Reynolds number, S is MHD interaction parameter, K_0 is the load parameter and β_0 is the Hall parameter.

The deceleration of supersonic flow of electrically conducting gas in the 2-D duct of constant height is investigated. The duct entry cross-section is located at coordinate x=-6 and the exit cross-section - at x=5.5. The flow deceleration is provided by crossed electric and magnetic fields in the central part of the duct. The magnetic field smoothly abates to the entry and exit cross-sections of the duct. The electric potential difference is supported between upper and lower duct walls in central part of the duct. The duct is operated in the regime of MHD generator when the upper and lower walls have correspondingly negative and positive electric potential in the central part of the duct. The electric potential on each wall approaches to zero in directions to the entry and exit cross-sections of the duct. The flow at the duct entry is supposed to be supersonic and uniform. The flow Mach number M at the duct entry is equal to 5.

This problem was solved using both quasi 1-D approach for electromagnetic field and accurate 2-D formulation of the electrodynamic problem. The perfect gas with adiabatic constant γ=1.4 is considered. The electric conductivity σ is assumed to be a constant isotropic value. The MHD interaction parameter S in performed calculations is equal to 0.1. The load parameter K_0 estimated by the value $\delta\varphi_0$ is equal to 0.3 and Hall effect is ignored.

The first series of calculations was performed for 2-D flow using quasi 1-D electrodynamic approach. The Mach number fields for this case are shown in Fig.3. It is obvious that in the case of quasi 1-D electrodynamics the flow which is uniform at the duct entry remains uniform in vertical direction through all the duct for the inviscid flow (Fig.3a).

The next cases correspond to viscous laminar flow with the Reynolds number 5×10^3. The distinctive peculiarity of obtained separation flow picture in the symmetric duct is the asymmetric flow field structure (Fig.3b). The asymmetric flow field is realized with large separation region on the lower wall. Only small separation region is realized on the upper wall of the duct. The results presented in Fig.3.c were calculated for the comparison with previous case when only one half of the duct was considered. In this case, the symmetry condition on the duct symmetry plane is formulated. On can see the symmetric picture of flow pattern. It is possible to suppose that symmetrical flow with large separation region is unstable relative to small asymmetrical disturbances. The features of

computational procedure can be the reason of such disturbances.

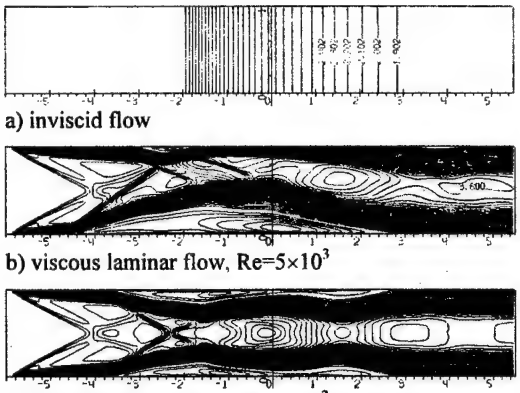

a) inviscid flow

b) viscous laminar flow, $Re=5\times10^3$

c) viscous laminar flow, $Re=5\times10^3$, symmetrical formulation

Fig.3. Mach number fields, $M_0=5$, $S=0.1$, $K_0=0.3$, $\beta_0=0$ quasi 1-D electrodynamics

Further, some calculations were performed for this problem for 2-D flow using 2-D electrodynamic model. Both the gasdynamic parameters at the duct entry and magnetic field distribution are the same as in the case of quasi 1-D electrodynamics. Therefore it is possible to compare results obtained with quasi 1-D and 2-D electrodynamics solutions both for inviscid and viscous flows.

The following data are presented in 2-D case: the lines of equal electric potential (a), the "streamlines" of electric current (current lines) in (b) and Mach number fields (c). Mach number fields comparison for inviscid calculations (Fig.4) shows that the influence of 2-D electrodynamic effects on the deceleration is negligible in comparison with quasi 1-D electrodynamics.

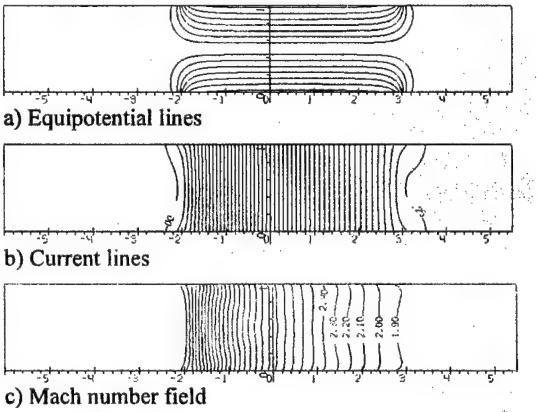

a) Equipotential lines

b) Current lines

c) Mach number field

Fig.4. $S=0.1$, $K_0=0.3$, $\beta_0=0$, inviscid flow, 2-D electrodynamics

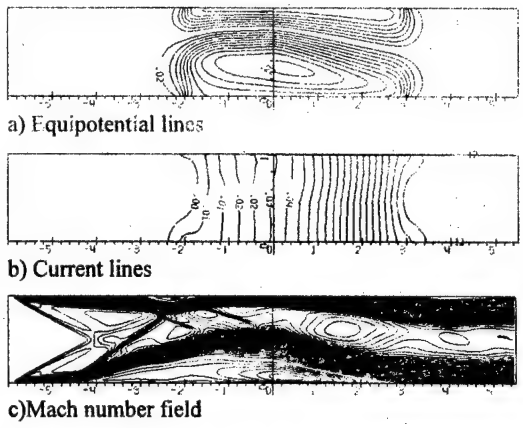

a) Equipotential lines

b) Current lines

c)Mach number field

Fig.5. $S=0.1$, $K_0=0.3$, $\beta_0=0$, viscous laminar flow, $Re=5\times10^3$ 2-D electrodynamics

For the viscous laminar flow at the Reynolds number 5×10^3, the electric potential, current and Mach number fields are shown in Fig.5. In this case, the asymmetrical separated flow similar to this one in Fig.3b is realized. The comparison of obtained results in 2-D case with those for 1-D electrodynamics shows that the difference in the flow fields is not appreciable. At the same time, the viscous and inviscid flow patterns differs significantly.

Conclusions

Thus, the presented examples testify to significant influence of the wall boundary layer on the structure of the hypersonic flow at its deceleration by magnetic field. This fact must be taken into account at the efficiency estimations of the MHD flow control applied to hypersonic propulsion system.

Acknowledgments

This work is partially supported by EOARD and by RFBR (project № 98-01-00923).

References

1. *Bityurin, V.A. Zeigarnik, A.L. Kuranov.* On a Perspective of the MHD Technology in Aerospace Applications // AIAA 96-2355, 1996.
2. *Evgeniy P. Gurijanov, Philip T. Harsha.* AJAX: New Directions in Hypersonic Technology. // AIAA 96-4609, 1996.

3. *Kacnelson S.S, Zagorskiy A.V.* Magnetohydrodynamic Flow Control in Scramjet Duct. // Thermophysics and Aeromechanics, 1997, V.4, No.1, P.41-46.
4. *Biturin, V.A., Lineberry, J.T., Potebnia, V.G., Alferov, V.L., Kuranov, A.L., Sheikin, E.G.* Assesment of Hypersonic MHD Concepts. - AIAA 97-2393, 1997.
5. *Brichkin D., Kuranov A., Sheikin E.* MHD Control Technology for Hypersonic Vehicle. // 2-nd Weakly Ionized Gases Workshop. AIAA 8-th International Space Planes and Hypersonic Technologies Conference, April 27-39, 1998, P.239-261.
6. *Frishtadt, V.L., Kuranov, A.L., Sheikin, E.G.* The MHD System Use on the Hypersonic Flight Vehicles. // Journal of Technical Physics. 1998, V.68, No.11, P.43-47.
7. *Brichkin D., Kuranov A., Sheikin E.* MHD - Technology for Scramjet Control. // AIAA 98-1642, 1998.
8. *Claudio Bruno, Paul A.Czysz.* An Electro-Magnetic-Chemical Hypersonic Propulsion System. // AIAA 98-1582, 1998.
9. *Bezgin L.V., Ganzhelo A.N., Gouskov O.V., Kopchenov V.I.* Numerical Simulation of Viscous Non-Equilibrium Flows in SCRAMJET Elements // 13th ISABE 97-7131, Chattanooga, Tennessee, USA, September 7-12, 1997, V.2, P.976-986.
10. *Vatazhin A.B., Ljubimov G.A., Regirer S.A.* Magnetohydrodynamic Flows in Channels. // Moscow: Nauka, 1970.
11. *Ivanov V.A.,* A Method for Calculation of MHD Flow with Boundary Layer Separation // High Temperature. – 1994, V.32, No.5, P.909-912.
12. *Vatazhin A.B., Isakova N.P.* Deceleration of Supersonic Flow of Conducting Gas in Strong Magnetic Field // Izv. AN USSR, Fluid Dynamics, 1972, No.5, P.145-155.
13. *Gulyaev A.N., Kozlov V.E., Secundov A.N.* A Universal One-Equation Model for Turbulent Viscosity // Fluid Dynamics, 1993, V.28, No.4, P.485-494.
14. *Borghi C.A., Cristofolini A., Ribani P.L.* A Time-Dependent Two-Dimensional Analysis of Transients in Plasma MHD Generators // 12th International Conference of Magnetohydrodynamic Electric Power Generation, Yokohama, Japan, Oct.15-18, 1996, P.807-814.

THE ELABORATION OF PHYSICAL BASES FOR FLOW CONTROL IN HYPERSONIC DIFFUSER BY MHD METHOD

S.V.Bobashev, A.V.Erofeev, V.G.Maslennikov, R.V.Vasil'eva
(Ioffe Physico-Technical Institute RAS, St.Petersburg, RUSSIA)

The work presents a model experiment undertaken to study the MHD effect on shock-wave configurations in the supersonic diffuser. Given is a description of the setups of the shock tubes with the exit nozzles incorporating the models of diffusers. The proof of employing rare gases as a working fluid is presented as well as the estimations of the MHD interaction parameters at various regimes of the setup operation sufficient to change the locations of discontinuities at the inlet.

It is well known that a flow in the supersonic diffuser experiences a change when a departure occurs in the calculated regimes under the supersonic velocities. Particularly, the shock location and shape vary resulting in the decrease in the total pressure and consumption coefficients. Commonly, the control of the supersonic diffusers is accomplished through the changes in their geometry. We suppose that the MHD method gives a possibility to control a flow in a diffuser. Solving this problem does be the goal of the work.

The first experiments are intended to be carried out with the relatively small Mach numbers at the diffuser's entry (M=4). Their results will be compared with those of the calculations and employed to elaborate the physical model of such a flow.

The general difficulties in the experiment performing in air are due to its ionization. The air ionization must be obtained, practically, continuously throughout a whole vessel [1]. For this purpose the complex nonstandard instrumentation is needed, whereas a simple inexpensive modeling employing the rare gases makes a possibility to solve a number of problems raised when performing the actual MHD control method.

To confirm this, in Fig.1, the characteristic times of recombination τ_r versus T_e are given for the initial electron density of $n_e^0=10^{20}m^{-3}$ and different gases [2,3]. The characteristic time of recombination of the molecular ions depends on the initial electron density as $1/n_e$, for the monatomic ions, as $\tau_r \sim 1/n_e^2$. Required life-time of the given plasma volume in the laboratory facilities is of the order of 10^{-3}s. As it can be seen in Fig.1, in a case of rare gases, practically, always there are the conditions to initial ionization conservation in a course of an experiment. The relatively slow recombination does be a main gain when choicing of the rare gas as the working fluid in the MHD experiment.

Flow modeling in a diffuser with a flow-magnetic field interaction is accomplished via the general similarity criteria: the Mach number of a flow, the Stuart and Hall parameters.

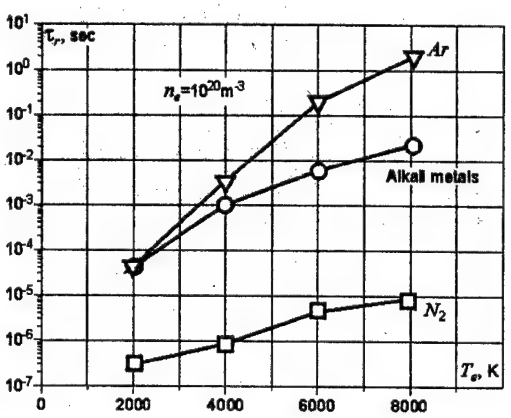

Fig.1 Characteristic recombination time versus electron temperature for various gases.

In the experiment under consideration, the preliminary ionization of a gas has been performed past a reflected shock wave in the shock tube. Then, a plasma enters an accelerating nozzle where the ionization of a gas becomes slightly lower due to the recombination but the conductivity at the outlet turns out to be sufficient to perform the MHD experiments. Further, the plasma accelerated in the nozzle enters a supersonic diffuser supplied with an electrode system. The diffuser is situated in a domain of an exterior magnetic field.

The study is accomplished in two stages. At the first, a common single-diaphragm shock tube of 50mm in diameter (so called a "small shock tube") is a base of the experiment. The second stage of this study is intended to be performed on a Large Shock Tube of the Ioffe Institute.

The large two-diaphragm shock tube of 100mm in diameter is a high-energy facility. Stored energy is as high as 4MJ. Its description is in [4]. With it, the regimes with «tailored» contact surface have been successively performed,

increasing the life-time of a shock-heated gas under the constant parameters, the operation time of this shock tube is as great as 1ms and more.

Figure 2 illustrates this presenting the operation time of the shock tube at various intensities of an incident shock wave. Dashed region corresponds to a range of a change in operation time of a single-diaphragm shock tube at the regimes employing H_2 or *He* as a pushing gas and air, N_2, or *Ar* as a working gas. Little vertical columns denote the time realized in a regime closed to the «tailored» contact surface. It follows, that the two-diaphragm tubes give rise in the operation time. Black squares denote the operation times realized with the Ioffe institute shock tube. In *Ar*, at the Mach number of an incident shock wave M_1=11 the operation time as great as more than 1ms, the *Ar* parameters being as follows: T_5=14400K, p_5=3MPa, α_5=0.11 in the stagnation region. A total tube length is about 20m. The high-pressure chamber can be supplied with H_2 or He by a compressor of 500atm pressure. This chamber can be heated up to 450^{0}C. The experimental setup is supplied with a shear polarization interferometer made on a base of the serial optical device IAB-451 and rapid camera ZhLV-2.

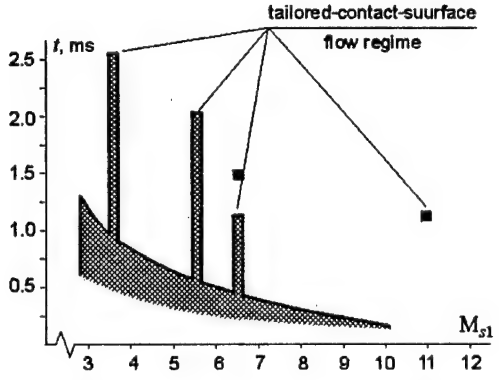

Fig.2. Operating time of shock tube versus shock wave intensity in working gas.

When planning the experiment, the results of a numerical modeling [5] for the single-shock diffuser have been used as a base. Calculation showed that there is a significant flow reshaping in a perfect sectioned short-circuited Faraday channel under condition of a constant conductivity at the initial value of the local Stuart parameter $S_0=\sigma B^2/(\rho_0 u_0)=1m^{-1}$. Subscript "o" denotes the parameters at the diffuser's inlet, the length scale is L=1m. With this value, a cross point of the shock is 15% shifted towards the diffuser's inlet. The selection of the optimum parameters of the shock tube was aimed at obtaining the values $S_0 \geq 1$ under condition that the maximum value of magnetic induction B=1.5T.

It is supposed that the parameters at the diffuser's inlet are of the same values as those at the nozzle's outlet. To find them, the stagnation parameters past the reflected shock wave were determined as well as the plasma parameters in a critical cross section of a nozzle and the problem of the non-equilibrium flow of a two-temperature plasma was solved in a flat diverging nozzle [6].

Plasma parameters at the diffuser's inlet are the functions of a pressure in the high- and low-pressure chambers and a kind of gases filling these chambers. These values determine the Mach number of an incident shock wave M1. Since these functions are known, the work regime of a shock tube is characterized by the number M1 and an initial pressure p1 in the low-pressure chamber. Experimental p1>20Torr value ensures a gas density at the nozzle outlet such that to obtain the high quality shadow pictures.

In Fig.3, shown are the initial values of the Stuart parameter for *Ar*, *Kr*, and *Xe* at various Mach numbers of the incident shock wave attainable on the small shock tube. A low limit of the Stuart parameter should be raised several times compared with the calculated value $S_0=1m^{-1}$ for a case of the actual channel under load. Set $S_{0\,min}=4m^{-1}$. From Fig.3, one can see that such values of S_0 are obtained with B=1T. Taking into consideration that a magnetic field can be raised 1.5-fold, when decreasing a gas density, we have a multiply reserve on the values of the MHD interaction parameter.

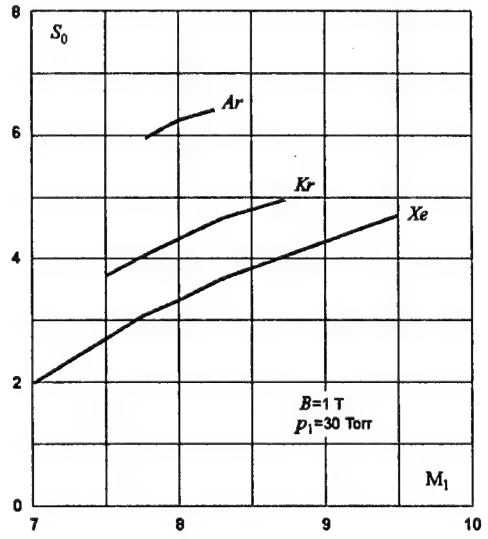

Fig. 3. The values of the initial local Stuart parameter versus the Mach numbers of the incident shock attained at the small shock tube for various gases.

The work is made in cooperation with Computer Simulation sector of Ioffe PTI.

This work is supported by the RFBR, grant No. 98-01-01121.

References

1. *A.V.Erofeev, R.V.Vasil'eva, T.A.Lapushkina and A.D.Zuev*, On possibility of preionized air using in an MHD generator an aerospace plane, Proceedings of the 34th SEAM, pp.4.3.1-4.3.12, Starkville, MS, 1997.
2. *Yu.P.Raizer*. Gas Discharge Physics (in Russian). Nauka, Moscow, 592p., 1987.
3. *L.M.Biberman, V.S.Vorob'ev, I.T.Yakubov*. Kinetics of the Non-Equilibrium Low Temperature Plasma (in Russian). Nauka, Moscow, 376p., 1982.
4. *V.G.Maslennikov and V.A.Sakharov*. Double-diaphragm shock tube at the Ioffe Physico-Technical Institute, Tech. Phys., **42,** No.11, pp.1322-1328, 1997.
5. *Yu.P.Golovachov and S.Yu.Suscikh*. Weakly Ionized Flows in Supersonic Inlets Subjected to the External Electromagnetic Field, Proc.of the Conference «Perspective of MHD and Plasma Technologies in Aerospace Application», Moscow, March 24-25, 1999.
6. *R.V.Vasil'eva, A.L.Genkin, V.L.Goryachev, A.V.Erofeev et al.*, Low-Temperature Plasma of Inert Gases with Non-Equilibrium Ionization and MHD Generators (in Russian). Ioffe Physico-Technical Institute RAS, St. Petersburg, 206p., 1991.

MHD AUGMENTED HYPERSONIC PROPULSION SYSTEMS

J.Cole (NASA Marshall, Huntsville, USA), J.T.Lineberry, R.Litchford (ERC INC., Tullahoma,TN,USA), V.A.Bityurin (IVTAN, Moscow).

This paper presents simplified analyses of MHD thrust augmentation for rocket and airbreathing primary propulsion systems. The basic idea behind MHD thrust augmentation is the redistribution of available on-board energy. Typically, this is the chemical energy of the fuel or propellants. In principle, total propulsive performance may be enhanced by extracting enthalpy (energy) from the flow in one stage of the engine cycle and transferring it to a different stage of the engine cycle. This paper examines two unique jet propulsion systems, one rocket based and one airbreathing based, which utilize MHD as an energy transfer mechanism for thrust augmentation.

First, the performance potential of the a Rocket-Induced MHD Ejector (RIME) engine concept for redistribution of momentum and energy between a primary rocket and a secondary by-passing air flow was organized using a simplified first order thermodynamic analysis. The flow processes were organized in full analogy with rather well known systems in conventional gasdynamic applications.

Second, it has been proposed (AJAX Concept) that MHD generator/accelerator coupling can significantly improve the performance of airbreathing ramjet/scramjet engines during operation at hypervelocity flight speeds. Here again, the basic idea is to transfer energy from one stage of engine cycle to another in order to minimize the entropy rise of the total aircraft system. This energy management objective is accomplished by extracting a portion of the aerodynamic heating energy at the engine inlet and converting it to kinetic energy in the engine exhaust. In this study, our goal was to assess the physical and thermodynamic feasibility of an AJAX type propulsion system for hypersonic flight.

Introduction

In this report a simplified analysis of the thrust augmentation of jet propulsion systems both for rocket and airbreathing type of primary thrusters is presented. The general idea of such an augmentation technique is so called a momentum transformation during the motion through fluid environment (atmospheric air, ocean water or others similar).

A more particular case of an application of such an idea to jet propulsion of launching operation system has been proposed and preliminary discussed by J.Cole et.al in Ref.1.

In this paper an MHD generator/accelerator coupling was proposed as a tool providing the momentum and energy redistribution between a primary rocket engine and a secondary by-passing flow. The latter assumed is organized in full analogy with the rather well known systems in conventional gasdynamics applications.

The utilization of MHD generator/accelerator coupling for a jet propulsion thrust manipulation was considered and earlier, for example, to improve significantly performance of ramjet/scramjet operation in supervelocity flights. Probably, the first of such a proposal known as AJAX concept has been proposed and developed in Russia (see Ref.2). Unfortunately a few studies of both mentioned above and any others similar to those is available now in literature.

The primary goal at this of this study is to assess physical and thermodynamics background for such an application.

. Simplified theory of a by-pass augmentation of a rocket engine thrust

Let us consider the thrust of a system presented in Fig.1 taken from Ref.1. In this Chapter any non-gasdynamics components given in this picture are neglected. Thus a conventional gasdynamics by-pass thrust augmentation system is considered.

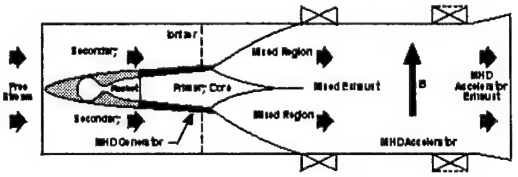

Fig.1

In this case the rocket jet is a ejecting gas. The ejected gas is the ambient air coming into mixing chamber directly from atmosphere, and the mixed flow is ejected into atmosphere again.

Let us assume for simplicity that the nozzle and diffuser are designed in such a way that the static pressure at the nozzle exit and at the exhaust of the mixture from the diffuser are equal to the ambient pressure p_a. In this case the effective thrust acting on the whole ejector system being in the rest in respect to ambient media is

$$T_p = (m_p + m_a) V_{ex}$$

where m_p and m_a are the mass flow rates of the rocket propellant and the ejected air,

correspondingly, and V_{ex} is the mixture velocity at the diffuser exit.

For comparison note that the thrust of the rocket engine alone at the assumed thermodynamics parameters in the combustion chamber is

$$T_p = m_p V_p ,$$

where V_p is the rocket ejection velocity.

Due to so called the impact losses the kinetic energy of the mixture is less the initial kinetic energy of the propellant flow

$$\frac{m_p + m_a}{m_p}\frac{V_{ex}^2}{V_p^2} = \eta < 1 .$$

The value η can be treated as an ejector efficiency. From the previous expression one can easily obtain that

$$\frac{m_p + m_a}{m_p}\frac{V_{ex}}{V_p} = \sqrt{\eta \frac{m_p + m_a}{m_p}}$$

or

$$\frac{T_{eff}}{T_p} = \sqrt{(1+f)\eta} ,$$

where f is air-to-propellant ratio.

The latter expression means that for given value of the ejector efficiency η the sufficient amount of air can be added to the propellant flow so that $1+f > 1/\eta$ and, consequently, $T_{eff}/T_p > 1$.

Basing on a standard approach of the conservation laws applied to the properly chosen control volume one can derive the final expression of the thrust augmentation of the rocket engine

$$\vartheta = \frac{T_{eff}}{T_p} = \frac{1}{\sqrt{1-\alpha^2 f^2 + \omega^2}}\left[\frac{1}{\varphi}\frac{\alpha}{\alpha+1}(f+1)^2 - f\omega\right] ,$$

where $\alpha = A_{rocket}/A_{by-pass}$,

$\varphi = A_{exit}/(A_{rocket} + A_{by-pass})$, $\omega = V_{light}/V_p$.

and for air-to-propellant ratio the following expression can be obtained (for details see for example Ref.3)

$$f = \frac{\varphi(1+1/\alpha)\sqrt{(2\alpha+\alpha^2(\varphi^2-1)+(1+\alpha^2\varphi^2)\omega^2)} - 1 - \varphi^2}{1+\alpha^2\phi^2}$$

When the system is in a rest in respect to the ambient air $\omega = 0$ and the formulas are simplified to

$$\vartheta = \frac{T_{eff}}{T_p} = \frac{1}{\sqrt{1-\alpha^2 f^2}}\left[\frac{1}{\varphi}\frac{\alpha}{\alpha+1}(f+1)^2\right]$$

and

$$f = \frac{\varphi(1+1/\alpha)\sqrt{(2\alpha+\alpha^2(\varphi^2-1))} - 1 - \varphi^2}{1+\alpha^2\phi^2} .$$

It can be shown that the thrust augmentation coefficient ϑ and by-pass coefficient f are monotonic functions on geometry parameters α and φ. It is important that $\vartheta > 1$ and can reach a rather high value. Thus, for the system resting in respect to the ambient atmosphere the thrust augmentation can be very significant. The maximum of the thrust augmentation coefficient $\vartheta = 2\varphi$ is defined by the exit-to-entrance ratio and for $\varphi = 1$ can be as high as 2.

When the propulsion system is moving in respect to the ambient atmosphere the thrust augmentation coefficient is always less. When the flight velocity approaches sonic and supersonic values the shock wave losses result in fast reduction any positive effect.

Thus, the expectation of the thrust augmentation of a rocket engine with increasing value of the by-passing coefficient is probably overestimated by neglecting of significant mechanisms of losses.

2. General concept of MHD assisted rocket thrust augmentation

2.1. Reference case

The conventional case of the thrust production system is a jet propulsion system converting the chemical energy of a fuel+oxidant mixture into the heat of the (compressed) gaseous combustion products. The expansion of this combustion product from the initial (combustion chamber) pressure to the pressure approximately equal to the ambient pressure (the best case then both are equal to each other) through the nozzle of a proper shape results in conversion of the heat energy into the kinetic energy of the jet. It can be easily shown that such an energy transformation results in the thrust acting on the jet creating system. When the whole amount of fuel and oxidant is located on-board of the system the case of the rocket jet propulsion is presented. When the ambient air is used as an oxidant to support of combustion process releasing the chemical energy of the fuel the case of airbreathing propulsion is presented.

Two main type of jet propulsion will be considered below: a rocket engine and ramjet/scramjet as an example of airbreathing device.

A general expression of the thrust valid for both cases is

$$T = (m_a + m_p) V_{ex} - m_a V_a .$$

Here m_a and m_p are mass flow rate of air and propellant component moving with propulsion system, V_a and V_{ex} undisturbed air flow velocity in respect to the propulsion system under consideration and (mass averaged) jet velocity at the exit of the propulsion system. When the only driving force to accelerate the propellant through the nozzle is heat energy of combustion products the maximal achievable exhaust velocity can be defined as

$$V_{ex,\max}=\sqrt{2C_p T_{stag,p}}=$$

$$=\sqrt{2\left(C_p T_{stag,init}+q_{fuel}\frac{1}{1+f}\right)}\ .$$

(As always in this simplified analysis the ideal gas properties are assumed for all cases.) The air-to-fuel ratio $f=m_a/m_p$ is an important parameter in this analysis.

In particular case of a rocket engine $m_a=0$ and $f=0$.

The thrust is maximal when the expansion process is completed at the pressure equal to ambient pressure p_a. For the ideal (is entropic) expansion the temperature drop is defined by

$$\left(\frac{T_{stag,p}}{T_{ex}}\right)=\left(\frac{p_{stag,p}}{p_a}\right)^{\frac{\gamma}{\gamma-1}},$$

then

$$V_{ex}^2=\left(1-\left(\frac{p_a}{p_{stag,p}}\right)^{\frac{\gamma-1}{\gamma}}\right)V_{ex,\max}^2=\left(1-\varepsilon_p\right)V_{ex,\max}^2,$$

with

$$V_{ex,\max}^2=2C_p T_{stag,p}$$

and

$$\varepsilon_p=\left(\frac{p_a}{p_{stag,p}}\right)^{\frac{\gamma-1}{\gamma}}.$$

The basic idea of the thrust augmentation is a redistribution of energy available on a vehicle board. In the typical case the only energy on-board source is a chemical energy of fuel this redistribution consists of two steps: the first one is the extraction of some fraction of the total enthalpy flux of the rocket engine $Q_{extr}=\eta_{extr}Q_p$ and, the second one, the utilization of this extracted energy to create an (extra) thrust T_{air} accelerating the ambient air (or any other surrounding fluid). Obviously that the extraction of some enthalpy decrease the residual thrust of the rocket engine. The final result is defined by the balance of the thrust loss due to power extraction from the rocket jet and the thrust benefit received by accelerating of ambient fluid.

Let us estimate these two components.

2.2. Thrust losses

After the extraction of some enthalpy from the rocket jet the residual enthalpy flux is

$$Q_{res}=Q_p-Q_{extr}=Q_p\left(1-\eta_{extr}\right).$$

Any real process of heat conversion (or transformation) results in some losses which can be described in terms of stagnation pressure losses

$$\frac{p_{stag,extr}}{p_{stag,p}}=\left(1-\eta_{extr}/\eta_i\right)^{\frac{\gamma}{\gamma-1}},$$

where $p_{stag.extr}$ is the stagnation pressure in the flow after the energy extraction process is competed, η is a so called internal (isentropic) cycle efficiency defined as the ratio the enthalpy extracted in given process between an initial and final stagnation pressure to the enthalpy extracted in an ideal (isentropic) process with the same pressure drop. Thus,

$$\eta_i=\left.\frac{\Delta H_{actual}}{\Delta H_{isentropic}}\right|_{\substack{p_{stag,init}=fixed\\ p_{stag,out}=fixed}}.$$

With these definitions one can obtain an expression for the residual exhaust velocity of the rocket jet after the enthalpy extraction and the following expansion in the nozzle from the residual stagnation pressure $p_{stag.extr}$ to the ambient pressure p_a

$$\frac{V_{ex,p,res}^2}{2C_p}=T_{stag,p}\left(1-\eta_{extr}\right)\left(1-\varepsilon_p\frac{\eta_i}{\eta_i-\eta_{extr}}\right)$$

and consequently

$$V_{ex,p,res}=V_{ex,p}\sqrt{\frac{\left(1-\eta_{extr}\right)}{\left(1-\varepsilon_p\right)}\left(1-\frac{\varepsilon_p\eta_{extr}}{\left(\eta_i-\eta_{extr}\right)}\right)}.$$

The rocket jet thrust loss due to the enthalpy extraction is as following

$$\delta T_p=-T_p\left[1-\sqrt{\frac{\left(1-\eta_{extr}\right)}{\left(1-\varepsilon_p\right)}\left(1-\frac{\varepsilon_p\eta_{extr}}{\left(\eta_i-\eta_{extr}\right)}\right)}\right].$$

For the further analysis it is important to define the behavior of these parameters when the enthalpy extraction ratio goes to zero. One can find for this case

$$V_{ex,res}=V_p\sqrt{\frac{(1-\eta_{extr})}{(1-\varepsilon_p)}\left(1-\frac{\varepsilon_p\eta_{extr}}{(\eta_i-\eta_{extr})}\right)}\Bigg|_{\eta_{extr}\to 0}\to$$

$$\to V_p\left[1-\frac{\eta_{extr}}{2}\left(1+\frac{\varepsilon_p}{1-\varepsilon_p}\frac{1}{\eta_i}\right)\right].$$

2.3. Thrust benefit

The total enthalpy extracted from the rocket jet is supplied afterwards into the flow of ambient air (surrounding fluid). Let us define the device providing such an energy transfer into the air flow as an *accelerator*. This device transferring the energy to the air flow can produce some mechanical work (acceleration or/and compression) and heating.

$$T_{stag,a,\sup}=T_{stag,a}+\eta_{extr}Q_{prop}/m_aC_p=$$
$$=T_{stag,a}(1+\Lambda),$$

with

$$\Lambda=\frac{\eta_{extr}q_{prop}}{fC_pT_{stag,a}}.$$

The final result of a thrust augmentation depends strongly upon the ratio of these two contributions. It is convenient again to characterize such an energy conversion in terms of the process efficiency defined in full analogy with the preceding analysis of the thrust losses as a ratio of the enthalpy transferred in an ideal (isentropic) process with the stagnation pressure change given to the those in real process within the same stagnation pressure change interval, thus

$$\eta_Q=\frac{\Delta H_{Q,isentropic}}{\Delta H_{Q,actual}}$$

and

$$p_{stag,Q}=p_a\left(\frac{T_{stag,a}}{T_a}\right)^{\frac{\gamma}{\gamma-1}}\left(1+\Lambda\eta_{extr}\eta_Q\right)^{\frac{\gamma}{\gamma-1}}=$$
$$=p_{stag,a}\left(1+\Lambda\eta_{extr}\eta_Q\right)^{\frac{\gamma}{\gamma-1}}.$$

It should be noted that for given definition of η_Q the latter can varies from η_Q=1, corresponding to ideal isentropic compression till a negative value corresponding to a strong dissipative process resulting in $p_{stag,Q}=p_a$.

The expansion factor is now equal to

$$\varepsilon_Q=\left(\frac{p_a}{p_{stag,Q}}\right)^{(\gamma-1)/\gamma}=\varepsilon_a\frac{1}{\left(1+\Lambda\eta_{extr}\eta_Q\right)}.$$

Applying a conventional procedure of the exhaust velocity definition one can obtain consequently

$$V_{a,Q}=V_{a,Q}^{\max}\sqrt{1-\varepsilon_Q}=V_a\sqrt{(1+\Lambda)\frac{1-\varepsilon_Q}{1-\varepsilon_a}}.$$

An important case $\Lambda\to 0$ (low enthalpy extraction) the preceding expression can be simplified as

$$V_{a,Q}\Big|_{\Lambda\to 0}\to V_a\left[1+\frac{\Lambda}{2}\left(1+\frac{\varepsilon_a}{1-\varepsilon_a}\eta_{extr}\eta_Q\right)\right],$$

that leads to

$$T_{a,Q}=m_aV_{a,Q}-m_aV_a\to$$
$$\to m_aV_a\frac{\Lambda}{2}\left(1+\frac{\varepsilon_a}{1-\varepsilon_a}\eta_{extr}\eta_Q\right)\approx$$
$$\approx m\ V\ \frac{V}{V_a}\frac{\eta_{extr}}{2}$$

with additional assumption that the compression factor for thr primary rocket jet propulsion system small enough, i.e.

$$\varepsilon_p<<1.$$

2.4. Total thrust

The total thrust augmentation is now defined as a sum of the residual primary rocket engine thrust and benefit with extra thrust provided by by-passing accelerated air flow.

$$T_\Sigma=T_{a,Q}+T_{res}.$$

The general expression is too complicated for a fast analysis. For this reason let us consider the case of low enthalpy redistribution bearing in mind that this case provides the most optimistic results.

$$T_\Sigma=T_{a,Q}+T_{res}\Big|_{\eta_{extr}\to 0}\to$$
$$\to m_pV_p\frac{V_p}{V_a}\frac{\eta_{extr}}{2}+m_pV_p\left[1-\frac{\eta_{extr}}{2}\left(1+\frac{\varepsilon_p}{1-\varepsilon_p}\frac{1}{\eta_i}\right)\right]$$
$$\to m_pV_p\left\{1+\frac{\eta_{extr}}{2}\left[\omega-1-\frac{\varepsilon_p}{1-\varepsilon_p}\frac{1}{\eta_i}\right]\right\}$$

with the additional assumption of the previous section.

Here $\omega=V_p/V_a$ is a velocity ratio. It is clear that the positive augmentation effect can expected only for cases of relatively low the flight speed.

Of course, more reliable conclusion needs accurate calculation.

2.5. T-S diagram cycle analysis

The thermodynamics cycle characteristics can be qualitatively explained with simplified T-S diagram technique. The ideal gas properties are assumed as always.

In Fig.2 the T-S diagram cycle analysis from Ref.6 is presented. The cycle (dashed lines) represents a reference cycle of a rocket engine driven by a chemical propellant (see Fig.3). The heat supply to the propellant in combustion process assumed as isobaric process with pressure $p_1=p_{comb}$. The expansion process in the nozzle from the combustion pressure p_{comb} to the pressure assumed for simplicity equal to ambient pressure p_B. The curve closing a cycle represents the ejected gas cooling process in the atmosphere. The nozzle efficiency is typically rather high so the expansion curve is very close to vertical (isentropic expansion) line. In this case the thrust (per 1kg/1sec mass flow rate of propellant) is defined by the exhaust velocity V_{ex}. The velocity square i.e. equal to doubled kinetic energy of the ejected flow which equal to enthalpy difference at points upper and loner points respectively.

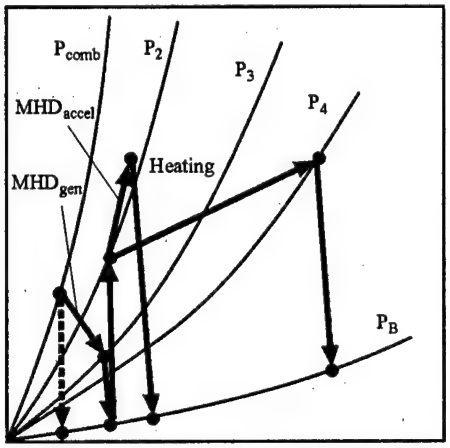

Fig.2

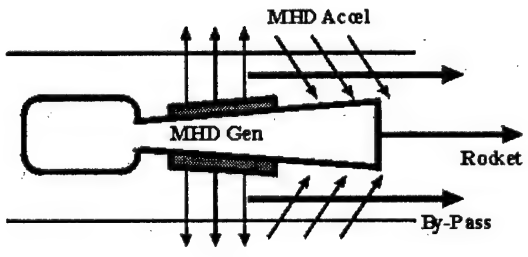

Fig.3

The process in questions involves two different working media: primary propellant and ambient air. For this reason the following 'double media' analysis is even more qualitative.

Let us consider the primary propellant cycle. It starts again from the same initial point and goes along the same heating curve. Further the curve from $p_1=p_{comb}$ to $p=p_3$ represents the process of enthalpy extraction from the primary propellant jet. It is qualitative outlined that such a process could be very dissipative so the entropy growth can be significant. The important consequence of such low efficiency is a significant stagnation pressure drop in comparison with ideal isentropic expansion. The energy extracted in this process is represented by the enthalpy drop between points upper and loneer. The following nozzle expansion process from (from an intermediate pressure p_3 to the ambient pressure p_B) provides some residual thrust by primary propellant defined by the kinetic energy of the exhausting flow. This kinetic energy is equal to the enthalpy drop. Note that the sum of energy extracted in the process of Enthelpy extraction and kinetic energy of the exhausting flow is less then the total enthalpy drop in the reference case due to lower efficiency assumed for energy extraction process.

The ambient air acceleration cycle is presented in the diagram by doubled solid curves. Assuming a rather high efficiency of air compression in the intake system one can define the compression process as a vertical line from p_B to $p=p_2$. So the enthalpy at the upper point represents approximately the stagnation enthalpy of the flow. The process of injection of the energy earlier extracted from the primary propellant jet to the air flow is presented alternatively by two curves. The difference between these cycle trajectories is defined by isentropic efficiencies along each trajectory. So, the first case is an ideal isentropic process, the second represents a process can be called as 'heating' and less desirable process. The expansion process in a by-passing nozzle is represents by one of alternative lines between one the upper point and the corresponding point at ambient pressure isobar. The thrust defining value is now the difference of the incoming air velocity V_a and the exhausting air velocity V_{ex}. Note that the kinetic energy difference available in such an expansion process is equal to the injected energy only in the case of the maximal cycle efficiency of the energy injection).

The mass flow rate correlation has to be included into this analysis also.

The conclusion is not obvious. The final result can be as positive and negative as well.

3. The simplified thermodynamics analysis of an ajax type concept

3.1. Input data and basic definitions

Let us assume that the working media is an ideal gas with constant specific heat capacities C_p and C_v, so the specific heat capacity's ratio $\gamma=C_p/C_v$ is also constant.

Let us introduce several values to characterize the process efficiency following after standard approach given in textbooks (see, for example, Ref.4).

Compression (or diffusion) efficiency to characterize the efficiency of the compression process in the intake diffuser of an ramjet/scarmjet engine

$$\eta_D=\Delta h^D_{actual}\Big/\Delta h^D_{isentropic},$$

and similar one for the expansion process through the nozzle

$$\eta_{ex}=\Delta h^{ex}_{actual}\Big/\Delta h^{ex}_{isentropic}.$$

Energy conversion in the MHD generator/accelerator can be also characterized by thermodynamics efficiencies that define the ratio of the total enthalpy change along the process to the those under isentropic condition assumed, thus

$$\eta_{MHDgen}=\Delta h^{MHDgen}_{actual}\Big/\Delta h^{MHDgen}_{isentropic},$$

and

$$\eta_{MHDacc}=\Delta h^{MHDacc}_{actual}\Big/\Delta h^{MHDacc}_{isentropic}.$$

Due to the fact that the entropy can growth through the combustion process occurring in the flowing gas mixture under the constant static pressure condition let us define also the combustion efficiency as a ratio of the stagnation pressure at the inlet of the combustion chamber to the stagnation pressure at the combustion chamber outlet

$$\eta_{comb}=p_{stag,flow}\Big/p_{stag,rest}.$$

One of the main feature of ramjet/scramjet operation in supersonic flight is the rather high stagnation temperature at the combustion chamber inlet which is practically equal to stagnation temperature of the free stream

$$T_{stag,D}\approx T_{stag,a}=T_a\left(1+\frac{\gamma-1}{2}M_a^2\right).$$

Some fuel heat is also added to the gas mixture the temperature in the combuster can reach the level unacceptable for a device operating in long duration (steady state) mode. Thus, the temperature limitation should be introduced into consideration as the condition, that the stagnation temperature of the flow at any location from the intake inlet till outlet nozzle must be not higher then the limiting temperature defined by a designer

$$T_{stag,flow}\le T_{limit}.$$

Under these definitions and assumptions let us consider the process performances in natural consequence.

3.2. Compression

The ideal values of the free stream are the free stream stagnation pressure

$$p_{stag,a}=p_a\left(1+\frac{\gamma-1}{\gamma}M_a^2\right)^{\frac{\gamma}{\gamma-1}},$$

the free stream stagnation temperature

$$T_{stag,a}=T_a\left(1+\frac{\gamma-1}{\gamma}M_a^2\right),$$

the free stream Mach number

$$M_a^2=\frac{V_a^2}{\gamma RT_a}$$

with p_a, T_a, $V_a=V_{flight}$ the static pressure, the static temperature and the free stream velocity. The latter is equal to the flight velocity.

Using the diffusion efficiency introduced earlier one can obtain the stagnation pressure at the end of the inlet diffuser as follows

$$p_{stag,D}=p_{stag,a}\frac{\left(1+\frac{\gamma-1}{2}M_a^2\eta_D\right)^{\frac{\gamma}{\gamma-1}}}{\left(1+\frac{\gamma-1}{2}M_a^2\right)^{\frac{\gamma}{\gamma-1}}}.$$

With no heat losses through the wall the stagnation temperature before the combustion chamber is equal in this case to the free stream stagnation temperature

$$T_{stag,D}=T_{stag,a}.$$

3.3. Combustion

In the combuster the stagnation temperature of the incoming flow is to increase due to a fuel heat release.

$$h_{stag,comb}=h_{stag,D}+q_{fuel}\Big/f=$$
$$=C_pT_{stag,comb}\le C_pT_{limit}.$$

In preceding expression q_{fuel} represents the specific heat of the fuel under stoihiometry condition and f is the air-to-fuel ratio. For given stagnation conditions and fuel characteristics

there is the only possibility to satisfy to the right inequality it is to change air-to-fuel ratio f

$$f \geq \frac{q_{fuel}}{C_p T_{\text{limit}} - h_{stag,D}} .$$

Even more for certain flight conditions when

$$h_{stagD} \geq C_p T_{\text{limit}}$$

no combustion (fuel injection) is possible because of the combuster temperature limitation. This means obviously that no positive thrust can be produced in such a jet propulsion system.

Meanwhile the limitation conditions is acceptable to produce some thrust let us continue the analysis of the cycle.

In practice the combustion process occurs in the flow with some Mach number greater than zero. It means that the static temperature in the combustion chamber is less then stagnation temperature that results in additional losses of the stagnation pressure. The estimation of these losses (made with approach given in Ref.5) is

$$\frac{\delta p_{stag}}{p_{stag}} \cong -\frac{\gamma}{2} M_{comb}^2 \frac{\delta T_{stag,comb}}{T_{stag,comb}} .$$

Here all values involved are as averaged ones along the process.

Defining again the combustion efficiency one can obtain

$$\eta_{comb} = \frac{p_{stag,comb}}{p_{stag,D}} = 1 - \frac{\gamma}{2} M_{comb}^2 \frac{\delta T_{stag,comb}}{T_{stag,comb}} \leq$$

$$\leq 1 - \frac{\gamma}{2} M_{comb}^2 \frac{T_{\text{limit}} - T_{stag,D}}{T_{\text{limit}}} .$$

For RAMJET $M_{comb}<1$ and for SCRAMJET $M_{comb}>1$ operating modes that can create again some problem in realization such a process. Anyway, the efficiency η_{comb} should be positive that results in an inequality

$$\frac{T_{\text{limit}} - T_{stag,D}}{T_{\text{limit}}} \leq \frac{1}{\frac{\gamma}{2} M_{comb}^2} .$$

The latter looks like a very difficult condition for high speed flight operation.

Thus the combustion yields outlet flow parameters

$$T_{stag,comb} \leq T_{\text{limit}},$$

$$p_{stag,comb} = p^*_{stag,D} \eta_{comb} =$$

$$= p^*_{stag,D} \left(1 - \frac{\gamma}{2} M_{comb}^2 \frac{T_{\text{limit}} - T^*_{stag,D}}{T_{\text{limit}}} \right).$$

In previous expression the values $p^*_{stag,D}$ and $T^*_{stag,D}$ are reserved for the MHD assisted case (see section 5). With no MHD assist $p^*_{stag,D} = p_{stag,D}$, consqeuntly $\eta^*_D = \eta_D$, and $T^*_{stag,D} = T_{stag,D}$, so

$$p_{stag,comb} = p_{stag,a} \frac{\left(1 + \frac{\gamma-1}{2} M_a^2 \eta_D \right)^{\frac{\gamma}{\gamma-1}}}{\left(1 + \frac{\gamma-1}{2} M_a^2 \right)^{\frac{\gamma}{\gamma-1}}} \times$$

$$\times \left(1 - \frac{\gamma}{2} M_{comb}^2 \frac{T_{\text{limit}} - T_{stag,D}}{T_{\text{limit}}} \right).$$

It is convenient to define the expansion factor

$$\varepsilon_{comb} = \left(\frac{p_a}{p_{stag,comb}} \right)^{\frac{\gamma-1}{\gamma}} =$$

$$\frac{1}{\left(1 + \frac{\gamma-1}{2} M_a^2 \eta_D \right) \left(1 - \frac{\gamma}{2} M_{comb}^2 \frac{T_{\text{limit}} - T_{stag,D}}{T_{\text{limit}}} \right)^{\frac{\gamma-1}{\gamma}}} .$$

3.4. Expansion

Using the expansion efficiency one can easily find that

$$\Delta T_{ex} = \frac{V_{ex}^2}{2C_p} = \eta_{ex} T_{\text{limit}} \left[1 - \varepsilon_{comb} \right].$$

The thrust reduced to the 1kg/sec mass flow rate of the propellant of such a propulsion system is equal to

$$\frac{T}{m} = V_{ex} - V_a \frac{f}{f+1} = \sqrt{\frac{2T_{\text{limit}}}{C_p} \eta_{ex}} \times$$

$$\sqrt{1 - \frac{1}{\left(1 + \frac{\gamma-1}{2} M_a^2 \eta^*_D \right) \left(1 - \frac{\gamma}{2} M_{comb}^2 \frac{T_{\text{limit}} - T^*_{stag,D}}{T_{\text{limit}}} \right)^{\frac{\gamma-1}{\gamma}}}} -$$

$$- \frac{f}{f+1} V_a .$$

In this expession $T^*_{stag,a} = T_{satg,a}$ and $\eta^*_D = \eta_D$ if no MHD convertor is involved.

3.5. MHD assisted thrust augmentation of ram/scramjet

As it follows from results of the previous section too high stagnation temperature arisen due to high flight Mach number blocks any fuel injection ($f\to\infty$) and consequently no positive thrust can be produced. In order to solve this problem energy by-passing was proposed (Ref.2). The qualitatively the idea is rather simple: the first of all to extract some fraction of the total enthalpy of the incoming air flow before combustor, the second step is the combustion of the fuel in amount providing the limiting temperature at the combuster exit, the third step is to supply the enthalpy extracted in pre-combuster area back into the exhausting flow. The expected result is to increase the total thrust by extended fuel combustion when the flight conditions approaching the critical point $T_{stag,a}\to T_{\lim it}$. Because of the high temperature environment the MHD energy conversion can be considered as a main candidate for such an energy by-passing mechanism. Disadvantages of MHD are rather low isentropic cycle efficiencies both for MHD generation and MHD acceleration.

Let us consider this process in more detailed.

Assuming that MHD generator can extract some power from the air flow. Than

$$T^*_{stag,a}=T_{stag,a}-q_{MHDgen}/C_p$$

or

$$T^*_{stag,D}=T_{stag,D}\left(1-\eta_{e,MHD}\right).$$

The stagnation pressure during MHD electrical power generation stage decreases because of the dissipation accompanying processes. These stagnation pressure losses can be expressed with earlier defined efficiencies as following

$$p^*_{stag,D}=p_{stag,MHD}=$$

$$=p_{stag,D}\left(1-\eta_{e,MHD}/\eta_{i,MHD}\right)^{\frac{\gamma}{\gamma-1}}.$$

Thus, the MHD generator modifies the inlet parameters of the combuster to $T^*_{stag,D}$ and $p^*_{stag,D}$. Substituting these values in formulas of the preciding section one can obtain

$$\varepsilon^*_{comb}=\frac{\eta_{i,MHD}}{\eta_{i,MHD}-\eta_{e\,MHD}\left(1+\frac{\gamma-1}{2}M_a^2\eta_D\right)}\times$$

$$\times\frac{1}{\left[1-\frac{\gamma}{2}M^2_{comb}\left(1-\frac{T_{stag\,D}}{T_{\lim it}}\left(1-\eta_{e,MHD}\right)\right)\right]^{\frac{\gamma-1}{\gamma}}}.$$

As it was indicated above the final stage of the AJAX' type cycle is an ijection of (probably some fraction of) electrical power extracted in upstream section of such a divice. The fractioning of the extracted power is connected with energy pre-ionization needs. With these definitions one can get

$$T_{stag,MHD}=$$

$$=T_{\lim it}+\eta_{e,MHD}\left(1-\chi_{pre-ionization}\right)T_{stag,D}=$$

$$=T_{\lim it}\left(1+\Delta_{MHD}\right),$$

where

$$\Lambda_{MHD}=\frac{T_{stag,D}}{T_{\lim it}}\eta_{e,MHD}\left(1-\chi_{pre-ionozation}\right)$$

and

$$\chi_{pre-ionization}=q_{e,MHD}/q_{pre-ionization}\le 1.$$

Then the effective stagnation pressure available in nozzle expansion process can calculated with

$$p_{stag,MHDacc}=p_{stag,comb}\left(1+\Lambda_{MHD}\eta_{i,MHDacc}\right)^{\frac{\gamma}{\gamma-1}}$$

and the corresponding value of the expansion factor in the nozzle

$$\varepsilon_{ex,MHDacc}=\left(\frac{p_a}{p_{stag,MHDacc}}\right)^{\frac{\gamma-1}{\gamma}}=$$

$$=\frac{1}{\left(1+\Lambda_{MHD}\eta_{i,MHDacc}\right)}\varepsilon^*_{comb}.$$

These yield the exhaust velocity

$$V_{ex}=\sqrt{2C_pT_{\lim it}\left(1+\Delta_{MHD}\right)\left(1-\varepsilon_{ex,MHDacc}\right)}$$

and the thrust

$$T_{AJAX}=m_aV_a\left(\frac{V_{ex}}{V_a}\left(1+f\right)-1\right).$$

3.6. T-S diagram of the AJAX type cycle

The calculation performed in the previous sections are to be qualitatively explained with a simplified T-S diagram analysis.

In Fig.4 the similar cycle analyses is shown corresponding to AIAX type concept from the Fig.5 and Fig.6. The latter represents the schematic gragram of MHD augmented

scramjet with characteristics points indicated along the slow train.

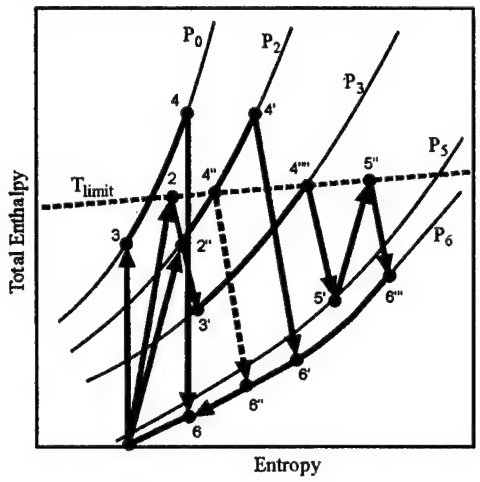

Fig.4

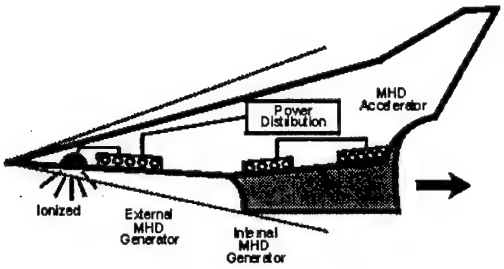

Fig.5

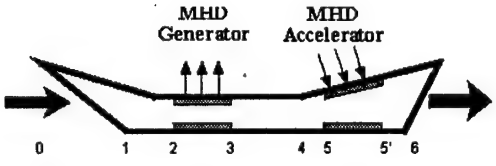

Fig.6

It can be shown also that the final result of MHD augmentations is very sensitive to non-isoentropic losses along the MHD processes both in generator and accelerator models.

Conclusion

The analysis carried out in two study is has shown that the MHD augmented jet propulsion system can be provided in frame of existing approaves wever the significant improvement of scramjet characteristics is limited by the rather high level of non-isoentropic losses typical of MHD systems.

At the same time the possible MHD applications can be found to extend the Mach number range of seeramjet operation.

References

1. *J.Cole, J.Campbell, and A.Robertson,* Rocket-Induced Magnetohydrodynamic Ejector – A Single-Stage-to-Orbit Advanced Propulsion Concept, AIAA Paper 95-4079, AIAA 1995 Space Programs and Technologies Conference, Huntsville, AL, September 26-28, 1995.
2. *Novichkov, N.,* Space Wings of Russia and the Ukraine, Echo of the Planet/Aerospace, Moscow,Sept,1990.
   Harsha P. and Gurjanov E., *AJAX: New Directions in Hypersonic Technology,* AIAA 96-4609, 8th Aerospace Planes and Hypersonic Technologies Meeting, Norfolk, Virginia, April 1996.
3. *G.A.Abramovich,* Prikladnaya Gasodinamika (Applied Gasdynamics), Moscow, Nauka, 1971, (pp.761) (in Russian).
4. *Philip G.Hill and Carl R.Peterson,* Machanics and Thermodynamics of Propulsion, Addison-Wesley publishing Company, Third printing, 1970.
5. *G.G.Cherny,* Gasovaya Dinamika (Gasdynamics), Moscow, Nauka, 1988, 424 p. (in Russian)
6. *V.A.Bityurin and J.T.Lineberry,* Overview of MHD Applications (MHD Assisted Hypersonic Flight), In: Plasma/ Electromagnetic Advanced Propulsion Workshop, 10-11 Dec., 1997, UTSI, TN.

T-LAYER MHD IN AEROSPACE APPLICATIONS

V.S.Slavin, V.V. Danilov M.V., (Krasnoyarsk State Technical University),
Kraev (The Siberian AerorSpace Academy, Krasnoyarsk),
A.V.Romashko, K.A. Finnikov, U.M.Ermoshkin (SPC of Applied Mechanics, Zheleznogorsk),

Abstract. The problem of electricity production on board of the hypersonic airplane, is considered can be solved applying the MHD method of energy conversion, that allows to converse the kinetic energy of incident flow into the electricity directly.
For these proposes the MHD generator with T-layers is proposed to be used.
Numerical simulation of the MHD process in the generator channel has shown that in the given conditions the regime with multi-structure of T-layers can be organized.
The new type of electric rocket engine is also proposed, using the T-layer effect. As the T-layer is a product of development of the overheating instability that at the nonlinear phase leads to forming of stable plasma piston (T-layer), artificial creation of T-layers in the flow of working gas allows to suppress the catastrophic development of instability in the whole flow. Numerical simulation of the corresponding process has shown that effective processes of acceleration of nonuniform gas-plasma flow in the channel of MHD accelerator can be organized.
The ionization kinetics of nonequilibrium current layers (T-layers) in the Faraday channel of closed cycle MHD generator has been investigated. Various noble gases (helium, neon, argon) not containing alkali seed have been considered as a working body of such generator. The calculations have shown that the optimal characteristics of generator process are achieved in the neon flow with stagnation pressure 2 MPa, stagnation temperature 2000 K and maximum value of magnetic field 10 T. The calculated efficiency of MHD conversion has amounted 41% for the enthalpy extraction ratio and 79% for the adiabatic efficiency.

I. AIRBORNE MHD GENERATOR FOR A HYPERSONIC AIRPLANE

It is well known that the main problem of application of MHD generators aboard an airplane is bulky and heavy magnetic systems. Traditional MHD method of energy conversion deals with very low efficient electric conductivity of a uniform flow of a working medium. In order to adjust this drawback according to the formula for specific power of MHD generator

$$W=\sigma K(1-K)u^2B^2 \qquad (1)$$

it is necessary to increase magnetic field. The required value ($B\approx4$T) is realized in superconducting electromagnets whose weight and size characteristics are not suitable for airplane conditions.

In a MHD generator with T-layers there is formed a non-uniform stream where T-layer occupies no more than 10% of the MHD channel volume. Plasma electric conductivity in current layers $\geq10^3$S/m and under these conditions average electric conductivity of the whole flow considerably exceeds a uniform case. Therefore, it is possible to considerably decrease magnetic field to the parameters ($B\leq1$T) which are realized by means of permanent magnets.

A MHD generator on a hypersonic airplane converting kinetic energy of a running on air flow into electric energy won't make on very strict demands to isentropic efficiency of the process. Hence one can decrease a load factor here and turn to maximum specific power mode in the MHD channel, that is to work with K=0.5. In its turn it changes relation of factors: Joule dissipation j^2/σ and force $j\times B$. Now execution of conditions of plasma self-maintenance won't be followed by extremely strong magnetohydrodynamic interaction of T-layers and a flow which enables to reduce losses in shock waves arising in the course of such interaction. Finally, work with air and not with combustion products enables to reduce radiation losses which changes the structure of a T-layer. It becomes thicker and accordingly more stable. Summing up all these, one should acknowledge that the conclusion on uselessness of a MHD generator with T-layers for work in open cycle [1] has proved to be wrong for a hypersonic airplane conditions. It will probably turn out to be the most efficient facility as an airborne source of electric energy.

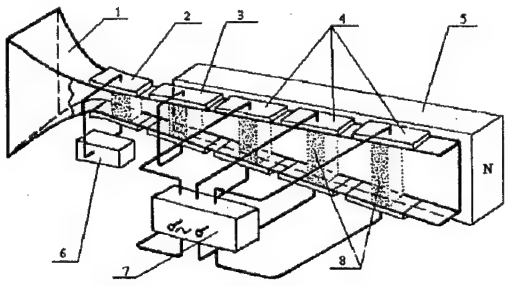

Fig. 1

Consider an unsteady one-dimensional process in MHD channel shown in Fig.1. Here an input

device accomplishes deceleration of a running on flow from M_{flight} to M≈3. Thus decelerated flow enters into a rectangular channel which has short electrode inserts in the narrowest part connected to the outer system of a periodic impulse discharge. The discharge forms a plasmoid in an air flow which is picked up by the flow and injected into the MHD channel with the cross magnetic field. Electrode walls of the channel are sectionalized, the first pair of electrodes being short-circuit and the load on the following ones is selected so as to satisfy a condition $K=E_y/(\mathbf{u}\times\mathbf{B})=0.5$. A short-circuit section is needed for production a T-layer structure from a plasmoid, on this T-layer force

$$\Delta P=\int_{\delta} j dx \qquad (2)$$

and power

$$j^2/\sigma=\mathrm{div}\mathbf{S_r} \qquad (3)$$

balances are being performed. Here δ — T-layer thickness, $\mathbf{S}_r$ — radiation energy flux.

The system of impulse discharge works at a set frequency and transforms an air flow into a stratified structure where T-layers interact with each other through gas-dynamic disturbances. Extreme disturbances can break down condition of balances (2)-(3) for the following T-layers due to which they can disintegrate and not to form a periodic structure. The aim of this numerical simulation is the demonstration of the generator mode where efficiently working periodic structure of T-layers is being formed.

Assume that the flight is performed at the altitude of 30km at a speed of a M_{flight}=7 and flow deceleration to M_0=3 occurs isentropically. Flow and MHD generator parameters are given in Table 1.

Table 1.

	Parameters of the simulated airborne MHD generator :	
1.	Static Pressure in a running on flow	10^3 Pa
2.	Air temperature overboard	240K
3.	Flight speed	2135 m/s
4.	Pressure in the throat of the channel (M_0 =3)	1.13×10^5 Pa
5.	Temperature in the throat of the channel	925 K
6.	Speed of air in the throat of the channel	1796 m/s
7.	Cross-section of the throat	57×10^{-4} m^2
8.	Width of electrodes	0.1m
9.	Height of the channel in the throat	0.057 m
10.	Height of the channel in the output	1m
11.	Initial temperature of a plasmoid	7×10^3 K
12.	Initial thickness of a plasmoid	0.05 m
13.	Length of the MHD channel	6 m
14.	Load factor	0.5

The value of magnetic field should be selected in order to find an optimal mode.

Mathematical model.

The process will be described by the system of quasi-one-dimensional equations of magnetohydrodynamics

$$\frac{\partial \rho A}{\partial t}+\frac{\partial \rho u A}{\partial x}=0 \qquad (4)$$

$$\frac{\partial \rho u A}{\partial t}+\frac{\partial\left[\left(\rho u^2+P\right)A\right]}{\partial x}-P\frac{\partial A}{\partial x}=jBA \qquad (5)$$

$$\frac{\partial \rho e A}{\partial t}+\frac{\partial\left[\rho u A\left(e+P/\rho\right)A\right]}{\partial x}=\left(jE-q_r\right)A \qquad (6)$$

Here $A(x)$ - cross-section of the channel, $e=\varepsilon+u^2/2$ — complete gas energy, q_r — power of radiation losses of energy from a unit of volume. For current density and electric field the following equations are used:

$$j=\sigma\left(E-uB\right),\quad E=KuB \qquad (7)$$

Equation system (4) – (6) is complemented with thermodynamic relationships for pressure $P(\rho,\varepsilon)$ and temperature $T(\rho,\varepsilon)$ given in tables and dependence on them of electric conductivity $\sigma(T,P)$. Volume radiation losses for air can be estimated by a model of a volume radiator

$$q_r=4\sigma_r T^4\left[\frac{\varepsilon_r\left(P,T,x-x_1\right)}{2\left(x-x_1\right)}+\frac{\varepsilon_r\left(P,T,x_2-x\right)}{2\left(x_2-x\right)}\right] \qquad (8)$$

Here $\sigma_r=5.67\times10^{-8}W/m^2\cdot$K^4; $x_1<x<x_2$, where x_1 and x_2 are distances from the calculated point up to the left and right boundaries of a T-layer correspondingly; $\varepsilon(P,T,l)$is radiation ability of hemispheric isothermal volume with radius l. Relationship (8) was checked in correlation with more accurate calculation [2] for a non-isothermal layer of air plasma. In a wide range of changes P, T and l deviation did not exceed 50%.

Boundary conditions of the problem are determined by its formulation: at the MHD channel input (cross-section x=0) stationary conditions with the parameters : $P_0=1.13\times10^5$Pa; T_0=925K; u_0=1796m/s are being set. At the channel output (x=6m) the flow has a pulsating nature but still remains a super-sonic one which enables to prescribe conditions $\partial f/\partial x=0$. Steady isentropic flow is an initial condition of the problem.

For numerical solution of the (4)–(6) set of equations the two-step difference Lax-Vendroff scheme is used modified by means of the local dissipation method.

Results of simulation.

In Fig.2 one can see distribution of speed, pressure and temperature in a MHD generator channel on one of the moments of steady-state periodic process. Steady distribution of magnetic field shown in Fig.3 corresponds to the given mode. In this moment of time there are five current layers (see relationship T(x)) in the MHD generator channel and their maximum temperature reaches 12×10^3K. The current layers actively interact with the flow which results in arising of shock waves and expansion waves. These waves can be well identified on the curves P(x) and u(x), the gradient zones with $\partial P/\partial x>0$ corresponding to the fronts of shock waves and zones with $\partial f/\partial x<0$ being current layers where overfall of pressure is balanced by electrodynamic force.

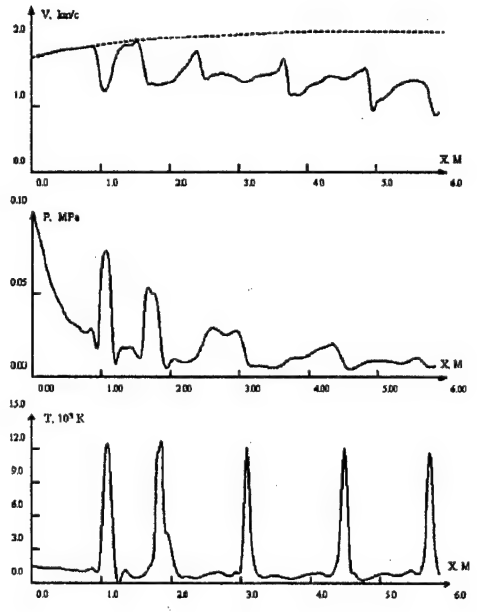

Fig. 2

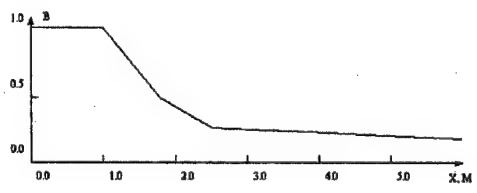

Fig. 3

In development of T-layers one can underline the following stages:

1. Stage of "picking up" of temperature disturbance set at the MHD channel input. In the flow of air not containing alkali seed at the initial temperature about 7000K disturbance has low electric conductivity and is moved by the flow practically without force interaction. However, in a short-circuit section of the channel the power of Joule dissipation in plasma exceeds cooling due to expansion of the flow. Then the mechanism of overheating instability turns on which results in explosive-like dynamics of the process. Pressure in a T-layer does not have time to level off and, as seen from the graph $P(x)$ for current layer turned out in the cross-section x=1m, the pressure peak corresponds to the thermal spike. Temperature of the T-layer at that moment of time reaches 12000K and its farther elevation is decelerated by energy losses to radiation.

2. Working stage. T-layer is thermally stabilized by radiation loss and temperature in it does not rise. The pressure peak decays and instead of it there arises the pressure gradient balancing electrodynamic force. At this stage the flow acting upon a T-layer as if on a plasma piston does work a part of which is released m the load and the remained part maintains self-support mode of a T-layer in the form of Joule dissipation.

As the T-layer travels along the channel, gas pressure is continuously dropping and, hence, the power of radiation losses is dropping too. Limitation of unwanted temperature rise is attained by means of decreasing of magnetic field along the channel. Efficient periodic mode of operation with five current layers in the working section of the MHD channel is supported by magnetic field with average value $\langle B\rangle$=0.3T. Such a field is easily created by permanent magnets.

In the process of numerical simulation electric power of a MHD generator was being determined which made the value N=3MW in the periodic mode. Expenditure for own needs, i.e. for initiating current layers made N_{exp}=0.5MW in this investigation. This is net expenditure ignoring losses which in real discharge systems can make up to 50% but even in this case there remains a considerable store of useful power which makes the idea of the MHD generator with T-layers attractive for the given applied utilization.

II. EFFICIENCY ANALYSIS OF THE SPACE MHD POWER PLANT

Efficiency of a power plant, as a rule, is associated with the high value of thermal efficiency that defines the transforming ratio of the heat energy received from a heat source. Thermal efficiency of any heat machine can be conceived of as a product

$$\eta=\eta_{carnot}\cdot\eta_{perfect},$$

where $\eta_{carnot}=(T_{max}-T_{min})/T_{max}$ is the efficiency of the Carnot cycle carrying out isothermal heating of the working body at temperature of a heat source - T_{max} and isothermal cooling at the temperature of a refrigerator - T_{min}; $\eta_{perfect}$ is a parameter reflecting thermodynamic perfection of the concrete power plant. The meaning of the second factor is defined by the irreversibility degree of heat exchange processes which is proportional to the temperature difference between heat exchange mediums. The temperature rise T_{max} does not have to be accompanied of the general thermal efficiency upgrowth. So for example the transition from steam-gas installation with $T_{max}\approx1500K$ to the MHD generator with $T_{max}\approx3000K$ at common $T_{min}=300K$ increases η_{carno} from 80% up to 90%, i.e. only by 10%. As this takes place the gas turbine has at the output the temperature about 900K and the MHD generator about 2300K while the bottom cycle of the steam turbine has in both cases T_{max} about 800-900K. By inevitable losses, which appear because of the irreversible heat exchange processes, the MHD generator will lose to steam-gas installation in thermal efficiency in earthly conditions ($T_{min}\approx300K$).

To reveal the most effective type of a space power plant it is necessary to carry out the elementary thermodynamic analysis of possible cycles of heat machines. We shall consider gas turbines and MHD generators for which the heat source heats up a working body without phase transitions that much simplifies a heater design. In space conditions it can be of paramount importance. Clearly in space only a closed cycle installation may be used having a heat source and device carrying out a working adiabatic process, together with the refrigerator and compressor restoring the gas pressure. To reduce the compressor work it is necessary with the help of refrigerator to down the temperature T_{min} so far as possible. In space conditions cooling of the working body in a refrigerator can be carried out only by dispersing heat energy in the form of thermal radiation. The power of this radiation from a unit of surface is proportional to the fourth degree of temperature. Hence, decrease of the surface temperature of refrigerator radiating panels will result in sharp growth of their surface, and with it the growth of the total installation weight. On the other hand, temperature rise leads to reduction of thermal efficiency of installation. In these conditions there is an optimum temperature of a refrigerator which provides the maximum value of specific power. The thermodynamic analysis of power plant cycles that are based on the gas turbine and MHD generator given below, permits to define thermal efficiency of installations, their specific power and, in the end, to find the value of the optimum characteristics. We shall consider that the structure of installations corresponds to the scheme shown on Fig.4 where the block "converter" represents either a gas turbine with the electrogenerator or a MHD generator. This scheme is simple enough but at the same time its efficiency is close to the limiting value achievable for this type installations.

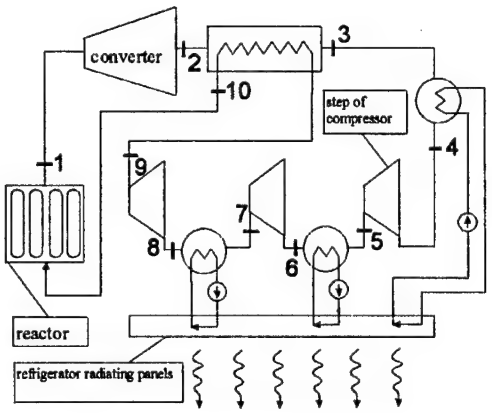

Fig. 4

The appropriate thermodynamic cycle of these installations is shown on Fig. 5.

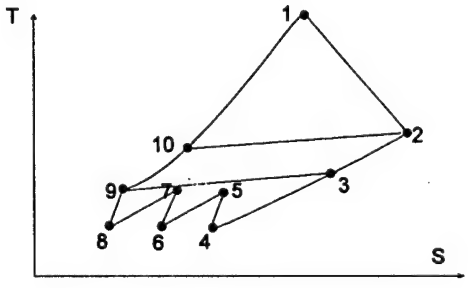

Fig. 5

The thermal efficiency of the given installations will be defined as the relation

$$\eta=\frac{W_{gen}-W_{com}}{Q_{heat}}, \qquad (9)$$

where W_{gen} - the power of a heat energy converter, W_{com} - the power of a compressor, and Q_{heat} - heat power of a heat source. A working body of a closed cycle will be noble gas which is on the one hand a good heat-carrier, and on the other hand, because of its chemical inertness, does not cause chemical erosion of the channel walls. For noble gas the specific heat could be conceded as a constant value and, hence, the parameters in the formula (9) can be expressed as $W_{gen}=G\cdot C_p\cdot(T_1-T_2)$, $W_{com}=3\cdot G\cdot C_p\cdot(T_5-T_4)$, $Q_{heat}=G\cdot C_p\cdot(T_1-T_{10})$. Therefore, the ratio (9) is written down as:

$$\eta=\frac{T_1-T_2-3(T_5-T_4)}{T_1-T_{10}} \qquad (10)$$

Here the temperatures T_1 and T_4, being the temperatures T_{max} and T_{min}, are defined accordingly by conditions in a heat source and in the refrigerator. In this analysis value of Tmax is set which is 1200K for the gas turbine and is 2500K for the MHD generator. The value of T_{min} will vary for search of an optimum value. The value of the temperature T_2 is defined by work conditions of the heat energy converter in which an irreversible adiabatic process proceeds. Let there be given the ratio of the inlet pressure to the outlet one as a parameter $\beta=P_1/P_2$ and the parameter of adiabatic efficiency $\eta_s=(T_1-T_2)/(T_1-T_{2i})$ which is defined as the ratio of a real difference of temperatures to an ideal isentropic one. Then the temperature T_2 is defined as

$$T_2=T_1\left[1-\eta_s\left(1-\beta^{-(\gamma-1)/\gamma}\right)\right] \qquad (11)$$

For a compressor step the ratio of compression is $\pi=\beta^{1/3}$ and adiabatic efficiency is $\eta_{sK}=(T_{5i}-T_4)/(T_5-T_4)$ therefore the temperature T_5 at the compressor step outlet is defined as

$$T_5=T_4\left[1+\frac{1}{\eta_{sK}}\left(\beta^{(\gamma-1)/3\gamma}-1\right)\right] \qquad (12)$$

The temperature at the heat source inlet is defined by the temperature difference on a wall of a tubular heat exchanger which is used for utilization of the heat energy of the working body after the converter. As a rule, this difference ΔT is set equal 50K. Thus the of temperature value at the heat source inlet will be defined as $T_{10}=T_2-\Delta T$.

Finally, the formula for calculation of thermal efficiency will look like

$$\eta=\frac{T_1\left[\eta_s\left(1-\beta^{-(\gamma-1)/\gamma}\right)\right]-3T_4\left[\frac{1}{\eta_{sK}}\left(\beta^{(\gamma-1)/3\gamma}-1\right)\right]}{T_1\left[\eta_s\left(1-\beta^{-(\gamma-1)/\gamma}\right)\right]+\Delta T} \qquad (13)$$

Let us use this formula and define the dependence $\eta(T_4,\beta)$, thus hitherto not determined parameters in the formula (13) will have the values:

η_s=0,7 for the MHD generator and 0,9 for the gas turbine;

η_{sK}=0,87 is assimilated level for the axial compressors.

The results of the calculation are submitted on a Fig. 6 where (A) corresponds to the conditions of a MHD generator and (b) those of a gas turbine. The area of parameters for which the thermal efficiency has appeared to be less than zero is given by zero value on diagrams.

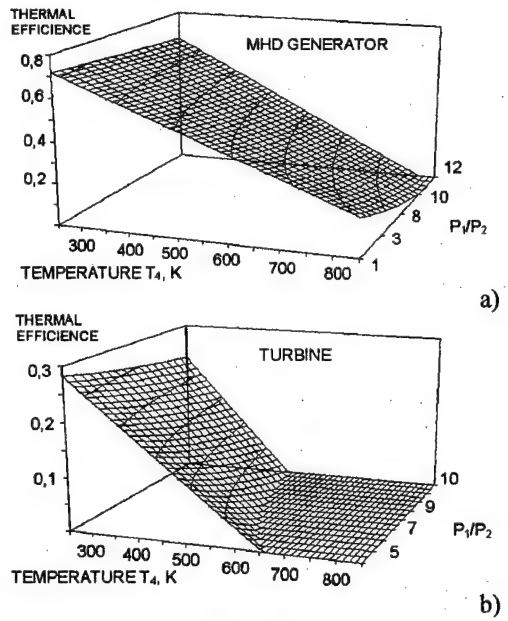

Fig. 6

In conditions of space the value of thermal efficiency itself is not of prime importance. Here, as stated above, the determining parameter φ is the specific power calculated as the ratio of electrical power to the total weight of installation. For calculation of this parameter it is necessary to estimate the weight of all units making up the power plant. Let us use the data [3] that analyzes a nuclear space power plant

with open cycle disk MHD generator created on the basis of the space nuclear rocket engine (the so-called project NERVA with high-temperature gas-cooling nuclear reactor). The reactor parameters: heat power ≈300MW; the heat-carrier - hydrogen; temperature of heating ≈2500K; pressure of hydrogen ≈30atm. This reactor, apparently, can be altered for noble gas with preservation of a former temperature level. The mass characteristics this installation are the following:

1. Nuclear reactor	2200kg
2. MHD generator	2100kg
3. Superconducting electromagnet	1500kg

In addition to this list the closed cycle installation should include a further compressor group with electric motors and system of start, tubular heat exchanger, radiating refrigerator, and besides, for the gas turbine the installation should contain the turbine generator instead of the MHD generator and electromagnet. The weight of these elements can be estimated only by convention. Let us consider, that for a given heat power all additional units, except a refrigerator, have the same weight of 2000kg and the weight of the turbine generator is equal to the weight of the MHD generator and the electromagnet. Thus, we establish the following conformity of weights:

4. Compressor group	2000kg
5. Electric motors and system of start	2000kg
6. Tubular heat exchanger	2000kg
7. Turbine generator	3600kg

Weight of a radiating refrigerator should depend on the dispersed heat power. Let us consider the weight of one square meter surface of heat-dispersing panels equal 1 kg, and flow of energy from a surface appropriate to the radiation law of the black body. In this case the weight of the refrigerator is $M_{ref}=Q_{heat}(1-\eta)/(\sigma_r T_4^4)$kg where $Q_{heat}=3\cdot10^8$W and parameter σ_r - is Stefan's constant $=5.67\cdot10^{-8}$W/(m^{2}K^4).

Finally the specific power of installation is defined as

$$\varphi=Q_{heat}\eta/M, \text{ where } M=11800+M_{ref}\text{kg}.$$

Fig.7 shows the results of specific power calculation for installations with the MHD generator (Fig.7a) and with the gas turbine (Fig.7b) as functions of parameters β and T_4. It is clear that the specific power really has optimum value in both cases, for the MHD generator it being reached at T_4 ≈600K and for the gas turbine at ≈350K. For technical reasons the heat power circulating into the installation should be comparable with the generated electrical power that implies the necessity to use the installations with a high value of enthalpy extraction. Let us accept for optimum value $\beta=P_1/P_2=10$ that at $\eta_s=0,7$ corresponds to the enthalpy extraction ratio

$$\eta_N=\eta_s\left(1-\beta^{-(\gamma-1)/\gamma}\right)=0.4=0,4 \qquad (14)$$

At these parameters the specific power of the MHD generator makes 2000W/kg and that of the gas turbine about 300W/kg. Since, there is a large uncertainty degree in the definition of the weight characteristics, this result should be estimated as a qualitative one which demonstrates that the gas turbine and solar photo cells have identical levels of efficiency and the MHD generator can lift efficiency of the space power plant to an order.

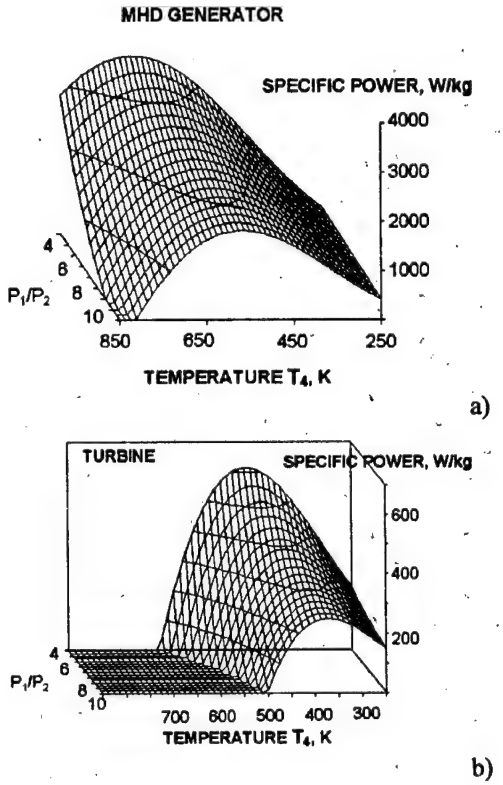

Fig. 7

III.NUMERICAL SIMULATION OF MHD PROCESS IN THE CHANNEL OF THE ELECTRICAL ROCKET PROPULSION USING THE T-LAYER PHENOMENON

For the first time the problem of creation a MHD accelerator using T-layers was analyzed in the work [4] considering the mechanism of gas flow acceleration by a separately taken T-layer. As this takes place, the channel of the accelerator had a constant section that interfered with effective work of electrodynamics force. In work [4] a phenomenon of acceleration is fixed, though the additional gain of velocity appeared to be small. In this research the problem of definition of conditions is posed at which velocity of the flow reaches about 20km/s. If the working body is neon with initial stagnation temperature about 2000K then at such a velocity the kinetic energy of gas at the outlet of electrical rocket propulsion more than 100 times exceeds the initial enthalpy. At the length of MHD channel equal 1m the average gas acceleration is $a=2\cdot10^7$g. If the induction of magnetic field equals 10T then from a ratio $\rho\cdot a=j\cdot B$, in which average mass density of the flow is $\rho\sim0{,}1$kg/m^3, find the average current density as $j\sim2\cdot10^5$A/m^2. Current density in the T-layers is an order higher, i.e. $j_{max}\approx200$A/cm^2 that corresponds to a current density in the equilibrium plasma of an arc discharge stabilized by radiation losses.

Let the stagnation parameters of the neon flow at the inlet section of the accelerator channel be equal P_s=1MPa, T_s=2000K, Mach number M=1.5. Then the parameters of the flow at the inlet are equal to P_0=0,247MPA, T_0=1142K, ρ_0=0,52kg/m^3, u_0=1334m/s. At the area of the inlet section A_0=1cm^2 a mass flow will make 70g/s. The expected thrust force of the propulsion is about 1400N. The accelerator channel linearly extends along the length up to the outlet section and equals A_1=10cm^2. At the inlet site of the channel there are periodically set local isobaric perturbations of the temperature in which T_{max}=9000K and half-width δ=5cm. The frequency of occurrence the new perturbations is selected so that into the MHD accelerator channel in an established periodic mode 6-7 T-layers would be acting simultaneously.

Contrary to the MHD generator in which the external electrical field is formed by the voltage fall on the load and its value is less than the product **uB**, in the MHD accelerator electrical field created by an external source exceeds the value of **uB**. As a result the vector of current density **j** is facing away from the MHD generator direction and interacting with magnetic field creates accelerating electrodynamics force **jB**. Electrode walls of the channel will be considered ideally sectional that allows to set intensity of an electrical field as a function of coordinate x and time value t.

Numerical simulation carried out during the course of the decision of magnetohydrodynamics equations:

$$\frac{\partial(\rho A)}{\partial t}+\frac{\partial(\rho A u)}{\partial x}=AM,$$

$$\frac{\partial(\rho A u)}{\partial t}+\frac{\partial(\rho A u^2+Ap)}{\partial x}=jBA+\frac{\partial A}{\partial x},$$

$$\frac{\partial}{\partial t}\left[A\rho\left(\varepsilon+\frac{u^2}{2}\right)\right]+\frac{\partial}{\partial x}\left[A\rho u\left(\varepsilon+\frac{p}{\rho}+\frac{u^2}{2}\right)\right]=$$
$$=jEA-AQ_r-AM(\varepsilon-\varepsilon_0)$$

in which the traditional symbols for designations the gasodynamic parameters of the flow and the electromagnetic ones of the field are used. Parameters A, M, Q_r, ε_0 corresponding: A- cross-section of the channel [m^2]; M- extra mass flow connected with arc erosion of electrodes [kg/m^{3}s] ; Q_r- the loss of energy from plasma with radiation [W/m^3]: ε_0 - specific energy of the erosion products [J/kg].

A current density is defined from the Ohm's law $j=\sigma(E-uB)$ where B=10T=Const, and the intensity of the electric field is set as a function

$$E=E_0(1+t/T_0)(1+x/X_0) \qquad (15)$$

The parameters T_0 and X_0 have been selected so as to ensure the growth of electric field in the first 10^{-4}s after the start ($T_0=t$ for $t\geq10^{-4}$s) and continuous linear growth of the field on the length of the MHD accelerator.

The plasma conductivity is set as a function of gas temperature and pressure in conformity with the model for noble gas [5]. For function of radiating losses a simplified model is accepted $Q_r(T)=Q_0\cdot T^4$ where factor $Q_0=10^{-7}$W/m$^3\cdot$K^{-4} is selected so as the stabilization of a T-layer occurred at the temperature $\leq$20000K. The source of mass in the equation of mass conservation is defined in conformity with experimental data about the arc erosion on copper electrodes which can be summarized in the form of a ratio between the vaporized mass and the amount of electricity gone through the arc, $K_q=2\times10^{-6}$kg/C . Let define a factor of proportionality between current density and the

right part of the mass conservation equation with condition $MA=K_q \cdot j \cdot a$ where a is the width of electrodes =0,01m.

The initial condition of the problem is a stationary isentropic flow which does not interact with magnetic field. The non-stationary process begins with the task isobaric perturbation of the temperature on an inlet site of the accelerator channel. The electrodynamics force operating in a volume of plasma perturbation causes its acceleration that is accompanied by formation of the waves of both compression and divergence. The wave of divergence moves to the up flow with a sound velocity but the supersonic flow maintained at the channel inlet keeps stationary conditions here that can be used as the boundary conditions. A boundary condition at the outlet section of the channel are the conditions of "transference", i.e. condition of equality to zero derivative on x for all parameters of flow.

Thus in this section the statement of the problem of numerical simulation of the MHD process in the channel of the electrical rocket propulsion is formulated. The problem was decided with the use of algorithm constructed on the basis of the Lax-Wendroff's method which was used at the simulation of the MHD generator processes.

Simulation results of the MHD process in the ERP channel

On Fig.8 the acceleration process of the flow in the form of dependencies: $u(x)$, $\rho(x)$, $T(x)$ is submitted. Specially selected electric field dynamics in the channel corresponds to this mode (see dependence $E(x,t)$ on Fig.9), which includes the increasing of E both temporal and spatial in the working part of the channel according to a condition (15), but also temporary growth of value E_0 which defines an electrical field in the formation section of the T-layers. This growth appeared to be necessary for formation of new T-layers following the first one.

The new layers appear in the zone of a rarefied wave generated by the first T-layer. As a result they receive additional acceleration not connected to the action of electrodynamics force. The growth of velocity in this case reduces the total electric field $E^*=E-uB$ which without increase of an external field E is not sufficient for formation of selfmaintained current layer.

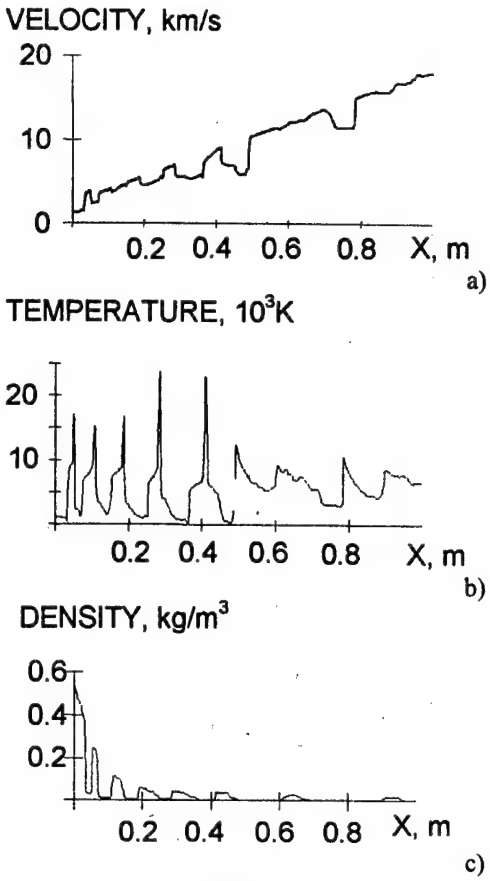

Fig. 8

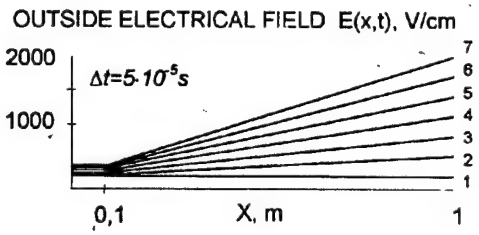

Fig. 9

Presented on Fig.8 distributions of the main gasodynamic parameters correspond to the established periodic mode. From this figure we notice that the average flow velocity grows linearly and on the channel length per 1m the velocity about 16km/s is reached. The flow of the working body gets a pulsing character that is well visible from distribution of pressure in the channel of the accelerator. Thus the T-layer are placed in the sites of the flow appropriate to the zones with minimum density which are formed under the influence of two factors: thermal expansion of the gas heated up in a T-layer and

action of a rarefied wave. Density of plasma in T-layers is on average two orders of magnitude lower than in the surrounding gas flow that leads to the development of overheating instability. As a result the current layers become thinner (1-2cm instead of 5-7cm of initial perturbation) and its temperature is stabilized at the level ~2×10^4K. Conductivity of plasma reaches the values about 10^4S/m at which for maintenance of a T-layer, as differentiated from the conditions of the formation, very small value of the field E^* is required. On Fig.10 the distribution of $E^*(x)$, appropriate to the same time moment as on Fig.8 is given. On this curve it is possible to see a series of "holes" which correspond to the zones of T-layers. At the inlet site of the channel, where the mode of T-layer formation takes place, the minimum value of E^* in the "holes" is about 10V/cm while in the other part of the channel these minimums are practically about zero.

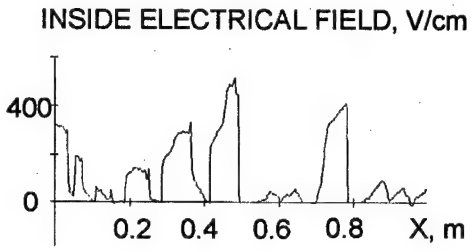

Fig. 10

Therefore, the autoregulation takes place at which changing the electric field it is possible to set a velocity of T-layers and through it the flow velocity too. On the channel length about 1m the acceleration process proceeds in a regular mode that allows to increase the velocity of a flow up to the desirable value by simple escalating of the channel length with preservation of linear growth of E.

IV. IONIZATION AND RECOMBINATION PROCESSES IN THE NONEQUILIBRIUM PLASMA IN CONDITIONS OF FARADAY CHANNEL OF MHD GENERATOR

Molecular Ions Kinetics

A significant part of ions can exist in the molecular form. Molecular ions are generated as a result of the atomic ions conversion with the scheme $A^+ + 2A \leftrightarrow A_2^+ + A$ and in the associative ionization process $A^* + A \leftrightarrow A_2^+ + e$, where A^* is an atom in the high excited state, which excitation energy differs from the ionization potential by the value close to the molecular ion dissociation energy E_D=1.4eV. The process, reverse of the associative ionization is the dissociative recombination of molecular ions and electrons, causes the additional electron losses. At a low gas temperature the equilibrium in these reactions shifts to the conversion of atomic ions into molecular ones and dissociative recombination. The equation of the molecular ions density balance, formed by these reactions, is written as

$$\frac{\partial n_m}{\partial t} = c_1 n_a^2 n_i - c_2 n_m n_a + \beta_m n^* n_a - d_m n_m n_e \quad (16)$$

The reaction rate constant of atomic ions conversion [9] depends on the gas temperature as $c_1 \sim T_g^{-3/4}$. At 300K $c_1=4.1\cdot10^{-32}$cm^6/s^3. The ratio of the reverse process is found from the thermodynamic equilibrium:

$c_2 = K_m c_1$;

$$K_m = \frac{g_i g_a}{g_m} \frac{\exp\{-E_D/T_g\}}{2\pi r_0^2} \sqrt{\frac{\mu T_g}{2\pi h^2}} \left(1 - \exp\left\{\frac{-h\nu}{T_g}\right\}\right)$$

This expression includes the following characteristics of the molecular ion Ne_2^+: statistic weight g_m=3; oscillation quantum energy $h\nu=7.7\cdot10^{-2}$eV; dissociation energy E_D=1.4eV; distance between nuclei r_0=1.7A [4]. According [5] $d_m = 1.8\times10^{-7} T_e^{-0.43} T_g^{-1.1}$ cm^3/s, as a result of dissociative recombination two atoms appear, one of which is in the base state and another in the $3p$, $3p'$ state.

The atomic ion converts into the molecular one during the time of the order of $\tau \approx c_1 n_a^2 \approx 10^{-6} \div 10^{-4}$s, which is significantly less than the characteristic diffusion time of ion. That is why the diffusion is not taken into account in the equation of balance of molecular ions density.

Electron-Atom Non-elastic Collisions

In the excited atoms of noble gases due to the high potential of the first excited level there is one electron on the higher shell, weakly bounded to the atomic residual. Due to this the collision transitions between the excited levels can be considered as the diffusion of electrons in the discrete energy space. Solving the Focker-Planck equation for the discrete spectrum [6,app.2] the following expression is obtained for the transition probability from the level k to k+1, in the case of the maxwellian energy distribution of free electrons:

$$z^0_{k,k+1}=\frac{4\sqrt{2\pi}n_e e^4\Lambda_k E_{k-1}\exp\left\{-\frac{E_{k+1}-E_k}{T_e}\right\}}{\sqrt{m_e T_e}(E_{k+1}-E_{k-1})(E_{k+1}-E_k)} \quad (17)$$

Here Λ_k is the Coulomb logarithm of transition. The reverse processes probabilities are defined from the equilibrium correlation.

The electron-electron energy transfer collision frequency is much more than that against electron-heavy particle, i.e. the main body of the electron energy distribution is maxwellian. Due to small values of ratios of electron and atom masses and also electron-atom and coulomb cross sections it becomes true at the ionization ratio $\approx 10^{-7}$ [6,7,1]. Nonelastic electron-atom collisions with the transitions between the excited levels with the energy ≈2eV, only change the temperature of the main body of the distribution function, so we can use the equilibrium values for the probabilities of transitions between the excited levels $z_{k,k+1}$, when $k\geq 0$: $z_{k,k+1}=z^0_{k,k+1}$.

It is seen from (17) that closely located levels exchange the electrons very intensively. That is why we can combine closely-spaced levels adding their statistical weights and averaging out the energy [6,app.3]. Lets choose the following effective levels:

	Combined levels	Average energy E_k, eV	Total statistical weight g_k
0	$1S_0$	–21.56	1
1	3s, 3s′	–4.86	12
2	3p, 3p′	–2.94	36
3	4s, 4s′	–1.87	12
4	4p, 4p′, 3d,3d	–1.46	96

The fourth effective level includes the states which ionization energy is close to the dissociation energy of the molecular ion; in the equation (16) $n^*=n_4$.

To find the cross section of excitation from the base state the half-empiric formula is used [7]:

$$q_{01}(u)=\frac{\pi e^4 f_{01}}{(E_1-E_0)^2}\left[\frac{u}{(u+1)^2}\ln(1.25(u+1))+\frac{0.3}{u+1}\right] \quad (18)$$

where $u=(E-E_1+E_0)/(E_1-E_0)$. With the approach $t=(E_1-E_0)/T_e<<1$ the frequency of the excitation from the base state

$$z^0_{01}(t)=\frac{2\pi e^4 n_e f_{01}}{(E_1-E_0)^2}\sqrt{\frac{2T_e}{\pi m_e}}\exp(-t)\left(\frac{\ln(1.25)}{t}+0.3\right) \quad (19)$$

The collisions with the excitation from the base state strongly influence the high energy part of electron energy distribution. Let us estimate the derivation of the electron energy distribution from the Maxwellian, following [6.7.2.2]. The estimation expression obtained there, is

$$z_{01}=z^0_{01}F,\ F=\frac{1\sqrt{1+4C}-1}{C\sqrt{1+4C}+1},\ C=\frac{z^0_{01}n_a}{\nu_{ee}n_e} \quad (20)$$

Ionization from the low excited states can be a significant source of electrons. The following half-empiric formula is derived in [7] for the cross section of ionization from the k level:

$$q_k=\frac{\pi e^4}{E_k^2}f_k N\frac{u-1}{u^2}\ln(1.25u) \quad (21)$$

where N — the number of equivalent electrons in the atomic shell (for the excited states of noble gases N=1), f_k — oscillator strength. The ionization rate

$$\beta_k(t)=\frac{2\pi e^4 f_k N}{E_k^2}n_e\sqrt{\frac{2T_e}{\pi m_e}}\ln(1.25)\exp\{-t\} \quad (22)$$

The ionization from the 4th level and three-body recombination to the 4th level are described within the framework of the diffusional approach, giving for the three-body recombination coefficient the expression called the "9/2 law":

$$\alpha_d=\frac{4\sqrt{2\pi}}{9}\frac{e^{10}\overline{\Lambda}}{\sqrt{m_e}T_e^{9/2}} \quad (23)$$

The ionization coefficient is found from the equilibrium correlation.

Radiation Transitions

Let us consider that in a dense plasma, with the parameters like the described above, the radiation transitions to the base state are suppressed by the reabsorbing of radiation. At the same time we must take into account the atom impact quenching of the resonance state that strongly influences the populations of low excited levels. in the case of low ionization. The opposite situation is observed in the case of transitions between the excited levels, where the radiation transitions prevail over the atom impact quenching. In the nonequilibrium plasma under the given conditions the density of the excited atoms amounts to 10^8–10^{10}cm^{-3}. That is why we can consider the plasma to be transparent for the radiation of transitions between the excited levels. As approaching the continuous spectrum the influence of radiation processes, as compared with the processes of electron impact excitation and quenching, sharply decreases. The estimations of the collision and radiation transitions intensity [6.5.1] show that the influence of radiation processes becomes negligibly small at the level energy

$$E_{[\mathrm{eV}]} > -\left(n_{e[\mathrm{cm}^{-3}]}/4.5\cdot10^{13}\right)^{1/4} T_{e[\mathrm{eV}]}^{1.8}$$

Under the conditions of contracted discharge the boundary energy is about 0.5eV. Among the transitions between the low excited states the most intensive are transitions between 3s, 3s′ and 3p, 3p′ (1 and 2 groups) and between 3p, 3p′ and 3d, 3d′ (2 and 4 groups) Averaging the probabilities of transitions between the different pairs of states of effective levels we obtain the following probabilities of transitions between the effective levels:

$A_{21}=3.87\cdot10^7\mathrm{s}^{-1}$; $A_{42}=9.49\cdot10^6\mathrm{s}^{-1}$.

The probability of atom impact transition to the base state

$$Q_{10}=\frac{2}{\sqrt{\pi}}n_a\sqrt{\frac{2T_g}{M}}q'_{aa}\frac{1}{g_1(2T_g+E_1-E_0)}, \quad (23)$$

where q'_{aa} is the tilt of the cross section of the atom impact excitation at the threshold energy. The experimental data about its value lies within the limits $10^{-19}\div10^{-20}$cm^2/eV. This value strongly influences the discharge model characteristics. That is why this value was chosen so that the discharge model were most close to the real characteristics. The optimal value appeared to be $q'_{aa}=8.7\times10^{-20}$cm^2/eV

The Kinetic Equations System

The populations of four effective levels and the density of the molecular ions are described by the following system:

$$\begin{aligned}
&z_{01}^0 F n_a-(z_{10}^0 F+Q_{10}+\beta_1)n_1+(z_{21}+A_{21})n_2=0\\
&z_{12}n_1-(z_{21}+A_{21}+\beta_2)n_2+z_{32}n_3+A_{42}n_4+\\
&\qquad+d_m n_e n_m=0\\
&z_{23}n_2-(z_{32}+\beta_3)n_3+z_{43}n_{43}=0 \quad (24)\\
&z_{34}n_3-(z_{43}+\beta_d+\beta_m n_a)n_4+\alpha_d n_e^2(n_e-n_m)=0\\
&c_1 n_a^2(n_e-n_m)-c_2 n_a n_m+\beta_d n_4 n_a-d_m n_e n_m=0
\end{aligned}$$

The schematic view of this system is presented on Fig. 11

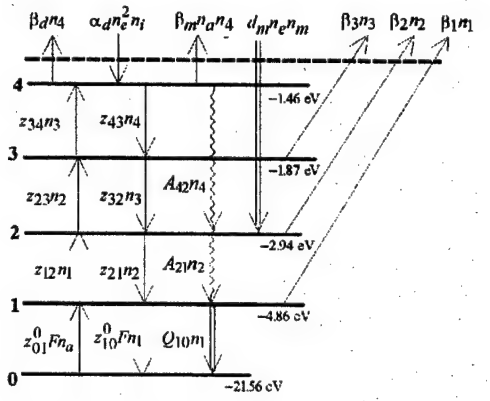

Fig.11. Scheme of fluxes in the discrete energy space. Simple arrows — the electron impact transitions, wavy arrows — the radiation transitions, thick arrows — the atom impact transitions and processes with participation of molecular ions

The system is linear relatively to n_1... n_4 and n_m. As a result of its solution we obtain the dependency of these values on n_e, n_a, T_e and T_g. The speed of electrons delivery or the electron flux in the energetic space is found from the expression

$$j_E=z_{01}^0 F n_a-z_{10}^0 F n_1-Q_{10}n_1 \quad (25)$$

The electron gas energy losses in the line radiation and with the decay of the molecular ions are described by the expression

$$\begin{aligned}
q=&(E_1-E_0)Q_{10}n_1+(E_2-E_1)A_{21}n_2+\\
&(E_3-E_2)A_{32}n_3+(3/2T_e-E_4)d_m n_m n_e
\end{aligned} \quad (26)$$

Results of simulation of MHD process

To organize the working regime in which the plasma clots are slowly recombinated it is necessary to set a high ionization in them at the beginning. Besides, the gas in the ionized layer must be heated because in cold gas the dissociative recombination is strong and phenomenon of "frozen" ionization is impossible. The task of creation of the plasma clot with needed parameters is the object of

further investigations. Apparently, the plasma clot with the needed ionization and gas temperature may be created by the means of high current diffusive discharge. This type of discharge, described in [8], develops in a strong electric field. It remains diffuse during the characteristic time of gas rarefaction. In the same period electron density grows sharply.

The expense of energy to the plasma clot creation, which consists of the ionization and gas heating expenses, must be deducted from the thermal efficiency of the MHD generator. The working ionization ratio is less than 10^{-4} and, since the plasma is about the tenth part of the gas in the MHD channel, the electron gas energy is about 10^{-3} of the gas energy. Thus we can neglect the ionization expense. The expense for gas heating was estimated as the heat delivered in the equilibrium isobaric process.

The simulation was conducted with the following parameters of flow and MHD-channel:

Stagnation pressure	2 Mpa
Stagnation temperature	2500 K
Mach number at the inlet	1.5
Channel length	2 m
Channel expansion ratio	10
Magnetic field	10 T
Load factor	0.7 (at the inlet) ÷ 0.97 (at the outlet)
Initial electron density	7×10^{14}cm^{-3}
Initial gas temperature in the T-layer	2500 K
Periodicity of the T-layers forming	1.8×10^{-4} s

With time the periodic regime of flow establishes in the MHD channel. Its character is shown on fig.12,13. Interaction between the plasma layers leads to the deceleration of flow as a whole. The obtained characteristics of the MHD generator efficiency are the following: enthalpy extraction ratio η_N=0.412; adiabatic efficiency η_S=0.788. The expenses on the plasma layer creation amount 0.029 of the whole heat power. The working regime by the means of the load factor varying was chosen such that the plasma clots are slowly recombinating, as seen on Fig.14. The situation is observed in which the both ionization and recombination are weak in T-layers during the work time. In this conditions the ionization ratio keeps practically constant. It leads to that the conductivity of plasma decreases with the increase of the electron temperature, which suppresses ionization and overheating instabilities.

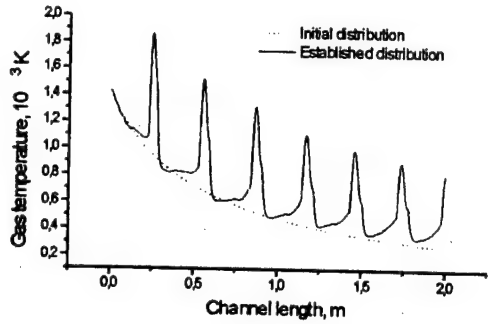

Fig. 12. Gas temperature in the isentropic and established flow

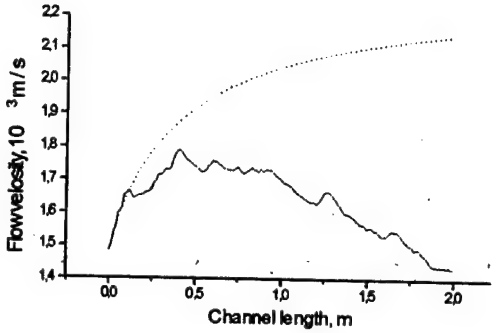

Fig. 13. Flow velocity in the isentropic and established flow

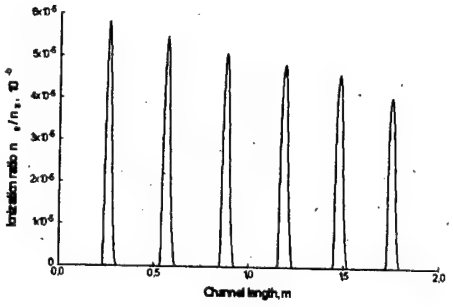

Fig.14. Momentary distribution of ionization ratio in the established mode

Conclusion

As conclusions let us enumerate the main results:

1. The program of industrial exploitation of space will require the creation of a powerful electrical rocket propulsion with thrust force up to 1000N. To feed such an engine aboard of a spacecraft we need a source of energy with the power level up to 10MW. The attractive decision of this problem can be a combined installation including both a source of electric power on the basis of a closed cycle MHD generator and a propulsion on the basis of the MHD accelerator.
2. Comparison of the efficiency has shown that in space conditions the MHD generator is about an order superior both to the gas turbine and the perspective solar cells in specific power (W/kg).
3. As shown, the use of a MHD effect of the formation of selfmaintained high-temperature current layers (T-layers), which are electrical arcs stabilized by the losses of radiation, allows to realize in the MHD channel a mode of quasi-continuous acceleration of the gas flow. For this purpose in the linearly extending channel with outlet section ~10cm^2 it is necessary to set both a constant magnetic field B ~ 10T and a linearly increasing electrical field with the value of coordinate derivative $E'(x)\approx 2\times 10^3$ V/cm.
4. In a simulated mode the neon was considered as a working body with stagnation parameters at the inlet of the channel P_s=1MPa, T_s=2000K and with the value of mass flow 70g/s. In the established periodic acceleration mode the average increase of gas velocity per 1m of the channel length is about 15 km/s. The used electrical power (without considering the expenses for the initiation of initial temperature perturbations) is equal 8×10^6W thus, efficiency of the MHD accelerator is 95% at the thrust force about 1000N.
5. The model of ionization and recombination kinetics has been created for the simulation of the gas-plasma MHD processes in the noble gas flow.
6. The possibility of realization of the MHD process with nonequilibrium ionized plasma clot in the condition of "frozen" ionization, has been shown. This regime is the most effective for transformation of the heat energy into the electric one and, besides, in this condition the plasma clot do not run the risk of the ionization-overheating instability.
7. The results of simulation of the process in the Faraday MHD generator channel has demonstrated the possibility of reaching of the high performance in the both enthalpy extraction ratio and adiabatic efficiency. The effective working regime has been obtained at the stagnation pressure of working medium 2MPa, which allows to use the gas-cooled nuclear reactor as a heat source in the one-contour cycle. In this case the space power plant will be compact and with low specific mass.

References

1 *Slavin V.S.* Final Results of the Theoretical Study of the Development Problems of an MHD Generator with Self-Maintained Current Layers, J. Magnetohydrodynamics, Vol.2, No.2-3, 1989.

2. *Nemchinov I.V.* On the averaged equations of the radiation transfer and its use in the solution of gasdynamic tasks. PPM, 1970, Vol.34, No.4, p.706 (In Russian)

3. *W.D. Jackson, et al.,* Non-equilibrium MHD Disk Generator Using Cesium-Seeded Hydrogen, Proc. of 11-th Intern. Conf. on MHD Electrical Power Generation, Vol.4, p.1224-1231, Beijing, October, 1992.

4. *B.C.Lin, et al.,* An Assessment of Unseeded MHD Accelerator Using T-layer Concept, Proc. of 33-rd SEAM, p.V.7-1-10, Tullahoma TN, June, 1995.

5. *Frommhold L., Biondi N.A.* Interferometric study of dissociative recombination radiation in argon and neon afterglow. Phys.Rev., 1969, vol.185, 1, p. 244

6. *L.M. Biberman, et al.,* book "Kinetics of Non-Equilibrium Low-Temperature Plasma", Moscow, Nauka, 1982 (in Russian)

7. *Drawin H.W., Emard F.* Instantaneous population densities of the excited levels of hydrogen atoms and hydrogen-like ions in plasmas. Physica, 1977, v. 35c, p. 333

8. *Yu.A.Bichkov.* Plasma physics, 1991, v.17, No.2, p.196

9. *G.Huxley, R.Crompton.* The diffusion and drift of electrons in gases. N.Y.: Wiley, 1974

10. *B.M.Smirnov.* Ions and excited atoms. Moscow: Atomizdat, 1974 (in Russian)

PLASMA AERODYNAMIC WT TESTS WITH 1/6 SCALE MODEL OF NOSE PART OF FLIGHT TEST LABORATORY (F-15).

Warren Beaulieu (BOEING, USA),
V.Byturin, A.Klimov, A.Kuznetsov, S.Leonov (Institute of High Temperature RUS),
A.Pashina (Institute of Radio Engineering, MTC), B.Timofeev (Moscow State University/MTC)

Abstract. The preliminary experiment results on plasma aerodynamics study of the 1/6 scale model of F-15 noe part are reported. Several types of plasma generating systems are described.

Plasma/ aerodynamic study supersonic flow around 1/6 scale model of nose part of flight test laboratory (F-15) were fulfilled in the frame of Program of Flight Test Experiment. This experiment is very important for study of possible application of plasma technology in aviation.

Present work is a part of mutual BOEING/ IVT RAN researches in the field of plasma/ aerodynamics, which included the following tasks also:

- Study of supersonic flow around 1/3 scale model (with TsNIIMash),
- Optimisation of on board plasma generators (PG) for 1/3 and 1/6 scale models,
- Microwave plasma/ wind tunnel experiment (with St.-Petersburg Univ.),
- Plasma diagnostics for WT tests and flight test experiment (with MSU).

The main goals of the future WT tests 1/6 scale model were the following:

1. Measurement of reliable aerodynamic characteristics of the model in WT experiment (Drag, Lift, Moments and others). It is very important to note that integral characteristics (such as Drag, Lift and others) have to be measured with differential ones (for example, surface pressure distribution) simultaneously.
2. Decrease of EM noise up to 5% of measured sensor's signal.
3. Study of possibility of plasma parameters measurements by new diagnostic instrumentation in real plasma/ WT experiment.
4. Prepare the proposals for future experimental Program on plasma/ WT experiment with 1/3 scale model.

Experimental set up

Experimental researches were carried out in WT- 113 (TsAGI). This WT has square cross section 60x 60 cm^2.

Parameters of supersonic flow were following in this work:

- Mach number M~ 2
- Static pressure P_{st}=100-200torr
- Reynolds number Re~10^5-10^6
- Incidence angle α= 0°, ±2°, ±5°

1/6 scale model consists of (see Fig.1):

- Cylindrical metal body with diameter D_c=168 mm and length L_c=225mm,
- Conical dielectric head part (Nilon-6, D_h=168 mm, L_h=173mm),
- On board plasma generator
- Pressure sensor of ESP type (commutator, 32 channels) for measure of pressure distribution and total pressure in model boundary layer.

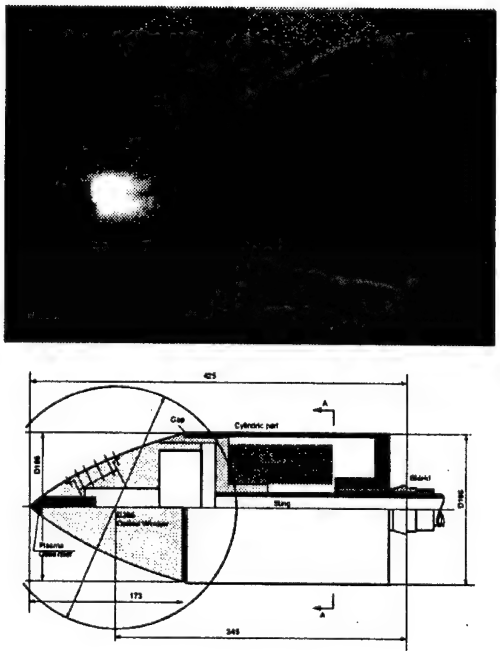

Fig.1 Schematic diagram of the 1/6 scale model and shadow photo of supersonic flow around this model with working PG PR: M=2, P_{st}=200Torr, F_r=40Hz

There are 15 tubes on the surface of the model for the measure of surface pressure distribution. These tubes are connected with sensor ESP (commutator).

3 Preston's tubes are located on the surface of this model near orifices of surface tubes also. These Preston's tubes are connected with commutator.

8 tubes posed in base model area measure base pressure distribution.

Sensor ESP is located in cylindrical part of model.

PG is installed in nose part of the model.

Electric probe is posed in nose part of the model near PG.

Head part of this model is connected with the sting of mechanic balance only. Cylindrical part of this model is disconnected with balance.

We have possibility to change 5 different types of PG in nose part of this model.

Diagnostic instrumentation of the 1/6 scale model.

- Mechanical balance for measurement of Drag, Lift, Moment M_z,
- Shadow photos of supersonic flow around model (time exposure was about ~2mcs).
- Surface pressure distribution on head part of 1/6 scale model was measured by ESP commutator (15 sensors),
- Measurement of base pressure distribution on the 1/6 scale model (8 sensors),
- Measurement of stagnation pressure inside model boundary layer by 3 calibrated Preston's tubes,
- Measurement of surface temperature by threshold thermo- tabs,
- Measurement of Volt- Ampere characteristics of electric discharge by calibrated resistive dividers,
- Measurement of electron concentration by electric probes (with MSU),
- Measurement of rotation and vibration temperatures by optic spectroscopy,
- Video and photo of discharge.

Plasma generators of various types for the 1/6 scale model were designed and manufactured in IVT RAN/ MTC:

- **PG PR** for creation of the pulse repeated longitudinal electric discharge,
- **PG AC** for creation continuous longitudinal and transverse AC discharges,
- **PG HF** with Helium injection for creation of HF streamer discharges in supersonic flow (Tesla's coil generator with Helium injection),
- **PG- jet** for creation of erosive plasma jet,
- **PG- Comb** for creation of combined discharge (PG PR+ PG AC).

* Small injection of Helium or Argon were used in all discharges for decrease value of breakdown electric intensity and improve of stable burning and homogeneity of the discharge.

Main characteristics and parameters of PGs.

HF plasma generator (PG HF).

- Primary frequency — 13,6 MHz,
- HF power < 2,5 kW,
- Output voltage < 5kV,
- Operation mode: continuos mode, or modulated power mode (F_m~100 Hz).

Plasma generator of pulse repetitive discharge (PG PR)

- Pulse power, N_i=8-13 kW,
- Mean power, N_m=1-4 kW,
- Pulse duration, T_i=1-10 ms,
- Repetitive pulse frequency, F_r=20-100Hz.

Plasma generator of continuous transverse AC discharge (PG AC).

- AC current, I_{max}< 5 A,
- AC voltage, U_{max}< 9 kV,
- Mean power, N_m< 23 kW,
- Frequency F=50 Hz

PG- jet

- Mean power, N_m< 3 kW,
- Pulse power N_i< 10 kW
- Discharge current I_d=3-50 A
- Operation time, T_i= 2 s,
- Repetition frequency F=100Hz
- Operation mode: continuous, pulse-repetitive.

Main experimental results

1. Stable operation modes of ignition and burning of different types of discharges on the 1/6 scale model were studied in supersonic flow (M~2, P_s=100-200Torr, α=0°, ±2°, ±5°)
2. Parameters of these discharges were measured in dependence of change of initial

pressure, location of discharge on the model, total pressure of Helium injection.

3. It was revealed that small injection of Helium (Argon) extends the range of discharge burning at high initial pressure (up to 1bar).
4. Using of different cones on the needle for generation of vortex separation zones, helps us to create more stable discharge on the model.
5. Drag and lift were measured in plasma/aerodynamic experiment. It was revealed that maximum mean drag decrease was 5-6% at mean power input in plasma ~2kW. It is very large value, if we remember that Drag power of 1/6 model is about N_d~150-200kW. It was shown that maximum drag decrease was at case of PRD. It is need to note that Drag decrease has to be about 30% during power pulse because of ratio of pulse duration / time duration between pulses in PRD was 4-6 in our experiment.
6. Surface pressure distribution was measured on the model with plasma and without it. Maximal mean pressure decrease was ΔP_s~30% in the region near head top of model. It was shown that change of pressure distribution depended on location of plasma formation, type of discharge and power of discharge.
7. High efficiency η of PGs were obtained in plasma/aerodynamic experiment

$$\eta = \Delta F_d \cdot V / N_d \cdot 100\%$$

where F_d — drag force, V-flow velocity, N_d-discharge power.

- η~ 320% in case of PRD ,
- η~ 360% in case of longitudinal AC discharge,
- η~ 200% in case of HF streamer discharge in previous runs with the model 60mm, See below.

8. Base pressure of model head part (pressure inside model) was measured with plasma and without it. It was sown that base pressure practically was not changed during discharge in most of runs.
9. Surface temperature T_s on the model was measured by thermo/ tabs. Temperatures were T_s~200C on head top and T_s=116C on distant end of model.
10. Demonstration of operation of probe and optical spectroscopy in plasma/aerodynamic experiment was fulfilled. Gas temperature and vibration temperature were measured by optical spectroscopy, see below. Electron concentration N_e was measured also. N_e was about 10^{14}cm^3 at condition of PRD burning on the model in supersonic flow.
11. Stagnation pressure P_0 in boundary layer was measured by Preston's tubes. Maximum value of stagnation pressure decrease was about 20% in PRD.
12. It was demonstrated possibility of generation of HF streamer corona with Helium injection before head SW.

Conclusion.

1. Five types of plasma generators (PG) have been developed, deigned and fabricated.
2. All types of PGs have been successfully tested in WT experiments.
3. A stable HF streamer discharge was created in front of head shock wave of the 1/6 scale model
4. Integral aerodynamic characteristics (Drag, Lift and others) and differential ones (surface pressure distributions) were obtained in plasma/ aerodynamic experiments simultaneously.
5. Preliminary information about scale laws in plasma aerodynamic experiment was obtained during this work (for the 1/6 and 1/12 scale models with the same types of PGs).
6. It is clear that significant increase of positive effect of plasma on the control of aerodynamic characteristics could be expected with the accurate optimisation of plasma generators design. For example, for improvement of most promising PG HF it is need to study a possibility of HF streamer control both in space and time.

It is need development of theory, adequately described obtained experimental results, optimal parameters of plasma formations and optimal locations of plasma formations near model.

NUMERICAL SIMULATION OF THE FLOW WITH THE ENERGY SUPPLY REGION AROUND THE MODEL WITH A NEEDLE.

V.A.Bityurin, A.I.Klimov, S.B.Leonov (IVTAN, Moscow),
A.E.Lutsky (Keldysh IAM RAS, Moscow).

Abstract. The numerical simulation of plasma aerodynamics effects under conditions similar to the recent wind tunnel experiments are discussed. The qualitative one simetimes quantitative agreement with experimental are reported.

It was the purpose of the present work to study numerically the supersonic flow around the model with onboard plasma generators and compare the results with the experimental data. The plasma-aerodynamic experiments with the nose of flying laboratory model (model 1/6) were executed in wind tunnel T-113 (TsAGI).

The calculations were executed within the framework of 2D (axisymmetrical) time dependent equations of gas dynamics (without regard of viscosity and heat conduction). The numerical algorithm is based on the generalized Godunov scheme with piesevise linear representation of flow functions . The multiblock grid (29 blocks), containing 555 - cells along the body surface, 95 - between a body and external boundary was used.

Let's consider at first some problems concerning the flow calculation for uniform undisturbed inflow with Mach number M=2. It is well known from experimental and theoretical investigations (see. [1]), that the presence of a needle in front of a body results in essential restructuring of the flow. The large separation zone will be formed near to a surface of a needle, the main shock before a body is shifted upwards, the declination angle of the shock decreases. All this usually results in significant wave drag reduction of a body. The mathematical model, used in the presented work (Euler equations) admits existence of several steady solutions of such type satisfying the boundary conditions [4]. If time-stepping procedure is used, the limiting steady solution (if it exists) can depend, for example, on initial data.

Usually it is necessary to enforce complementary conditions (some experimental data or various empirical relations - see [2]) in order to select the unique steady solution of Euler equations for such flows.

There are some experimental data indicating that the needle influence on the shock position, its shape and wave drag is insignificant for the given flow. Therefore no special efforts for prescribing unique limiting solution and simulation of separation zone were undertaken.

On Fig.1-2 the steady solution obtained with the inflow parameters taken as initial data is shown. The structure of the flow appears to be rather complex. It consists of a shock attached to the nose point (x=-145) of a needle cone, rarefaction wave behind a cone, zone of circulating flow behind bottom of a cone between electrodes (-120<x<-100, 2<r<3.2), shock wave before the model. The value of a wave drag is $C_x(0)^1$=0.4117.

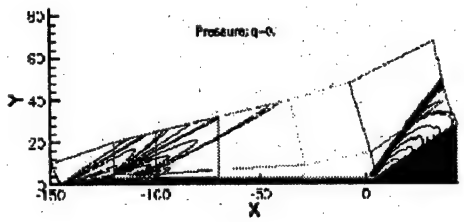

Fig. 1

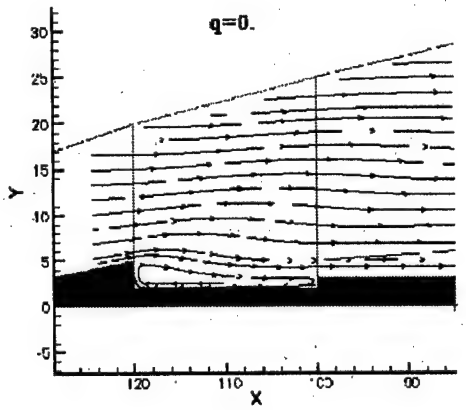

Fig. 2.

Further this solution will be referred as the nonperturbed solution 1. As it will be shown below, for the given problem other steady solutions for flow without energy supply can be obtained also.

It was supposed, that inside the given energy supply area the power value q is constant. The experimental data indicate, that the main part of discharge area is located near to the interelectrode space (-120<x<-100; 3.2<r<5).

Let us discourse the influence of some energy supply parameters on the flow structure and aerodynamic characteristics.

1. The pulsing energy source.

The position of energy supply area was set: -120<x<-100; 5<r<8. Further we shall refer this position as version À. According to the experiment conditions pulse duration Δt_e=4ms, total power q=10kW and repetitive frequency 60Hz were selected. Mean power is q=2.4kW. In the moment t=0 the parameters of a nonperturbed flow 1 were set.

The dependence $\tilde{N}_x(t)$ for 0<t<3T is shown on Fig.3. For a time unit the interval for which the undisturbed flow passes from a forward point of a needle up to a base shear of model is accepted. The pressure distribution near the conical head part of the model is shown on Fig.4. The surface segment approximately up to x=30 is in the region of circulating flow. The zone of the increased pressure near the nose point is due to the turn of a flow directed to the beginning of a needle. On some distance from model the trailing shock is formed which is intersected by streamlines initiated outside of a circulating zone.

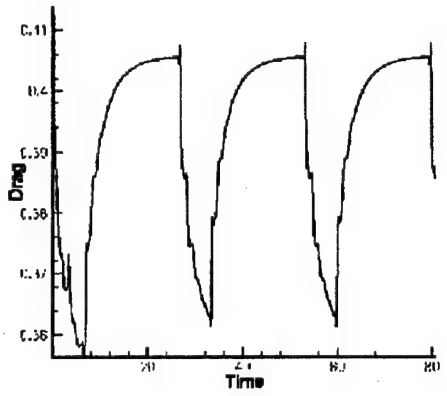

Fig. 3.

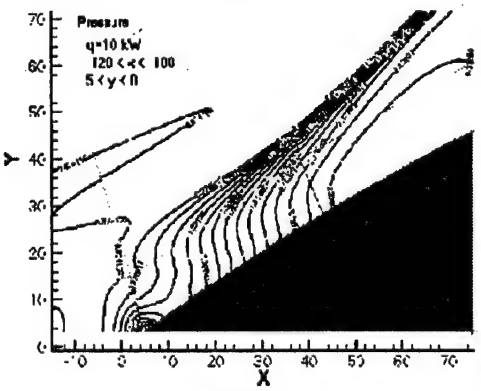

Fig. 4.

To the moment t=T the steady solution, distinct from an initial condition, is practically reached. This solution (further it will be referred as nonperturbed solution 2) corresponds to the undisturbed flow about the model as q=0 during the time interval Δt_e<t<T.

Fig.5-6 demonstrate differences in pressure profiles and axial speed for two nonperturbed solutions. In the new flow pattern the extended circulating zone is retained - see. Fig.8. However the arrangement of streamlines in a neighborhood of electrodes differs from that at the moment t=Δt_e (Fig.7). For the solution 2 the value of a wave drag is $C_x(0)^2$=0.4056. The available experimental data are not sufficient to determine the greater adequacy of any of these two steady solutions, corresponding q=0.

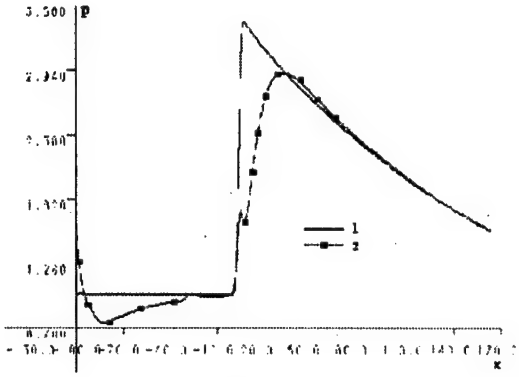

Fig. 5.

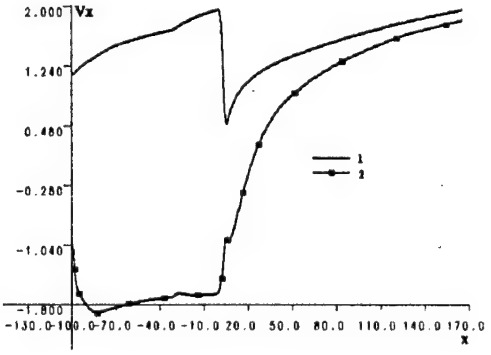

Fig. 6.

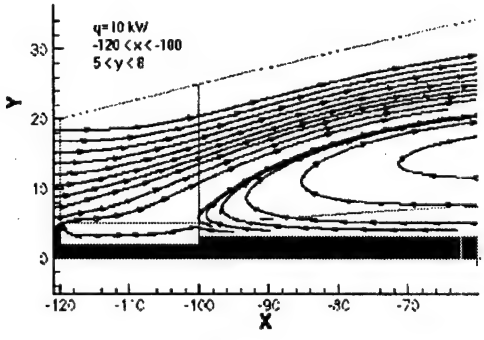

Fig. 7

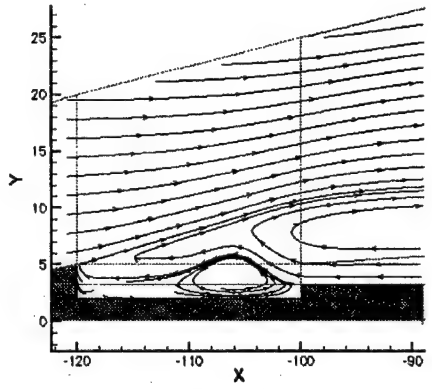

Fig.8

Fig.3 shows, that on the subsequent two periods the flow patterns appear to be practically identical.

The average value of wave drag for the first period ($0<t<T$) is C_x=0.3908, for three periods - C_x=0.3927.

The influence of energy supply on the wave drag we shall characterize by the value $\delta C_x = 100\% \cdot (C_x(0) - C_x(q))/C_x(0)$. Here $C_x(0)$ is a wave drag for uniform flow with a Mach number of M=2, $C_x(q)$ - drag at the presence of energy supply of power q per unit volume. As two nonperturbed solutions were obtained, we shall designate through $\delta^i C_x$ (i=1,2) values corresponding to solution i.

For the average value on the first period we have:

$\hat{C}_x$=0.3908, $\delta^1 C_x$=5.08%, $\delta^2 C_x$=3.18%

During three periods:

$\hat{C}_x$=0.3928, $\delta^1 C_x$=4.62%, $\delta\ C_x$=3.18%

On Fig.9 the relations $C_x(t)$ for following 3 cases are shown:

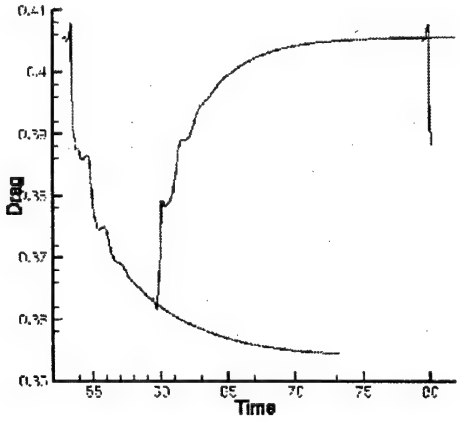

Fig. 9.

a) Steady flow with q=10kW
b) The steady solution 2,
c) The third period of the pulsing solution.

For the case à) the following values are obtained:

C_x=0.3544, $\delta^1 C_x$=13.92%, $\delta^2 C_x$=12.62%

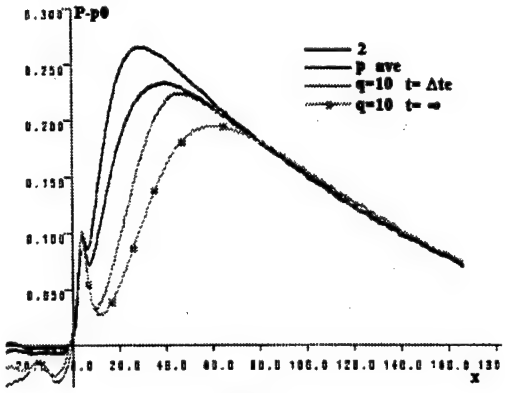

Fig. 10

On Fig.10 the pressure profiles (the values $(p-p_\infty)$, measured by kG/sm^2) on the model surface for steady supply with q=10kW, for pulsing supply at the moment $t=2T+\Delta t_e$, the averaged values and for nonperturbed solution 2 are shown.

2. The steady energy source location.

Two versions of source location are considered:

A) -120<x<-100, 5<r<8;

B) -95<x<-75, 3.2<r<7.

The first version corresponds to energy supply in the interelectrode region. At the expense of a of oscillatory energy relaxation the allocation of heat can also happen in the area located downstream from discharge. Version B) simulates this situation.

For q=1.4kW the nonperturbed solution 1 was set as initial data. On Fig.11 the relations $\tilde{N}_x(t)$ are shown. It is apparent that it takes much more time to reach steady state for version b).

For version B) the surface pressure appears to be noticeably lower, accordingly effect of the wave drag reduction appears stronger:

A) C_x=0.4080, $\delta^1 C_x$=0.90%, $\delta^2 C_x$=–0.59%

B) C_x=0.3954%, $\delta\ C_x$=3.96%, $\delta^2 C_x$=2.51%

The main difference in flow structures for these versions consists of existence for version B) of an extended zone of circulating flow near to a needle from a cone up to a nose of model.

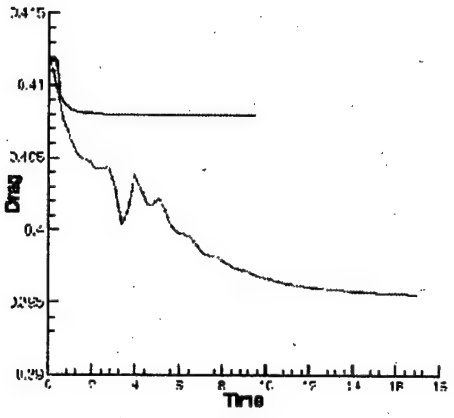

Fig. 11.

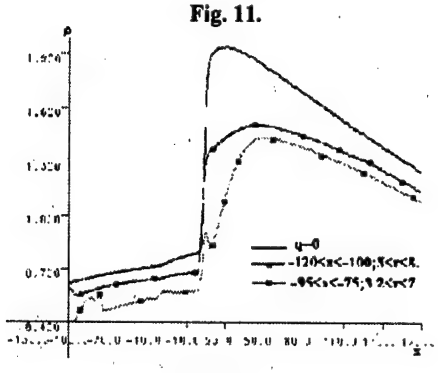

Fig. 12.

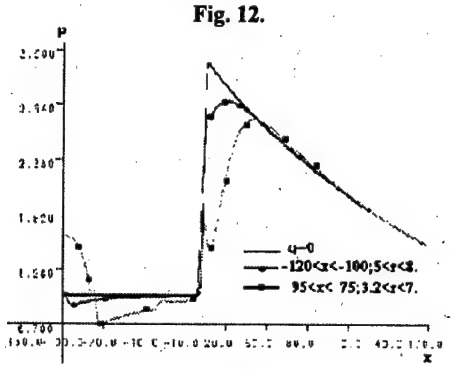

Fig. 13.

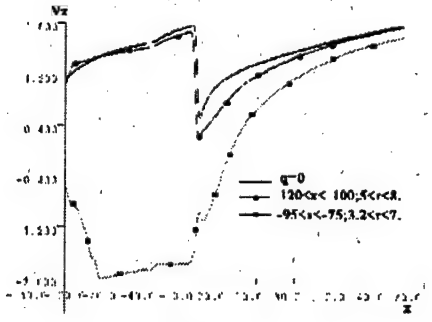

Fig. 14

On Fig.15,16 the streamlines near to electrodes on the needle are shown. For version A) the structure of flow here is similar to undisturbed flow 1. For version B) the beginning of an extended circulating zone can be seen.

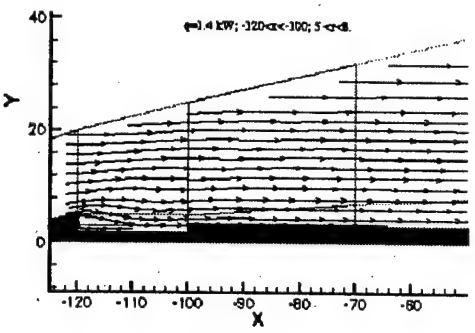

Fig. 15.

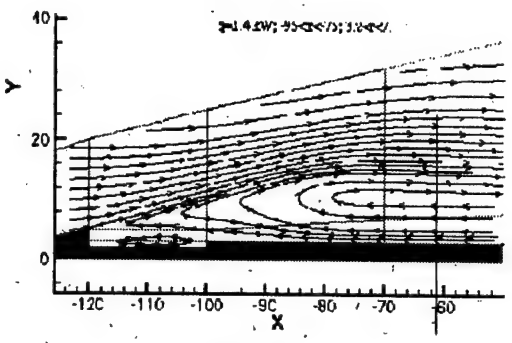

Fig. 16.

For q=2.4 (mean power at pulse energy supply) the variants A),B) of energy supply region were considered also. Besides for each of these versions the influence of initial data (unperturbed flows 1,2) on the limiting steady solution was researched, as well. Accordingly the 4 versions are designated: A1, A2, B1, B2.

On Fig.17 the relations $C_x(t)$ are shown. It can be seen, that in case of version B the limiting solution does not depend on the initial data. On Fig.18 the relations of pressure $P(x)$ on the needle and model surface are represented. For versions B1, B2 these values appear to be almost identical. The details of the solutions (pressure distribution and streamlines about a nose of model) A1, A2, B1=B2 are illustrated by Fig.19-20, 21-22, 23-24 accordingly. The values of drag are those:

A1) C_x=0.4024,

A2) C_x=0.3963,

B1=B2) C_x=0.3897.

As it is mentioned, for example in [5], the wave drag reduction due to energy supply in a flow before a body is stipulated by operation of two factors: by losses of full pressure in a thermal track behind a source and separation zone in front of a body nose. For the considered variants q=1.4kW A) and q=2.4·A1) the first factor acts

only. For variants B and A2 the action of both factors can be seen.

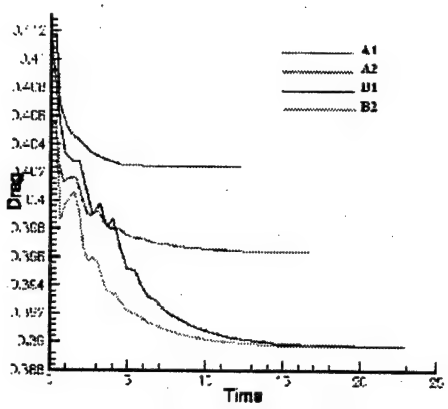

Fig. 17. Q=2.4 kW.

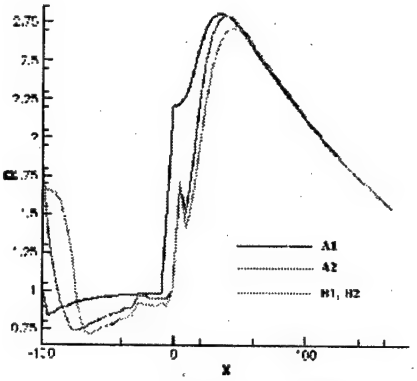

Fig. 18. Q=2.4 kW.

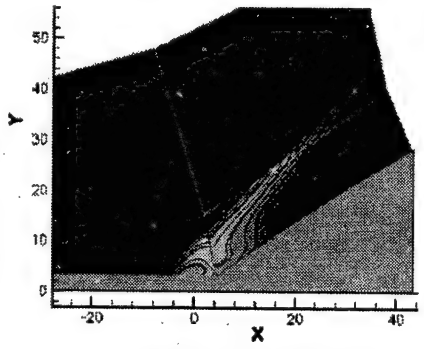

Fig.19. Q=2.4 kW A1.

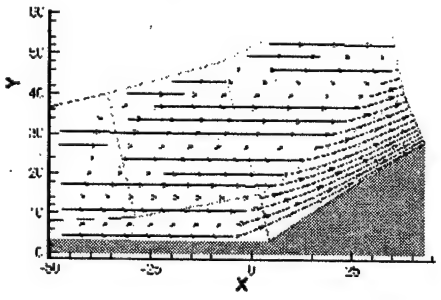

Fig.20. Q=2.4 kW A1.

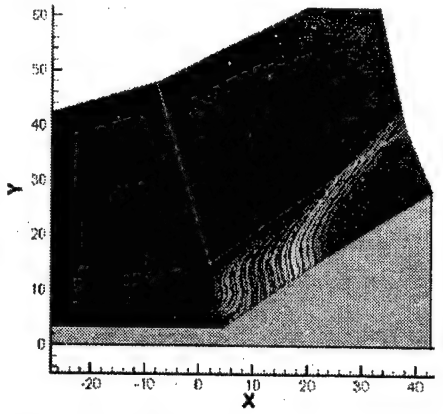

Fig. 21. **Q=2.4 kW A2**

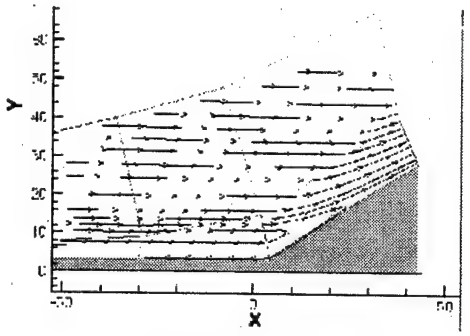

Fig.22. Q=2.4 kW A2

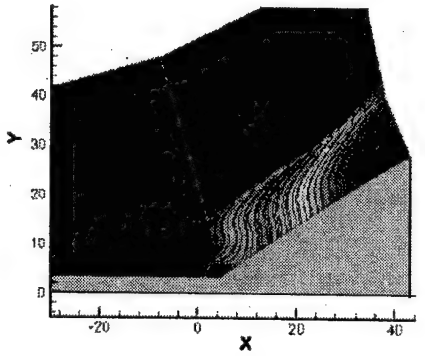

Fig.23. Q=2.4 kW B2

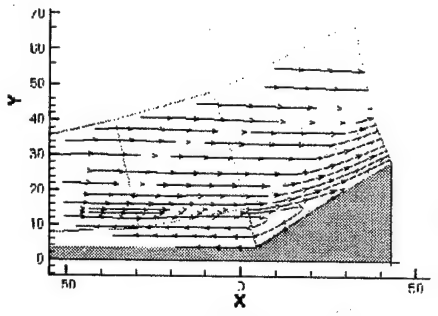

Fig.24. Q=2.4 kW B2.

3. Influence of power of fixed energy release.

The values $\delta^1 Cx, \delta^2 Cx$ for steady solutions, obtained in calculations, are shown in two tables.

Table 1. $\delta^1 C_x$

Q kW	A1	A2	B1	B2
1.4	0.90%		3.96%	
2.4	2.26%	3.74%	5.34%	5.34%
7.	9.59%		8.48%	
10.		13.92%		

Table 2. $\delta^2 C_x$

Q kW	A1	A2	B1	B2
1.4	-0.59%		2.5%	
2.4	0.79%	2.29%	3.9%	3.9%
7.	8.2%		7.1%	
10.		12.62%		

The data for versions q=1.4kW, q=2.4kW indicate to the greater efficiency of version Â) of area of energy release. The data for q=7kW Â) require some validation and refinement, as at calculation the existence of large density gradients can result in considerable errors.

Comparing the data for q=2.4kW with results of a pulse mode it is possible to make a conclusion about preferability of the latter, as the mean value in a pulse mode exceeds the value for mean power q=2.4 at the same energy source location (A1, A2).

The presented results allow to make some conclusions and to indicate the directions of future investigations.

1) The presence of the energy sources in the stream results in essential modification of the flow pattern around the model. The value of a wave drag and character of load distribution varies.

2) At the fixed value of total power the flow regime depends on the source position. In the considered cases version B) is characterized by large effect of a wave drag reduction .The further researches are necessary to check this assumption.

3) The existence of several distinct steady solutions of Euler equations for some problems is well known [4]. The problem on stability of these solutions and their physical sense in a particular case requires further researches concerning the equations of gas dynamics and properties of numerical algorithm.

References.

1. *P.K.Chang.* Control of Flow Separation .// Ì. "Mir" .1979 (in Russien)
2. *A.U.Gridin, B.G.Efimov, A.V.Zabrodin, A.I.Klimov, K.A.Kuzin, Yu.E.Kuznetsov, A.E.Lutsky, A.V.Severin, V.V.Skvortsov, N.N.Sukovatkin, K.V.Hodataev, V.A.Cherkashin.* Numerical and experimental research of supersonic flow over bluntnose body with the needle in presence of electric discharge at its head // KIAM RAS Preprint No.19.Moscow 1995. 31p. (in Russian).
3. *V.L.Bitchkov, L.P.Grachev, I.I.Esakov, A.A.Deryugin, A.V.Zabrodin, A.I.Kliov, I.V.Kochetov, T.Yu.Lutskaja, A.E.Lutsky, A.P.Napartovich, K.V.Hodataev, V.A.Cherkasin.* Numerical and experimental research of supersonic flow over of the blunt body at presence of longitudinal electrical discharge //KIAM RAS Preprint No 27. Moscow 1997. 50p. (in Russian).
4. *G.G.Chernyi.* Gas dynamics. // Moscow. "Science" 1988.(in Russian)
5. *Levin V.A.,, Afonina N.E., Gromov V.G., Georgievsky P.Yu., Terentieva L.V.* Influence of Energy Input by Electric Discharge on Supersonic flows around bodies. IM MSU Preprint N 36-98. Moscow. 1998. 92p (in Russian).

EFFECT OF INTERNAL ENERGY EXCITATION ON SUPERSONIC BLUNT-BODY DRAG.

Graham V. Candler (University of Minnesota), J. Daniel Kelley (The Boeing Company).

Abstract. The effect of upstream vibrational excitation on supersonic blunt-body drag is studied using computational fluid dynamics. The simulations model recent experiments in which a DC or microwave discharge excites the air upstream of a sphere. It is assumed that the discharge slightly dissociates the oxygen and excites the vibrational states of the diatomics. The computations show that the bow shock standoff distance increases, and the drag on the sphere decreases. Both of these effects depend on the degree of vibrational excitation in the flow. The results are in general agreement with the experimental observations. Preliminary calculations on a streamlined body do not show as large a drag reduction effect. Our plans for improvements to the simulation and for additional calculations will be discussed.

Introduction

- DC or microwave discharge is used to excite upstream air:

  1cm radius sphere
  M_∞=1.3, p_∞=60torr, T_∞=150K
  Chuvashev et.al (1998); Beaulieu et.al (1998)

- Drag reduced by 10 to 15%; bow shock standoff increased
- Simulate these drag reduction experiments

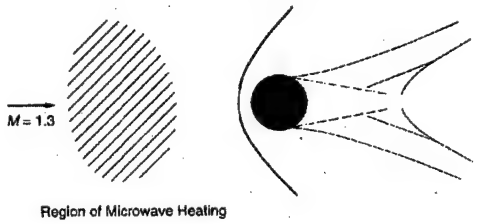

Flow field model

- Assume discharge causes:

Weak oxygen dissociation (0.5% mole fraction)
Vibrational excitation of molecules

- Model with:
  Finite-rate oxygen recombination reaction
  Finite-rate vibrational relaxation
  O-atoms dominate the relaxation process
  Laminar: $Re_D=10^5$

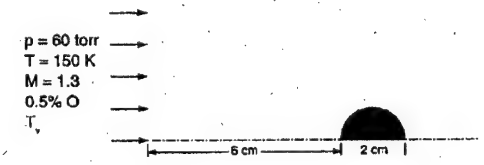

Sonic condition

- The gas relaxes as it flows toward the sphere
  T increases ⇒ a increases
- At some level of excitation flow becomes sonic: $a=u_\infty$
- Assume full relaxation and no change in u_∞

$1198 \le T_{vs} \le 1365$K for M_∞=1.3
depending on if a constant volume or constant pressure process.

Sphere pressure contours, M_∞=1.3

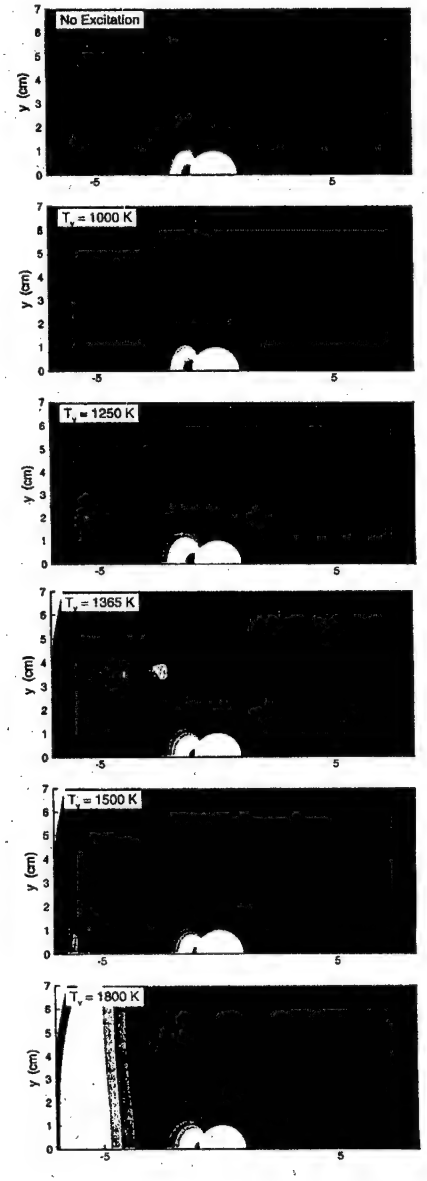

Sphere Mach number contours, M_∞=1.3

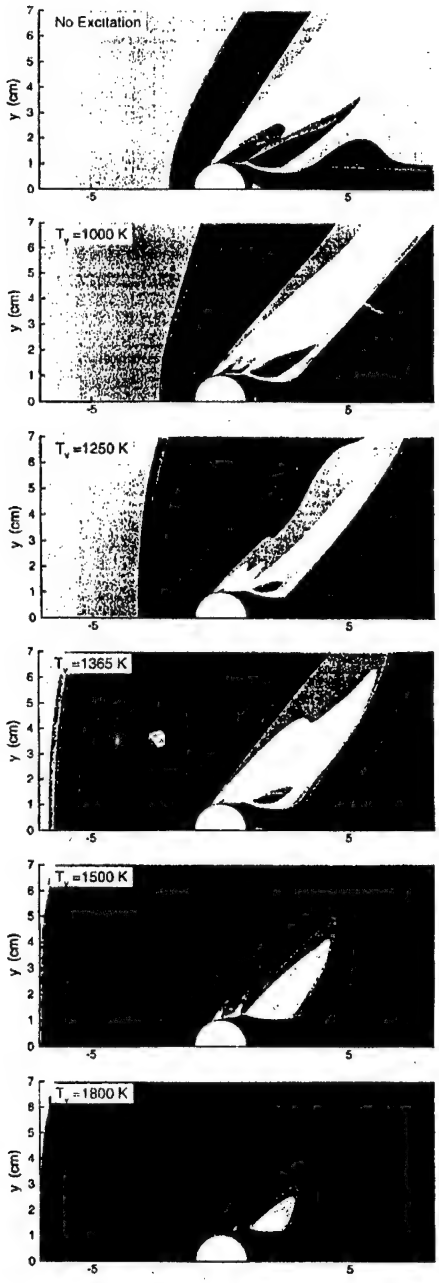

Sphere vibrational temperature contours, M_∞=1.3

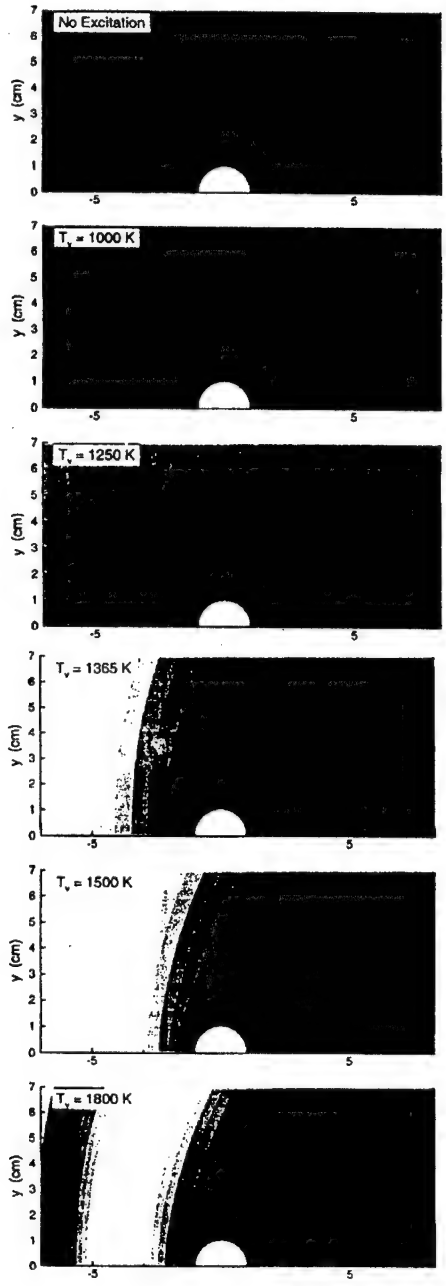

Sphere shock standoff and drag coefficien, M_∞=1.3

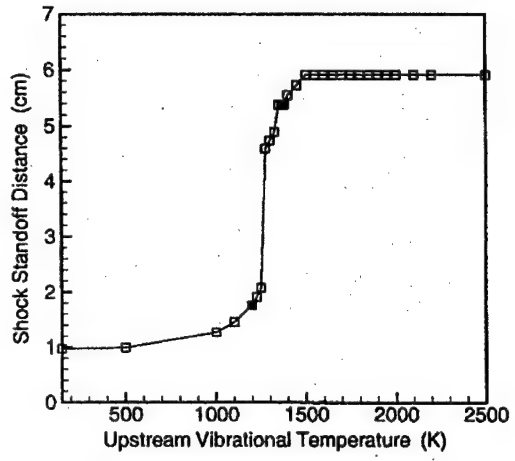

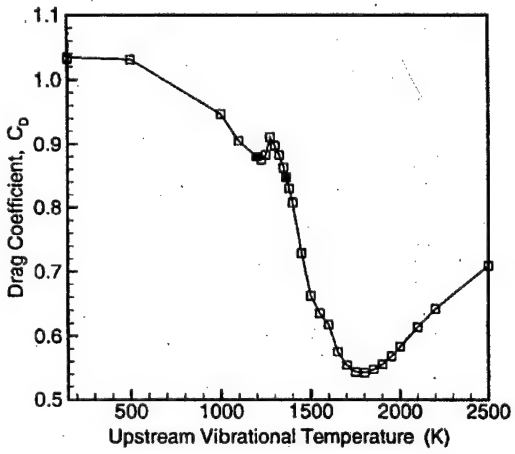

Sphere pressure distribution, M_∞=1.3

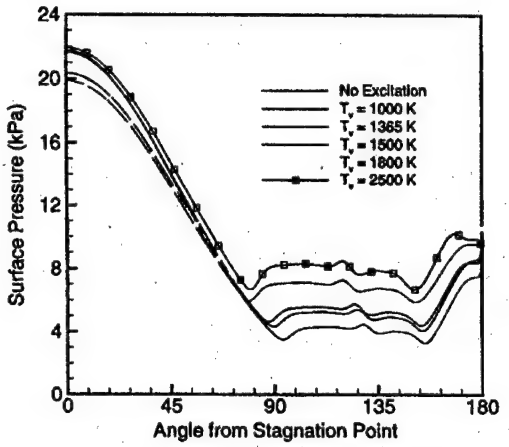

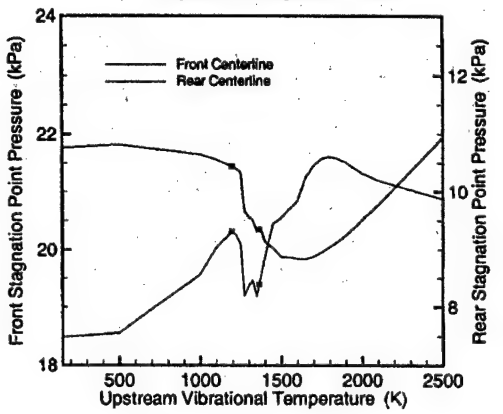

Drag coefficient as a function of Mach number

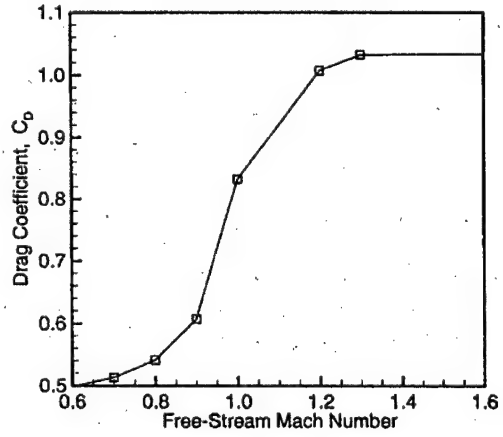

Sphere results, M_∞=2.0

- Increase M_∞ to 2.0; p_∞ and T_∞ unchanged

  Sonic condition: $2361 \le T_{vs} \le 2877$K
- Solution "unstarts" at high excitation
- Reduce region of upstream excitation to $2 \times r_n$

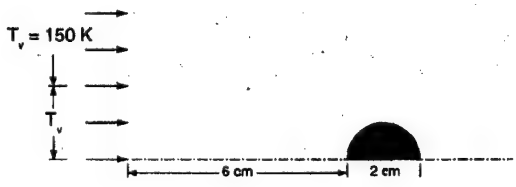

Sphere shock standoff and drag coefficient, $M\infty=2.0$

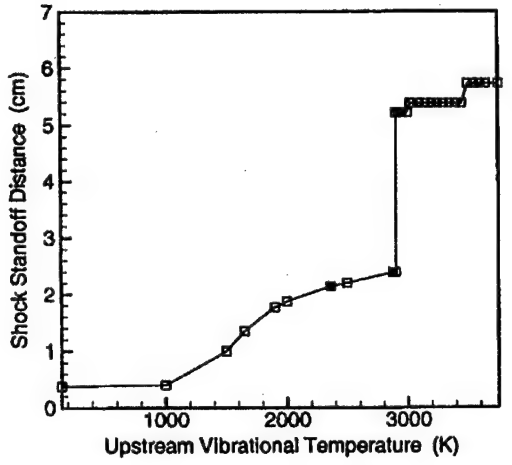

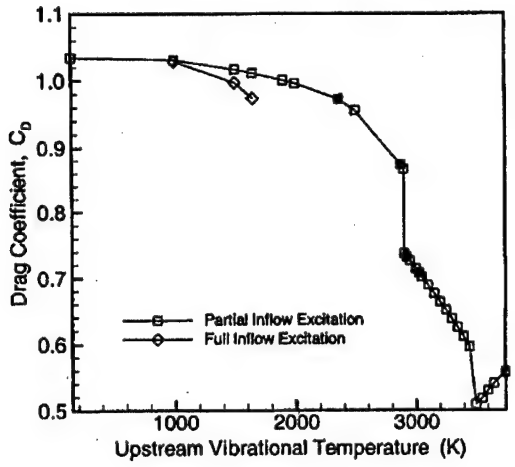

NACA 0012 airfoil results, $M_\infty=1.3$

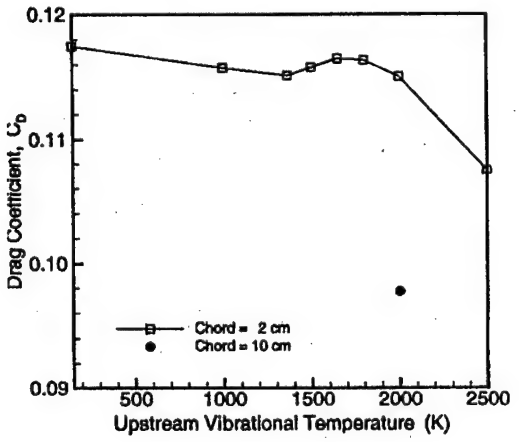

NACA 0012 airfoil, $M_\infty=1.3$

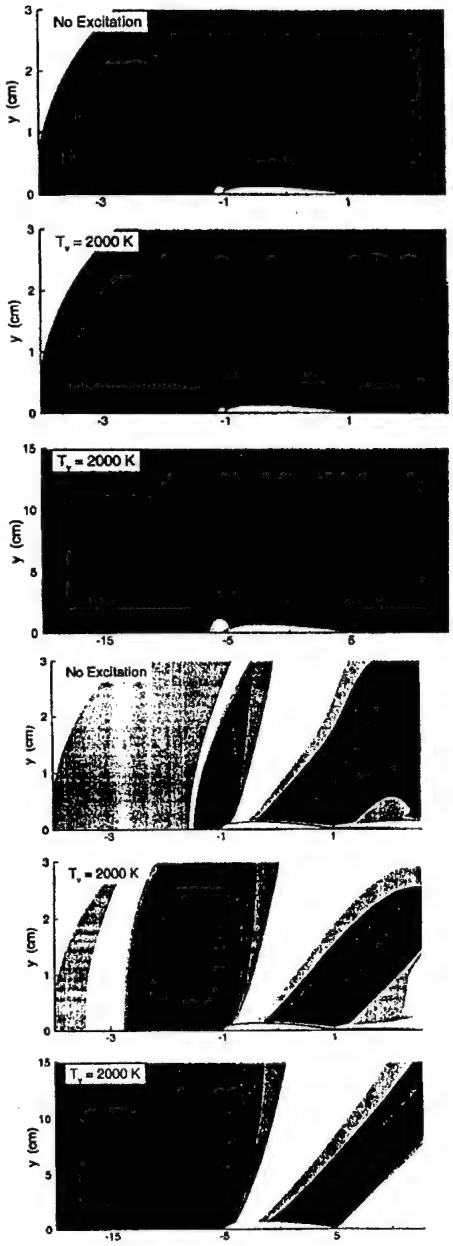

Scaling

- Non-dimensionalize the steady-state vibrational energy equation:

$$\frac{\partial \overline{E}_v \overline{u}}{\partial \overline{x}} = \frac{L}{u_\infty \tau_\infty}\left(\overline{E}_v^* - \overline{E}_v\right)$$

- Define the Damköhler number:

$$\mathrm{Da} = \frac{L}{u_\infty \tau_\infty} = \frac{\tau_f}{\tau_v} = \frac{k_v}{k_f}$$

- Note that $p\tau_v=\exp(AT^{-1/3}+B)$
- Then, for *fixed T*:

$$\mathrm{Da} = \rho L / u_\infty$$

- The effect *depends* on the binary scaling parameter and u_∞

Summary

- Bow shock moves out slowly until flow becomes sonic, then jumps to outer edge of domain
  - Transition is very sudden
  - Transition is bracketed by simple estimate
  - Self-reinforcing: τ_v decreases with p and T
- Once transition occurs, flow is effectively subsonic $\Rightarrow$ reduced C_D
  - Reduced forebody pressure
  - Increased pressure

Extensions to work

- Import energy addition:
  - Model energy deposition process
  - Prevent "bow shock" from leaving computational domain
- Improved vibrational relaxation kinetics:

Separate O_2 and N_2 nibrational temperatures
  - Include correct O_2 and N_2 V-V rates
  - Additional excited states
- Perform systematic study:
  - Binary scaling parameter, temperature
  - Mach number
  - Geometry
  - Region of excition

Temperature (K)

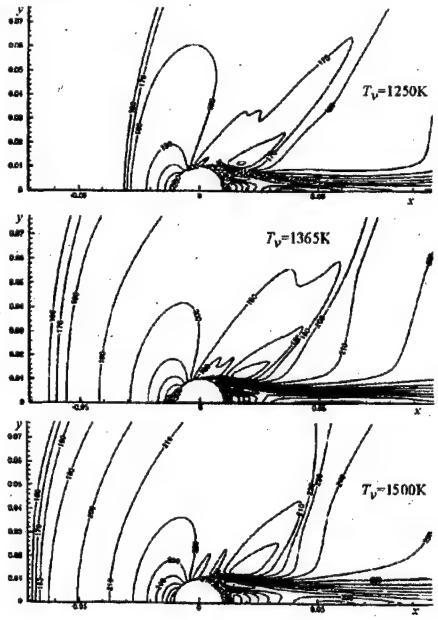

Conclusions

- Computations are consistent with experiments
- Up to 50% drag reduction achieved on spheres
- There is an optimal level of upstream excitation
- Effect appears to be weaker for streamlined geometries
- A more systematic study is needed

Pressure (Pa)

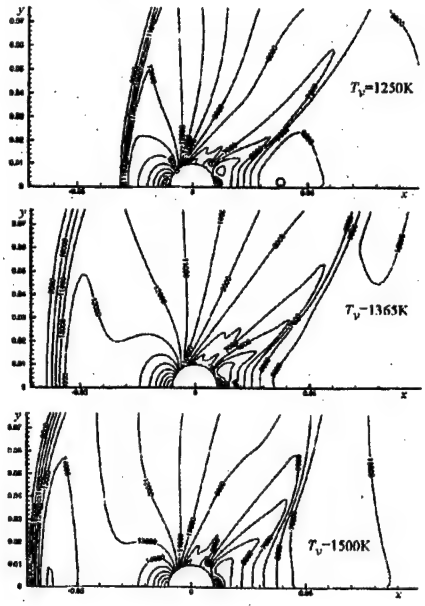

VIB temperature (K)

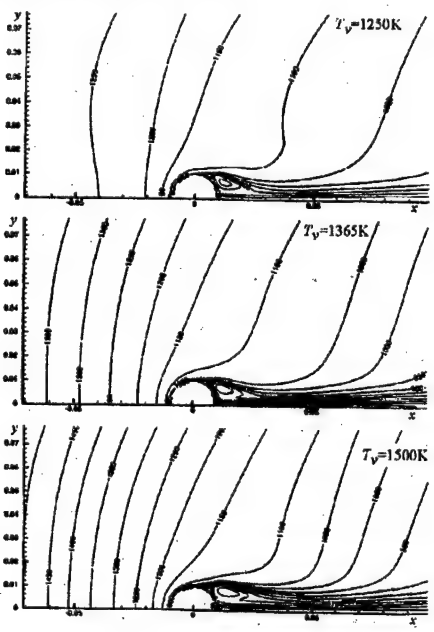

EFFECTIVENESS OF PLASMA JET EFFECT ON BODIES IN AIRFLOW.

S.Leonov (MTC-IVTAN), V.Nebolsin, V.Shilov (GosNIIAS), B.Timofeev (MSU), A.Kozlov (IVTAN)

Abstract. The description of results of model experiments on influence of erosive plasma jets on aerodynamic characteristics of axial-symmetric bodies in a supersonic and a subsonic airflow is presented. To achieve a high efficiency of interaction process, there was design a plasma jet generator with special properties: high enthalpy, high specific impulse, low full impulse and large specific length. A physical model of the jet is discussed. The results of aerodynamic modeling are compared with data of experiments, in which another types of plasma generators are used. The main results are going to be presented on graphs and photos.

Acronyms:

C_x	drag factor,
ΔC_x	change of drag factor,
F_x	axial force (drag),
AV	aero vehicles,
h	specific heat of fuel with kinetic energy,
Q	expence of gas,
V	airflow velosity,
ρ	gas density,
W_{pl}	electric input power of PG,
W_{kin}	kinetic power of airflow,
ADC-	aero-dynamic characteristics;
PG	plasma generator,
PJ	plasma jet;
BSW-	bow shock wave;
Ne-	electron concentration;
Te-	electron temperature;
Tg-	gas temperature;
M-	Mach number;
VAC-	volt- ampere characteristics;
Id-	discharge current;
Ud-	discharge voltage;
PD-	pulse discharge;
HF-	high frequency discharge.

Introduction.

The studied problem is a part of objective to increase of efficiency of vehicles and to safe or disturb stability and controllability at atmospheric flight, which could be provoked by change of AD characteristics. Latest, in this case, is due to influence of plasma formation of different types on aircraft's elements. Plasma generation could make by means of either external devices or on-board ones. In this work, on-board plasma jet generator has been used as an agent of modeling.

Methods to advance of ADC of AV and its parts are based on application of mechanical elements, which use an energy of streamlining airflow for re-distribution of pressure on surfaces and also to use of air jets power in local areas near the surfaces. So, it seems to be perspective to use methods of change of thermodynamic properties of medium and structure of boundary layer for a drag decrease (wave drag and skin friction). Such possibilities could be realized by means of plasma influence on approach airflow and, particularly, blowing out of high enthalpy plasma jets

The results presented here are a part of extensive work on plasma formation influence on ADC of models at WT conditions. An plasma jet of electro-discharge erosive source with hydro-carbon working medium have been used. Using of namely this plasma generator seems reasonable due to high specific power of PJ, controllability of spatial distribution, low mass density of plasma, high specific impulse, proper PG design. A historical continuity of the experiments was an important reason for a choice of PG.

A lot of papers were devoted to interaction of gas jets (including heated jets) with external flow [1,2]. Its application to effect on streamlining of bodies are discussed many times [3]. There were several works on interaction of plasma jets with bodies in airflow during last few years [4-12]. These works have shown, that:

- PJ allows obtaining significant decrease of drag of models both in a supersonic and a subsonic airflow.
- PJ is a quite convenient means for modeling of plasma and thermal influence on system body-airflow.
- The structure of PJ and interaction process with airflow and a body could be simulated numerically, at least, in first (gas-dynamic) approach.
- PJ are differed from gas jets by range of parameters, which can be achieved, and by rate of change of these parameters. A presence of ionized component allows us to apply electromagnetic methods of external control.
- Features of interaction process need to be studied carefully.

Last conclusion reflects a high probability of real application of PJ for the problem of flight control of AV in atmosphere.

Obviously, that perspective of a new technology's real applications directly depends on effectiveness in comparison with conventional ones. Such competitive methods in this case are geometric factor of AV and increase of power and

efficiency of AV engines, which use a chemical energy of fuel.

We can describe two criteria of effectiveness of plasma influence on body's drag in airflow: physical and technical. A physical one suggests, that change of integral drag factor should be related to specific input power of PG (electrical, as a rule):

$$\eta_1 = \frac{\Delta C_x / C_x}{W_{pl}/W_{kin}} = \frac{\Delta C_x}{C_x} \cdot \frac{C_x \rho V^3}{2 W_{pl}} = \frac{\Delta F_x V}{W_{pl}},$$

where change of axial force can be obtained from direct balance measurements at compensation of base effects.

A technical criterion is more complex. It includes fuel's and electrical efficiency of engine in accordance with diagram.

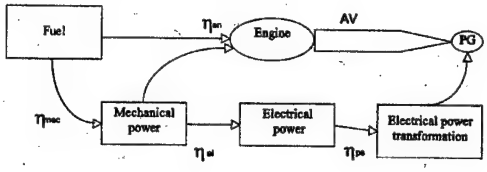

Here η_{en} is a total efficiency of energy transformation from fuel to an engine mechanical power, excluding secondary internal energy expenses:

$$\eta_{en} = \frac{FV}{hQ_{fuel}}$$

η_{mech}—efficiency of energy transformation to a mechanical power, η_{el}—efficiency of electric generator, η_{ps}—efficiency of power supply of PG. So, technical criterion looks as the following:

$$\eta_2 = \eta_1 \frac{\eta_{mech}\eta_{el}\eta_{ps}}{\eta_{en}}$$

At $\eta_2 > 1$ a technology promises a decrease of fuel expense by AV's engine. If we don't take into account exotic schemes of energy transformation, than the criteria are closed each other. A problem of applicability of plasma technology comes to achievement of reasonable physical effectiveness of PG, on a careful estimations, $\eta_1 > 2$.

Probably, three main ways to enhance of effectiveness of PGs could be described.

- Providing of optimal geometry (spatial) distribution of energy input near the AV.
- Decrease of BSW amplitude by means of plasma generation with optimal parameters in an area of interaction at supersonic streamlining.
- Use of time-alternative (variable) operation modes of PG, in particularly, pulse-repetition mode.

The last method assumes some non-linear mechanisms of effect, in respect of amplitude of interaction. Lets describe two ideas about result of pulse-repetitive operation, which have contrary conclusions.

Many times we can hear, that non-equilibrium plasma should be more effective to change parameters of airflow [5,6]. Actually, it is well known, that pulse operation mode of discharge allows to obtain non-equilibrium parameters of plasma (in respect of temperature distribution on degreases of freedom and ionization). Repetition rate can be in accordance of gas-kinetic (L/V) time or less in case of stagnation (circular) area presence, at influence on boundary layer and base area. An appropriate confirmation could be found in some works [13].

From the other side, an increase of pulse power, finally, might lead to saturation of effect during a pulse. So, a plasma influence will be less in average at the same mean power of pulse periodic and continuous operation mode of PG.

We can see, that problem of plasma influence effectiveness in pulse repetitive and continuous regimes is one of key problems of phenomenological description.

So, a field of optimization has a lot of direction. It forces us to solve specific problems. This work had following particular tasks:

- Comparison of pulse repetitive and continuous operation modes in frames of influence of plasma jet on drag of model in a supersonic airflow.
- Obtain of reliable data on drag decrease at different Mach numbers.
- Increase of statistical reliability of results of previous experiments.

Plasma Jet Generator's features.

A high enthalpy erosive plasma jet has features, which are important for application it as a factor of drag reduction: large specific length of initial laminar part of jet and high level of specific pressure counteraction [7,16,17].

Using a hydro-carbon working medium gives possibility to obtain less value of mass density in comparison with air at same temperature (due to large share of H2 in a thermo-destructive mixture) [14,15]. Besides, hydro-carbonic plasma has got high level of chemical activity: there is a lot of energy release at mixing with air.

PG was produced as changeable insertion to the model. An insertion from working substance could be substitute independently. Principal layout of PG is presented in Fig.1.

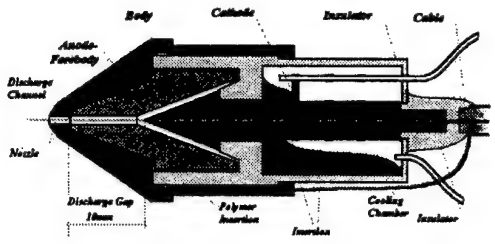

Fig.1.

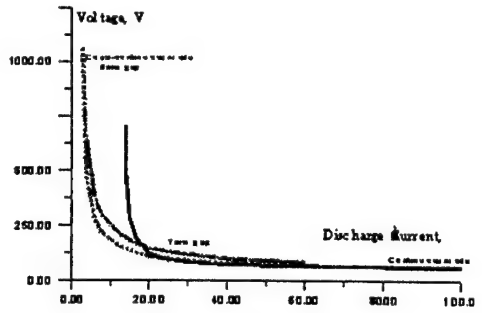

Fig.2.

Usually, electrodes are made from graphite, copper or special alloys. Working substance is polymethilmetakril (PMMA) or same on content and structure polymer. Position and orientation of anode allows discharge current to blow (output) out from an area of discharge channel. Duration of discharge pulse is much more than specific time of heat processes on a wall of discharge channel. Value of discharge current is chosen at taking into account of many factors, including absence of strong instabilities in discharge channel.

Parameters of PG were in the range of: diameter of nozzle d=1-2mm, length of discharge channel (gap) L=5-12mm; discharge current J=3-60A; mean input power W=0.3-3kW; operation modes continuous and pulse repetitive; repetition rate 0-1000Hz; pulse power up to W_p=3kW; operation time T=0.5-3sec.

Main physical parameters of PJ can be characterized by the following values: electron temperature at the axis up to 16кK; temperature in a plasma envelopeup to 2кK; electron density near the axis up to $3\times10^{17}cm^{-3}$; specific plasma enthalpy near the axis up to 10^8J/kg; plasma velocity near the axis 1-3km/s; penetration velocity into the atmosphere up to 300m/s; mass expense of working medium 0.02-0.1g/s.

In Fig.2 samples of V-A characteristics of discharge in PG at atmospheric pressure are presented.

Obviously, that heat loses on the electrodes relatively less at high voltage on discharge gap. In this work there was found and used namely high voltage operation mode of PG (in Fig.2 it is pointed as quasi-continuous). Power supply with alternative current at 80kHz of frequency and 3-6A of amplitude of discharge current was used in this specific case. The PJ was stable and with quite spatial structure. Actually, at current less than 15A the DC discharge didn't exist at atmospheric pressure.

A system of electronic control of power supply allows getting practically any variant of PG modulation. In the experiment there were three main variant of modulation: quasi-continuous operation mode, modulation at 100Hz (t/T=1/2 and depth 100%) and modulation 1kHz (t/T=1/2 and depth 100%).

Experimental set-up. Model.

The experiments were made in GosNIIAS on set-up MAS (wind tunnel plus control and measuring equipment). The layout of experiment is shown in Fig.3.

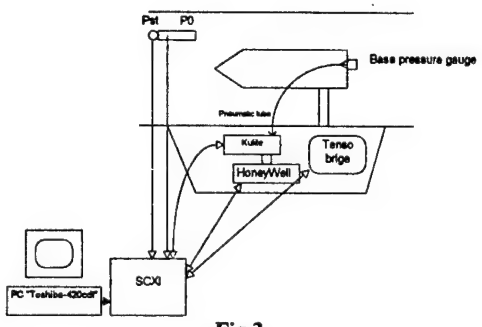

Fig.3.

The experimental set up MAS is a wind tunnel of close type and continuous operation mode with a flexible nozzle. An aerodynamic part of WT is used to produce airflow with needed parameters (Mach number and temperature) and providing of balance's and pressure distribution measurements. Control and measuring part is used to calculate loads and parameters of airflow from transducers' data and to control of gears.

Controlled flexible nozzle provides needed change of airflow velocity in a test section of WT. Cross-section of it is 400x400mm, Mach number of airflow can be tuned in a range 0,2-0,8<M<1,4-3,0 at non-homogeneity α<0,05. Reinold's number was in range Re=(0,1-1,0)$\times10^6$. Kern of airflow in test section has a dimensions

not less 300×300mm; aerodynamic force up to 10^4Pa; time of continuous work up to 10min.

A tenso-balance was used for the measurements of aerodynamic loads (forces). Metrology gives the following tolerance of it on the forces and moments: Y - 0,75%; X - 0,45% ; Mz - 0,65%. Some experiments include measurements of stagnation temperature of airflow.

Photographs and shadow-graphs (Schlieren) of plasma-airflow-body interaction have been used in the work. Some photos of model at and without plasma generation are presented below. To define both of plasma jet influence on balances without airflow and electric noises on measuring system special tests were produced. They demonstrate that the influence is small (less then tolerance of measurements) or/and can be take into account. Such kind of test was made at artificial external load and at working pressure.

The layout of model installation and some communications are shown in Fig.3. Aerodynamic model is fixed in test section of WT on vertical holder, which contains three-component tenso-balance. It was calibrate by means of standard loads. A supplying cable goes through console tube. A current and voltage on electrodes of PG are measured. A data from tenso-balances were transformed and filtered. It was done on recording devices through germetic connectors. Verifying of plasma presence was made by means of photo-diode and by sight. Plasma switching on was each 10sec on 0.5-2sec of duration. It was 3-4 times per a run.

Aerodynamic model was a combination of cylinder (60mm of diameter) and the cone with 30° of half angle. Base area was plain. Preliminary runs had shown that drag factor of such model was about 0.9 at Mach number 2.0. A comparison with reference shows that drag factor should be a little bit less (on about 10%). Probably, this difference could be explained by low level of Reynolds's number and interference of lateral holder. In general it might be defined as satisfactory.

Data Processing.

Measurement were carried out using a Data Acquisition system based on "National Instruments™" ADC DAQ-Card AI-16E-4 & 5 channels SCXI - block of pre-processing of a signal.

A tenso-metric bridge was connected directly to entrance of the SCXI-module 1121 (optoisolated 4-th channel amplifiers) to form an axial drag (weight) channel of balances. A power supply and the tuning of the bridge was provided with the circuits of support of this module.

The gauge of base pressure "Kulite™" was connected to as a previous one. (Power supply and the zero adjustment was provided with the SCXI-module 1121).

In the under-floor of a wind tunnel the gauge of absolute pressure "HoneyWell™" was established, reference of base pressure was deduced in a point of measurements of this gauge, and thus, the checking of reference of the base pressure gauge was made.

Flow control gauges P_0' and P_{st} of the IKD-24-0.25 type were used for calculations of the aerodynamic characteristics of a flow (Mach number, high-speed pressure). Their reference pressure was observed by means of liquid manometer and, at processing of the acquired data, was calculated on calibration curves according to the indications of the gauge of absolute pressure "HoneyWell™".

During processing the acquired information, all measured meanings were transformed to absolute physical values (stagnation pressure P_0 was iterated, in view of the amendments to P_0' due to losses in supersonic jump on a receiving pipe), the meanings of the characteristics of a flow and aerodynamic factor Cd were calculated. The estimation of Cd changes was carried out on the formalized statistical technique with use of pre-defined threshold probability (80% as a rule).

Main expressions for the calculations are presented below:

Measurements of input power to the discharge were made from data on current (by Rogovsky coil) and applied voltage (by compensated divider). Procedure of calculations was automated.

$$C_d=\frac{F_d}{qS}-C_b\ ,\quad q=\frac{\gamma}{2}\mathrm{M}^2 P_{st}\ ,\quad V=\mathrm{M}\sqrt{\gamma R T_{st}}\ ,$$

$$T_{st}=T_0\left(\frac{1}{1+\frac{\gamma-1}{2}\mathrm{M}^2}\right),$$

$$\mathrm{M}=\sqrt{\frac{2}{\gamma-1}\left[\left(\frac{P_0}{P_{st}}\right)^{\frac{\gamma-1}{\gamma}}-1\right]}$$

$$\frac{P_0'}{P_0}=\left[\frac{(\gamma+1)\mathrm{M}^2}{2+(\gamma-1)\mathrm{M}^2}\right]^{\frac{\gamma}{\gamma-1}}\cdot\left[\frac{(\gamma+1)}{2\gamma\mathrm{M}^2-(\gamma-1)}\right]^{\frac{\gamma}{\gamma-1}}$$

Results.

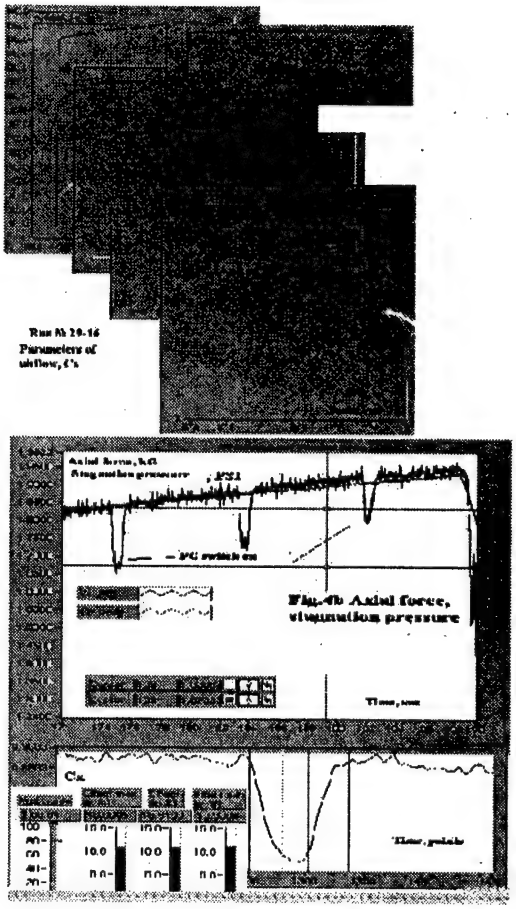

Fig.4.

A sample of measured parameters of airflow, forces and primary calculations for one of run at M=1.6 is presented in Fig.4(a-c). It is seen, that pressure in airflow is changes during a time of experiment. It happens due to blow in WT pumped contour and some increase of temperature of air in run. Resulting values of Cx are well compensated by taking into account all data at procedure.

A photograph and Schlieren photo of interaction process are presented in Fig.5. In the Schlieren photos a change of stand off of BSW is seen as well as generation of week turbulent heat layer around the model. Week parasitic shocks in a field of observation were due to mechanical junctures on a wall of WT.

In Fig.6 the results of measurements of drag reduction are presented in dependence on relative mean input power at Mach number M=1.5-2.4.

Fig.5.

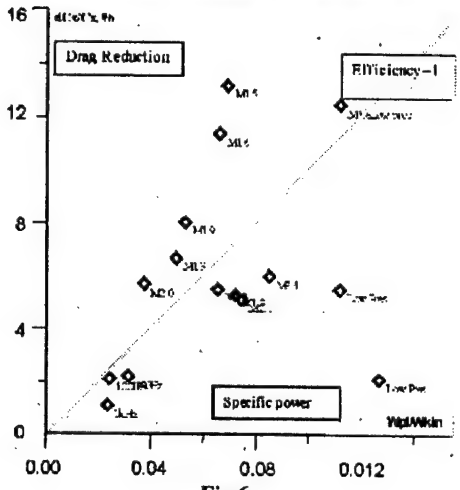

Fig.6.

In Fig.7 appropriate data on physical efficiency η_1 of PJ influence on drag on model are presented.

Well seen that the results could be divided on three groups: with high value of drag reduction and high efficiency of interaction, modulation mode and mode with low value of static pressure. At last case a stand-off of BSW due to PJ influence is relatively less.

In Fig.8 the dependence of efficiency of plasma influence on Mach number is presented. This chart looks like as another one for drag reduction, which was presented in papers [8-9]. But the value of efficiency in this work is much more and, important, more than 1.

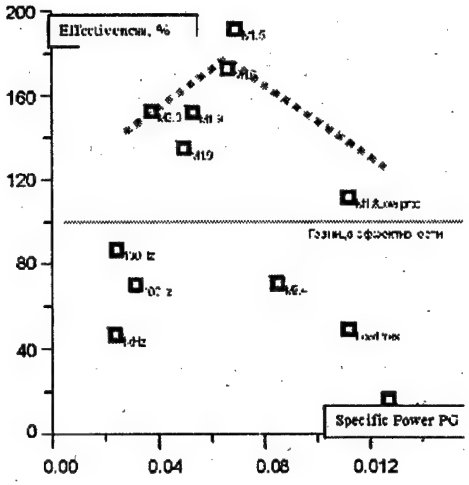

Fig.7.

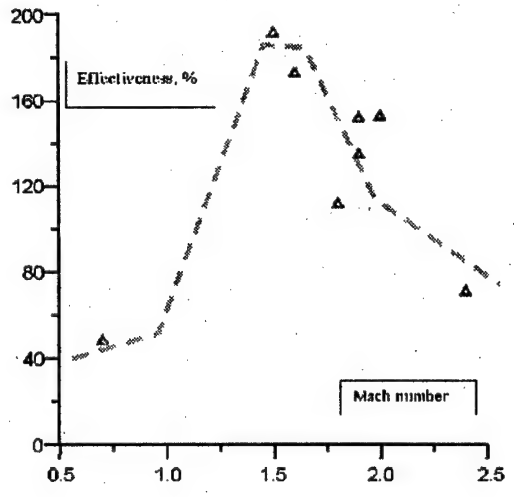

Fig.8.

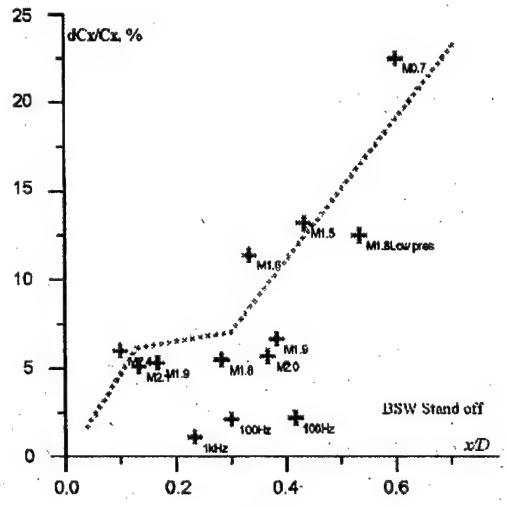

Fig.9.

In Fig.9 a correlation of plasma effect with stand-off of BSW is presented. Value of stand-off is related to diameter of a model. Obviously, that the function is an increasing curve. Such dependence points on significant share quota of wave reduction in effect (effective form-factor). At low stand-off drag reduction has a limited value, about dC_x/C_x=5%. This part could be confronted with change of parameters of boundary layer conditionally. It could be marked that this part is decrease significantly in modulated mode.

From the other side an input p[illegible]er was insufficient for saturation of effect.

It is important, that at increase of Mach number a static pressure in test section of WT decrease, as a rule. At M=2.4 static pressure in airflow is P_{st}<10Topp and PG is working in different mode (see below).

Discussion.

An interaction of plasma formation (PJ) with airflow happens by the following method: plasma jet is blew out from a cylindrical nozzle (which take place in critical point of fore-body). At interaction of PJ with approach airflow the BSW is stood off and change its shape. A loose of PJ's impulse results in turn of PJ, mixing with air, decrease of enthalpy and additional energy input near the model's surface by means of chemical reactions of plasma jet products with oxygen of air. Heated layer near the surface is created. Both: change of BSW structure and change of boundary layer parameters, lead to drag reduction in a supersonic airflow.

The influence of PJ on drag of model at subsonic streamlining was more, than at supersonic one, at the same input power (about 20% of drag reduction). In this case a specific input power was more. So, the resulting efficiency (about 0.5) was less than in case of supersonic airflow.

The results show that the efficiency of plasma influence is less in modulated operation mode of PJ than in continuous mode about 2-3 times. When the PG works the stand-off of BSW are the same practically for modulated 100Hz and continuous modes. At modulation 1kHz the stand off is decreased and so does effect. Seems that unsteady interaction (definite time of wave structure formation) can work at large time's periods.

At decrease of static pressure a spasmodic change of interaction regime was found. PJ's luminescence is decreased, stand-off of BSW is decreased and effect is decreased. This could be

connected with change of plasma chemical processes, including block of burning reactions.

In Figs.10 and 11 the results from different experimental investigations, which were made by teams at author's participation last years, are presented. A different types of discharges and models (with C_x from 0.09 up to 0.9) are presented here. Also methodical differences are been. Nevertheless, totality of results gives us possibility to make some conclusions.

The increase of efficiency of plasma influence more than 1 is the key moment of this work. Well known that calculations show such exceeding in many times [18]. But at experimental conditions and for "non-blunted" bodies it is not so simple problem. One method, for example is generation of re-circulating areas near the model. Figs.10-11 include such data, which labeled as "pulse discharge on a needle [19].

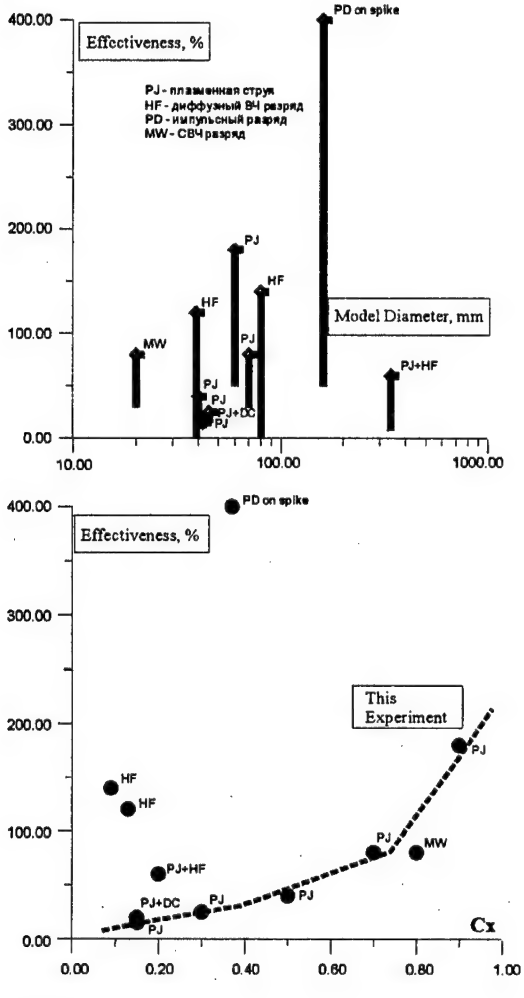

Figs.10,11

Note, that points in Fig.11, which lie above of approximating line, were obtained at high static pressure P_{st}=200-300Torr and Mach number M=1.8-2.0.

A comparison of data on HF discharge (HF points) with another results allows suggesting, that a main mechanism of drag reduction at HF discharge could differ specifically from PJ's one.

Conclusion.

Let formulate main results of presented work:

- Efficiency of drag reduction of cylinder-cone model at plasma jet influence on supersonic airflow higher for continuous operation mode than for pulse-repetitive operation mode at modulation frequency 0.1-1kHz.
- High-voltage mode of AC regime of plasma jet generator increases an energetic efficiency of plasma influence on drag of model.
- The efficiency of plasma influence on drag of model with C_x=0.9 more than η_1=1 was achieved.
- Statistically reliable results on drag reduction in dependence on Mach number of airflow were obtained.
- Two mechanisms of drag reduction in supersonic airflow were shown. Attempt of its separation was tried.
- The first summarizing of experimental results on plasma jets influence on airflow-body system was made. Dependence of plasma effect on parameters of streamlined body (C_x) is demonstrated.

Possible, that conclusion of the work would be changed if parameters of problem were in larger range.

Acknowledgements.

Specialists of GosNIIAS and IVTRAS (Drs. Bityurin and Klimov) help us to make this work and analyze the results.

References

1. *Abramovich V.G.* Applied Gas Dynamics. (rus.) – Moscow, Nauka, 1989.
2. *Kondrashov V.V.* "The study of interaction of supersonic plasma jets with approach flow.",- Minsk, Inst. heat- massexchange about Lykov, Prep. No.7, 1986.

3. *Love E.S.* The effect of the small jet of air exhausting from the nose of a body or revolution in supersonic flow.-NASA RM, 1952, NL52.
4. *Leonov S.B., Pankova M.B., Shipilin A.V.* "Modeling of ball lightning interaction with bodies in atmosphere" "Ball Lightning in Laboratory." ed. Avramenko R.F., Klimov A.I. and oth. Moscow: Chemistry, 1994.
5. Workshop on Weakly Ionized Gases, USAF Academy, Colorado, 9-12 June 1997. Proceedings.
6. 2nd Workshop on Weakly Ionized Gases, AIAA, Norfolk, 24-25 April 1998. Proceedings. P.193.
7. *Leonov S.B.* Plasma Jet Generation for influence on drag of bodies in a supersonic airflow.- Contributed Papers of HAKONE VI, Cork, Ireland, 1998, p.318-323.
8. *Gordeev V.P., Krasilnikov A.V., Lagutin V.I.* Experimental study of possibility of drag reduction by means of plasma, MLG (rus.), N2, p.177-182, 1996.
9. *Ganiev, Yu.Ch., Gordeev, V.P., Krasilnikov A.V. et al,* 2-nd Weakly Ionized Gases Workshop, Norfolk, VA, April 24-25, 1998.
10. *Hornung, H.,* in Plasma Aerodynamics Research at Rockwell Science Center, 2-nd Weakly Ionized Gases Workshop, Norfolk, VA, April 24-25, 1998.
11. *Burdakov V.P., Baranovsky S.I., Klimov A.I., Lebedev P.D., Leonov S.B., Pankova M.B., Puhov A.P.* Improvement perspectives of aerodynamic and thrust-energetic parameters of hypersonic aircrafts and engines when using algorithmic discharges and plasmoid formations., Proceeding of the International Conference of Advance Technology, Moscow, 1995
12. *Fomin V.P., Maslov A.A., Fomichev V.P.* Review of IPTM works on plasma aerodynamics. Proceedings of Meeting "Perspectives...", March, 24-25, IVTRAS, Moscow, 1999.
13. *Lutsky A.E.* Numerical modeling of model with needle streamlining at presence of energy release. Proceedings of Meeting "Perspectives...", March, 24-25, IVTRAS, Moscow, 1999.
14. *Vargaftik N.B.* Handbook on heat properties of gases and liquids. (rus.) - Moscow, Physmathgis, 1983.
15. *Boyko Y.V., Grishin Y.M. and oth.* Thermo-dynamic and optical properties of metals and dielectrics (rus.) – Moscow, Metallurgy, 1988.
16. *Leonov S.B., Lukyanov G.A.* "About structure of pulse erosive plasma jet",- "J.of Appl. Mech. and Tech. Phys.(rus.)", 5,1994, 13-18p.
17. Leonov S.B., Pankova M.B. "Structure and thermophysical properties of hydrocarbon plasma jet",- Proceedings Conf. of low temp. plasma, Petrosavodsk,20-26 June 1995, p.102-104.
18. *Levin V.A., Afonina,N.E., Georgievsky P.Y., Gromov V.G., Larin O.B., Terenteva L.V.* "Study of possibility of control of supersonic airflow...", Preprint IM MSU, N24-97, Moscow, 1997.
19. *W. Beauliew, V. Bityurin, A. Klimov, S. Leonov, A. Pashina, B. Timofeev,* Study of characteristics of 1/6 scale model...- Proceedings of Meeting "Perspectives...", March, 24-25, IVTRAS, Moscow, 1999.

CAN THE HYPERSONIC AIRCRAFT BE REAL.

Yu.V.Polezhaev . (Institute for High Temperatures RAS, Moscow, Russia)

Abstract. The report is devoted to the analytically survey of the heat transfer problems while the flight of the body with the hypersonic speed in the Earth's' atmosphere. It is shown that in spite of the experience of constructing the reusable transport aero-space systems like "Buran" and "Space-Shuttle" the realization of the hypersonic aircraft is steal a serious scientific problem. While solving it we have to find some all new methods of protecting the construction from aerodynamical heating.

Introduction.

The flight of the aircraft is named hypersonic when Mach numbers become greater than 6. From the position of aerodynamics the flow around bodies having simple shape (for example cone, wedge and so on), in this interval of velocities is even less complicated for the analysis than subsonic or supersonic interval. Stabilization of the head shock wave form while $M_\infty>6$ causes the self-similarity of the pressure and thermal flow distribution along the generative of the streamlined body. But the heat transfer theory shows several new physical phenomenon that take place in the airflow with high Mach numbers. First of all one of this phenomenon's is dissociation of the basic air molecular components - oxygen and hydrogen. Appearance of the atoms, ions and electrons behind the shock wave can considerably intensificate the heat effect of the over-running flow on the surface of the aircraft. This requires developing special methods of heat shield while construction of the air-space crafts [1]. The problem of shock wave interaction with elements of wings and rudder turned out to be not less complicated. Shock drop can cause the growth of the pressure on the surface by about an order and the intensive growth of the heat flow too [2].

All this problems had to be solved by constructors of the reusable transport space vehicles and were got over successfully. Although the shape of the returning vehicle didn't have the classical aircraft form it's said that the first hyper-sonic flight took place in April the 12th 1981. It' also known that before the constructing the Space-Shuttle returning device several experimental vehicles were manufactured (X-15, "Bor-4") and tested in flight conditions. But there was no hypersonic aircraft among them.

Aircraft in spite of returning vehicles of space-crafts can fly horizontally using high aerodynamical performance(quality) and the continuous work of engines. First condition allows to get the desired lift level and the gravity level and the second condition allows to overcome the drag forces such as tangential and normal to the outer surface of the craft (pressure forces).

Aircraft technique prepared to overcome the hypersonic barrier at the beginning of sixties. On Fig.1 taken from the Big Soviet Encyclopedia (Aviation) the diagram of soviet fighters and bombers velocities. If the tendention of velocity growth stayed the same that to the end of the sixties hypersonic barrier would be passed. But this didn't happen. Even at the beginning of new millennium we are not sure that the voyage with passengers across the Atlantic can be realized in the nearest future.

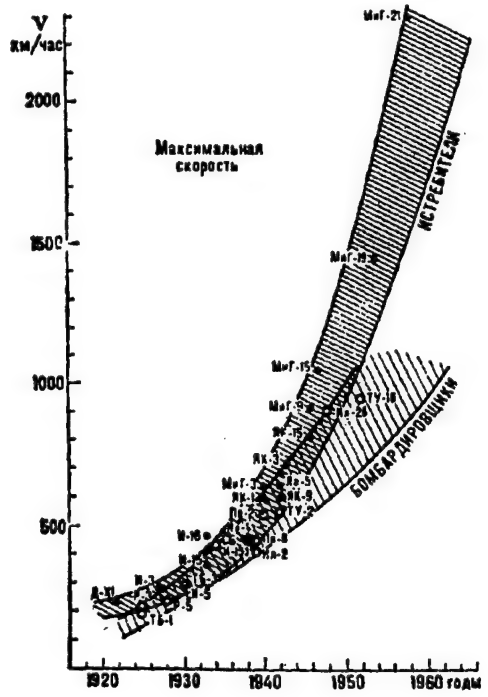

Fig.1.

Distinctive peculiarities of hypersonic aircraft.

In a first approach hypersonic aircraft differs from other planes only by the velocity of the flight V_∞. But even when the Mach numbers become grater than 3 we have to use without-

compressor straight-flow air-jet engines (SAJE) instead of common turbo-jet engines (TJE). While the velocity of the flight growth further the SAJE will be replaced by hypersonic straight-flow air-jet engines. It's not hard to see that all construction of hypersonic aircraft has to provide the desired air consumption for the straight-flow engine. Solving this problem of gas dynamics aircraft constructor has to combine in single system such parts as fuselage, wing and engine while the interval of attack angels and the place of head shock connection are bounded(restricted). We can see much more differences between returning device of reusable transport aero-space system (RTASS) like "Buran". In this case the priority values are the distance of the flight L and the weight of the useful cargo. To be more accurate the ratio of this weight to the whole weight of the flying vehicle.

The hypersonic aircraft differs from returning device of RTASS by having the long distance horizontal flight region in the atmosphere of Earth with constant velocity V_∞. Such a flight can be realized only when two conditions are fulfilled:

1. Thrust of the engines F_x must be equal to the drag force that can be calculated as an multiplication ($\left(C_x S\frac{\rho_\infty V_\infty^2}{2}\right)$).
2. The lift of the system consisting of the wing + fuselage that is equal to the ($C_y S\frac{\rho_\infty V_\infty^2}{2}$) have to equate the gravity force (m.g.).

Here C_x and C_y are the coefficients of aerodynamical drag and lift ratio of them is named aerodynamical performance of the aircraft $K=(C_y/C_x)$, S - a specific value of the aircraft's cross-section square, ρ_∞ - density of atmosphere at the altitude H that can be defined as

$$\rho_\infty=\rho_0\exp(-\beta H) \qquad (1)$$

in a first approximation. Here ρ_0 - density of atmosphere on the ocean level, $a\beta=(7100)^{-1}м^{-1}$ for the lower layers of atmosphere.

Thrust of the engines F_x depends on fuel consumption and its specific impulse I. On Fig.2 the data [3] of specific impulses of carbon-hydrogen fuel (T-1) and hydrogen (H_2) are shown. It's also shown that unlike fluid rocket engine ... specific impulse of TJE or SAJE varies in wide ranges while Mach numbers a flight grow. Specific impulse I plays a great role in maximizing the distance of a flight L. It's not hard to see while combining the Conditions 1 and 2 for realizing horizontal flight. With their help we can get the formula for calculating the distance of a flight L (Berge formula)

$$L=KIV_\infty\ln\left(\frac{m_0}{m_0-m_f}\right), \qquad (2)$$

where m_0 - aircraft' gravity at launching and m_β - weight of fuel.

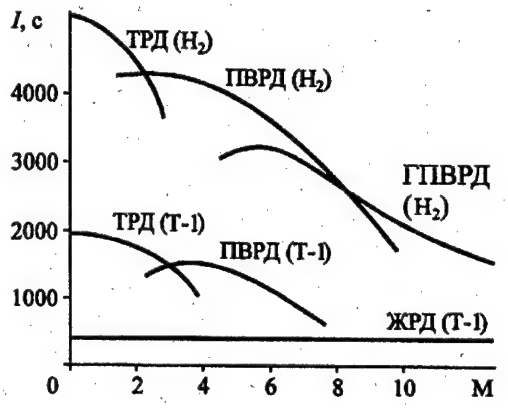

Fig.2.

Condition (II) gives an opportunity to get formula for altitude of a flight depending on admissible load on the wing. $(mg)/(C_y S)$:

$$H=\frac{1}{\beta}\ln\left[\frac{\rho_0 C_y S V_\infty^2}{2mg}\right] \qquad (3)$$

Typical range of H values depending on Mach numbers and load on the wing is shown on Fig.3.

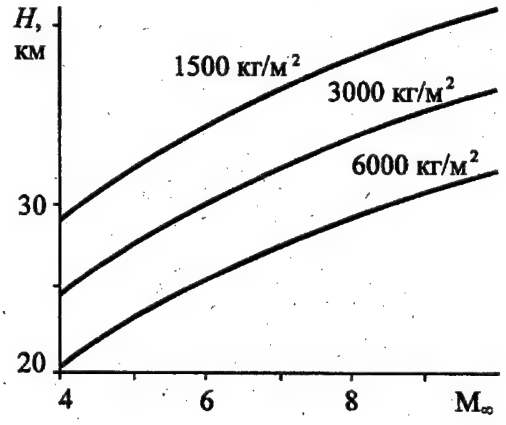

Fig.3.

Thermal regime of hypersonic aircraft.

Let us assume that specific distance of a flight L is about 10000km. Using formula (2) we can say that a flight of a hypersonic aircraft on such a distance can be realized with help of SAJE working on H_2 fuel and the Mach numbers will be 8-10. In this case the aerodynamical performance must be not less than 3. This value is by 2 times larger than the value of AP of the returning device of "Buran" system and it's by 1.5-2 times less than the AP of up to date supersonic crafts. The difference in values of K makes the constructors refuse the variant of arrangements used in "Buran" vehicle and use the shapes of supersonic aircraft. This means that head edges of wings will have radius of curvature about 10mm instead of "Buran" where $R_н \approx 1000$mm.

Optimal angle of attack in the flight must not be more than 5°. "Buran" had those angle equal to 20° and more. Stretched form of the aircraft can be realized due to the small values of specific thickness of the fuselage nd wings. At last not like the classical aircraft hypersonic vehicle will be constructed using composite scheme in which the lower surface of the fuselage will be playing the role of the flat nozzle's upper surface and the head shock wave must be connected to the entrance edge of the input air-duct.

As compared with the reusable "Buran" system and also with supersonic aircraft all this arrangement solutions greatly restrict the thermal regime of the hypersonic aircraft. On Fig.4 the growth of hit flow q and equilibrium temperature T_w of the aircraft's bow depending on flight velocity of the hypersonic aircraft is shown.

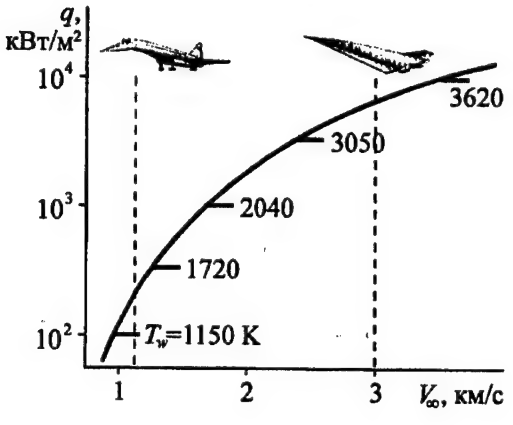

Fig.4.

You can see that in this case the as compared with the up to date supersonic aircraft the hit flow grows by 50 times and the temperature by 3 times. Fig.5 shows the isotherms on surface of the hypersonic aircraft when one of the arrangements is used (Mach number is equal to $M_\infty=8$ and the altitude of the flight is H=27km). The particular stress is generated by regions in neighborhood of the sharp wing, fuselage and input air-duct edges. Great temperature nonuniformity makes the use of airdusted covers impossible.

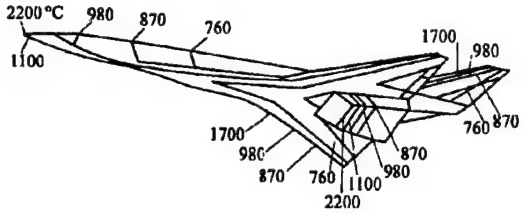

Fig.5.

The experience in constructing of the reusable transport air-space systems shows that the optimal variant is to use different combined heat-shield layers on the surface of the craft. It can be dense heat-resisting carbon composite materials up to the extra light fiber fabrics made of quartz glass. But the flight time growth up to the 5000sec causes the significant enlargement of heat-shield layer thickness.

$$\delta_T \approx 3\sqrt{a\tau}$$

where a - coefficient of the thermal conductivity. We also have to consider the higher value of the tangent stress (especially on the leeward surface) than the value that was calculated for "Buran" system, the problem of saturation of the porous isolation by moisture consisting in air, large linear dimension and so on. The methods of sharp edges heat protection must be made using all new methods. May be it's useful to use passive or active thermo-removal.

Heat exchange and heat insulation in zones of interference.

The effective functioning of straight-flow air-jet engines can be possible when the optimization of the input atmospheric air compression is realized in input air-duct. One of the solutions of the given problem requires the "closing" of the compressed layer it means connection of the head shock wave to the input air-ducts' edge. On Fig.6 the interaction of head shock waves in head edges'

neighborhood and the distribution of temperature on its' surface in cases with and without interference is shown. You can see that intersection of head shock waves from fuselage bow and own shock wave before the input air-duct creates the complicated interference picture with forming the highly-pressured stream headed to the surface. The pressure and the heat flow can increase by the order. Considering the small cross-cut dimension of this stream it is hard to find the definite way of heat insulation of this region.

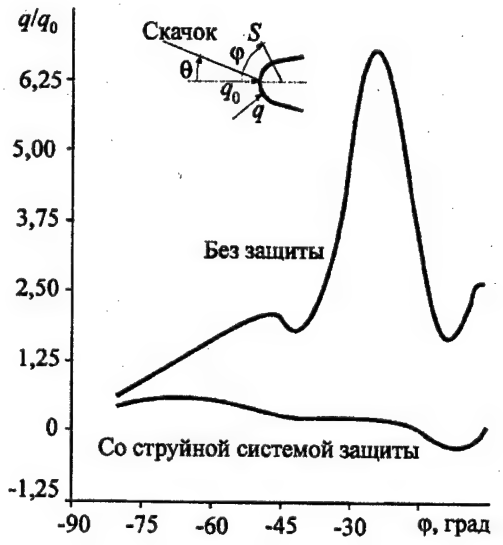

Fig.6.

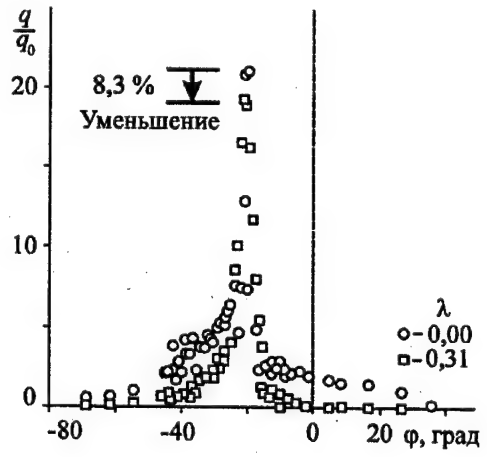

Fig.7.

Fig.7 shows experimental data [4] for reducing of the heat loads in zone of interference using the traditional method of penetrating cooling [1]. Even when dimensionless intensity of $G_w/(\rho_\infty V_\infty)$ coming up to 30% effect of the heat flow reducing didn't become more then 10%. We have to notice that the effect of penetrating cooling on some distance from the shock-wave is high. But the zone of high antipressure may cause the nonconformity of cooler filtration that means the local zone with low expense.

Conclusions.

Perspectives of constructing the hypersonic aircraft shows to be very assuring after tremendous achievements in aero-space technologies - creation the reusable transport systems "Buran", "Space Shuttle". But the analysis shows that aerodynamical arrangement, trajectories of the flight, and as a result thermal regime of the hypersonic aircraft differs from those characteristics of RTSS. This requires new technical ideas first of all among the methods of thermal insulation and analysis of different arrangement variants with there further optimization.

References

1. *Polezhaev Yu.V., Yurev F.B.* Teplovaya zatschita, Moscow, Energiya, 1976 (in Russian).
2. *Borovoy V.Ya.* Techenie gasa i teploobmen v zonakh vzaimodeystvia udarnykh voln s pogranichnym sloem, Moscow, Mashinostroenie, 1983(in Russian).
3. *Byushgens G.S., Bedrzhizky E.L.* TsAGI – zentr aviazionoy nauki, Moscow, Nauka, 1993(in Russian).
4. *R.J.Nowak, M.S.Holden, A.R.Wieting* Shock/Shock Interference on a Traspiration Cooled Hemispherical Model. AIAA-90-1643.

DIFFUSIVE DISCHARGE IN A FLOW IN FRONT OF BODY

V.M.Fomin, A.V.Lebedev, and A.I.Ivanchenko
(Institute of Theoretical and Applied Mechanics SB RAS, 630090, Novosibirsk, Russia)

An electrode system has been made to create a self-maintained glow discharge in a super- and hypersonic air flow for investigating a shock wave and nonequilibrium plasma interaction. A longitudinal discharge scheme, where the directions of flow and electric current coincide was used.

A technology has been developed to obtain a glow discharge with controlled transverse dimensions. Our experiments show that discharge the geometry is one of the most important factor for a shock wave and nonequilibrium plasma interaction.

The first experiments have been conducted for Mach numbers of 3.2 (the flow velocity is 620m/s), 7.1 (1000m/s) and 8.15 (1200m/s). The static pressure was varied from 1200Pa to 4000Pa. The characteristic current density was approximately 5 A/cm^2 in the discharge column and 0.2 A/cm^2 on the cathode.

For the first time a self-maintained glow discharge in a hypersonic air flow is obtained. The discharge reconstructs substantially the supersonic and hypersonic gas flow around the body. It induces the dissipation of the bow shock wave responsible for the main share of the body drag.

For the first time experimental data of spatial-energetic structure of the discharge have been obtained. The data show that the strength of electric fields in a volume is too small for the loss of particles in the volume to be compensating due to Townsend ionization. The pre-electrode regions proved in our experiments to have the most part of the voltage (up to 90%) applied to electrodes.

The work has been supported by the Russian Foundation of Basic Research, grant of RFBR X» 98-02-17936.

THE EFFECT OF THE POSITION AND SHAPE OF A LOCAL ENERGY SOURCE ON THE AERODYNAMIC CHARACTERISTICS OF A SUPERSONIC VEHICLE

V.M. Fomin, T.A. Korotaeva and A.P. Shashkin
Institute of Theoretical and Applied Mechanics SB RAS,
630090, Novosibirsk, Russia

Much interest in the research of skew fields by an inhomogeneous supersonic flow of gas is now exhibited. The non-uniformity of distribution of parameters in a flow can be caused by various reasons, including availability of a local energy source. It is shown [1-3 etc.] that the power effect on the free stream allows one to change flow regimes and to influence the aerodynamic characteristics of skew fields located in the wake behind the energy area. In the case when the energy source is not located on an axis of a body of revolution, there arises a complex spatial flow, which strongly influences not only the drag, but also the lift and pitching moment characteristics. However, such processes are poorly investigated both experimentally and from the point of view of computing gas dynamics. In the present paper, complex spatial flow structures are considered, which were derived as a result of the effect of local power sources both point and cylindrical. For research of the flow of skew fields (ogival, elliptical cones, skew field of the cone - cylinder), an energy source was set as in [1,2]. The position of a source varied not only on an axis of symmetry of a skew field, but also normal to it. In this case, the flow has an essentially spatial character and the local source influences not only the drag, but also the lift and pitching moment characteristics. The hot jet without plasma upstream of the bluntness also renders a large effect on the characteristics of a skew field. However, this flow pattern differs from the structure from a similar plasma jet in experiment.

References

1. *Georgievsky P.Yu.and Levin V.A.,* Supersonic flow around volume sources of energy// Mechanics: Modern Problems. Moscow, 1987. P.93-99.
2. *Korotaeva T.A., Fomin V.M., and Shashkin A.P.,* Numerical study of the influence of a local energy source on the flow around pointed bodies. -Novosibirsk, 1996.-36 p. - (Preprint /Sib. Branch, Russian Acad. Sci. ITAM; No.1-96).
3. *Bergelson V.I., Medvedyuk S.A., Nemchinov I.V., Orlova T.I., Hazins V.M.,* Aerodynamic characteristics of a body with different location of the heat spike// Mat. Modelirovanie. 1996. Vol. 6. No. 1. P.3-9.

INFLUENCE OF A COUNTERFLOW PLASMA JET ON THE INTEGRATED AND DISTRIBUTED AERODYNAMIC CHARACTERISTICS OF THE BLUNTED BODY

V.M.Fomin, N. Malmuth(USA), A.A.Maslov, V.P.Fomichev, A.N.Shiplyuk, G.A.Pozdnyakov, V.V.Postnikov, B.A.Pozdnyakov
Institute of Theoretical and Applied Mechanics SB RAS, 630090, Novosibirsk, Russia

The large interest recently is attracted to researches of flow around of bodies in inhomogeneous flow. A non-uniformity of flow can change structure of flow and to influence the integral aerodynamic characteristics of flight vehicles. Sources of a non-uniformity can be other bodies, counter flow jets, artificially created areas of energy input [1].

The large number of papers, for example [2-4], are devoted to research of structure of cold counter flow jets of gas in supersonic flow. These activities are initiated by a capability of various practical uses, such as: maintenance of thermal protection of space vehicles, stabilization of supersonic combustion, control of thrust vector and etc. The essential influence on structure of flow makes heating of a flow before the flying body [5]. The effects of a counterflow jet and heating of a flow, supplement each other at counter flow plasma jet [6-8]. To these effects are added also plasma effects. The interest to use of plasma jets grows in connection with development of plasma process engineering and searching of ways of flight vehicles drag reduction.

The experimental researches on effect of a counterflow hot plasma jet on aerodynamics of the blunted body [6-8] have shown, that the impulse of a counterflow plasma jet can significant reduce of flying body drag. The influence of a plasma jet on the distributed aerodynamic characteristics was not investigated. In the present paper the experimental result on influence of a counterflow plasma jet on the integrated and distributed aerodynamic characteristics of model a cone - cylinder in a supersonic flow are presented.

The researches were carry out in the supersonic wind tunnel T-325 ITAM SB RAS of a continuous - periodic operation. The size of the test section of the wind tunnel is 200x200x600mm. The researches were conducted at a Mach number M=2.0, total temperature - 300K and stagnation pressures 1-3atm, that corresponded to unit Reynolds numbers Re_1=(13-40)×106 1/m.

Test model - truncated cone - cylinder with lengthening 5. The apex angle of a cone is equal 60 degrees, diameter of a cylindrical part - 40mm. The model is made as a thin-walled cylindrical shell with conical nose cone. It was set on single-component strain-gauge balance, which was fastened to a wall of a wind tunnel with the help of a pylon. The model had replaceable noses with sharp and truncated cones, solid and drainage. Diameter of a truncated cone nose d_2=9mm. All measurements were carried out at a zero angle of attack of the model.

In truncated top of a cone the nozzle of the plasma generator with diameter of the nozzle 2mm (Fig.1) was placed. The plasma generator was fastened to a wall of a wind tunnel with the help of a pylon separately from model.

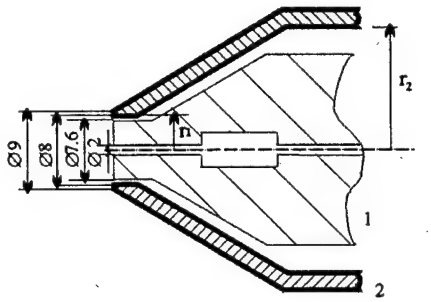

Fig.1.

A efflux from the nozzle plasma generator was sound. The plasma generator of a direct current with gasdynamic vortical stabilization of an arc on the cathode and self-aligning length of an arc in an anodic part was used in experiments. The current of an arc was 30-60A, voltage - 100-200V. The characteristic value of power input in gas was 6kw/g. The plasma generator allowed to receive a hot jet of nitrogen with temperature 5000K and gas flow rate 0,7g/sec. The body of the plasma generator had an effective system of water cooling, that allowed to execute continuous tests of model. Current, voltage, gas flow rate and pressure in a prechamber of plasma generator were measured in experiment.

In an offered design of the model attachment to wind tunnel walls the strain-gage registered forces acting only on a thin-walled shell. The forces which are acting on plasma generator (including force of a jet response), were compensated by force of a pylon response and were not measured by balance. 10 drainage orifices was located on a conical section of the

model for measurement of distributions of static pressure and 3 orifices - on a cylindrical part. Diameter of drainage orifices was 0.5mm. The pressure inside the model was measured by static-pressure gages in 5 points.

For visualization of flow the optical device IAB-451 and standard procedure of schlieren pictures obtaining was used.

Thus, in the given work the drag forces of model a cone - cylinder were measured, the pressure distributions on a surface of conical and cylindrical parts of model are obtained and the schlieren-pictures of flow are made.

The plasma generator was actuated after beginning of a wind tunnel operation. The actuation of plasma generator resulted in appearance of glow enveloping all models and making flow visible. Visually in experiments two steady modes of flow were observed: with short penetration of a jet into incoming airflow (SPM) and with long penetration of a jet (LPM) Fig.2.

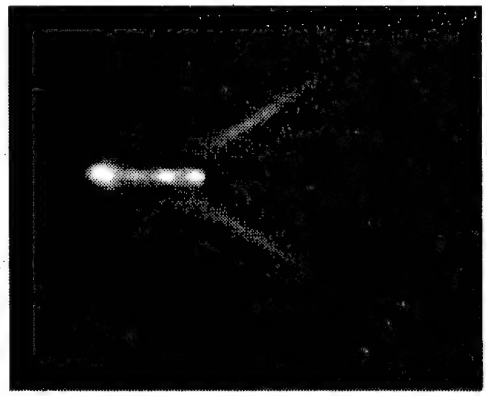

Fig.2

Both modes of flow were observed in the same experiment. The transition from one mode to another was accompanied by non-stationary phenomena, at which all flow pattern changed. During transition regimes there is a reorganization of flow from multibarreled structure of a jet, characteristic for LPM-mode, to flow with one barrel intrinsic to SPM-mode. Qualitatively such phenomena were observed at the efflux of cold gas jets towards to a supersonic flow [2,3].

The examples of schlieren-pictures verifying visual observations, are presented in a Fig.3.

All of them are obtained sequentially in one running at constant parameters of a wind tunnel and growing pressure in a prechamber of plasma generator . The flow with LPM-mode was realized in the beginning of experiment, then it was transformed in SPM-mode. Let's characterize, following [2,3], mode of flow by the parameter $p=P_{0j}/P_{0f}$, where P_{0j} - full pressure of a plasma jet, P_{0f} - full pressure after bow shock. The Fig.3a corresponds to LPM-mode (p=3.8). The bow shock and oblique shock are well visible. The Fig. 3c concerns to SPM-mode (p=5.0). In Fig.3b the example of an transitional regime (p=4.4) is shown. In the pictures both modes (exposure time » 0,01sec) are as though imposed. The transitional regime with the expressed instability of flow in a zone of interaction of a jet and counter flow was observed in range $4.1<p<4.5$. For critical value p it is possible to accept pcritical = 4,3, that is a little bit higher expected for similar conditions at cold counterflow jet (pcritical =3) [2]. Probably, it is possible to explain by presence of specific plasma effects [9].

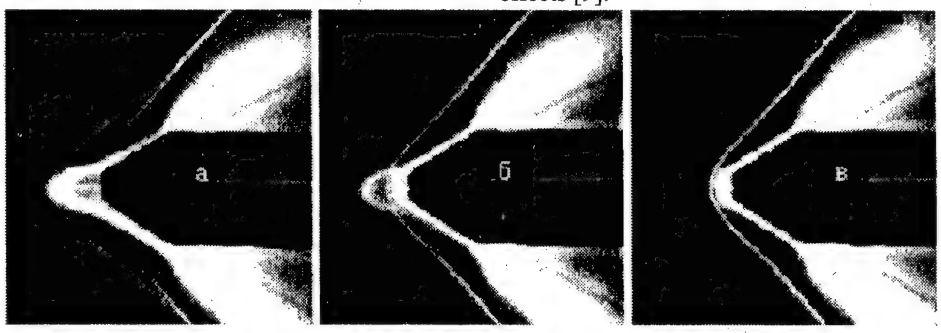

Fig.3

In a Fig.4 the values of a drag coefficient of model $cd=X/qS$ (X -drag of the model, q - dynamic heat, S - area of model cross-section) for various stagnation pressures of a flow P_{0f}, obtained from results of balance measurements are presented. The experiments were carried out with a sharp cone (point 1), with a blunted cone without a plasma jet (point 2) and with a jet (point 3). The greatest drag has the sharp cone in all the investigated range of parameters. The blunted cone has some less drag . It is explained by the fact that even in a model without a jet on a lateral area in a neighbourhood of a leading edge of a truncated cone the zone with the reduced pressure

is formed [10]. Besides in experiments the force which is acting on a nose of model was not measured.

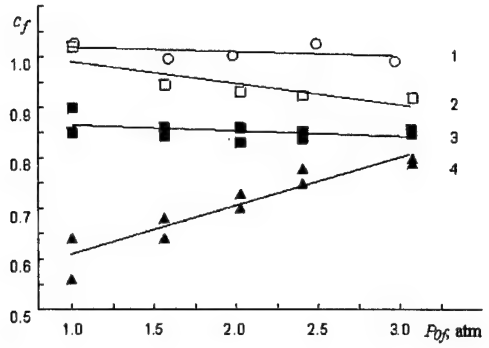

Fig.4.

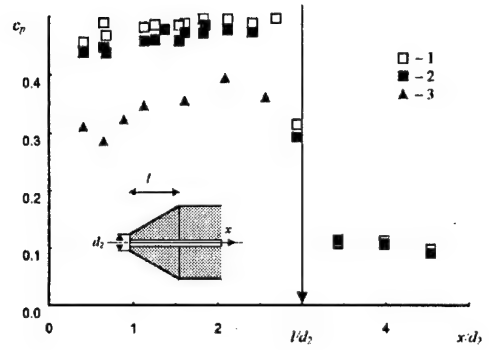

Fig.5.

Efflux of a plasma jet essentially reduces drag of the model. The experimental data form two groups of points - with strong influence (correspond to LPM- mode) and with weak (correspond to SPM- mode). In the first case the greatest effect of drag reduction (up to 45%) was observed, in second - the drag reduction was insignificant (about 15 %). Result looks like obvious in the whole, as at LPM-mode the jet penetrates much further into a flow, that reduces an effective angle of a cone.

In Fig.5 the relative pressure $c_p=P/2q$ (P - surface pressure on the model) are shown as a function of dimensionless coordinate X/d_2 (d_2=9mm). The points 1 correspond to a flow regime without a jet, point 2,3- with a jet in modes SPM and LPM, accordingly. In figure the position of a fracture on a contour of model by the letter l is marked. It is possible to see, that two modes are again observed. In both cases the essential pressure variation at efflux of a plasma jet happens on a conical section of model, that is that the drag reduction of the model is stipulated by reorganization of flow at a nose cone.

The integrals from pressure distribution on a surface, with taking account of inner-model pressure, will be well agreed with balance measured forces .

Thus in the given work two steady flow regimes around of the blunt body are obtained at counterflow plasma jet, with one and many barrels. Qualitatively this result coincides with cold jets one. The drag reduction at counterflow plasma jet is confirmed and for the first time pressure distributions on a surface of model are obtained which show, that the drag reduction is connected with a pressure decrease on a conical section of the model.

Acknowlegements

The work was supported by Boeing and the Rockwell Science Center, LLC. Agreement No.B8X413840, RSC NM 98-3.

References.

1. *G.G.Chernyi,* The Impact of Electromagnetic Energy Addition to Air Near the Flying Body on its Aerodynamic Characteristics, (Russian contribution), Proc. American Institute of Aeronautics and Astronautics, 1998
2. *P.J.Finley.* The flow of a jet from a body opposing a supersonic free stream. JFM, 1966, V.26, pt2, p.378-368 .
3. *Yu.N.Yudintsev., V.F.Chircashenco,* Gas dynamics and acoustics of jet flows. ITPM SO AN SSSR. Novosibirsk, 1979. p.75-106.
4. *B.L.Zhirnicov, K.P.Petrov.* Modern problems of aerodynamics. Engineering. M: 1987.
5. *P.K.Tretyakov, A.F.Garanin, G.N.Grachev, V.M.Fomin,* DAN, 1996, V.351, No.3, p. 339-340.
6. *Yu.Ch.Ganiev, V.P.Gordeev, A.V. Krasilnikov, V.I.Lagutin, V.N.Otmennikov.* Experimental Study of the Possibility of Reducing Aerodynamic Drag by Employing Plasma Injection," Proc. Third International Conference on Experimental Fluid mechanics, Korolev, Russia, June3-6, 1997.
7. *A.Klimov,* Anomalous Supersonic Flow and Shock Wave Structure in Weakly Ionized Plasmas, 1st Workshop on Weakly Ionized Gases Proceedings, USAF Academy, Colorado, June 9-13, 1997.
8. *S.Leonov,* Experiments on Influence of Plasma Jet Lift and Drag of Wing 1st Workshop on Weakly Ionized Gases Proceedings, USAF Academy, Colorado, June 9-13, 1997.
9. *G.G.Chernyi.* Flow of gas with a large supersonic velocity, 1959.
10. *G.A.Lukyanov.* Supersonic jets of plasma, 1985.

INFLUENCE OF HOT COUNTER JETS ON THE DRAG OF THE BLUNT SKEW FIELDS (CALCULATION)

Fomin V.M., Maslov A.A., Shashkin A.P., Korotaeva T.A. (ITAM SB RUS, Russia)

Malmuth H.D. (Roclwell Sience Center, USA)

The importation of a local disturbance in a free stream with the help of a counter jet can result in desirable changes of the aerodynamic characteristics of the body. This way is practically realizable. The available data show that the effect of the jets depends on the form of skew fields and initial parameters of a gas in the jets and in a free stream . The purpose of the present activity is an attempt to conduct complex preliminary researches of the flow of skew fields in the presence of jets, counter flow, with allowance for plasma effects, a combination of the data of experiments and numerical researches.

In this activity, numerical researches of the flow of skew fields are conducted in the presence of a thin high-temperature counter flow jet. The flow around a truncated cone with a cylinder at a zero angle of attack is considered for Mach numbers of M = 2.0. Two modes of penetration of a plasma jet in a free stream are experimentally established: a mode a short (SPM) penetration of a jet and long (LPM) penetration of a jet. It is shown that modes with a counter jet, especially LPM result in a significant decrease in drag of a skew field. The results of calculations for a hot jet in a perfect gas in an inviscid flow approximation agree with the results of experiment with a plasma generator in the mode of short (SPM) penetration of a jet.

THERMAL MODEL OF GAS FLOW PLASMA CONTROL

M.N. Kogan (TsAGI, Zhukovskyi)

The possibility of thermal explanation of some facts showing plasma influence on aerodynamic characteristics will be discussed.

Introduction.

In the present report connection of the processes in WINP with thermal processes in gases and possibility of their utilization for flows with WINP regions modeling is analyzed. The problem of shock waves and bodies motion in the pre-prepared WINP in electric or electromagnetic fields differs considerably from the problem of gas flows past bodies with WINP regions created by some kind of discharge. Here the main attention is paid to alterations of flows past bodies caused by WINP regions.

Simplified WINP model.

For weakly ionized and weakly nonequilibrium cold plasma one may neglect by momentum transformed by electrons and ions to neutral component. The force of the flows of such mixture on a body is also defined by neutral component. The electrons with energy of an order of 1-2eV disturb, ionize and slightly "heat" neutral molecules. The electrons can transfer the energy of the same order as neutral component not changing molecule translational energy transport considerably. The disturbed molecules transfer their energy to translational mode increasing its temperature or irradiate it.

Concrete character and generic times of the processes are defined by type, molecules kind, pressure, flow over the body, etc. So one can roughly considered WINP flows as flows of neutral gas with disturbed molecule internal degrees of freedom and distributed heat sources and with internal energy sources and sinks.

Energy of charged particles at small n_e/n ratio may be neglected. Under these assumptions the system of neutral component transport equations may be written in the form (for monatomic gas for simplicity)

$$\frac{\partial n}{\partial t}+\frac{\partial n u_j}{\partial x_j}=0\,;\quad p=knT \tag{1}$$

$$\frac{\partial u_i}{\partial t}+u_i\frac{\partial u_i}{\partial x_j}=-\frac{1}{\rho}\frac{\partial P_{ij}}{\partial x_j} \tag{2}$$

$$n\left(\frac{\partial}{\partial t}+u_i\frac{\partial}{\partial x_j}\right)\left(\frac{3}{2}kT+\varepsilon\right)= =-\frac{\partial q_i}{\partial x_j}-P_{ij}\frac{\partial u_i}{\partial x_j}+E_T \tag{3}$$

Here n, u_j and T are number density, velocity and translational temperature of neutral gas, q_i and P_{ij} are energy flux vector and stress tensor, $\varepsilon(t,x)$ is the international energy per molecule, E_T is the total energy transferred to neutral component, k is the Bolzmann constant. The stress tensor has an usual form. The energy flux vector can be divided in two parts $q_i=q_{itr}+q_{in}$ where q_{itr} is the flux of translational energy and q_{in} is the internal energy flux. For internal energy the Landau-Teller type equation may be written

$$n\left(\frac{\partial}{\partial t}+u_j\frac{\partial}{\partial x_j}\right)\varepsilon= =\frac{n[\varepsilon_0(T)-\varepsilon]}{\tau}-\frac{\partial q_{j\,in}}{\partial x_j}+E_{in} \tag{4}$$

where $\varepsilon_0(T)$ is equilibrium value, τ is relaxation time and E_{in} is the energy translated to internal degrees of freedom by electrons. Strictly speaking in a general case more exact level by level description is required. The value $E_T=E_{in}+E_{tr}$ with E_{tr} being the energy transferred by electrons and ions to translational degrees of freedom. Using eq. (4) the equation (3) may be rewritten in the form

$$\frac{3}{2}R\rho\left(\frac{\partial T}{\partial t}+u_j\frac{\partial T}{\partial x_j}\right)+P_{ij}\frac{\partial u_i}{\partial x_j}+\frac{\partial q_{j\,tr}}{\partial x_j}= =-\frac{n[\varepsilon_0(T)-\varepsilon]}{\tau}+E_{tr}=E(t,x) \tag{5}$$

Here $E(t,x)$ is a heat source per unit volume and unit time, $R=k/m$ and $\rho=nm$, m is a mass of a molecule. The values E_{tr} and E_{in} include the energy transmitted at collisions as well as at electron-ion recombination. Electron can transfer energy of the same order as neutral gas. But in the bulk of the they show themselves through local values of E_{in} and E_{tr}. On the body surface the electron energy may be transferred directly to the surface. But this situation needs special consideration. To determine the forces acting on the body electrons and ions serve only as energy transmitters from electric or EM field to the neutral component which parameters define the flow and force on the body. Prescribing $E(t,x)$ it is possible to model flows with different types of discharges and for different gases.

Using this simplified model the problem of WINP flow over the body may be divided in two parts.

At the first stage the flow may be investigated with prescribed energy surface $E(t,x)$. If one succeeds to find $E(t,x)$ function providing energetically efficient body aerodynamics improvement (if only !?) the possibility of designing the discharge creating, the flow with found heat release distribution $E(t,x)$ must be solved. The first problem is much easier that the second one.

MICROWAVE PLASMA - BODY INTERACTION IN SUPERSONIC AIRFLOW

V.Brovkin, Yu.Kolesnichenko (MRTI RAS, Moscow),
A.Gorynya, M.Gurevich, M.Ryvkin (RDI Radio Apparatus, St.-Petersburg),
A.Klimov, S.Leonov (IVTAN, Moscow),
A.Krylov, V.Lashkov, I.Mashek (St.-Petersburg State University),
Yu.Serov (Ioffe Institute, Moscow)

Abstract. The effect of microwave plasma-body interaction in a supersonic airflow is experimentally studied. Plasma is created in front of the body (upstream the flow) by the free localized microwave discharge. The existence of phase of bow shock wave instability under its interaction with plasma is confirmed. The reduction of the drag force of the model due to the microwave plasma action is measured. The gas temperature in the discharge by the end of microwave pulse is defined with using vibrational-rotational transitions of the second positive nitrogen system. The maximum temperature raise does not exceed 50K for the pulse. Self-consistent values of electron and vibrational «temperatures», average concentration of electrons in microwave discharge are also obtained. However, additional studies are necessary to conclude explicitly the reason for plasma-shock wave interaction effect.

Introduction.

Studies of interaction of nonequlibrium low-temperature plasma with high speed bodies and airflow were conducting intensively last 15 years [1,2]. There were revealed effects, which can be used in aviation, bringing about increasing range of flight and spare fuel. One of the most perspective methods of remote plasma creation in front of the moving object is microwave (MW) discharge. The beginning of realization of this method was getting started in 1997 by our work [2], when free localized MW discharge in supersonic airflow was received for the first time.

The unique experimental installation was created for a given method realization. The installation consists of three main blocks: MW, gas-dynamic and diagnostic. MW generator forms pulses with peak power about 200kW, pulse duration 1.3 to 2.25μs, repetition frequency up to 1.5kHz in X-range. By means of a horn radiator and parabolic reflector MW radiation of linear or circular polarization is focused on the axis of supersonic flow in the area between the working nozzle and the AD model. The gas-dynamic installation creates a uniform working flow of 20mm diameter with Mach number M=1.45, static pressure 60Torr and static temperature 200K. Diagnostic part of the installation includes: Schlieren-system, allowing to visualize the flow under investigation with separation of the needed phase of a process to the account of time gating; spectral system, allowing to obtain emission spectrums of plasma with the temporary resolution near 1μs; pressure sensors, with the possibility to select a necessary phase of a process. All this allows to research in detail the processes of interaction of MW plasmas with AD bodies in supersonic flow.

As it was already noted above, exactly on this installation a free localized MW discharge in linear and circular polarized radiation beam in the supersonic airstream was received for the first time. The possibilities of MW plasma technologies were demonstrated, in particular for changing of drag reduction [2]. Our last studies were directed on the detailed study of process of interaction of plasma with gas-dynamic structure of a flow near the bodies and determination of MW discharge plasma parameters.

MW discharge in supersonic flow.

The discharge existed stable both in the free flow, and at the presence of aerodynamic models. In accordance with maximums in MW field distribution in the region of focusing there were observed two or three denominated areas of discharge light emission. The nearest to the AD model plasmoid was located just before the front of the bow shock wave (BSW). As in the case of MW discharge in the steady-state gas [3], there were observed two main structures of discharge: in the manner of half-wave dipoles, encircled by the shining plasma, and in the manner of curved and branched channels with the base in the form of quarter-wavelength sinusoid. In the majority of experiments the first structure was realized, demonstrating a good spatial reproducibility that is characteristic of discharges with the small threshold excess. Coming from the values of a discharge time formation (measured by means of photo-electric multiplier and MW sensor) equal to 0.2μs for peak MW power 180kW, the initial value of reduced field E/p turned out to be equal to 40V/(cm·Torr), where E is electric field strength of the wave, p is a normalized pressure. Breakdown occurred under minimum peak

power 120-130kW that corresponds to the value of reduced field in maximums of MW field distribution 32-34V/(cm·Torr). Measurements also have shown that the discharge absorbs not more than 30% of the led MW power. Thereby, the specific energy input in the discharge did not exceed several tenth J/(cm^3·atm).

Study of MW plasma influence on gas-dynamic.

By means of Schlieren-system with time gating aerodynamic spectrums of airflow with time step 2-10μs in the interval of delays comparatively MW pulse from 0 to 200μs were received. Hemispherical model of 16mm diameter was used, which was installed in the region of the 20mm diameter even kernel of a flow. MW discharge was burned up in front of the model, the nearest to the model plasmoid being located at the distance 4-8mm. Experiment has newly demonstrated (earlier refer to [2]) particularities in the picture of plasma flow around the model. As from 10-16μs and up to 80-100μs an unstable character of BSW behavior in front of the model was observed. At a moment of MW discharge plasma coming, a division of a BSW into layers occurs. In this process are consecutively observed the phases: twist of the front, its crushing, fluctuations and, finally, division into layers in the area of interaction. A fragment of BSW front is «displaced» and is disposed closer to the surface of the model, simultaneously another shock upstream the flow is formed. The pressed and the moved away shocks are fluctuating in the space. Under the greater delays, i.e. after MW discharge plasma drifting below the main BSW front, a recovering of the main shock and a picture of a flow occurs.

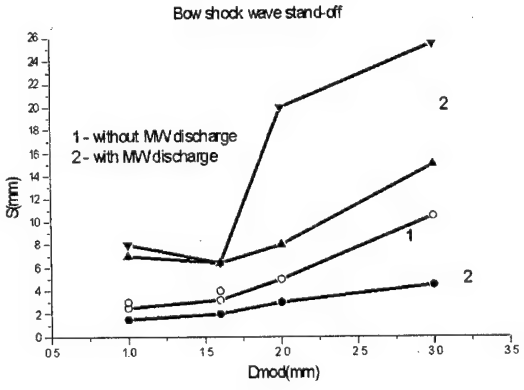

Fig.1.

The described above patterns of plasma flow-body interaction are summarized in Fig.1, where the BSW stand-off in a flow without discharge and BSW fragments — the pressed and the moved away shocks in plasma flow are shown. The models are spheres of the appropriate diameter. It is well seen that the amplitude of fluctuations of the moved away shock position increases greatly when the model diameter becomes equal or exceeds the diameter of the working flow.

For the study of plasma influence on the drag of a body, sensors of stagnation and static pressure, working at the base of piezoelectric effect were used. Investigations of stagnation pressure behavior during interaction with plasma at the leading edge of AD body under different MW conditions were conducted. Reduction of full pressure on the value $\Delta p \cong 30$Torr at time delay near 70μs is fixed. The characteristic time of interaction of plasma flow with the body — near 150μs — correlates well with Schlieren-system data. However, the experimental data obtained by means of the pressure sensor should be considered as preliminary, characterizing sooner qualitative picture of a flow near the model and the value of its drag changing.

Measurement of gas temperature by the optical method.

Overview spectrum of discharge in the flow by the end of MW pulse was prescribed in the interval 3700-4100A through 2Å (Fig.2).

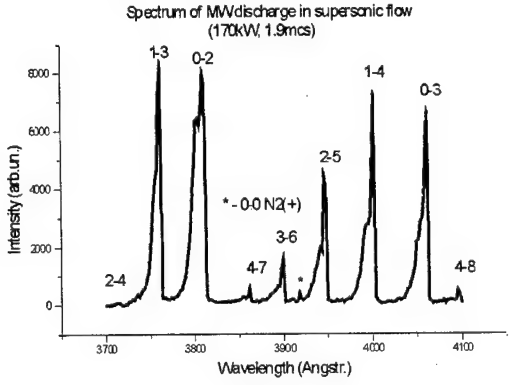

Fig.2.

Each point (on the wavelength) was averaged on 50 realization. Overview spectrums of air in the bulb under 15Torr and 50Torr were received in the same interval of wavelengths. In all overview spectrums sequences Δv=-3 (up to 4-7 in the flow and 3-6 in the bulb) and Δv=-2 (up to 2-4) are seen. In the flow transition 4-8 is also

seen. In spectrums of air flow and of air in the bulb under 15Torr 0-0 transition of the first negative system of nitrogen ion is observed. When getting the spectrums of MW discharge in the flow registration of light emission took place from the first (upper on the flow) plasmoid.

When getting the spectrums of band edgings, 200 points were fallen on the interval 50-70 A, herewith each point was also shown by the result of averaging on 50 realization (Fig.3). The rotational temperature of gas in the discharge in the flow by the end of MW pulse was defined using vibrational-rotational transitions 0-3, 1-4, 0-2, 0-0 of the second positive nitrogen system. For processing the spectrums the program was developed, allowing to define rotational temperature of gas on unresolved rotational structure of a spectrum. Processing the spectrums has confirmed that distribution over rotational levels is Boltzmann (Fig.4). Determination of rotational temperature was produced in the interval from 10 up to 20 rotational levels of R-branch. In this interval (with provision for low temperature of a gas) the contribution of P- and Q-branches is already insignificant and the inaccuracy in the determination of intensity is not yet too great.

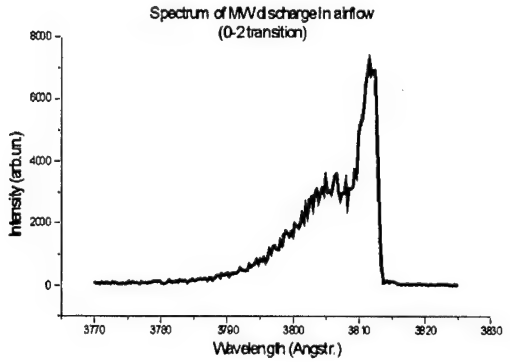

Fig.3.

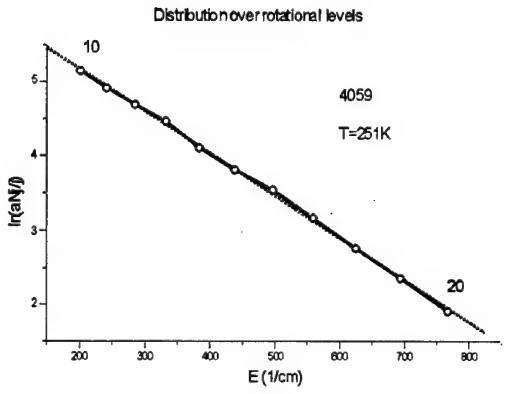

Fig.4.

At MW power radiation 180kW, duration of MW pulse 1.9μs the temperature of the gas turned up equal to 240±10K. Thereby, the maximum temperature raise did not exceed 50K for the pulse. When reducing the peak MW power to 145kW the temperature raise was halved: T=220±10K. We assumed the rotational and translational temperatures to be equal.

Temperature of the gas in the bulb under the same MW power, duration of MW pulse and repetition frequency of the pulses 900Hz and 20Torr air pressure turned up near 540K.

Measurement of gas temperature by means of thermocouple.

Measurements were conducted under the same parameters of the flow and MW, as in optical ones. Thermocouple had a time constant 0.2s. Signal level reproduction in different runs without discharge was very good.

Measurements were conducted in three positions of a sensor. In the first position there was no discharge in front of the sensor. Accordingly, the gas temperature raise was not fixed. In the second position (this is the staff place of AD models) the temperature growing on 2.5K was fixed when including a discharge. In the third position a sensor was displaced on 4cm down the flow, herewith the temperature increase in 1K was fixed. Such a noticeable reduction of temperature raise can not be explained by heat conduction of a gas.

The true value of gas temperature in the discharge can be obtained using the results with thermocouple. Supposing that averaging is related only with a time of a flow warmed and cool regions interaction with a sensor, brings about the evaluation $\Delta T_{disch}=\Delta T_{sens}\cdot Q\cdot\gamma$, where Q — time factor of interaction ($Q\sim v\cdot T_{rep}/\Delta x$, v — the velocity of a flow, T_{rep} — the period of following of MW pulses, Δx — a longitudinal size of the discharge plasma), γ — the adiabatic constant. Substituting the values of the incoming parameters leads to estimation $\Delta T_{disch}\sim$40-50K that corresponds to the optical measurements.

Parameters of MW plasma in the discharge.

Determination of vibrational temperature of the ground state of nitrogen molecule on relative intensities of edgings of a given sequence (Δv=const) is referred to the class of inverse problems (generally speaking, incorrect). For the correct determination of vibrational temperature T_V the necessary condition is an

occupying an upper electronic state ($C^3\Pi_u$) by the direct electron impact from the main state ($X^1\Sigma_g^+$). Alternative to the direct electron impact channel of an occupying a $C^3\Pi_u$ state is the process

$$2\,N_2(A^3\Sigma^+_u) \rightarrow N_2(C^3\Pi_u) + N_2(X^1\Sigma_g^+, v),$$

with the velocity constant $k^* \approx 7.7\times10^{-11}cm^3/s$.[4] Comparison of the population fluxes of a $C^3\Pi_u$ level via the both channels under average concentration of electrons in the discharge $3\times10^{12}cm^{-3}$ and reduced electric field in the plasma near 110Td has shown that there is a basis to consider the population of $C^3\Pi_u$ level by direct electron impact to be the main mechanism.

Processing on the sequence Δv=-3 (transition 0-3, 1-4 and 2-5) enables to define the relative population of the level v=1 of the nitrogen ground state $X^1\Sigma_g^+$ and the corresponding vibrational «temperature», and electron temperature of vibrational levels excitation. Hereinafter on these values the electric field strength in plasma and the specific energy input in the discharge are (independently) calculated, with using these values the average concentration of electrons in the discharge is defined.

The following results were received: vibrational temperature 1500±200K, electron temperature 2.1-2.3eV, specific energy input in the discharge 0.4J/(cm^3·atm), average concentration of electrons in the discharge $3\times10^{12}cm^{-3}$.

Conclusions.

As it was already noted above, the main aim a given investigation was a detailed study of influence of MW discharge plasma on flowing around aerodynamic models by the supersonic airflow and determination of parameters of plasma of discharge. The existence of phase of BSW instability under its interaction with MW plasma in the supersonic flow of air is experimentally confirmed. This phenomena is well reproduced. The reduction of the stagnation pressure and the drag force of the models due to the MW-plasma action was measured. Self-consistent values of electron and vibrational «temperatures», translational temperature of the gas, average concentration of electrons in the discharge are obtained.

However we consider that the findings are insufficient to do a choice in favor of one or another mechanism of interaction and additional studies are necessary. Only after these investigations being carried out it will be possible to formulate a reliable raw data for full-scale modeling and making clear that aspects of interaction of shock wave with the plasma, which did not find hitherto rational explanation.

References

1. Proceedings of Weakly Ionized Gases Workshop, USAF Academy, Colorado, 9-12 June, 1997.
2. *W.Beaulieu, V.Brovkin, I.Goldberg, A.Klimov, Yu.Kolesnichenko, A.Krylov, V.Lashkov, S.Leonov, I.Mashek, M.Ryvkin, Yu.Serov,* «Microwave Plasma Influence on Aerodynamic Characteristics of Body in Airflow», Proceedings of the 2nd Weakly Ionized Gases Workshop, AIAA, Norfolk, VA, April 24-25, 1998, pp.193-198.
3. *V.G.Brovkin, Yu.F.Kolesnichenko.* «Structure and Dynamics of Stimulated Microwave Discharge in Wave Beams», J. Moscow Phys. Soc. 5 (1995) pp.23-38.

THE TRANSFORMATION OF ENERGY OF A LASER-MICROWAVE DISCHARGE INTO GAS-DYNAMIC DISTURBANCES MOVING AT A SUPERSONIC VELOCITY IN THE ATMOSPHERE.

A.G.Ponomarenko, V.N.Tischenko, G.N.Grachev, V.M.Antonov, A.V.Melekhov, S.A.Nikitin, V.G.Posukh, I.F.Shaikhislamov (Institute of Laser Physics, Siberian Division RAS, Russia), A.I.Gulidov (Institute of Theoretical and Applied Mechanics, Siberian Division RAS, Russia)

The promising methods for the control over the flight of supersonic bodies (decreasing the resistance, creation of side forces) are based upon the energetic effect on the structure of the incident flow. Schematically we may divide all the methods into three groups: a) a blowout of a gas jet or plasma into the incident flow; b) a discharge among the elements of the construction of a flying apparatus; c) entirely contactless ones based on the usage of laser or SHF beams. The first two groups seem to be simpler in practical realization of the devices for their creation and in this item we have obtained the positive experimental results (see, for instance, the papers presented in this collected volume). The investigations on contactless effect upon the flow are presented (in part) in papers [1-6].

SHF and laser generators are more complex devices. The main advantage of them is the feasibility of power supply into the required area in the incident flow. Moreover, we may suggest that there exists an area of the flow parameters (ρ,V) in which this group will have some merits. SHF beams as means of ionization, excitation and heating of gas by a free-localized SHF discharge [7-9] at high altitudes are more preferable from the energetic point of view than laser radiation [5]. At increased density and high velocity of gas an optical pulsating discharge [10,11] being generated by pulse-periodic radiation of a CO_2-laser may be a matter of interest. But under such conditions it is necessary to have high powers even for the realization of a narrow channel method [3]. In [12] a laser-microwave discharge (LMD) enabling to approach high powers is proposed. Here the main power supply occurs by comparatively «cheap» SHF radiation (high efficiency and power of the generators). The laser radiation generates a «trace» of the ionized gas with low density in which SHF radiation is being absorbed.

The given paper reviews our works on the problem of injection of laser and SHF radiation into the supersonic flow. The investigations have been conducted in two directions at different experimental set-ups of the Institute of Laser Physics of SD RAS. I - generation and investigation of a quasi-continuous optical pulsating discharge in the supersonic gas flow and using this discharge in the experiments on the control over flow around body in a stream (together with the Institute of Theoretical and Applied Mechanics of SD RAS [10,11,13]). The discharge was generated by the CO_2-laser radiation with average power ~2,5kW and pulse repetition rate up to ~100kHz. II - at the KI-1 set up we investigated LMD satisfying the conditions for the formation of an extended channel which can move in the atmosphere at a supersonic velocity. At the energy of the CO_2-laser ~1kJ (~1μs) in the experiments on the generation of laser plasma in the atmosphere we used up to ~20J. The absorption of the pulse-periodic SHF beam in decaying laser plasma was investigated.

V. A Model of LMD

In Fig.1 a scheme of the LMD formation and some of its characteristics such as radius of both a channel and a shock wave temperature and relative gas concentration in the channel are presented [12, 14]. The focal area of pulse-periodic laser radiation moves relative to the surrounding gas with velocity V along the beam axis. Every laser pulse creates a gas breakdown near the focus. Laser plasma length L exceeds substantially the radius. If during the pause between the pulses ~ L/f the laser beam focus is displaced at distance L (that is, $f \cdot L/V \approx 1$ is satisfied), then the separated optical breakdowns form a channel, the length of which is limited by cooling (f - is the repetition rate of laser pulses).

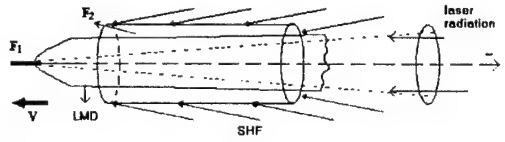

Fig.1. A LMD scheme. F_1, F_2 are the focal areas of laser and SHF beams; V - velocity of the motion of F_1 and F_2 with respect to gas.

The pulse-periodic microwave radiation is introduced into the channel through its lateral surface. The length of a cylindrical focal area of the beam is not less than the channel length. The beam parameters are such that the microwave discharge is localized in the channel. Besides, there exist some conditions under which the

microwave radiation compensates the medium cooling in the channel. In this case the temperature and conductivity of medium can be set at the level being optimal for the absorption. This allows us to increase substantially the power and length of LMD. We should point out that at small duration of laser and microwave pulses the medium in the channel is stationary (along Z-axis) relative to the undisturbed gas. The heated gas is expanded mainly with radial direction. Here there are no effects of flowing of a heat source by the external flow. The microwave radiation field moves along the channel. If the length of channel L_c is long $L_c>>L$ and the interaction of the regions of the separate optical breakdowns (mainly through the shock waves) is weak then the distribution of LMD parameters in the channel may be studied on the basis of the investigation of the interaction of the microwave radiation with decaying plasma of the isolated optical breakdown. Further, replacing t by Z/V we can get the dynamics of the medium in the channel. The value $Z=0$ corresponds to the position of the laser beam.

Generation of a Channel under the Influence of Laser Radiation

Intricate physical-chemical and gas-dynamic processes take place in the gas subjected to the optical breakdown. One can recognize 4 stages with characteristic times differed from each other by more than an order of magnitude:

1. heating and ionization by optical radiation during the period $t_1<<r_1/C_0\cong 2\mu s$ (r_1 - 0.3cm is the characteristic radius of the optical breakdown, C_0 is the sound velocity in undisturbed gas);
2. heat expansion (explosion) of laser plasma at $t_1<t<t_2<r_2/C_0$; at $t\cong t_2$ the pressure in a cavity decreases up to the pressure of undisturbed gas ($r_2(t_2)$ is the radius of the cavity boundary);
3. $t_2<t<10\cdot t_2\approx 3$ ms isobaric cavity expansion, temperature is ~4000K, density is small, the boundary moves with velocity of several meters per second, to the moment $t\geq 10\cdot t_3$ the density and temperature of the medium in the cavity become equal to the values in undisturbed gas;
4. stage of long-lived small-scale vortex structures t_4 .

The typical values of the characteristic times are as follows: $t_1\cong 1\mu s$, $t_2\cong 10\mu s$, $t_3=0.3\mu s$, $t_4\geq 20ms$ (see below). A great t_i difference in values allows us to separate the processes and obtain the approximated relations of LMD model.

The optical breakdown

The optical gas breakdown is initiated in the focal area where the intensity of laser radiation is a maximum and must exceed a threshold value. A plasma front moves to the radiation. Both breakdown threshold and mechanism of breakdown propagation depend strongly upon the radiation wavelength. In this paper the breakdown under the influence of CO_2 -laser radiation ($\lambda\cong 10.6\mu m$) and with duration ~1μs is considered in the air under atmosphere pressure.

While generating a continuous channel it is necessary to choose optimal radiation energy Q of the separate laser pulse and angle of beam focusing $\alpha=d/F$ (d - is the beam diameter at the focusing lens, F is the distance from the lens to the focus). Minimal value Q is limited by breakdown threshold $Q>Q_0$. Maximum value Q and minimal angle α are limited by the condition of continuity of the optical breakdown. At the same time Q/L energy supply (per unit of breakdown length Q/L) mustn't be small (see below) that is necessary for the generation of a channel with the diameter comparable with the wavelength of the microwave radiation.

From the experiments it follows that at $\alpha<0.05$ in a one-mode beam the optical breakdown is continuous at Q slightly exceeding value $Q_1=0.5\div 1$J. At large values of Q the breakdown consists of separate plasma formations with characteristic parameter ~1cm. Such structure is formed as a result of breakdown initiation at aerosol particles at intensity of radiation in the beam being $100MW/cm^2$. At $\alpha\cong 0.1$ the breakdown is close to one at $Q_0\leq Q\leq 7$J. Here the isolated plasma formations may be formed but the distance between them is small as compared to their dimensions. Maximum value $\alpha\cong 0.1$ is limited by the technical reasons, namely: a need for using the focusing lens of large diameter. In the experiments with multi-mode radiation the optical breakdown was continuous in the whole range of measurements $Q\leq 10Q_0\cong 10$J and at $\alpha\cong 0.01$-0.1. The reason for such a difference in the effect of one-mode and multi-mode radiation is not clear at present.

Length L of the continuous optical breakdown of gas may depend upon the mechanism of plasma front propagation during the development of the breakdown. In the energy range mentioned above the mode of a light detonation wave is the most probable one. For this case we have obtained an analytical expression for L and the density of the radiation energy absorbed per unit of breakdown length.

$$L=\frac{b_i}{\alpha}\left(\frac{W_L}{P_0}\right)^{\frac{1}{2}}\times$$

$$\times\left\{6.3+\ln P_0+\ln\left[b_i\left(\frac{W_L}{P_0}\right)^{\frac{1}{2}}(6.3+\ln P_0)^{\frac{3}{4}}\right]\right\}^{\frac{3}{4}}$$

$$g(Z)=1.2\times10^{-4}W_L^{2/3}(Z\alpha)^{2/3}\left(\frac{A}{\gamma^2 1}\right)^{\frac{1}{3}}$$

$$b_i=\frac{A^{1/4}(\gamma-1)^{5/4}}{I^{3/4}(\gamma-1)}$$

Here $Z\leq L$; A, I, γ is the atomic weight of gas, ionization potential [K^0], adiabatic index. At $T_0\cong300K^0$ gas concentration is expressed through pressure P_0 of undisturbed gas. Laser radiation power W_L is constant during the whole pulse and the duration is not less than the time of upset of the propagation mode of the light detonation wave.

$$t_i=4.5\cdot10^{-5}b_i^{5/3}\left(\frac{W_L}{P_0}\right)^{\frac{1}{2}}\left(\frac{A}{\gamma^2-1}\right)^{\frac{1}{3}}\alpha^{-1}\times$$

$$\times\left\{6.3+\ln P_0+\ln\left[b_i\left(\frac{W_L}{P_0}\right)^{\frac{1}{2}}(6.3+\ln P_0)^{3/4}\right]\right\}^{\frac{5}{4}}$$

If radiation duration t_i is less than value t_i, then the length of the optical breakdown is equal to:

$$L=360\cdot\alpha^{-2/5}\left(\frac{\gamma^2-1}{A}\right)^{\frac{1}{5}}\cdot\left(\frac{W_L}{P_0}\right)^{\frac{1}{5}}\cdot t_j^{3/5}=$$

$$=360\cdot\alpha^{-2/5}\left(\frac{\gamma^2-1}{A}\right)^{\frac{1}{5}}\cdot\left(\frac{Q}{P_0}\right)^{\frac{1}{5}}\cdot t_j^{2/5}$$

We should point out that value αL corresponds to the maximum diameter of the region of the optical breakdown.

The experimental data may be approximated by the following expressions:
One-mode radiation P_0=1atm, α=0.1:

$$L=2.2Q^{1/2}\ [\text{cm}]\quad d_p=0.6Q^{0.77}.$$

Multi-mode radiation P_0=0.05÷1atm, α=0.03÷0.1

$$L=1.6\cdot Q^{0.4}/P_0^{0.1},\ d_p=0.66\cdot Q^{0.45},$$

$$Q_0=0.3/P_0^{0.43}\ [\text{J}].$$

Value d_p corresponds to the luminescence of the expanded laser plasma at t ≅ 20 μs.

So, while forming the channel the following parameters of laser radiation, namely: $Q\cong5$J, $\alpha\cong0.1$, $L\cong5$cm, $Q/L\cong1$J/cm may be considered as the optimal ones. The duration of radiation is to be $t_r\cong1\div2$μs. The optical pulsating discharge moving with velocity V generates a continuous channel of rarefaction in case frequency f and the average power of the pulse-periodic laser radiation satisfy the conditions:

$$f=V/L=0.45V/Q^{\frac{1}{2}}\ [\text{Hz}]\quad W_L=0.45\cdot V\cdot Q^{\frac{1}{2}}\ [\text{W}]$$

Here V [cm/s] and radiation is one-mode.

Supersonic Expansion of Laser Plasma

The main characteristics of this stage are as follows: first $t\cong t_1$ the temperature makes up dozens of thousands of degrees, then at $t=t_2$ supersonic plasma expansion stops by pressure equalization in the cavity and the surrounding gas medium. At $t=t_2$ the shock wave moves away from the cavity boundary. In the cavity the medium density decreases in 10-20 times and the temperature drops according to the measurements [15] up to ~8000K. At this stage the electron concentration is much greater the critical one for the microwave radiation. To construct an approximated model of both channel and LMD (on the whole) it is necessary to know the cavity parameters (radius, temperature) at $t=t_2$.

The dependence of these values upon the parameters of medium and laser radiation can be obtained in the approximation of strong cylindrical explosion. At $t\leq t_1$ the relation of the maximum diameter of the optical breakdown to the length is small; $2r_1/L=\alpha\leq0.1$.

In the optical discharge the density of the absorbed energy calculated for one particle of the initial gas (ignoring dissociation and other chemical reactions) equals:

$$U=\frac{Q}{KN_0\omega}$$

where $k\cong1.38\ 10^{23}$J/deg. and the volume of the optical discharge (of a conical shape) is equal to:

$$\omega\approx\frac{1}{3}\pi r_1^2 L\ [\text{cm}^{-3}]$$

Expressing r_1 in terms of L and α we obtain:

$$U=\frac{2.54\cdot10^{22}}{\alpha^2N_0Q^{0.5}}=\frac{10^3}{\alpha^2P_0Q^{0.5}}\cong4\cdot10^4\text{K}$$

Here U [K], N_0 [cm^{-3}], P_0 [atm].

At α=0.1, $Q\cong5$J and atmospheric pressure we get the value of energy $U\cong4.5\times10^4$K being average in volume that is much larger than the initial energy corresponding to T_0=300K.

A velocity of the shock wave motion D may be deter mined from the relation for a cylindrical point explosion [16]

$$\frac{r}{r^*}=\frac{k_1}{M-1/M},\quad k_1=\left[\frac{(\gamma-1)}{\pi}\right]^{0.5}\cdot\frac{(\gamma+1)}{2\gamma}$$

where $M=D/C_0$ is the Mach number, $r^*=(Q/LP_0)^{1/2}$ is the dynamic length.

Dependence M on r/r^* differs from the experimental data obtained in a wide range of equations ($P_0\cong 0{,}05\div 1$atm.) and radiation energies. This is caused by the fact that the explosion is not point one. The experimental data fall well on one curve. At $r/r^*\geq 0.1$ both experimental M_1 and theoretical M dependencies are linked by the relation $M_1\cong 1.6\cdot M-0.6$. In the range $r/r^*\leq 0.1$ $M>M_1$ as here the shock wave is being formed. At $r/r^*\geq 1$ the shock wave velocity decreases up to $M_1\cong 1.2\div 1.3$ and, besides, the cylindrical shock wave is changing into spherical one.

By time $t\cong t_2$ the pressure of medium in the cavity decreases up to the pressure of undisturbed gas, the *velocity* of the plasma boundary reduces sharply up to several meters per second, the shock wave moves away from the plasma cavity carrying away a major portion of energy.

At $t\cong t_2$ radius of the cavity r_2 may be defined by using the explosion theory:

$$r_2=\frac{1}{2}\left[\frac{120\,(\gamma-1)}{\pi}\frac{\alpha^{2(\gamma-1)}Q}{P_0\,L^{3-2\gamma}}\right]^{\frac{1}{2\lambda}}$$

For dependence $L=2.2\sqrt{Q}/P_0^{0.1}$ we get:

$$r_2=1.1\left[3.6b(\gamma-1)\right]^{1/2\gamma}\cdot\alpha^{1-1/\gamma}\cdot\frac{Q^{\frac{1}{2}(1-1/2\gamma)}}{P^{0.35/\gamma}}$$

Here $b\cong 0.9$ is the coefficient taking into account the energy losses by plasma radiation. Value r_2 is ~20% larger the measured one in papers [11,17] where the energies of the laser radiation were 0.1 and 15J, respectively.

The cavity boundary reaches radius r_2 at the moment $t_2\cong t_1+r_2/2C_0$. For LMD $Q\cong 5$J, radius is ~0.9cm and the duration of the stage of a supersonic expansion makes up ~15-20μs. In the interval $t=t_1\div t_2$ the temperature and the concentration of particles in the cavity decrease up to the values:

$$T_2=\frac{200}{(\gamma-1)^{1-1/\gamma}}\left[\frac{3}{P_0^{0.7}Q^{0.5}\alpha^2}\right]^{\frac{1}{\gamma}}$$

$$N_2=N_0T_0/T_2$$

For the conditions of LMD we get $T_2=8000$K and $N_2\cong 0.04\cdot N_0\cong 10^{18}$cm^{-3}. This value T_2 is close to the measured one in [15] and here the dependence of T_2 on Q has been observed.

At $t\cong t_2$ the shock wave moves away from the cavity boundary carrying away a part of energy:

$$\frac{E_s}{Q}=1-\left[\frac{\pi\alpha^2P_0L^3}{118b(\gamma-1)Q}\right]^{\frac{\gamma-1}{\gamma}}$$

At $\alpha=0.1$, $\gamma=1.18$, $b=0.9$, $L\cong 2.2\cdot\sqrt{Q}/P_0^{0.1}$ we shall obtain

$$E_s/Q=1-0.51Q^{0.075}P_0^{0.1}$$

At $Q\cong 5$J, $P_0=1$atm it follows that the shock wave carries away ~38% of the laser radiation energy absorbed in plasma of the optical breakdown of gas. The experimental value E_s/Q makes up 20÷30 %.

The gas pressure P_s and temperature T_s behind the shock wave front equal:

$$P_s=P_0+2\cdot 10^{-6}\frac{M^2c_0^2\rho_0}{(\lambda+1)}\left(1-\frac{1}{M^2}\right)$$

$$\frac{T_s}{T_0}=\left(\frac{P_s}{P_0}\right)\frac{(\gamma+1)P_0+(\gamma-1)P_s}{(\gamma-1)P_s+(\gamma+1)P_0}$$

Here P_0 [atm], ρ_0 [Gr/cm^3], c_0 [cm/s], $\gamma=1.4$ are the pressure, density, sound velocity of undisturbed gas, respectively. At the characteristic distances from the optical axis r_2 and r^*, values M, T_s/T_0 and P_s have the following meanings:

at $r=r_2$ — M≅2, P_s=4,7 tm., $T_s/T_0\cong 1.72$;

at $r=r^*$ — M= .26, P_s=1.73atm., $T_s/T_0\cong 1{,}.18$.

The experimental values P_s are ~25% less than the calculated ones. Typical value of r^* is 1÷3cm. The duration of a compression phase depends weakly upon r and makes up 15-20μs.

In LMD the shock waves of separate breakdowns generate a common shock wave in the form of a cone the vertex of which is located in the focal point of the laser beam. An angle between axis Z of the optical radiation and the cone formative is determined from the relation $\mathrm{tg}\beta=c_0/V$ (V is the velocity of the focus motion relative to gas).

Isobaric Stage of Laser Plasma Decaying

The given stage begins at $t\geq t_2$. During the period $t_2<t\leq\tau=10\cdot t_3\cong 3$ms in the cavity the temperature falls from $T_2\cong 8000$K up to the temperature of the surrounding gas $T_0\cong 300$ K, and the medium density increases. The main mechanism of cooling is a turbulent heat transfer. This

phenomenon is known from the papers on the recovery of electrical strength of the spark gaps. The turbulence of the medium of the optical breakdown has been observed or investigated only in a few papers, performed under substantially different conditions.

Schematically we may recognize 2 modes: 1- a convective motion of medium with the characteristic size of inhomogeneity close to the cavity diameter [25]; 2- only small-scale (δ~2mm) inhomogeneities (vortex structures) are being formed [17,18]. In [11,13,18] one can see the shadow pictures of density made at different times of exposition $t_f \cong 0.01 \div 0.05$; $1 \div 5\mu s$ and at continuous exposure as well. In the pictures the small -scale structure hasn't been registered in the third case. Consequently, the characteristic value of the velocity of travel of inhomogeneities makes up $V_G \cong \delta / t_f \cong 500$ m/s. In this case the Peckle number is estimated as P_e=30. The small-scale structure of density was observed both at $t \cong t_1 \cong 2\mu s$ and within the large time >3ms when the averaged values of the temperature and density of medium in the cavity had been equalized with the surrounding gas.

The turbulence of the optical pulsating discharge burning before a supersonic body can affect its aerodynamic properties, namely: it limits the length of the rarefaction channel and turbulent an incoming flow. In the known papers on the control over the body flow this phenomenon hasn't been considered [2-6].

The isobaric stage of decaying is the most complicated for a precise theoretical description. At the medium cooling from 8000K up to 1000K intricate physical-chemical and gas-dynamic processes are taking place. But for the estimation of the discharge energetic we can use the empirical relations based on the measurement of the effective time t_3 of the medium cooling of isolated breakdown. In this case by t_3 we take into account not only cooling at turbulent mixing but also heating of medium as a result of the chemical reactions and transferring the energy of the turbulent motion into heat. In [15] t_3 and the effective temperature conductivity φ were determined by the measurements of temperature $T(t)$ of the cavity. In the formula $\varphi = \lambda / C_p \cdot \rho$ such parameters as the coefficient of heat conduction, heat capacity C_p and density ρ of the medium in the channel are taken into account. In [17] t_3 and φ have been obtained from the shadow measurements of the characteristic cavity radius $R_c(t)$ and with using the relation for R_c:

$$R_c(t) = r_2 \left[1 + (t - t_2)/t_3\right]^{-} \equiv r_2 \cdot \psi^{-}$$

which is in a good agreement with the experimental data. In the experiment [17] on the measured r_2, t_2, R_c (t) the effective time t_3 has been found which according to [15] is in agreement with the decrease of temperature in ~2 times as compared to T_2.

In the air $t_3 = 1.74 \cdot 10^{-4} \cdot Q^{0.25}$s and in the argon $t_3 \cong 1.63 \cdot 10^{-4} \cdot (Q/L)^{1/2}$ (the pressure is close to the atmospheric one). The effective temperature conductivity is connected with t_3 by the relation:

$$\varphi = r_2^2 / 4t_3$$

The dynamics of a cylinder cooling can be obtained from the simplified model (as in the case [15]) solving the equation of heat conduction with φ obtained by the method mentioned above. The solution can be represented in the form:

$$T(R,t) = T(t_2) \cdot \psi^{-1} \exp\left(-1.75\left(\frac{r}{R_c}\right)^2\right)$$

The concentration of particles in the cavity is taken from the condition of equality of pressures and is equal to $N = N_0 T_0 / T$.

The concentration of ions may be determined from tables in [19] or approximately from the Saha equation:

$$n_e = 6.3 \cdot 10^9 \left(N_0 T_0 G_+ / G_a\right)^{\frac{1}{2}} \left(\frac{T_2}{\psi}\right)^{\frac{1}{4}} \times$$

$$\times \exp\left[-0.44 (r/R_c)^2 - I/2T\right]$$

These expressions determine the cavity radius, the temperature, density of molecules (atoms) and electrons in it. Substituting t for Z/V we may get the distribution of the given parameters along the channel being formed at pulse-periodic optical breakdown of medium. Length L_c of a continuous channel is defined by temporary cooling t_3 and the velocity of travel of LMD relative to the gas: $L_c = V \cdot (t_2 + 10 \cdot t_3)$, with his plasma part having length $L_p = V \cdot (t_2 + t_3)$,. At $0 < Z < L_p$ the temperature is larger than $4000K^0$ and the concentration of ions is 10^{16}cm^{-3}. Dependence of t_2 and t_3 upon the laser radiation energy is presented above.

If it is necessary to have the channel of L_c length than the pulse repetition frequency of the laser radiation and the average power have to satisfy the following requirements:

$$f = 3.8 \cdot 10^{-7} \frac{V^{3.2}}{L_c^{2.2}} \text{ [Hz]}$$

$$W_L = 4.2 \cdot 10^4 \frac{L_c^{1.8}}{V^{0.8}} \text{ [W]}$$

Here V [cm/s], L_c [cm].

Thus, the laser radiation may form the channel with low concentration of particles $N/N_0 \leq 0.1$, high temperature ~5000K. The channel length may be of several meters and the diameter -not less than 10cm.

A microwave discharge in laser plasma

The microwave discharge in the channel is possible and energetically more effective on the right branch of the microwave analogue of the Pashen curve at gas concentration exceeding in an order of magnitude the value corresponding to the curve minimum. The microwave discharge is located in the channel under the following conditions: a self-maintained, low-threshold discharge (the velocity of its front is $\sim 10^4 \div 10^5$cm/s) is not propagated opposite the beam, that is, the pulse duration must be $\leq 5\mu s$. The pulse intensity is lower the threshold of the gas breakdown outside the cavity but is sufficient for the breakdown of medium in the channel at $L_p < Z < L_c$. Pulse repetition frequency $f_2 \leq 30$kHz is limited by the requirement of the channel transparency for the passing laser radiation. In the plasma part of the channel $Z \leq L_p$ both a semi-self-maintained discharge and a self-maintained discharge of the diffuse type [17] are possible. At $L_p < Z < L_c$ the plasma concentration is much less the critical one for the microwaves of the centimeter range $\lambda \cong 2$-5cm. Here only the self-maintained discharge of the diffusion or spark type (depending on the field intensity in the channel) is possible. Pulse-periodic microwave radiation is focused by an axicone along the total length of the channel L_c. In this case the average power of the microwave discharge in the channel equals:

$$W' \cong 3.7 \cdot 10^{-3} \eta V J \tau f_2 Q^{\frac{1}{2}} \text{ [W]}$$

Here J, τ, f_2 are the intensity on the surface of the channel, duration and pulse repetition frequency, respectively and $\eta \cong 0.7$ is the efficiency of absorption. The radiation energy of one pulse is $Q' = 3.7 \cdot 10^{-3} V J \tau \sqrt{Q}$ [J]. The energetic efficiency of the laser-microwave discharge may be characterized by the relation of W' to the average power of laser radiation required for the channel formation $W'/W_L \cong 8.2 \cdot 10^{-3} \eta J \tau f_2$. At the atmospheric pressure of gas $J = (1 \div 2) \cdot 10^4$W/cm^2. Value W' is limited by the channel length. To remove this limitation it is necessary to stabilize the temperature in the channel at $Z \geq L_p$ at the optimal for the absorption level $T \cong 4500$K (depending on λ and frequency of the collision of electrons with gas molecules). It is possible if the energy supply of the microwave radiation compensates the turbulent cooling of the channel. The average power absorbed per a unit of the channel length is to be $W'' \geq 4 \cdot 10^3 Q^{1/4}$ W/cm, length (along Z) of the energy supply of the microwave beam is $L_b = 2.5 \cdot 10^{-4} W' / Q^{1/4}$ [cm] (W' is the required LMD power). In paper [17, 18] the experimental results on the microwave discharge in decaying laser plasma in the air and argon are presented.

Let us estimate the conditions at which LMD may be efficiently used for the control over the flight of a supersonic body. Let us assume that in the atmosphere is moving a body with diameter d and velocity V and at a small angle of attack. From the theoretical works it follows that for the decreasing the aerodynamic resistance of body it is necessary to form a channel with lower density of gas or a powerful heat source at some distance from the body [1–6]. Its optimal length L may be connected with diameter d-L=k d, where k=2-3. As the condition of efficiency of the method let us assume that the energy of radiation is small as compared to the kinetic energy of the gas flow passing through the cross-section that is equal to the cross-section of the body $\pi d^2/4$. While using only laser radiation the velocity V must satisfy the condition:

$$V \geq \frac{1500 \cdot k^{0.47}}{(b \cdot \rho_0)^{0.26} \cdot d^{0.053}}$$

where ρ_0 is the gas density in the flow, b is the relationship of powers of laser radiation and the flow. Value b must be small ~0.001. Consequently, the Mach number must be sufficiently large M>3. At d>1.5m the requirements for the laser radiation are realized with difficulty. In this case a laser-microwave discharge is required with the body velocity being equal to:

$$V \geq 5000 \cdot \left(\frac{k}{b \cdot d \cdot \rho_0} \right)^{0.} \approx 10^5 \text{ cm/s}$$

Here $b \approx 10$ and equals the relationship of LMD power to the power of the flow.

VI. Laboratory Simulation of LMD

In the model and in the experiment [14,17,18] the dynamics of the processes in laser-produced plasma of a single optical breakdown was under investigation. The distribution of the parameters in a LMD $Y(Z)$ channel was obtained by changing $t = Z/V$ from the measured dependence $Y(t)$. This

holds true at the channel radius $r_k << L$, when heat and mass transfer in Z is small as compared with radial processes (UV, convective mixing of gas). By experiment we determined the parameters of the channel and laser radiation, which are optimal for the LMD initiation and investigated a SHF discharge localized in decaying laser-produced plasma. The scheme of the experiment is partially shown in Fig.2.

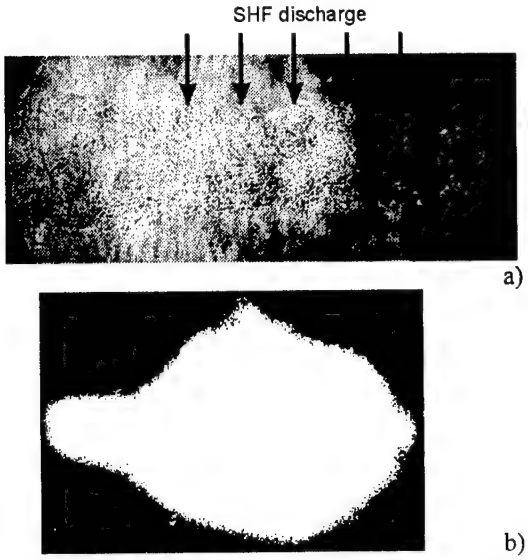

Fig.2. A shadow picture of the channel of optical breakdown at t=100μs (a) and SHF discharge in the channel (b) at delay time t_1=20μs, argon, Q=15J.

An optical breakdown in air or argon (P=1atm) was generated by a pulse of the CO_2 -laser with energy Q=0-20J and duration t_i~0.2-1.5μs. Four SHF pulses with the following parameters: λ≅3cm, peak power ~100kW, pulse duration ~2μs, repetition interval ~25μs were introduced into the laser-produced plasma. Laser-produced plasma was generated in the focal plane of the SHF beam (E=1.5kV/cm, diameter ~λ) or at the distance ~1.5cm from the open wave guide (SHF=E=3kV/cm) isolated from the plasma by a thin dielectric (<<λ). Delay time t_1 of SHF beams with respect to the initiation of the optical breakdown, energy, focusing angle α and the structure of a laser radiation field varied. We measured the parameters of laser and SHF pulses, radii of both UV and channel, the gas density structure (shadow photography, a piezoprobe), plasma luminescence of the optical breakdown and SHF discharge (gated imager and the picture being integral in time). In Fig.3 showing the energy expenses of laser radiation for the creation of the channel one can see Q-dependencies of the values of the maximum diameter of luminescence of the optical breakdown d_p (2) and average energy value $q=Q/L_1$ (1.3) being absorbed at a unit of the breakdown length (1- α≅0.1; 3- α=0.03). Here length $L_1 \sim \sqrt{Q}$ changed in the range L_1=1-30cm. In Fig.4 we present radii of UV and channel (▲ - α=0.1, • - α=0.03 air; ■ - α=0.1, Ar). $R(t)$, $q(Q)$, $L(Q)$ are necessary for the calculation of the length and radius of the channel, temperature, density and conductivity, repetition frequency and average power of the laser radiation.

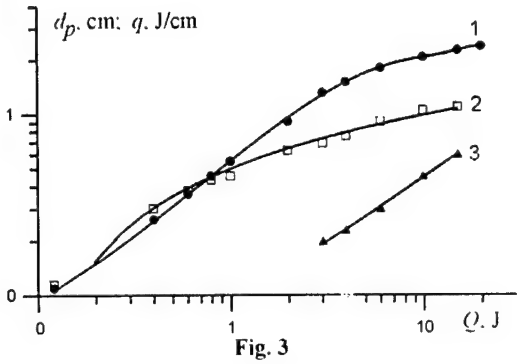

Fig. 3

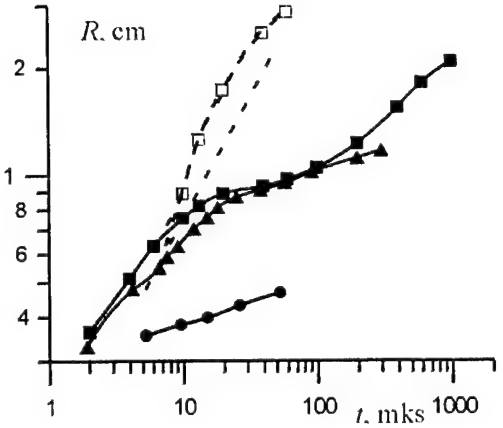

Fig. 4

In Fig.2 one can see a typical form of the density structure in the channel (a) and luminescence of SHF discharge in it under different conditions. In the measurement range of t=0.002-2μs inhomogeneity of the laser-produced plasma with characteristic scale δ~0.3cm was observed. A turbulent medium in the channel causes its cooling at characteristic time τ=0.2-0.35μs (q=0.8-1.5J/cm) that, in its turn, limits the channel length to value $L=10\tau V$≅300cm.

It is obvious that the average power of laser radiation necessary for the «burning

through» the channel in gas equals $W_L=q\,V$. Value q must not be too small because $\tau\sim q$ and $r_k\sim q$, and both τ and r_k define the channel length and efficiency of the interaction of microwave radiation with the channel. So in [11,13] a channel in a supersonic flow was formed at $q\sim 0.1$J/cm. Here $\delta\sim r_k$ that, judging by the shadow pictures, caused fast decaying of the channel. The energy expenses for the «burning through» the channel in LMD must be equal to q=1J/cm and repetition frequency of the laser pulses $f<1/\tau_a$ (τ_a=10μs is the time of adiabatic expansion of dense laser plasma). Optimal radiation energy is in the range Q=5-20J. At small focusing angles α and large Q the optical breakdown consists of separate plasma formations, the uniform structure of which can also absorb SHF radiation.

In LMD channel in axis Z (Z=0 is a laser beam focus) we may distinguish three areas. In $0<Z<Z_1=V\tau<30$cm the gas temperature makes up $8000>T>3500$K, and concentration of electrons maintains the effective absorption of SHF under the conditions of a semi-self-maintained discharge. The discharge is of diffusion structure. At $Z_1<Z<Z_2=KV\tau$ only a self-sustained SHF discharge is possible. The measured value $K\sim$6-10 and discharge structure (spark or diffusion one) depend upon the intensity of SHF field in the channel. SHF discharge in the range $Z>Z_2$ may exist if the cooling in the channel is compensated by SHF heating. Thus, LMD may be efficient for the formation of extended plasma channels moving in the atmosphere. Higher power of radiation is necessary.

VII. A High-Power Optical Pulsating Discharge (HPOPD) in a Supersonic Flow

In 1992 on the initiative of A.G.Ponomarenko (Institute of Laser Physics) and P.K.Tretyakov (Institute of Theoretical and Applied Mechanics) in the frame of the "Planet" program and at the laser-technological set-up of the Institute of Laser Physics we initiated the joint experiments on verification of using laser-produced plasma for the control over the flight of bodies moving at a supersonic velocity. By that time in a number of works a feasibility for the control over the flight of a high-speed body had been shown (decreasing the resistance, formation of the side forces) by the formation of a heat source in front of it [2] or a narrow channel with low density of gas [3] or an air needle being generated by a high-power optical discharge [5]. In method [3] while «burning through» the channel a mass removal is negligible as compared to the mass of the incident flow or the mass being removed by shock waves or at flow over the heat source in methods [2, 5]. The channel was suggested to burn through by a thin laser beam [3] so that to reduce the energy expenses for the control. The authors didn't consider the formation of the channel, a limitation on its length as the result of cooling.

The main problem in using laser radiation lies in the fact that a continuous optical discharge exists in the gas flow with velocity up to several meters per second and the energy of one or tandem laser pulses may be absorbed in the flow at the optical breakdown of gas [20]. But the influence upon the structure of the incident flow must be quasi-stationary and satisfying the conditions of decreasing the aerodynamic resistance of body. In experiments [10, 11] this problem has been solved by using HPOPD in which laser produced plasma exists continuously and the energetic influence is quasi-continuous in a gas –dynamic aspect.

A scheme of the experiment. The CO_2-laser ($\lambda\cong$10.6μm) with the average power up to ~2.5kW was used. At constant pumping power of the active medium by the electric discharge an optical resonator allowed us to generate continuous or pulse-periodic radiation with duration of separate pulses ~1.5μs. In the experiments the repetition frequency changed in the range f=10-100kHz at the fixed power of the electric discharge. Besides the energetic parameters of the output radiation could change (see below). As a threshold of HPOPD existence in air exceeds the power of our laser in several times, the radiation was focused at the argon jet axis having the following parameters: diameter ~2cm, velocity up to ~500m/s and the density was a bit less than 1.6kg/m^3 .The axes of the beam and jet coincided and the radiation propagated downstream. If the radiation power exceeded a threshold value, then an optical discharge pulsating with laser pulse repetition frequency was being formed in the jet. We measured the following parameters of laser radiation: incident, reflected and scattered radiation, the radiation passed through plasma and intrinsic radiation of plasma as well.

Results of the Measurements

HPOPD was being formed if the average and pulse powers of radiation exceeded the threshold values depending upon the velocity of flow and laser pulse repetition frequency. At $V\sim$400m/s depending upon f=12.6, 25, 32, 50, 78. 100kHz the value of threshold average power W takes the following meanings of W_*=480, 790, 940, 1100, 1190, 1390W. Burning HPOPD decayed at the

value of power being less than W_s by ~10–20%. The increase of W_s depends upon the fact that with increase of f both peak power and laser pulse energy decrease. Simultaneously at repetition frequency f~12–100kHz the decrease of threshold peak intensity from 300 up to 100MW/cm^2 was observed. The following processes may be considered as possible mechanisms of such HPOPD effect, they are: ionization of the incident flow by proper radiation of plasma and the location of the focal area of laser radiation at the moment of breakdowns in the region of gas pressing by a shock wave from the previous pulse (threshold intensity is known to be decreased with the increase of density).

Laser radiation power absorbed in HPOPD also depends upon repetition frequency f and at f=12.6, 25, 32, 50, 100kHz makes up ~75, 75, 64, 60% of the incident radiation power. The measurements of the forms of both incident and passed through HPOPD pulses have shown that with increase of f delay time of the optical breakdowns with respect to the initiation of laser pulses increases. As a result, the energy of the front part of pulses passes through HPOPD, being weakly absorbed in decaying plasma (from the previous breakdowns) which is drifted downstream. A part of the absorbed energy may be increased up to ~95% with laser radiation power exceeding repeatedly the threshold of HPOPD initiation. As the measurements have shown, the part of power being lost for the reflection from HPOPD is negligible in its energy balance.

At high repetition frequency $f>V/L$>50kHz the effects of quasistationarity of HPOPD and its gas-dynamic influence upon the flow have been observed. In a time between the pulses the power of proper radiation of plasma decreases by an order of magnitude and not more as well as a continuous channel with low density of gas (~0.1 of the undisturbed density) and high temperature is being formed. In Fig.5 one can see a shadow picture of the density structure in the flow and channel. The channel diameter (~0.3–0.4cm) and the wave structure are in good agreement with the calculations presented above and an approximate model.

The gas density in the channel is highly inhomogeneous that is a consequence of the influence of two mechanisms [18]: the optical discharge in a mode of the light detonation wave generates turbulent plasma with inhomogeneity scale ~0.1–0.3cm; a part of the energy of heat micro-explosions by the optical breakdowns is removed into the channel. Thus, HPOPD allows us to form the channel with low density which may be used for the HPOPD creation and was used in the experiments on decreasing the aerodynamic resistance of a small-sized body [13].

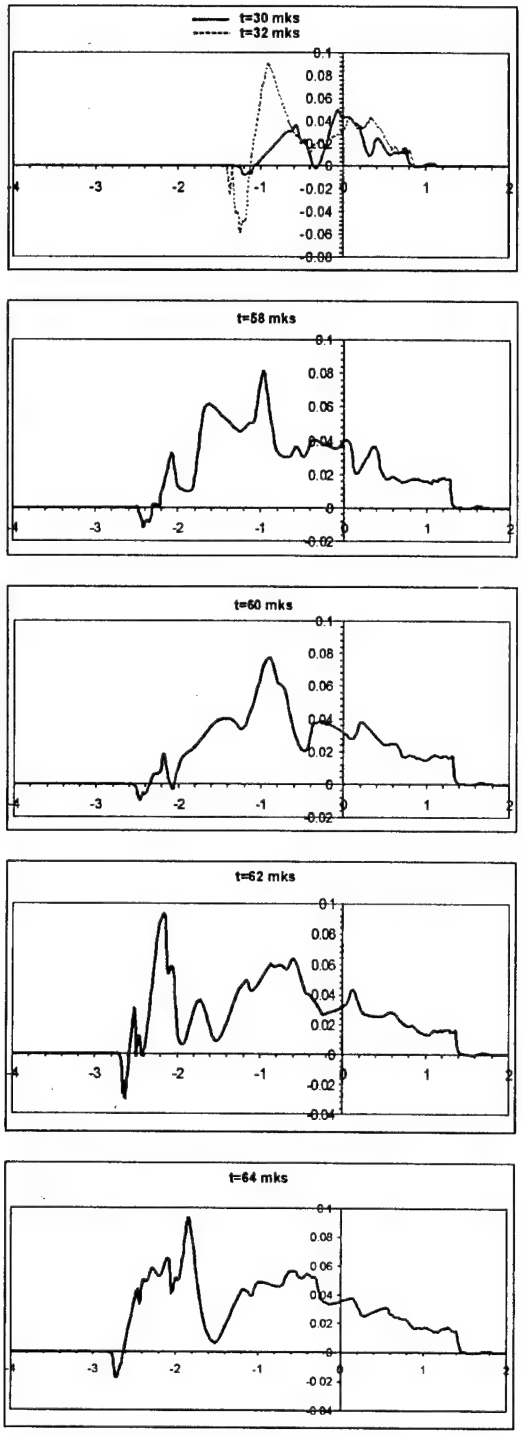

Fig.5. A longitudinal velocity of medium in the channel at different times. Units – Z [cm], V_z [cm/s]

VIII. Numerical Simulation of the Interaction of Radiation with a Supersonic Gas Flow

By present we have performed two-dimensional and three-dimensional calculations of flow over body while supplying energy into the incident gas flow [1-6,20-24]. The aim of our calculations is the development of a model taking into account all the experimental data on the laser and SHF discharges; investigation of the interaction of radiation with the flow at large Mach numbers; transformation of beams' energy into local and non-local gas-dynamic disturbances (out of the region of energy absorption). But at the present stage of investigations the problem of flow over body is not dealt with. The work is being performed in cooperation with the Institute of Theoretical and Applied Mechanics of the Siberian Division of the Russian Academy of Sciences.

It is shown that LMD can generate pulse-periodic shock waves (SW) with controlled amplitude and spectrum. This can be achieved by changing the energy and repetition frequency of SHF beams. The results of these investigations may be a subject-matter of another communication.

We have performed the calculation of HPOPD influence upon the supersonic stream for the conditions of the experiment [11,13]. The numerical simulation was made under the conditions of ideal gas in two-dimensional axisymmetric geometry. The model describes the channel diameter and structure of density in the flow (the location of density jumps).

In [24] it is shown that stationary absorption of laser radiation in the flow may be accompanied by the formation in the channel a high speed gas jet with a smooth velocity profile. Slight inhomogeneity was observed only close to the area of the energy absorption In [6,20,21] the authors calculated the influence of the repetition frequency of the pulse - periodic source upon the aerodynamic resistance of the body and the structure of the incident flow. In [12,23] the parameters of a shock wave (SW) and the radius of the channel with lower density have been approximately determined. And in [12] the evaluations of the channel length in view of its cooling have been made.

The SW under the HPOPD conditions is weak and that's why at a small distance it moves with velocity close to the sound one. We believe that the effect of modulation of a longitudinal plasma velocity at the channel axis is more interesting. In Fig.5 on can see the distribution of axial velocity V_z for different times. The calculation is performed for the following conditions of the experiment: the velocity of gas (Ar) is 425 m/s, laser pulse repetition frequency - f=100kHz. the breakdown length - L=0.3cm, diameter D~0.05cm, the absorbed energy in the pulse is 0.08J, pulse duration t_i~1μs. In the present case value t_i is comparable with characteristics dynamic time ~$D/(2\times C_0)$ (C_0~250m/s is the sound velocity in the flow). For this reason the optical breakdown of gas in HPOPD is not instantaneous. The pictures are given in such a coordinate system in which the flow velocity is V_0=0. The first optical breakdown took place at Z=0. The every next breakdown drifts to the right at the distance $Z_1=V_0/f$ during the pause between the pulses ~$1/f$=10μs. The positive value V_z corresponds to the motion of gas to the right.

From the calculations it follows that a part of energy of the optical breakdowns of gas may be removed into the channel having the diameter ~0.4cm with disturbances moving downstream and being formed in the channel. Their velocity is less than the local sound velocity in the channel. The velocity of a plasma jet (in the given variant) is ~1.5 or 2 times larger than the velocity of the incident flow.

The evident condition $f\times L/V$=1 for the formation of the continuous channel is overrated and may be not optimal in the energetic aspect. In the given calculation at $f\times L/V$=0.7 the join of the areas of the separate breakdowns into the channel occurred as a result of a longitudinal expansion. In some cases the left boundary of the channel could lead the area of energy extraction of separate pulses. The energy absorption in the channel is accompanied by the formation of a strong axial disturbance of the plasma. This mechanism seems to be important and requires an experimental checkout.

References

1. *Chernyi G.G.* The impact of Electromagnetic Energy Addition to Air near the Flying Body on its Aerodynamic Characteristics (Russian Contribution). Published by the American Institute of Aeronautics and Astronautics, 1998.
2. *Georgievsky P.Yu., Levin V.A.* In the Papers of the Institute of Mathematics of the Academy of Sciences of the USSR, 1989, v.186.
3. *Nemchinov I.V., Artem'ev V.I., Bergelson V.I., et al.* Shock Waves, 1994, No.4.
4. *Borzov V.Yu., Rybka I.V., Yuriev A.S.* Engineering and Physical Journal, 1992, v.63, No.6.

5. *Myrabo L.N., Raizer Yu.P.* AIAA Papers 94-2451.
6. *Guvernyuk S.V., Samoilov A.B.* Letters to the Journal of Technical Physics, 1997, v. 23, No.9.
7. *Zarin A.S., Kuzovnikov A.A., Shibkov V.M.* Freely-localized SHF Discharge in Air. "Neftegas", M., 1996.
8. *Zarin A.S., Mitsuk V.E., Petrukhin V.D. et al.* In the Collected Book "Radiophysics" (Scientific-technical Collected Book), Moscow Institute of Radiotechnics, 1991.
9. *Brovkin V.G., Bykov D.V., Golubev S.K. et al.* Journal of Technical Physics, 1991, v.61, No.2.
10. *Tretyakov P.K., Grachev G.N., Ivanchenko A.I. et al.* Reports of the Academy of Sciences, 1994, v.336, No.4.
11. *Grachev G.N., Ponomarenko A.G., Smirnov A.L. et al.* Laser Physics, 1996, v.6, No.2.
12. *Tischenko V.N.* Optics of the Atmosphere and Ocean. 1998, No.2.
13. *Tretyakov P.K., Garanin A.F., Grachev G.N. et al.* Reports of the Academy of Sciences, v.351, No.3.
14. *Ponomarenko A.G., Tischenko V.N., Grachev G.N. et al.* Proceeding Papers of the Conference on Physics of Low-Temperature Plasma, 1998, Petrozavodsk, Russia.
15. *Kabanov S.N., Maslova L.I., Tarkhova T.I. et al.* Journal of Technical Physics, v.60, No.6.
16. *Korobeinikov V.P.* The problems of the Point Explosion Theory. The transactions of the Institute of Mathematics , "Nauka", Moscow, 1973.
17. *Tischenko V.N., Antonov V.M., Melekhov A.V. et al.* Letters to the Journal of Technical Physics, 1996, v.22, No.24.
18. *Tischenko V.N., Antonov V.M., Melekhov A.V. et al.* J. Phys. D: Appl.Phhys., 1998, v.31.
19. *Kuznetsov N.M.* Thermodynamic Functions and Shock Adiabates of Air at High Temperatures, "Mashinostroyenie", Moscow, 1965.
20. *Borzov V.Yu., Mikhailov V.M., Rybka I.V. et al.* Engineering and Physical Journal, 1994, v.66, No.5.
21. *Levin V.A., Afonina N.E., Georgievsky P.Yu. et al.* The influence of the Energy Extraction Source upon the Supersonic Flow over Body. Papers N 36-98, Institute of Mechanics of the Moscow State University, Moscow, 1998.
22. *Korotaeva T.A., Fomin V.M., Shishkin A.I.* Journal of Applied Mechanics and Technical Physics, 1998, v.39, No.5.
23. *Tretyakov P.K., Yakovlev V.I.* Reports of the Academy of Sciences, 1999, v.365, No.1.
24. *Thomas P.D.* AIAA Journal, 1977, v.15, No.10.
25. *Buphetov I.A., Phrohorov A.M., Phedorov V.B. et al.* Annual Reports of Russian Academy of Sciens. 1991, v.261, No.3.

MECHANISMS OF SHOCK WAVE DISPERSION AND ATTENUATION IN WEAKLY IONIZED COLD DISCHARGE PLASMAS

V.Soloviev, V.Krivtsov, and A.Konchakov (Moscow Institute of Physics and Technology)
N.D.Malmuth (Fellow, AIAA, Rockwell Science Center)

Abstract. Both mechanism of shock wave filamentary discharge interaction, and shock wave propagation through transverse temperature non-uniform discharge region are shown to describe available experimental data for shock acceleration and diffusion. A criterion for stable filament formation is obtained for high current discharge giving filament parameters that agree with experimental measurements. 2-D model calculations for the shock propagating through the filamentary discharge give good agreement with experiment for both the shock wave velocity and the shock layer structure. The effect of shock diffusion and attenuation is due to supersonic disturbance propagation from downstream to the upstream region across the shock along the filaments.

Introduction

Shock wave (SW) propagation into weakly ionized plasmas has been investigated for the last 20 years [1-6]. The main features of this phenomenon, such as SW acceleration in a plasma, SW intensity decrease, and dispersion of SW front are still not understood. These phenomena were observed both in atomic (Ar) and molecular (N_2, CO_2, air) gases.

The experimental results were initially simulated analytically as a penetration of a SW into a heated region (thermal model). For a steady state discharge with a gas temperature T of approximately 1500-2000K, this model gave a good approximation of SW speed measurements [7,8] and shock front diffusion [9]. In later experiments, a pulse discharge cold plasma (T_a =350-400K) was examined [3,4]. The SW velocity increase in the plasma region was almost the same as that of a steady state discharge plasma, and it could not be explained by the thermal model.

However the idea that microscale plasma inhomogeneity may play a role was advanced in Russia a long time ago by, for example, Khodotaev and Klimov. Related filamentary discharge structure was observed in microwave (MW) and high frequency (HF) discharges. The calculations for plane SW propagation through a periodic layered structure with hot and cold regions along the SW propagation direction (modeling the filaments) show the SW transformation into a wave packet consisting of shocks and rarefaction waves [10], giving a SW structure resembling that observed in discharge experiments. Supporting calculations using high temperature layers modeling discharge experiments will be reported in [11]. A single streamer interaction with a SW has been modeled and will be reported in [12]. All this research lends credence to the role of streamers in creation of SW precursors and diffusion.

This paper is devoted to experimental results reported in [3,4] and explanation of SW interaction with pulsed discharge cold plasma. First, the situation is analyzed, that SW really propagates through quasi-state discharge plasma with transverse parabolic temperature profile (thermal model).

As an alternative version, a self-consistent, first order physics model for filamentary structure creation in pulsed high current discharge is proposed. The discharge parameters variation due to SW entering a discharge region is investigated numerically, leading to a conclusion, that initial discharge maintenance conditions should be analyzed more carefully to compare theory predictions with experiment. This analysis permits to assume the filamentary structure existence in the discharge under consideration. The criterion for stable high temperature and high ionization degree filament formation is obtained. Estimated filament parameters are close to experimentally observed in MW and HF discharges. The SW interaction with such filamentary discharge structure is analyzed numerically, and the results are compared with experimental data of [3,4].

The foregoing is illustrated by viewgraphs below.

Summary

- Quasi-stable filamentary discharge structure was shown to be possible
- Both filamentary discharge and thermal model give approximately the same shock acceleration coinciding with experimental data
- Calculated shock precursor length agrees with experiment for both thermal and filamentary discharge model

- Pressure jump across the shock and the shape of precursor are different for these models, pressure jump is less for thermal model
- Experimental data available are not sufficient and accurate enough to permit a solid conclusion, what model is more appropriate to describe the experimental results
- Additional experiments should be performed with incident shock wave profile more clear for simulation (like 'piston-driven' shock) to compare the shock attenuation (pressure jump) with experiment
- More careful theoretical analysis and experimental proof for filamentary discharge structure are necessary

Thermal model conclusions

- SW velocity in plasma predictions are in good agreement with experimental data both for 2-D and 1-D calculations.
- Calculated SW layer pressure profile is diffused with precursor length the same as in experiment. The shape of diffused pressure profile differs from experimental one, but this difference could be attributed to not exactly the same temperature over the radius profile compared to experiment.
- SW front curvature predicted is much greater than in experiment ($\Delta x_{sw}/R_d \cong 1$ compared to 0.08 value in experiment, where Δx_{sw} is x coordinate difference for SW position on the tube axis and near the wall, R_d is a tube radius). But there are some doubts the SW front curvature could be measured with accuracy giving $\Delta x_{sw}/R_d \cong 0.08$, because this value corresponds to $\Delta x_{sw} \cong 1.2$mm, and $\Delta \tau_{sw} \cong 1$mcs. However the pressure transducer time accuracy is reported to be around 1mcs.
- Pressure jump through the shock differs from experimental one.
- Thermal model predictions are qualitatively and quantitatively close to experimental data for impulse discharge, if someone does not take into account the details of SW precursor profile

Shock wave discharge region interaction conclusions

- Significant E-field and electron-ion density space redistribution takes place after SW entering discharge region
- This redistribution is sensitive to gas flow parameters behind the SW in all the region between gas-discharge boundary and SW front
- Foregoing leads to more close to experiment SW simulation is necessary to explain the experimental results
- Initial discharge parameters should be analyzed more carefully

References

1. *Klimov A.I., Koblov A.N., Mishin G.I., Serov Yu.L. and Yavor I.P.,* Sov.Tech. Phys.Lett. **8**, 192 (1982).
2. *Klimov A.I., Koblov A.N., Mishin G.I., Serov Yu.L., Khodataev K.V. and Yavor, I.P,* Sov.Tech.Phys.Lett. **8**, 240 (1982).
3. *Gorshkov V.A., Klimov A.I., Mishin G.I., Fedotov A.B. and Yavor I.P.,* Sov.Phys. Tech.Phys. **32**, 1138 (1987).
4. *Klimov A.I., Mishin G.I., Fedotov A.B. and Shakhovatov V.A.,* Sov.Tech. Phys.Lett. **15**, 800 (1989).
5. *Avramenko, R.F., Klimov A.I. and Nikolaeva V.I.,* Journal of Tech.Phys. **63**, 101 (1993) (in Russian), Sov.Phys. Tech.Phys. (1993).
6. *Ganguly B.N., Bletzinger P. and Garscadden A.,* Physics Letters **A 230**, 218 (1997).
7. *Voinovich P.A., Ershov A.P.,* Ponomareva S.E. and Shibkov V.M., High Temp. **29**, 468 (1991).
8. *Naidis G.V. and Rumyantsev S.V.,* High Temp. **25**, 389 (1987).
9. *Macheret S.O., Martinelly L., and Miles R.B.,* 37th AIAA Aerospace Science Meeting and Exhibit, Reno, NV, January 11-14, 1999.
10. *Voinovich P.A., Fursenko A.A., Yuferev C.V.,* Ioffe Physical Technical Institute AS USSR, preprint N1321, Leningrad (1989)
11. *Klimov A.I., Lutskii A.E.,* (to be published)
12. *Bityurin V.A. et al* (to be published)

THERMAL MODEL PREDICTIONS FOR SHOCK WAVE VELOCITY AND PRECURSOR LENGTH ARE IN GOOD AGREEMENT WITH EXPERIMENT

Physical system for calculations

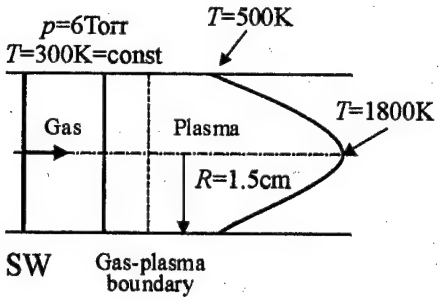

SW velocity versus initial SW velocity dependence

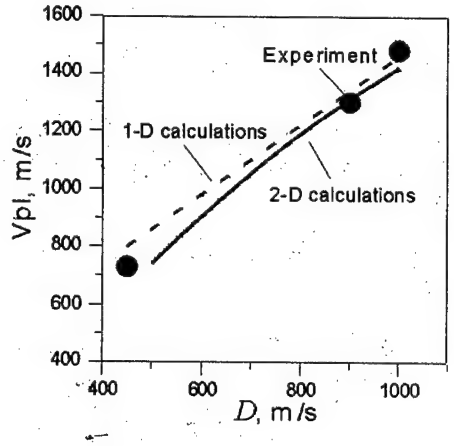

Experiment

SW passed L_{SW}=10cm distance through plasma, D=1000m/s

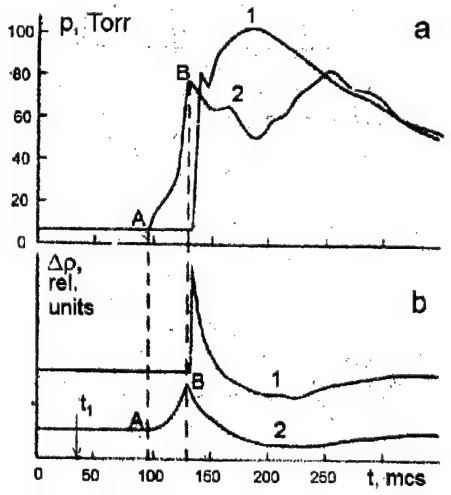

t_1= SW into discharge entrance time, AB=SW precursor, 1-without plasma, 2-with plasma

Theory

Pressure profile on tube axis (2), near the wall (3) for L_{SW}=10cm

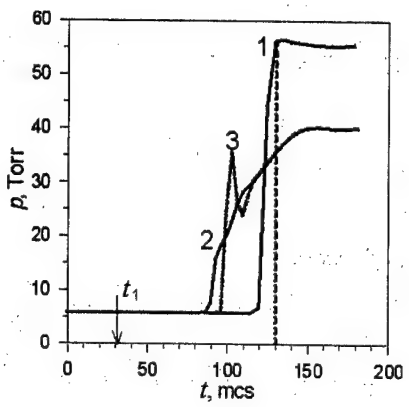

Schlieren signal

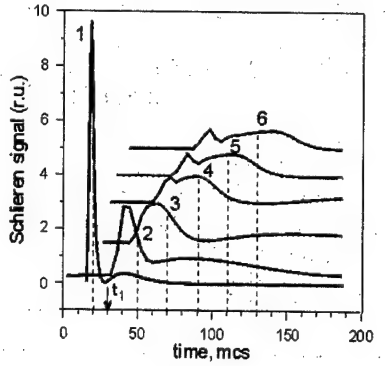

1- Incident SW

2-6 - for L_{SW}=2,4,6,8,10cm respectively

SHOCK WAVE INDUCES A DRAMATIC E-FIELD AND ELECTRON-ION DENSITY SPACE REDISTRIBUTION IN THE DISCHARGE

Physical system sketch

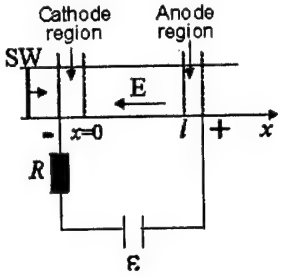

System of equations

$$\frac{\partial n_i}{\partial t}+\frac{\partial}{\partial x}[n_i v+J_i]=k_i(E/N)Nn_e-\alpha_r n_e n_i-\frac{D_a n_i}{\Lambda^2} \qquad J_i=-D_i\frac{\partial n_i}{\partial x}+n_i K_i E,\ \Lambda=R/2.4$$

$$\frac{\partial n_e}{\partial t}+\frac{\partial}{\partial x}[n_e v+J_e]=k_i(E/N)Nn_e-\alpha_r n_e n_i-\frac{D_a n_e}{\Lambda^2} \qquad J_e=-D_e\frac{\partial n_e}{\partial x}+n_e K_e E \qquad \frac{\partial E}{\partial x}=4\pi e(n_i-n_e)$$

E - electric field, k_i, α_r – ionization and recombination rate constants, N, v – gas concentration and velocity defined by SW, D_e, D_i, D_a – electron, ion and ambipolar diffusion coefficients, K_e, K_e – electron and ion mobility, Λ - diffusion length in radial direction, R – tube radius.

DRAFT SOLUTION OF ELECTRON-ION DENSITY AND E-FIELD DISTRIBUTIONS FOR DIFFERENT TIME MOMENTS (SW POSITIONS)

Shock wave structure

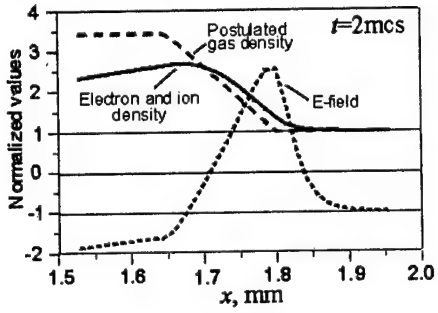

Ion density distribution

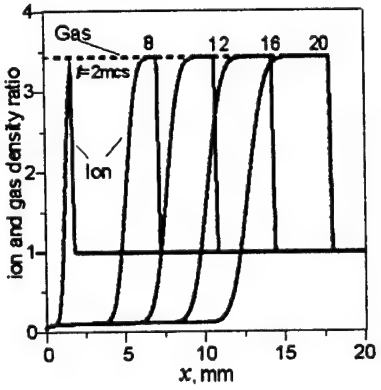

E-field distribution

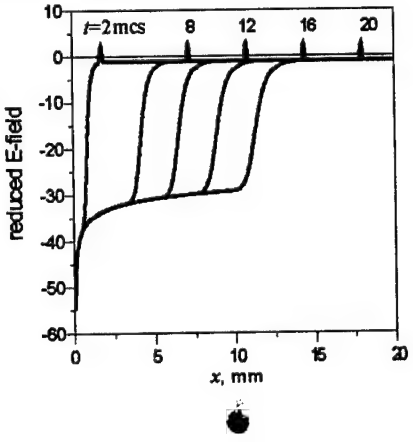

Discharge potential drop

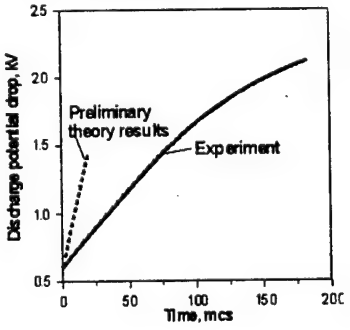

FILAMENTARY DISCHARGE STRUCTURE COULD EXIST TO ENFORCE THE SW DIFFUSION AND ATTENUATION

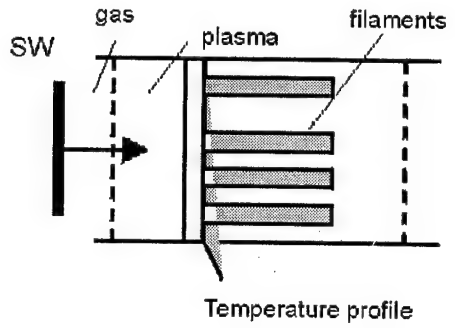

- To obtain the equilibrium between ionization and electron disappearance much higher E/N values are necessary corresponding to filamentary discharge structure
- The temperature in the filaments should be around 1500K leading to density about five times less than average density

Calculated electron appearance and disappearance frequencies for Klimov's experiment conditions

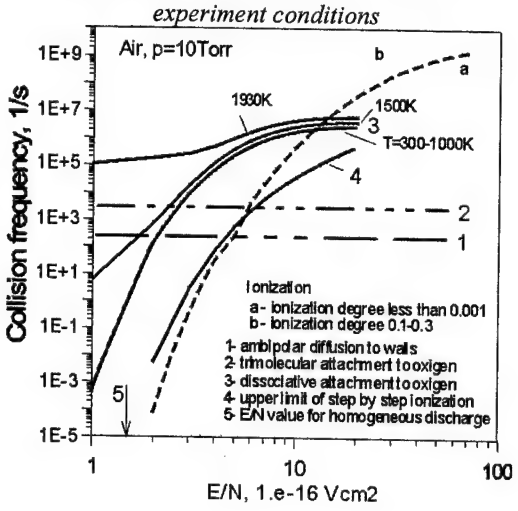

MECHANISM EXISTS STABILIZING HIGHLY IONIZED FILAMENTS FORMATION

Heat balance equation

$$Nc_p\frac{\partial T_f}{\partial t}=\eta^* e n_e v_{dr} E-\frac{8\lambda\left(T_f-T_0\right)}{r_f^2}$$

$$r_f^2=\frac{4D_a}{k_r n_e+0.22N_f k_{at}}$$

Discharge maintenance equation

$$\frac{\partial n_e}{\partial t}=n_e\left(k_i N-0.22N_f k_{at}-k_r n_e\right)$$

Pressure balance equation

$$N_0T_0=N_fT_f+n_eT_e$$

Filament parameters obtained:

E/N=2.7×10^{-15}V·cm^2, T=2900K, T_e=5.24eV, n_e=10^{15}cm^{-3}, α_i=0.062, r_f=0.4mm

The stability criterion

$$\frac{\delta T_f}{T_f}=\left(\frac{x_E}{C_{K_i}}-\alpha_i\frac{T_e}{T_f}\right)\frac{\delta n_e}{n_e},\quad \alpha_i\geq\frac{x_E T_f}{C_{K_i}T_e},$$

$$k_i\sim\exp\left\{-\frac{C_{K_i}}{x_E}\right\},\quad x_E=\frac{E}{N}\,(10^{-16}\text{V}\cdot\text{cm}^2$$

Sound speed inside filament:

$$c_f^2=c_T^2\left(1+\frac{\alpha_i T_e}{\gamma T_f}\right),\qquad c_T^2=\gamma RT_f$$

The region of stable solution

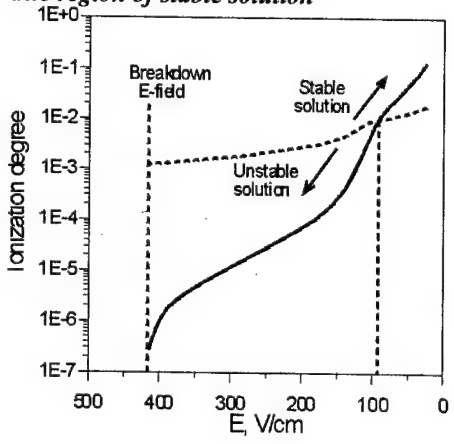

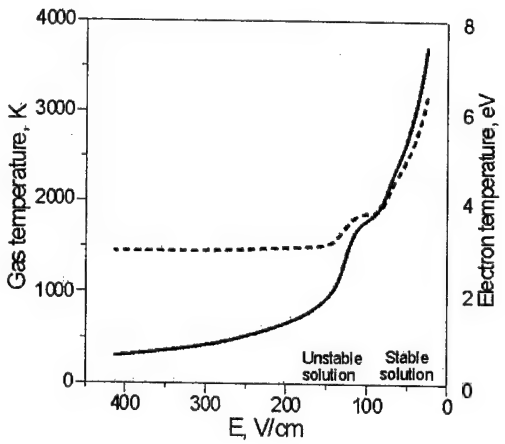

INCLUSION OF STREAMER DISCHARGE STRUCTURE DRAMATICALLY IMPROVES AGREEMENT OF THEORY WITH EXPERIMENT FOR 1-D SHOCK PENETRATING INTO A PLASMA

Physical system

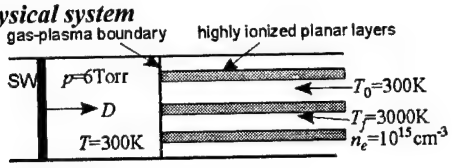

Physical model for SW diffusion and attenuation

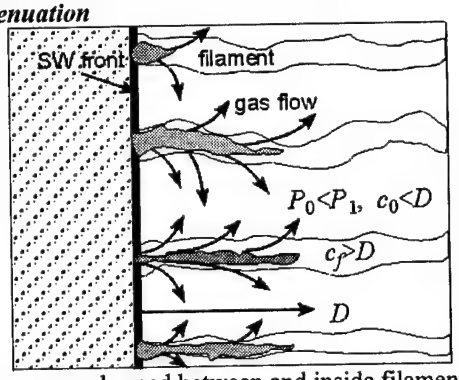

c_0, c_f - sound speed between and inside filaments

The dependence of SW velocity in plasma versus initial SW velocity

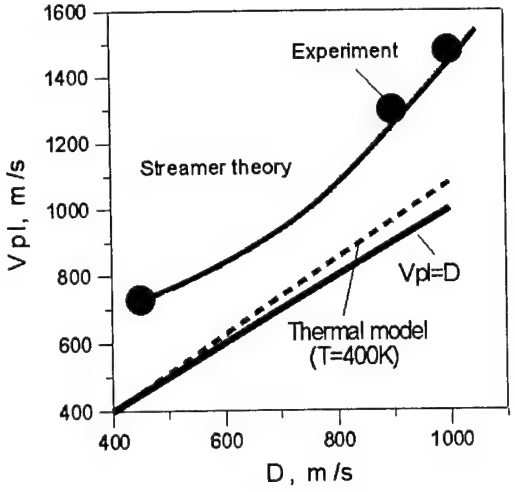

FILAMENTARY DISCHARGE THEORY SW PROFILE PREDICTION IS IN GOOD AGREEMENT WITH EXPERIMENT

Theory

SW pressure profile for L_{SW}=10cm

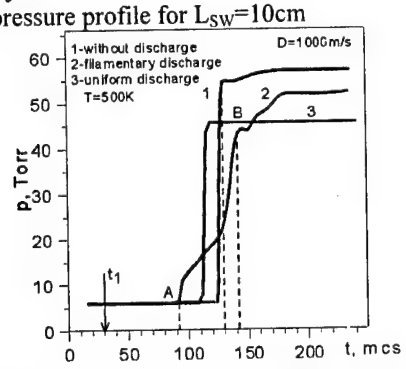

Schlienen signal variation for different distance L_{SW} SW passed through plasma

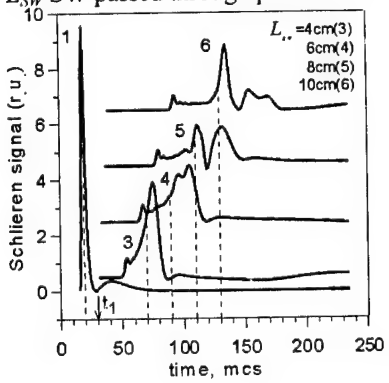

Experiment

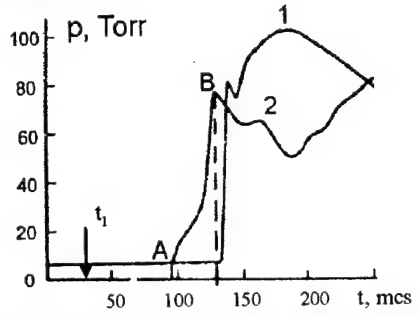

1-without discharge, 2-in filamentary discharge, 3-in uniform discharge with T=500K

Air, p=6Torr, T_{av}=500K, L_{SW}=10cm

t_1 - time moment for SW into plasma entrance.

AB = precursor position.

PLASMA AERODYNAMICS:PROBLEMS AND PHYSICAL MODELS

V.A.Pavlov, U.L.Serov, I.R.Smirnovskiy (Ioffe Physical-Technical Institute RAS, St-Petersburg).

There are several physical models considered by the authors for the explanation of the anomalous hypersonic plasma flow around bodies. The basic experiments carried out at the ballistic tunnel of Ioffe Physical-Technical Institute of Russian Academy of Sciences show that the above mentioned effect has an ion-sonic nature. Experiments were conducted with plasma formations of different characteristic size from 10 till to 50cm. The discharge current cut-off was used to avoid the effects connected with redistribution of the current in a glow discharge while the body moving. Parameters of the discharge - electron temperature and concentration were measured using the method of probes. The temperature of the neutral component was defined with a thermocouple. Experiments show that anomalous head shock wave departure can be observed in intervals of model velocities from V~1200m/s±50m/s up to V~3400m/s that corresponds to the maximum velocity of ion-sonic soliton $V_s = 1{,}6\sqrt{T_e/M_i}$ at the electron temperature T_e=1eV. Velocity of the disturbances propagation in plasma recorded in these experiments varies along with model velocity in the range of ion-sonic soliton as well. Anomalous shock wave departure can be observed in air, nitrogen, argon and xenon. Air admixture addition in barocamera did not exceed 3%. So the anomalous flow can not depend on the vibrational V-T relaxation. Reference experiments without discharge show the agreement of shock wave departure with calculated values by measurement accurate of error 2-3%. Modeling of the body movement in temperature non-uniformity with temperature like in plasma show that non-uniformity of medium temperature can be neglected. Today the theoretical investigation of back influence of the ion-sonic disturbances on neutral component in case of trans-ion-sonic flow around the body is not connected yet. The equations of three component colliding plasma including the non-linearity, dispersion and dissipation were solved. If the local ionic Mach number is introduced as $M_s = |C - V_i|\sqrt{(T_e + T_{i0})/M_i}$, where V_i - velocity of ions, C - body velocity, T_e - electrons temperature in perturbed state than near the body there is an ion-sonic surface M_s=1 separating the area M_s<1 and the area adgacent to the body, where M_s>1 is formed. Behind this surface the formation of the ion shock wave takes place. The local number can reach the value $M_s \approx 1.6$. This is a critical situation: in localized areas instability develops - blow-up of the soliton. As an consequence a hard impaciet on neutrals due to the ion-neutral collisions. This effect is observed obtained in the ballistic experiment on the shadow photos. Calculations using kinetic model show that the change of the discontinuity location the ion-sonic shock wave corresponds to the change of the head shock wave departure with the growth of the body velocity in the experiment. While the ion-sonic head shock wave propagation the kinetic effects can be observed, that can be caused by ions reflected from the potential barrier. As an result of this process the extra-thermal electrons are formed. The electrons are ejected by ion-sonic shock wave, and are recorded at the distance of 10-12 diameters of the model in ballistic experiment. In trans-ion-sonic regime the value of temperature plays a particular role. It establishes under influence of dissipation mechanisms, that form the structure of SW, external sources of nonisothermity and processes near the body surface. Numerical modeling of the scattering of ions on electrons show that regimes when M_s>1 and M_{s0}<0, where M_{s0} – nondisturbed Mach number are possible. Ions reflected from the potential barrier create the "Ion wind" and form the flow of atoms moving from body that changes the aerodynamical drag of the body. The velocity of this flow in the ballistic experiment was 450m/s. So anomalous plasma flow around the body and the decrease of the aerodynamical drag which is connected with this are caused by ion-sonic instability developing in the interval of ionic Mach numbers $1 < M_s < 1.6$.

ANOMALOUS FLOW OVER BODIES BY A MICRO-WAVE PLASMA

A.I.Kanzerov, A.A.Krylov, V.A.Lashkov, I.Tch.Mashek, M.I.Rivkin (St.-Petersburg SU).

Abstract. The outcomes of researches of anomalous flow effects on aerodynamics of blunt bodies in a weakly ionized non-equilibrium supersonic gas stream are given in the report. A micro-wave discharge was used to obtain a plasma. The description of a test bench, system for obtaining micro-wave plasmoids in a supersonic gas stream, as well as characteristic of methods for diagnostic is done. The outcomes of the research display a strong effect of a micro-wave plasma on a change of flow pattern and decreasing of aerodynamic forces acting on streamlined models.

The results of the work carried out by the team of representatives of S.Petersburg State University Institute of Mathematics and Mechanics, S.Petersburg State University Institute of Physics, Department of Physics of S.Petersburg State University, A.F.Ioffe Institute of Physics and Technology, Russian Research Institute of Radio apparature and Moscow Radiotechnical Institute.

The work has been started since the mid of 1997. The goal were to study possibilities of using microwave radiation for obtaining the plasmoids in supersonic air flow and to investigate the effect of plasmoid on aerodynamics of aircraft. To perform the goals the pilot facility has been created in the Gasdynamics Laboratory of S.Petersburg State University Institute of Mathematics and Mechanics consisting of the wind tunnel, microwave and measuring apparature.

1. The layout of the facility is shown in Fig.1. The air flow was generated by means of central supersonic conic nozzle with exit Mach number of 1.5. The outer supersonic nozzle, gas ejector, was set up to obtain the rarefaction in the working chamber. Geometry and parameters of the working jet were determined such that the jet boundary to be enclosed by the inlet part of diffuser. The geometry of the nozzle has been chosen to obtain the maximal rarefaction in the working chamber, namely the pressure level of 0.16-0.20ata. It is known that in the under-expanded jet there is a monotonous increase of gas velocity and decrease of pressure and temperature while gas passes from the nozzle to the Mach disk. In this the gas pressure may become lower than the environmental one. By moving the central nozzle relative to the outer one, one can change the static pressure of the outer media where the working flow is exhausted. The gas flow rate through the central nozzle and the stagnation pressure can be regulated by diaphragm, which cross-section can smoothly vary. With these measures, the following parameters of the working flow have been obtained: static pressure was 60Torr, flow Mach number was 1.5 and stagnation temperature was 200K. The flow field was controlled by virtue of shadow device. The probe tests confirmed that the non-uniformity in the Mach number distribution doesn't exceed 3-4% in the place where the studied models were dislocated.

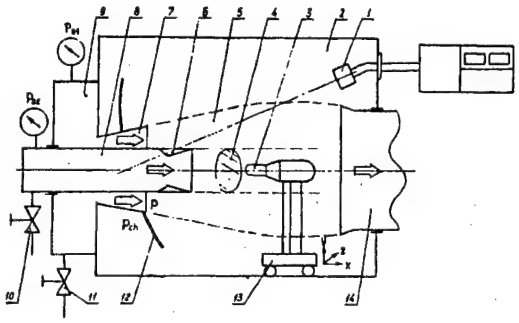

Fig.1

Nomenclature. 1- Radiator; 2- Working chamber; 3- Studied model; 4- Plasmoid; 5- Jet; 6- Working nozzle; 7- Nozzle; 8- Fore-chamber of working flow; 9- Fore-chamber; 10- Locking valve; 11- Valve; 12- Parabolic mirror; 13- Coordinate mechanism; 14- Diffuser; 15- Wave carrier; 16- Microwave generator.

2. The microwave unit is the klystron type generator of high power pulses with the X-range carrying frequency. The microwave pulses come to the mouth-piece radiator of parabolic mirror mounted in the working chamber through the wave carrier. The wave carrier is hermetically sealed, the radiator is closed up by the radio-transparent unit, the air pressure in the wave carrier is maintained at the level 1.8atm. The radiator is fixed just over the diffuser of the wind tunnel. The mirror is maintained on the main nozzle and focuses the microwave radiation on to the flow axis, in the region remote 210-240mm from the nozzle exit. Both position of the central nozzle and the studied models influence the distribution of microwave field in the focal region. The highest pulse power achieved the value of 210kWt. The pulse duration was in

between 1.2-2.2 microseconds. The pulse frequency can be as high as 1.5kHz. The mean power of the microwave facility is 400Wt. The facility can operate with both linear and circular polarization.

3. To investigate the influence of plasmoids on the drag the pressure counters have been used based on the piezoeffect. Two probes have been produced. One as total pressure counter and another - as the static pressure counter. The dimensions and the shape of the counters have been chosen following the recommendations on producing the usual gasdynamic receivers of total and static pressure. Piezoelectric counters were mounted on the total pressure probe and on the cylindrical surface of static pressure counter. The counters were dislocated within the metallic bandage of the probes and were halvanically isolated from them. The signal from counter came to the fore-amplifier, further - to standard U2-9 amplifier and, finally, to the F4226 AZP-device of KAMAK system. The probe gauging tests detected the time resolution as good as 0.5-1.0 microseconds and sensitivity as good as 3mV/torr. To avoid the appearance of discharge on the probe surface special ftoroplast shirts were mounted on the probe, which are the combinations of hemisphere and cylinder. This measure allowed one to control the position of plasmoid relative to probe. The influence of plasmoid on aerodynamic drag could be estimated from data obtained with total pressure probe. The scheme of the probe is given in Fig.2.

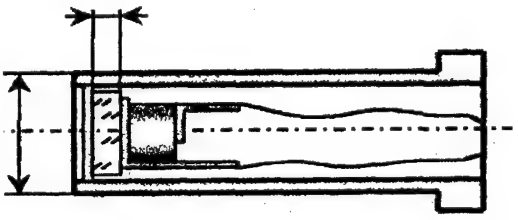

Fig.2

Special microwave/no-flow tests have been made to evaluate the influence of electrical hindrances on the probe operation. It was assumed that this influence was the same during plasmoid-in-flow experiments. In these the following parameters were varied: the distance between plasmoid and the model (total pressure probe) varied in the range 5 -50mm, the microwave power varied from 150 to 195kWt, the pulse duration changed from 1.3 to 2.2 microseconds. The influence of plasmoid on the drag can be seen from Fig.3. The curves on the plot correspond to three values of microwave power, 190, 150 and 130kWt. The pulse duration was 1.65 microseconds and the pulse frequency was 905Hz. The data presented are 10000 trial-averaged that. One can see from the figure that there is jump of the drag just after the microwave pulse. Then drag drops below the value corresponding to that in gas flow. Further, the drag increases. The process takes about 300-350 microseconds. It should be noticed that there are oscillations in drag behavior. The experiments revealed the non-linear influence of microwave power on the drag decrease: the latter is nearly same for 150 and 190kWt microwave power values, whereas the drag decrease effect is weakening for the power value 130kWt. The data presented should be considered as that characterizing the flow around the model and the drag change just qualitatively. Fig.4 shows that both the process phase and and the drag decrease depend on the position of plasmoid in front of the model while the time behaviour of the drag change remains the same.

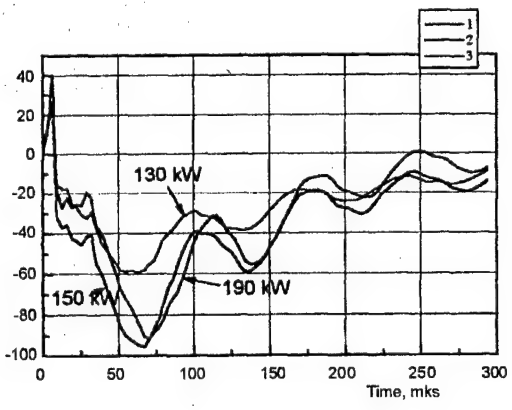

Fig.3

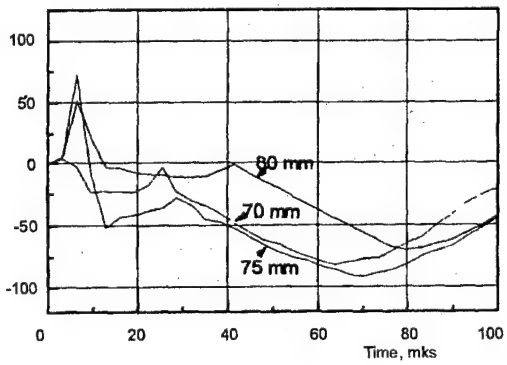

Fig.4

4. To carry out optical studies of influence of pulsed microwave discharge on the supersonic flow around the models experimental facility based on modification of IAB-450 measuring device was used. The facility includes CCD-matrix based TV camera, TV signal processing and fore-amplification complex, video recorder, pulse light feeder, control video monitors and the system for synchronizing, processing and managing experimental data constructed by means of KAMAK modules. TV camera can only register the integral in time the pattern of flow passed through the measuring system and cannot provide the required temporal resolution. In a rather high frequency of event repetitions (1kHz in our case), pulsed lighting of the flow synchronized with the discharge ignition instant and delayed for a fixed time relative to discharge ignition allowed the flow pattern corresponding to selected phase of process to be recorded on the integrating image receiver (CCD-matrix). The change in delay time during experiment allows to make a TV record of unsteady-state flow, the time resolution being determined only by the duration of pulse lighting and by rate of change in delay time. Further data processing is to select the representative pictures from the recorded set, digitize them and numerically process them with computer. Many important modifications have been made to IAB-450 device which allowed to get a good TV camera position and to provide good pulse lighting characteristics.

The experimental setup control panel have been remote from the facility as far as 15m. Fig.5 and Fig.6 represent the typical shadow patterns of flow around the model (hemisphere-cylinder).

They correspond to time moments 2 and 20 microseconds of the shock-layer plasmoid interaction process, respectively. Fig.7 and Fig.8 show the results of reduced-image processing: the optical gradient contours are given in the pictures.

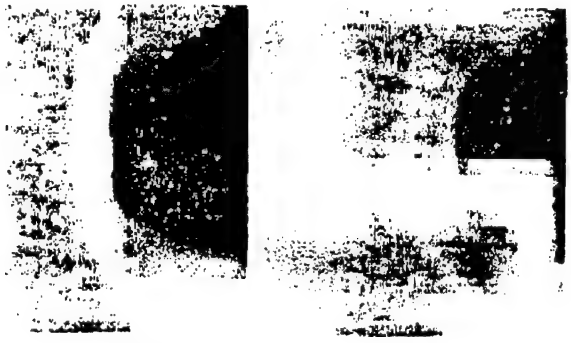

Fig.5 **Fig.6**

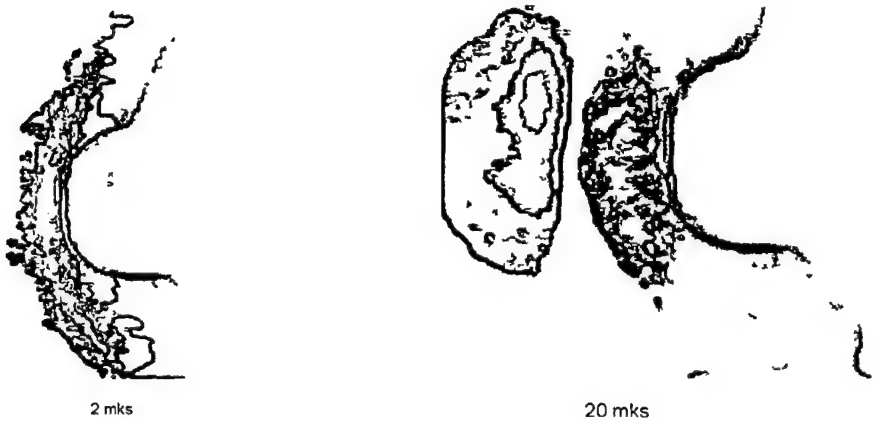

Fig.7 **Fig.8**

It can be concluded from the results that plasmoid significantly changes the thickness of shock layer before the model. The changes in flow pattern have oscillating behavior and oscillations last up to time 300 microseconds. The axial distributions of optical gradient of the density for the same time moments, 2 and 20 microseconds, are shown in Fig.9. The distance to the stagnation point of the model in mm is chosen as abscissa. It is seen that optical gradient of density and the gas density itself significantly vary both in time and space.

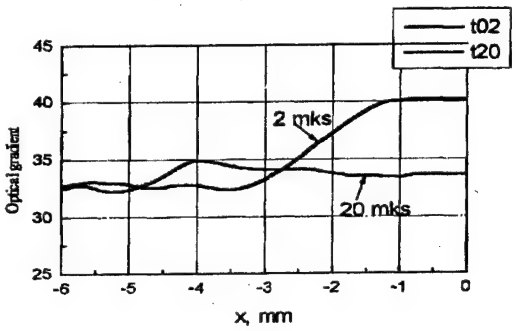

Fig.9

5. Spectral measurements. As the main spectral device for analyzing emission spectra of microwave discharge in a supersonic air jet the spectrometer based on the monochromator MDR has been used. Spectral device has been gauged in the range of wave lengths 300-600nm with a help of Hg-He spectral lamp of type of DRGS-12, worked in standard operation mode. Spectral sensitivity of the device has been gauged in the working wave length range by means of light-measuring lamp SIRSH8,5-200-1 with the color temperature about 3000K. The gauge data obtained allowed not only to calculate the relative spectral sensitivity of the device, but to evaluate its absolute spectral sensitivity in microWt/mV·nm. Fig.10 shows the radiation spectrum of plasmoid in a supersonic air flow.

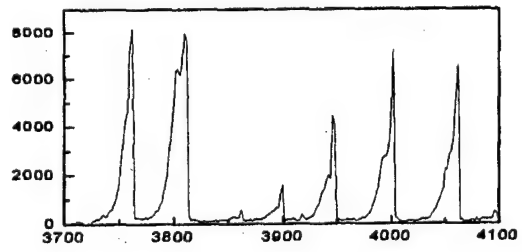

Fig.10

6. Thermal measurements have been fulfilled to observe the thermal aspects of plasma flow. Special temperature probe and measuring complex have been constructed to provide suitable accuracy and reliability of measurements. The scheme of the temperature probe is denoted in Fig.11. It was observed in experiments that the average flow temperature grow doesn't exceed 2-3K (cf. Fig.12) when the plasmoid ignites. The temperature measurements were made for different distances between the probe and nozzle exit. It was revealed that while plasmoid exists the temperature grow decreases with increasing the distance between plasmoid and probe.

Fig.11

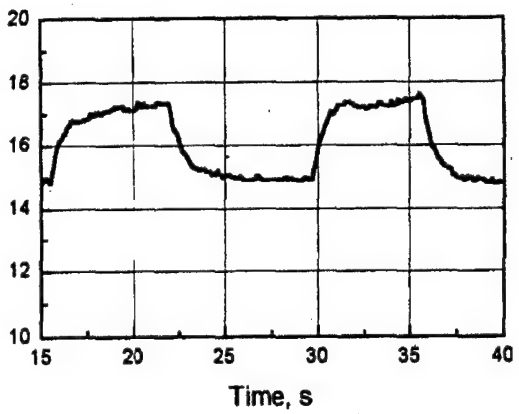

Fig.12

Conclusions

1. The experimental facility was constructed to study the influence of microwave-induced plasma on the characteristics of flow around the blunt body.
2. The plasma region was formed with the microwave generator in a supersonic flow with Mach number 1.5.
3. The measuring complexes were developed both to study the plasma flow characteristics and aerodynamic drag of the body in the flow of microwave-induced low-temperature non-equilibrium plasma.

4. The studies revealed an essential influence of microwave-induced plasma on aerodynamic body drag. It is emphasized that this influence cannot be explained by only thermal treating.
5. Up to date there is no physical model which adequately describes the plasma flow around the body. Therefore, further efforts should be made to investigate the elementary processes in relaxation plasmas.
6. The plasma diagnostics methods should be further improved so that they take into account the plasma relaxation. The accuracy and reliability of pulse pressure technique should be enhanced. Informative abilities of the optical measuring devices should be extended to better register the flow pattern around the body.

Finally, the authors would like to emphasize that the work intended to study effects in low-temperature non-equilibrium plasma flows around the body should be continued for improving the aerodynamic characteristics of aircraft.

WEAKLY-IONIZED GAS FLOWS IN SUPERSONIC INLETS WITH MAGNETIC FIELD

Yu.P.Golovachov, S.Yu.Sushchikh (Ioffe Physical-Technical Institute RAS, St.Petersburg, Russia)

Abstract. The results of calculations of stationary ionized electrically conducting gas flows in supersonic inlets are presented. Numerical simulation is carried out in the framework of magneto-gas dynamics approach using the space-marching high-resolution finite-volume method. The effects of applied magnetic field on the flow structure are investigated for various inlet geometry's, magnetic field orientations, and the values of MGD interaction parameter. The results demonstrate the possibility for flow control by applied magnetic field and provide the estimates for plasma electrical conductivity and magnetic field induction required for efficient flow control.

Introduction

The idea to control the flows of electrically conducting media with applied magnetic field is widely used in various fields of modern technology. The paper estimates the prospects of such mode of control as applied to gas flows in an inlet of supersonic aircraft. Development of a controlled inlet ensuring the rated operating regime with variation of the flight conditions is one of the urgent problems of supersonic and hypersonic aerodynamics. The method for supersonic inlet flow control which is under study in this paper consists in preliminary ionization of incoming flow following by its deceleration by applied magnetic field. To evaluate the prospects of such mode of flow control, electrically conducting gas flows in supersonic inlets are calculated using the simplest physical and gas dynamic models. The results provide the estimates for required plasma and magnetic field parameters.

1. Statement of the problem and numerical method

Under supersonic flight conditions the flows under study can be investigated within the framework of magneto-gas dynamics (MGD) approach, see for instance Mitchner and Kruger (1973). Beside that, one can use the following assumptions

a) $\alpha \ll 1$,

b) $\mathrm{Re} \gg 1$,

c) $\mathrm{Re}_m \ll 1$ (1.1)

where α is the ionization degree, Re is the Reynolds number, Re_m is the magnetic Reynolds number. Assuming (a), one can neglect the ionization effect on thermodynamic properties and regard plasma as one-component perfect gas with constant specific heat ratio. Assumption (b) allows the use of inviscid gas model for non-separated flows, and assumption (c) enables one to neglect the induced magnetic field. The applied magnetic field influences electrically conducting gas flow through the ponderomotive force and Joule heat release which are determined by the following formulae:

$$\vec{F} = \vec{j} \times \vec{B}, \quad Q = \vec{j} \cdot \vec{E} \tag{1.2}$$

where $\vec{j}$ is the electric current density, $\vec{B}$ is the magnetic field induction, E is the electric field tension. The above quantities are related through the generalized Ohm's law:

$$\vec{j} + \mu_e \left(\vec{j} \times \vec{B} \right) = \sigma \left(\vec{E} + \vec{V} \times \vec{B} \right) \tag{1.3}$$

where μ_e is the electron mobility, σ is the electrical conductivity. The magnetic field induction $\vec{B}$ being known, one needs in one more relationship to find the electric current density $\vec{j}$ and the electric field tension $\vec{E}$. In most our calculations the closing relationship is obtained from the fixed value of the external load coefficient, see Mitchner and Kruger (1973). Using the above algebraic model for MGD interaction, the boundary conditions are required only for gas dynamics functions. The results presented below pertain to supersonic flows governed by hyperbolic system of Euler equations. So the initial-boundary value problem is formulated. The initial conditions in the streamwise coordinate are given by oncoming stream parameters. On the inlet walls, normal velocity component is assumed to be equal to zero. Numerical solutions are obtained with the explicit space-marching high-resolution shock-capturing scheme by Rodionov (1989).

2. Results of calculations

The results of calculations pertain to plane flows of a perfect gas with specific heat ratio γ=1.4. Magnetic field is aligned with the z-axis of the Cartesian coordinate system in which the *(x,y)*-plane is that of gas flow. With this direction of the magnetic field induction B the flow under study remains to be two-dimensional and the MGD interaction manifests itself to the most extent.

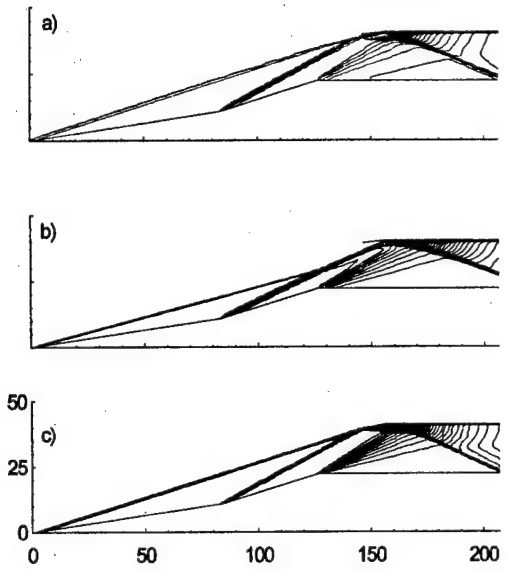

Fig.1. Density contours in supersonic inlet. $\Delta\rho$=1.0

a) M_0=6, S = 0, ρ_{min}=1.1, ρ_{max}=18.1
b) M_0=8, S = 0, ρ_{min}=1.9, ρ_{max}=39.0
c) M_0=8, $S \neq 0$, ρ_{min}=2.1, ρ_{max}=41.1

As an example, Fig.1 shows density isolines in the supersonic inlet which display the flow field structure including the shock waves and expansion fans arising in the wall slope discontinuities. In these calculations only the y-component of the electric field was taken into account, which corresponds approximately to flow in the MGD generator with continuous electrodes. Here $S=\sigma B^2 L/\rho_0 V_0$ is the MGD interaction parameter (Start number), $\beta=\mu_e B$ is Hall parameter, k is the external load coefficient. Figure a) corresponds to the rated operating regime of the intake at Mach number of the incoming flow M_0=6. In this case, the shocks arising in the points of the lower wall discontinuities meet at the intake lip. Figure b) presents the results for non-rated regime with Mach number M_0=8. Figure c) corresponds to the flow at Mach number M_0=8 with applied magnetic field. In the latter case, the Stuart number is taken to be constant S=0.005 when $0 \le x \le 12$, decreasing linearly to zero at $12 \le x \le 22$ and equal to zero when $x \ge 22$; the Hall parameter β=0.1, the load coefficient, k=0.5. The results display a recovery of the flow field structure inhering the rated operating regime of the intake by means of the applied magnetic field.

An inlet is intended to transform total pressure of incoming supersonic stream to static one in front of the combustion chamber at minimum loss. The calculations revealed a significant dependence of the outlet static pressure and Mach number on the electrode commutation. The calculations have been carried out for Faraday generators with continuous and segmented electrodes, and Hall generator. The results indicate that maximum effect is reached with electrode commutation according to the Hall generator scheme. However, the static pressure and Mach number profiles have been found to be most non-uniform in this case.

Conclusion

The results of numerical simulation demonstrate the possibility to control flow structure in supersonic inlets with the applied magnetic field. With length scale L=1cm, magnetic field induction B=2T, incoming stream Mach number M_0=6, and flight altitude H=15km electrical conductivity required for efficient control is estimate to be a few Sm/m .

The work is supported by Russian Fund for Basic Researches (RFBR, grant No-98—01—1121).

References

1. *M. Mitchner,. H. Kruger* // Jr. Partially Ionized Gases J.Wiley & Sons 1973.
2. *A.V. Rodionov* // Zh. Vychisl. Matem.i Fiz. 1989, V.27, No.12, P.1853-1860 (in Russian).

ON AN EXPERIMENTAL SET-UP FOR STUDY OF AERODYNAMICAL PROPERTIES OF BODIES IN A WEAKLY IONIZED PLASMA

V.G. Bondarenko, V.M. Gubchenko, V.P. Denisov, M.L. Khodachenko, A.V. Kozlov, V.E. Semenov
(Institute of Applied Physics, Russian Academy of Sciences, Nizhny Novgorod, Russia)

The effects of influence by means of electrodynamical forces on aerodynamical properties of bodies, submerged in hypersonic gas flows, are of great practical and theoretical interest. The sources of said electrodynamical forces are considered to be placed on/in a hypersonicaly moving body. Such an influence is possible only in a case of an ionized gas flow, when a medium around a moving body is electrically conductive and current-carrying. By this a moving body with a gas ionizing and force producing devices on board includes also a surrounding medium, and appears to be an active and complex object.

With a purpose of laboratory modeling of such effects an experimental set-up was created. The set-up has the following parts. An acceleration tube for experiments with a supersonic flow, it has a diameter 6cm and includes a Lavale nozzle. The nozzle produces a supersonic flow which is consumed in a receiver chamber with a volume $1m^3$. As a source of gas in a first case a chamber with a volume 10^3-10^4cm^3 and regulated pressure is used. Gas expands into a nozzle passing through a tearable membrane after an arch discharge. In a second case gas expansion from a chamber with a volume $5\times10^4cm^3$ and pressure from 0,1 to 5 *atm* is regulated by an electromagnetic valve. The Lavale nozzles used in a set-up have critical crossections 0.16-$30cm^2$ and allow to produce flows with Mach numbers from 0.8 to 7. Characteristic time of the set-up operation is 20-200ms. Gas ionization is produced by a HF induction discharge. The HF generator works at a frequency 10MHz. Power of the generator is 10kW. As a testing body we use a light ball which can easily move along a thin guiding rode.

During our experiments we have got the following parameters of a gas flow. Velocity of a flow is 100-500m/s. Static pressure of a gas in a flow is 1-15Torr, dynamical pressure is 50-200Torr, and plasma density is 10^9-$10^{11}cm^{-3}$ Ionization degree is 10^{-9}-10^{-6}, and concentration of neutrals (gas density) is 10^{16}-$5\times10^{17}cm^{-3}$. Drag force, acting on a testing body in a flow, appeared to be 0.5-5·*N*.

An effect of an aerodynamic drag force decrease up to 1,5 times in a weakly ionized plasma flow was confirmed for ionization degree, varying in limits 10^{-9}-10^{-7}.

Results, obtained on the experimental set-up, indicate a difference of a body and flow interaction in cases of an ionized and non-ionized gas flows. In conditions of a weak ionization the body-flow interaction looks like one in a case of neutral gas. At the same time there exists a certain value of an ionization degree when an effect of decrease of a drag force appeares. This effect could be explained by special properties of an ionized gas.

This work was supported by RFBR (grant No. 97-02-17062).

SIMULATION OF SHOCK WAVE PROPAGATION IN GAS DISCHARGE PLASMA REGIONS

Babaeva N.Yu. and Naidis G.V. (Institute for High Temperatures RAS, Moscow, Russia)

Abstract. Based on numerical simulation the results of shock waves (SW) propagation through gas discharge plasma are presented (wave acceleration, change of the wave front structure, etc.). Experiments show that discharge plasma is mostly (i) non-uniform (ii) non-equilibrium (iii) non-stationary. All the factors influence SW propagation in plasma regions. The most important is usually related with the spatial non-uniformity of the gas density in the discharges due to heating. In molecular gases an additional factor exists: the vibrational-translational non-equilibrium. Both these factors lead to SW acceleration, but their effects on the SW intensity are quite different.

In many experiments on shock waves (SW) propagation through gas discharge plasma some interesting effects have been observed, among them acceleration of the wave in the discharge region, dispersion of its front, formation of precursors, etc. (see [1,2] and references therein). Gas discharge plasma is normally non-uniform, non-equilibrium and non-stationary. For example, in broad range of experimental conditions microwave discharge has a form of successively developing plasma layers with temperature 1000 - 3000K (Fig.1).

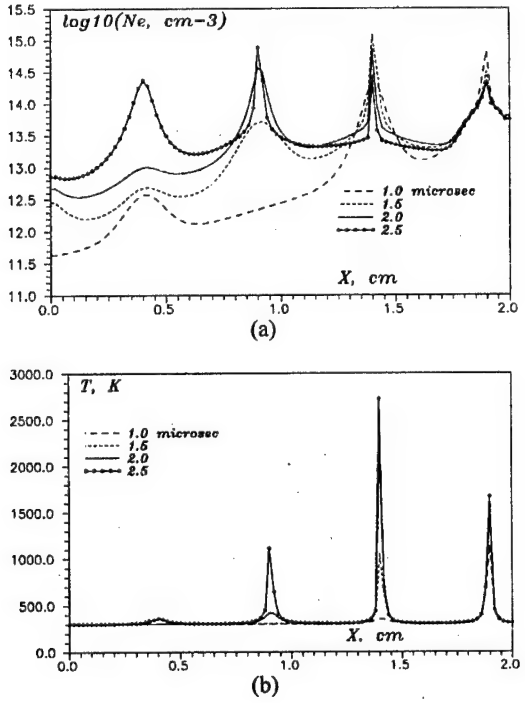

Fig.1. Distribution of electron number density (a) and gas temperature (b) at four successive time moments. Initial conditions are E_0/n=60Td, P=600Torr. Wave length of microwave radiation λ=2cm. Calculations have been performed for strong microwave fields using the discharge model proposed in [3].

When SW propagates in plasma with inhomogeneous gas temperature (and, consequently, gas density) distribution, complicated profiles of pressure and density signals can be recorded behind the SW front. Below the examples are presented on influence of different kinds of inhomogeneity on shock wave structure.

Fig.2 demonstrates the results of 1D modeling of Mach 2 plane wave interaction with thin hot gas layer (specific heat ratio is 1.4). At initial time moment t=0 the SW coordinate is x=0. Pressure is normalized by the value in unperturbed gas. Initial temperature distribution having the Gaussian form with 3000K in maximum is located at a point with x=0.3cm (Fig.2a, curve 1). The hot layer is moved away by the gas flow behind SW front. This is demonstrated by curves 2 and 3 in Fig.2. The "pressure probe" when placed at a point x=0.3cm (that is in density minimum) gives a peculiar record of pressure profile (Fig.2c). In the figure base pressure signal having the form of a plane wave is also presented.

An example of inhomogeneity with more complicated geometry is shown in Fig.3. Mach 2 plane wave propagates through plasma cylinder centered at x=0.3cm, y=0.5cm. Initial temperature is distributed according to the Gaussian law with maximal temperature 3000K. In this case 2D simulations were performed. In Fig.3 the SW front distortion can be seen. The signals from pressure probes set at points A, B and C are given in Fig.3c. The signals depend on the probe coordinate and have rather complicated forms.

In molecular gases the effects connected with vibrational-translational non-equilibrium can play the essential role [4]. In discharges in air a great amount of released energy is stored in vibrations of nitrogen molecules. VT relaxation in dry air is a rather slow process. It can be accelerated by a small amount of admixture (water vapor). The character of SW propagation in non-equilibrium gas is determined by the product of pressure and the dimension of a non-equilibrium region

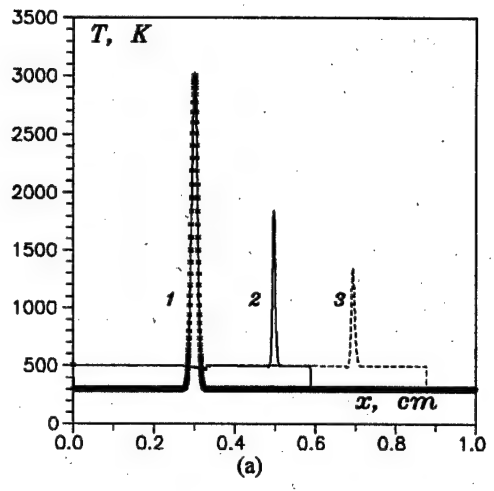

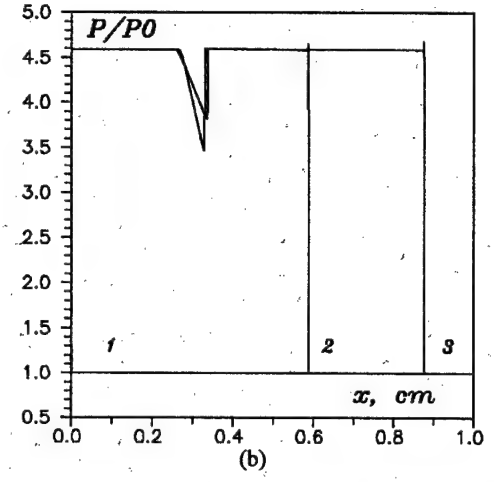

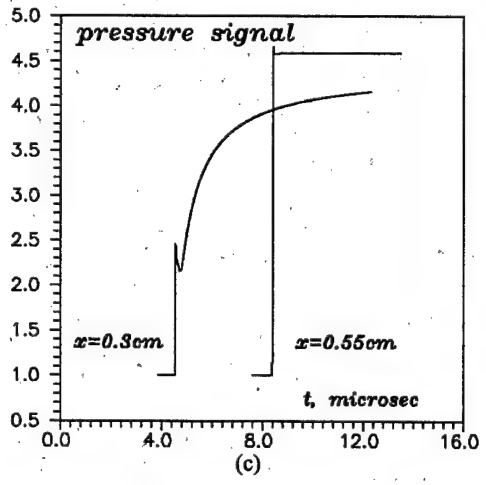

Fig.2. Temperature (a) and pressure (b) profiles at 3 successive time moments $t(\mu s)$: 0 - (1), 9 - (2), 13.5 - (3); (c) - pressure signal

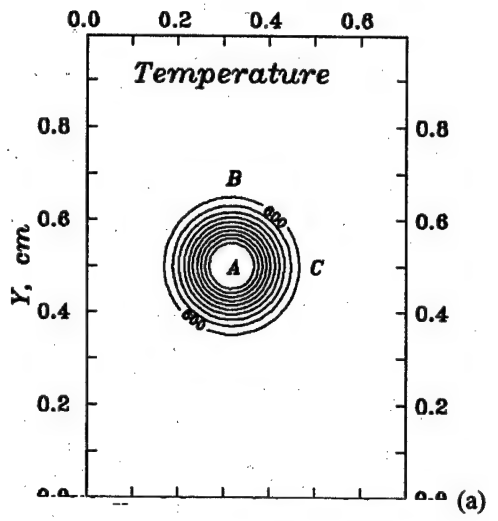

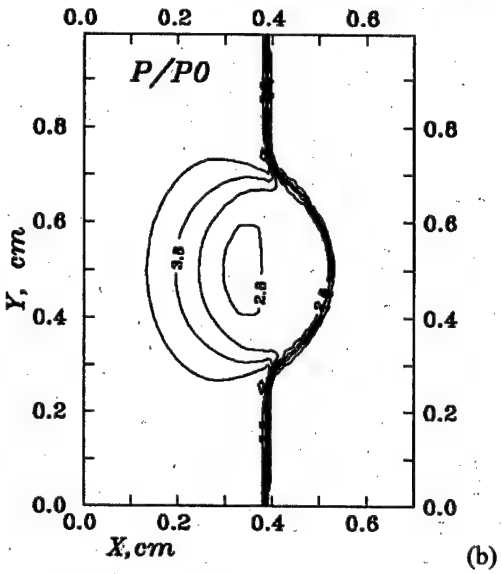

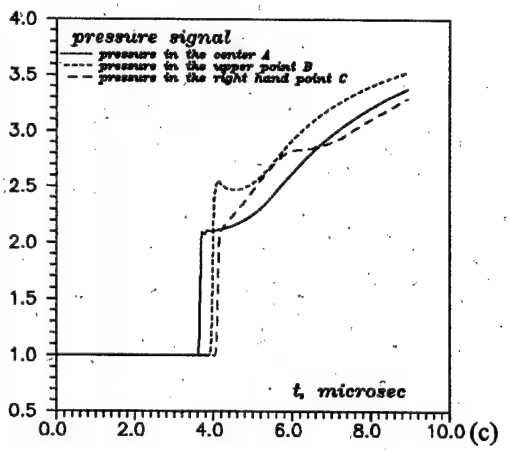

Fig.3. Initial temperature distribution (a); SW position at t=6μs (b); pressure signals from points A, B and C.

Fig.4 demonstrates Mach 2 plane SW propagation in the broad vibrationally non-equilibrium region in air at initial pressure 750 (a,b) and 50 (c) Torr. At high initial pressure rapid relaxation occurs and the detonation peaks appear on pressure profiles (Fig.4b). Fig.4c demonstrates essentially smaller relaxation at 50Torr initial pressure. For narrow vibrationally non-equilibrium gas regions relaxation is not observed even at high pressures (750Torr) and greater percentage of water vapor (Fig.5).

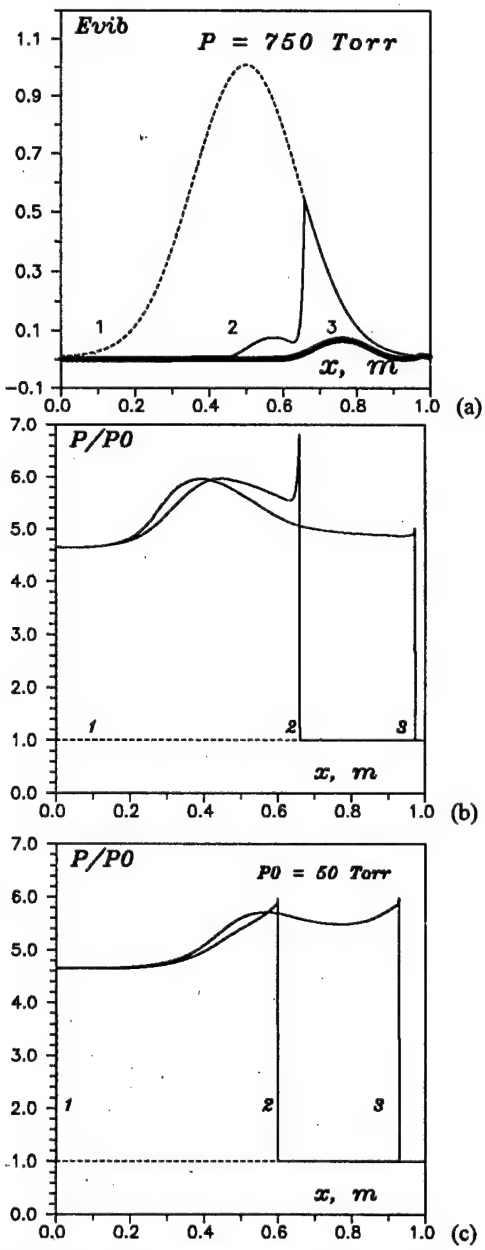

Fig.4. Profiles of vibrational energy (number of quanta per molecule) (a) and pressure (b) at P_0=750Torr, and also at P_0=50Torr (c) at 3 time moments; 1% H_2O.

In molecular gas discharge plasma both above mentioned factors (temperature non-uniformity and vibrational non-equilibrium) may be present simultaneously, and, depending on the discharge conditions, the SW intensity in plasma may be either decreasing or increasing. In Fig.6 pressure profiles are schematically compared behind plane Mach 2 SW propagating in cylindrical regions with Gaussian distributions of vibrational energy (region A, maximal number of vibrational quanta per molecule is 2) and temperature (region C, maximal temperature is 3000K). Pressure probes located at A and C positions show that in both cases SW accelerates (Fig.6c). SW intensity in hot inhomogeneous region C decreases, in contrast to vibrational region A where it increases and the pressure profile has a detonation peak. Base pressure signal for unperturbed gas at point B is also given (Fig.6c)

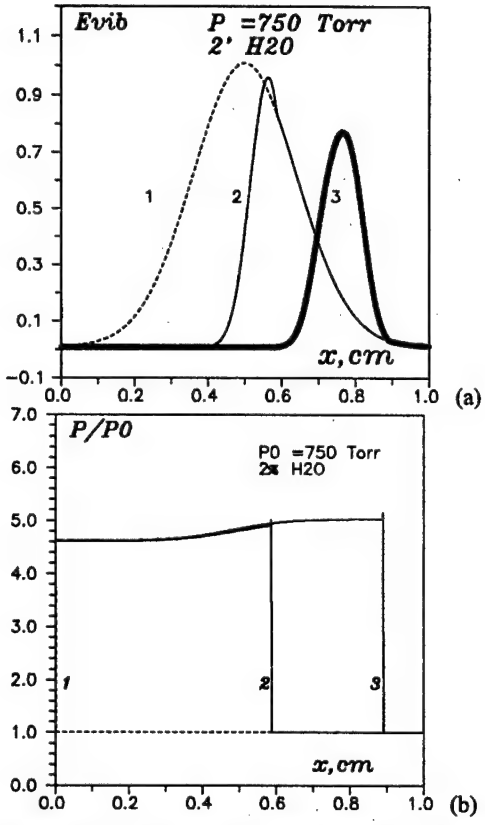

Fig.5. Profiles of vibrational energy (number of quanta per molecule) (a) and pressure (b) at P_0=750Torr at 3 time moments; 2% H_2O. Thin vibrational regions.

SW propagation through non-stationary discharges can reveal the effects connected with the peculiarities of gas temperature dependence on time. The heating of a molecular gas is a complex process involving the excitation of molecular vibrations and VT relaxation. Fig.7

shows the calculated vibrational energy and gas temperature versus time for the developing discharge in nitrogen [5]. It can be seen that, in a certain range of pressures, the curves are non-monotonous. Such character of gas heating can lead to non-monotonous dependence of SW velocity on the lag time between the instant of the discharge ignition and the beginning of SW-plasma interaction. Such dependence has been observed in [6].

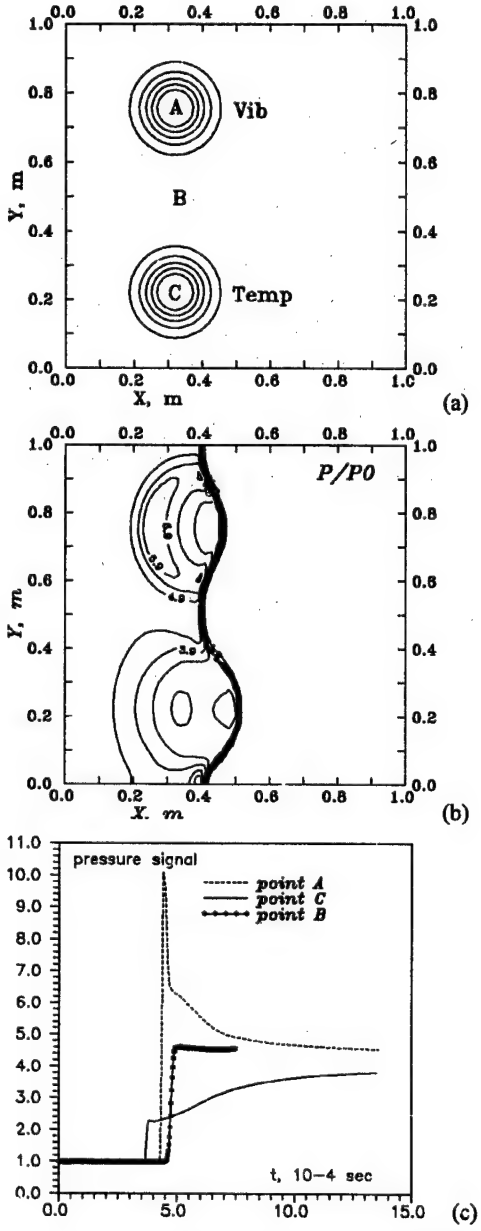

Fig.6: Initial distribution of a number of vibrational quanta per molecule (region A) and temperature (region C) (a); SW position at t=600μs (b); pressure signals at points A,B, and C (c).

Thus the detailed numerical modeling of SW propagation in spatially inhomogeneous and/or non-equilibrium regions gives a deeper insight into the effects observed in a number of experiments.

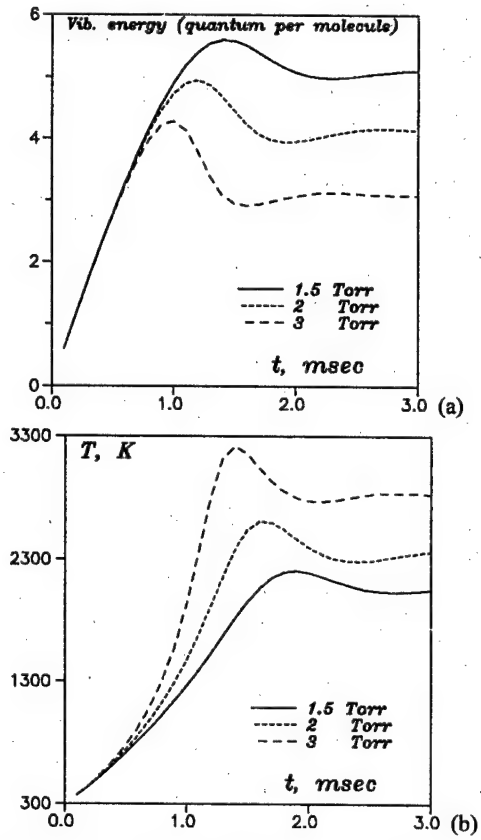

Fig.7. Dependencies of vibrational energy (a) and gas temperature (b) on time elapsed from discharge ignition for 3 values of initial pressure, j=0.3A/cm^2, E/n=10^{-15}V cm^2.

References

1. *Mishin G.I., Klimov A.I., Gridin A.Yu.,* Sov.Tech. Phys. Lett., **17**, 602 (1992).
2. *Ganguly B.N., Bletzinger P., Garscadden A.,* Phys. Lett.A, **230**, 218 (1997).
3. *Babaeva N.Yu., Mnatsakanyan A.Kh., Naidis G.V.,* Sov. J. Plasma Phys., **18**, 549 (1992).
4. *Mnatsakanyan A.Kh., Naidis G.V., Rumyantsev S.V.,* Proc.XVI Int.Symp. on Shock Tubes and Waves, Aachen, West Germany, 1987, p.201.
5. *N.Yu.Babaeva, A.Kh.Mnatsakanyan, G.V.Naidis,* High Temp., **31**, 617 (1993).
6. *Chutov Yu.I., Podolsky V.N., Brayon D.A.* Proc. XX Int. Conf. Phenomena in Ionized Gases, Pisa, Italy, 1991, p.550.

SHOCK SCATTERING ON FLUCTUATIONS OF THE NON-EQUILIBRIUM GAS.

E.Ya.Kogan, I.P. Zavershinsky (Aerospace State University, Samara)

The weak shock waves scattering in the fluctuating non-equilibrium gaseous media is considered. There are two types of fluctuations could be unstable in the non-equilibrium media, which formed the turbulent phone. The two-dimensional nonlinear equations for average acoustic field have been received. The possible mechanism of shock weakening and shock front widening in the non-equilibrium media is discussed.

There are two problems were considered.

The problem of slow evolution of artifically created high-frequency perturbation in the media with turbulent acoustic phone.

In the one-dimensional approach and accompanied count system after standard transformations we can lead to the equation

$$\partial u/\partial t + \Psi_\infty u \partial u/\partial x = (\mu_T + \mu_\infty)\partial^2 u/\partial x^2 \quad ,$$

where Ψ_∞ is nonlinearity coefficient, $\mu_T \sim M_S u_\infty/k$ is turbulent viscosity coefficient, M_S is acoustic phone Mach number. The estimation of the μ_T under conditions P=400Torr , $k \sim 10^{-2}$ м$^{-1}$, $M \sim 10^{-2}$ give value $\mu_T/\mu_\infty \sim 3\cdot 10^2$.

The problem of the definition of the acoustic field structure, created by the well streamlinied at the small attack angle body in the supersonic flow of the non-equilimrium gas.

We were proposed that the sound velocity is chaotic function. After the standard transformations for the high-frequency perturbances in the accompanied count system under condition $L/\lambda<<1$, where λ is wave length, L is correlation length at the second accuracy for the average velocity potential φ we have

$$\partial^2\varphi/\partial t^2 - u_\infty^2\left(1+3\sigma^2\right)\nabla^2\varphi = R[\varphi] + \mu_\infty \nabla^2 \partial\varphi/\partial t + (\mu_T, \nabla)\partial^2\varphi/\partial t^2 - \alpha_\infty u_\infty \partial\varphi/\partial t$$

where $\mu_T = 2/\pi \int |\mathbf{r}-\mathbf{r}'| \nabla^2 B(|\mathbf{r}-\mathbf{r}'|) d\mathbf{r}'$. The comparison of the turbulent viscosity coefficient and viscosity coefficient under conditions, descripted above give the value $\mu_T/\mu_\infty \sim 10^3$. The estimation of the shock front length l and dissipation length l_D lead us to conditions $l \sim |\mu_T| >> l_f$, $l_D \sim u_\infty/|\mu_T|\omega^2$, where l_f is free pass length.

Therefore, the turbulent transfer coefficients can sufficiently exceeded the shear viscosity and heat conductivity coefficients. These factors are lead to the shock weakening and shock front widening in the non-equilibrium media.

SHOCK WAVE DECAY UNDER PULSE IONIZATION

Znamenskaya I.A. (MAI, Moscow)

The method of impulse volume energy inlet into gas-dynamic flow is suggested. Use of the discharge with before-ionization by ultraviolet radiation from discharge sliding on the surface of nonconductor provide the most optimal conditions of impulse volume energy supply into gas-dynamical flow. Minimal time of break down evolution, homogenity of discharge area, diffusion kind of luminescence on first stages of discharge development are the peculiarities of the discharge of such kind. Proper shape of the discharge area makes possible to model instant energy supply into the one-dimensional, two-dimensional, three-dimensional flow, specifically into the flow in shock and aerodynamical tubes. Realization method of impulse volume energy supply into gas-dynamic flows by discharge with before-ionization from plasma sheets was made on shock tube-discharge-optics(STDO) UTRO. STDO is a shock tube which is connected to the discharge camera of special construction. In shock tube two flat sources of UV radiation are put mostly close to the investigated flow and bring minimal disturbances into the flow. Some nonstationary gas-dynamical effects that can be modeled in the shock tubes may be investigated with impulse uniform energy supply. Integral registration of discharge luminescence in the flow represent the visualization of the flow by impulse volume discharge [1]. Also the effect of energy supply into the stationary super-sonic flow around simple models in time of blockage existence after falling shock wave was simulated. Simulation of the flat boundary plasma - gas can be real when impulse uniform ionization of the area before the shock wave is held in idealized case - the instant energy supply into the volume gust before the front that appeares to be the hard technical problem. This problem is supposed to be solve by means of impulse energy supply with use of impulse volume discharge with before-ionization by UV radiation from plasma sheets. This method allows to simulate while the experiment the instant conditions of Rankin-Gugonio formulas violation on planar break up. Use the scheme with before-ionization by UV radiation from plasma sheets provide optimal conditions for impulse volume discharge development in the half-space before the shock wave. Time of the plasma area creation - up to 10ns discharge is burning about 150ns while this time the shock wave can travel not more than by 10-4m. One-dimention of the flow is breaked by four walls of the chamber, and by two plasma sheets. Effect of the plasma sheets existance is in impulse energy supply from upper and lower surface on the district of volume discharge before the shock wave. So the problem of break collapse with initial and boundary conditions is simulated in the experiment. Experiment is held in such a way : The SW with Mach numbers M-2-3,5 entered the discharge chamber; discharge was burned up when it was in discharge volume The SW becomes the surface of contact gas-plasma in time of 10ns because the plasma sheets were burned up only before the front in area of low pressure. At the time T=0 the energy supply of the volume discharge Q=UIT is made into the space before the SW. Energy density is determined by the dimension of the discharge area volume before the SW at the moment of the discharge initiation . It's minimal if the SW was at the entrance of the discharge area at the moment of discharge initiation. Parameters of gas before and after SW at the time T<0 are connected by Rankin-Gigonio formulas. Discharge area before SW (before the outlet of electrode area) is not one-dimension because of boundary conditions.

Structure and form of the SW after energy supply was investigated by shadow method. On the shadow photos taken with intervals about 10-30ns the space stratification can be detected. SW is propagating in air with pressure from 130Pa up to 50kPa with Mach numbers M=2-4 with impulse volume ionization before the front. Shock wave losses the stability with tendentious to restoring the front. In time of fluorescence photo-expositions in the area of the front the violation of the structure isn't discovered. Three-dimensions of instability are defined by boundary conditions.

References

1. *Znamenskaya I.A.* Discharge imaging technique for shock tube studies. // In: Proc 21th Int Symp on Shock Waves. 1997. Keppel p.489-491.
2. *Andreev S.I., Znamenskaya I.A., Stepanec I.V.* Shock wave in air excited by impulse volume discharge. // Chemical Phisics, 1993. 12. No.3. p.392-393.

ON INTERACTION OF LONGITUDINAL PULSE DISCHARGE WITH BOW SHOCK

V.A.Bityurin, A.I.Klimov, S.B.Leonov, V.G.Potebnya
(Institute of High Temperature of the Russian Academy of Sciences, Moscow, Russia)

Abstract. The concept of highly non-uniform discharge used for meekly ionized plasma creation is developed is treat the experimental results on anomalous feature of shock waves propagation in post discharge plasma flow. The first stage study is to cheek the possible effects by means of 2D time dependent numerical simulation of the ideal gas flows.

Introduction

One of possible explanation of an «anomalous» propagation of shock waves through non-equlibrium discharge plasma [1] is based on the model of a constricted breakdown penetrating a shock wave. Assuming that the average density of the energy input creating either uniform non-equilibrium plasma and strongly non-uniform discharge plasma channel are the same one can realize that plasma local parameters inside the discharge channel can be very high – the effective plasma temperature more than 10000K and the initial compression ratio is more than 100. It is significant that the sound velocity corresponding to such conditions inside discharge channel can be higher as compared with this value in bulk media for two order of magnitude. Thus, the overheated discharge channel can provide the intensive transport of gas dynamics perturbation through the shock wave.

The features of such an interaction of non-uniform pulse discharge with a bow shock are studied in frame of axial symmetrical flow of an ideal non-dissipating gas. The numerical solution of these non-steady state Euler's equations is obtained with the classic Godunov' scheme. Three shock wave configuration are considered: (1) a planar shock wave, (2) a bow shock at a sphere, (3) a head shock at a streamlined body. For the latter the evolution of integral characteristics and local parameters under pulse periodic discharge conditions are also presented and analyzed.

Formulation of Problem

In all cases presented below an axial symmetrical flow of an ideal non-dissipating gas is considered. It is assumed that the only result of gas discharge impact is an energy input with preset space and time distribution. Process as a whole is described by Euler's equations with corresponding source term in right-hand part of the energy equation.

The peculiarity of the problem considered is the process of energy input indeed. Utilizing the well known experimental fact (see, for example [2-4], and many papers presented at this workshop) that the typical energy input used in plasma aerodynamics experiments was between 0.01% to 10% of total enthalpy flux the level of averaged energy input was assumed as high as 1% of the total enthalpy flux. It is also assumed that the main part of the electrical energy is released in thin discharge channels like the streamer discharges, sparks or/and streamer-leader discharge channels (for details see [5]). The next important assumption is that only few such discharge channels can coexist at the same time. So the single discharge channel can be considered as an extreme case of energy input structure. Typically the so called fill-up factor that is the ratio of summarized discharge channel volume to the whole discharge gap volume, is about 10^{-3}-10^{-5}.

In Fig.1 a schlieren photography of pulse electrical discharge interacting with shock wave is presented. This picture can be considered as an experimental background for approach being developed it this paper.

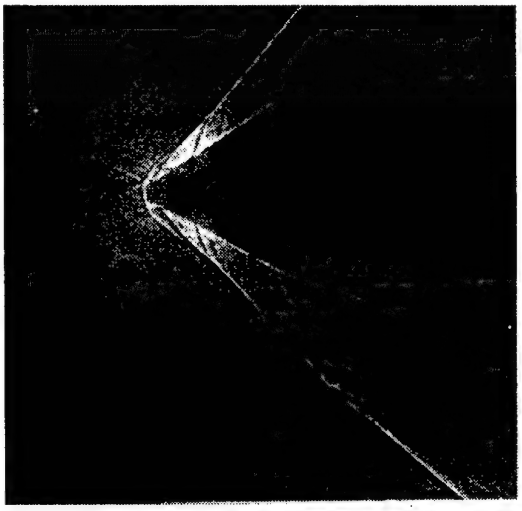

Fig.1

The pulse periodic nature of discharge results also in strong amplification of the local density of energy input. For these reason the characterization of the electrical discharge in air

flow is based on a high density $q \sim 10^{10}$–10^{12}W/m^3 electrical discharge. No other energy losses besides the gas internal energy change is taken into account. The rather short duration discharge pulses (tens of microseconds) are considered. The overheated compressed discharge channel created in such a way initiates a cylindrical shock wave interacting with primary shock wave. The relatively late stage of such an interaction is a subject of this paper.

The process is characterized as multi scale phenomena both in space and in time. In order to resolve the main details of the process the rather well developed grids are needed. The typical grids used in this study are 400 by 400 and 400 by 800 and several tens of thousands of time steps.

The numerical solution was obtained here with the classical Godunov's scheme.

Results and Discussion

Case 1. Planar Reflected Shock Wave

In Fig.2 the evolution of pressure distribution in vicinity of the intersection point of planar shock wave with a thin discharge channel is presented.

The calculating domain is a circular cylinder closed at the right side by a wall. From the left side open orifice, an ideal gas enters. In the figures below the one (upper) half portion of the axial cross-section is shown.

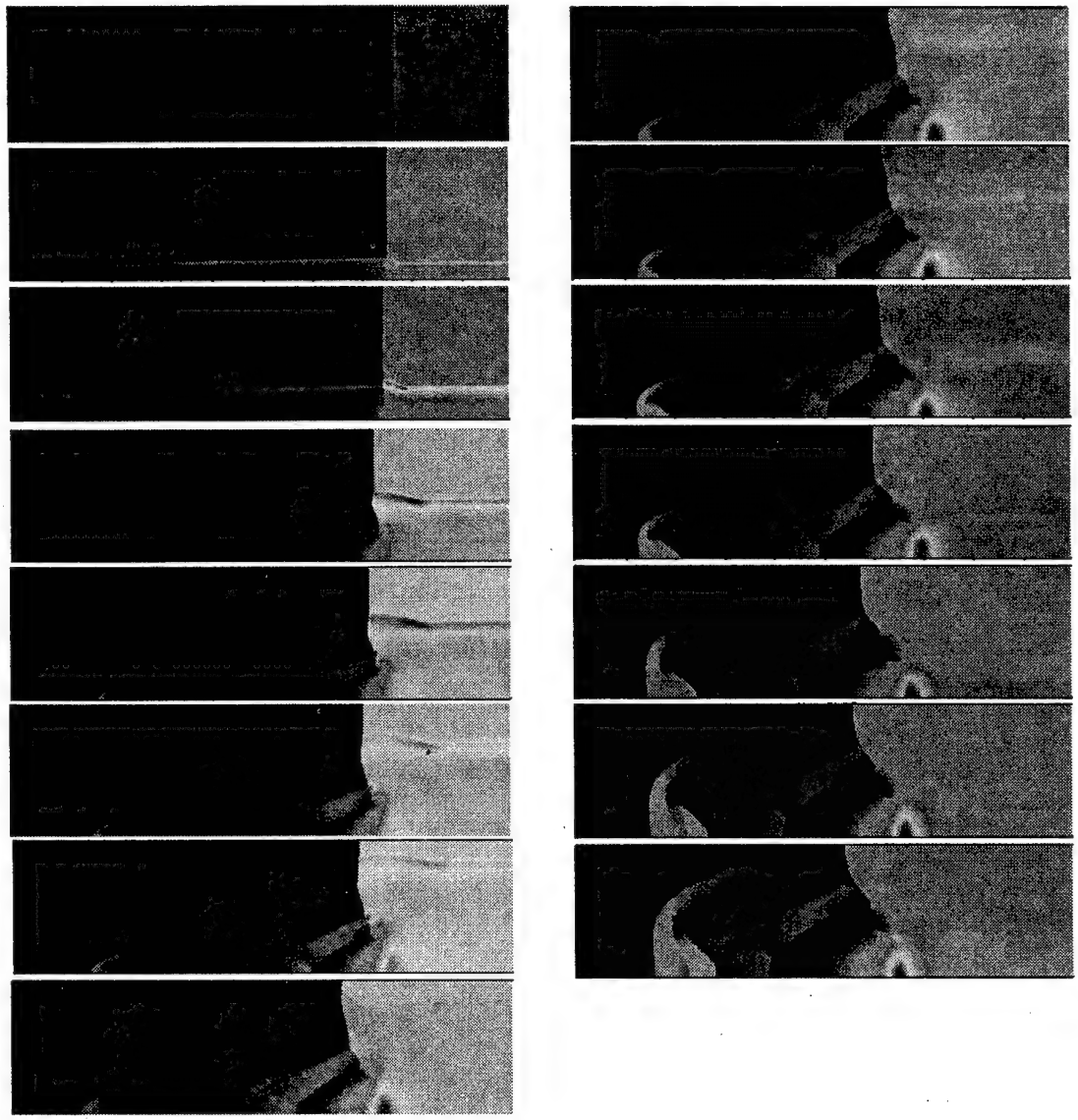

Fig.2

The gas parameters of incoming flow are as following: Mach number 3, static pressure 0.3atm, static temperature 250K. The shock wave is reflected from a wall located at the right hand side of the calculating domain. In several milliseconds after reflection, the energy input pulse is provided in the region along the domain axis (bottom border of the domain shown). The pulse duration is 10μs. The power density is 10^{12}W/m^3. The ratio of the radius of the energy input region to the radius of the domain r_s/r_0 is 1/200. The longitudinal distributions of energy input along the discharge channel is approximately linear increasing from the left side end to the right one that corresponds roughly to the electrode location assumed at the right side wall.

After the rather short phase of the energy input into the flow the second stage of the evolution develops. During this stage a strong cylindrical shock wave propagates outward the flow axis. At the initial moment this cylindrical shock wave propagates slower behind the primary reflected shock wave. However at the end of the second stage the cylindrical shock behind the primary shock decelerates slower due to higher temperature (initial compression ratio), and reaches the cylindrical shock wave in front of primary shock. Approximately at this moment the forming of a low (subsonic) Mach number flow region bridging incoming and compressed flow across the primary shock is completed. The temperature here is still very high (two-three times lower in respected to maximal post discharge value) and, consequently, the density is very low.

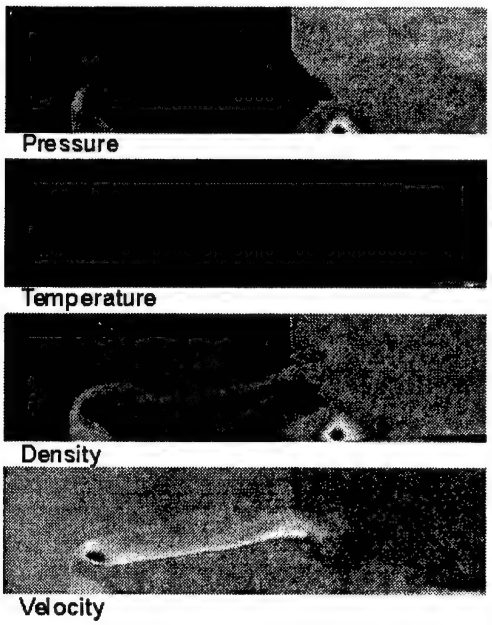

Fig.3

At the third stage of the interaction process a secondary strong shock wave created in this region by high pressure drop applied to high temperature low density propagates through this 'high sound speed' channel resulting in an intensive counter flow jet. The jet velocity can reach several km/sec.

At the later stage of the interaction process the jet creates the perturbed flow region with characteristic size of several hundreds on initial discharge radius. The perturbed flow looks as very well formed but complex flow with several Mach diamonds and a 'secondary' bow shock. At the same time, the corresponding area behind the primary reflected shock is characterized with significantly lower parameters.

In Fig.3 the distributions of pressure, temperature, density, and longitudinal velocity for a time moment of a late stage are presented. The counter flow region is clearly visible at the center part of the fragment of Fig.3. The residual high temperature area behind the primary shock is also clearly seen in the corresponding picture. The upstream temperature non-uniformity reflects the effects of "cold" counter flow jet.

Thus, a significant amount of momentum can be transferred from the compressed area behind the primary reflected shock wave into the upstream flow far from primary shock. It means in some way that effective propagation velocity of gas dynamics perturbances can be much higher in the presence of electrical (or laser) discharge penetrating of planar shock waves.

Case2. Bow Shock at Sphere.

In this case the initial stage of flow field development provided by a pulse periodic axial symmetrical discharge is similar to the previous case. The pulse parameter are the same as for the previous case as well. The new element beside the body and shock wave geometry is the periodicity of the process. In this particular case the pulsating period of 100μs is chosen. The difference from the previous case of a planar shock wave is revealed in the later stages when a slightly pulsating conical shock wave forms in upstream disturbed zone. The significant reducing of the pressure at the critical point is observed. On the other hand a markable pressure increase occur at the intersection of primary bow shock and secondary conic shock wave. In dependence upon the discharge parameters such as input power, periodicity, shape and others the integral result of the wave (pressure) drag reduction can be rather high.

In Fig.4 the example of the distribution of pressure, Mach number, density, and longitudinal

velocity are shown for a late stage after the third discharge was applied.

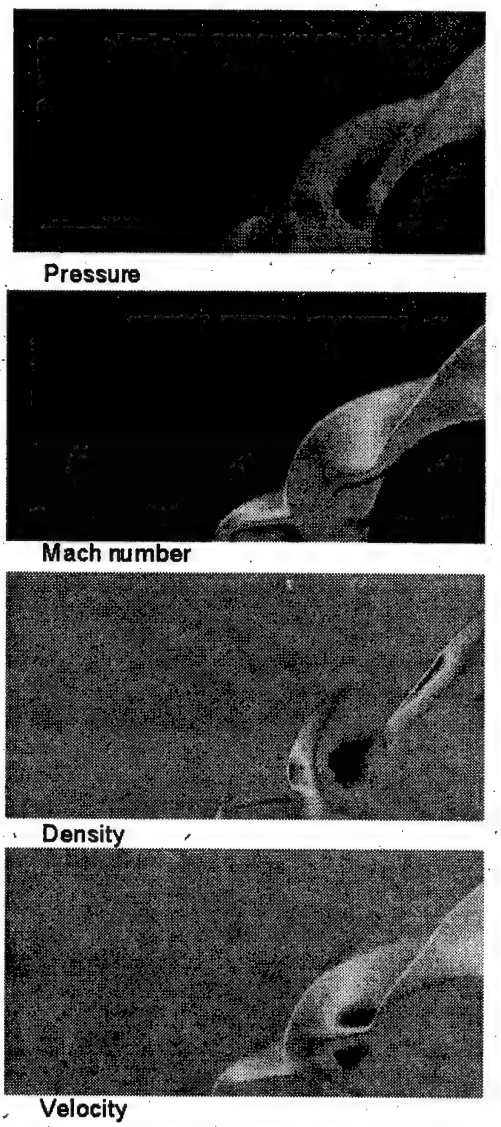

Fig.4

Case 3. Streamlined body

A streamlined body similar to those used in the recent experiments [6] is considered in the flow of the same parameters as in the previous case.

Furthermore, a pulse periodic mode of energy release is assumed. Thus, the actual energy release is characterized by two characteristics times: pulse duration t_p, and pulse repetition tr. Such a simplification is based on the fact that main (high) frequency of discharge (HF capacity type discharge is assumed) is about 10MHz and the macroscopic gasdynamics frequency is estimated as $Q_g=L/u \sim 0.1/10^3=10^4$Hz. The comparison of these two values leads to the conclusion that fast fluctuating electrical energy release can be averaged over a longer time interval comparable with gasdynamics time with no significant losses of accuracy.

Because of the electrode nature of the discharge it is also assumed that the energy release starts at the critical point on the body surface. The energy release is assumed to be uniform over the discharge channel described above.

One of the base physical idea used in this study is that the HF discharge under wind tunnel flow condition is consisted of series of fast created very thin discharge channels. The energy release with high power density results also in pressure jump inside the discharge channel. Thus, the first stage of the gasdynamics development starting after energy supply turn off is the channel decay with a cylindrical shock wave propagating outward. The feature of such a cylindrical blast is very low gas density at the primary channel axis. In principal this low density area can effect directly the integral pressure drag of the body due to decrease of the local dynamic pressure (see cases described above). Probably more important mechanism influencing the pressure drag is the indirect pressure redistribution provoked by the low pressure and high temperature area at the discharge channel axis. It should be noted, that the temperature in low pressure area after the cylindrical blast occurred is still rather high (only two-three times lower in comparison with the peak temperature reached at the end of energy release) and consequently the sound velocity is much higher than in undisturbed flow. For this reason the pressure disturbances propagate through the discharge channel very fast.

This scenario has basically confirmed by numerical simulation the interaction of a single discharge channel (streamer) with a normal shock and more recent study of the interaction of a single axis located streamer with the bow shock at the F-15 (see [6]) nose 1/6 model tested in wind tunnel.

Some of the examples of the results of the study are presented in Fig.5.

In Fig.5 the distributions of pressure, Mach number, density, longitudinal velocity are shown. The characteristics details are the rather low intensive disturbances of the pressure in up-stream part near the flow axis, the substantial pressure decrease at the model nose and the significant overpressure at the intersection primary bow shock and the secondary shock created by the discharge expanding channel. Downstream part of the flow (behind the

intersection point) is practically not disturbed. The latter is also found in experimental measurement during wind tunnel tests (see [6]). The integrated effect of the pressure distribution change over the model surface looks like as a value of the second order resulting from positive and negative pressure deviation from the reference (no discharge) case.

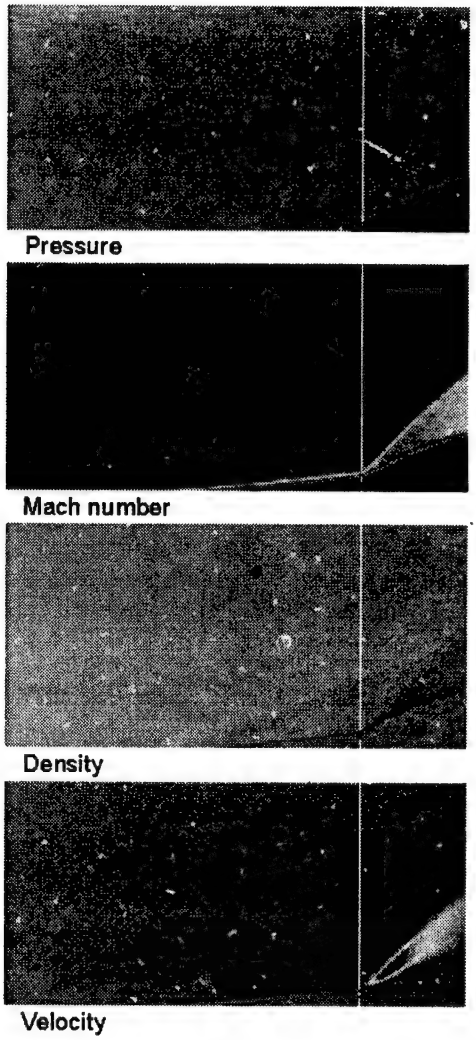

Fig.5

The nonmonotonic low amplitude disturbances of pressure resulted from the pulse periodic nature of the energy release used in this numerical simulation. The characteristics times of discharge – pulse duration t_p, and pulse repetition t_r, are to be carefully tuned to reach a 'resonance' conditions in respect to gasdynamics characteristics times: the cylindrical shock wave decay t_{cw} and the stream time t_s – gas sample travelling time over the interaction area. The investigation of such a resonance condition is in progress now.

The next fragment of Fig.5 represents the corresponding Mach number distribution confirms the general picture of the process described earlier as well.

The density distribution presented in Fig.5 shows the formation of the extremely low density channel along the discharge axis.

The Fig.6 summarizes the integral effects of the pulse periodic HF discharge.

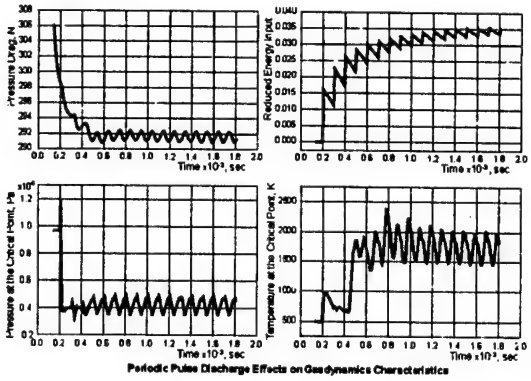

Fig.6

The pressure drag reduction is about 5%, the static pressure reduction at the critical point is about 30%. These values are in qualitative agreement with experimental observations. The temperature at the critical point found is rather high (approximately 2000K).

Concluding remarks

The preliminary study reported in this paper has shown that the concept of highly non-uniform discharge plasma can be very useful to treat the integral characteristics of shock waves interaction with weakly ionized plasma flow.

The avarage parameters both the non-uniform discharge plasma and the practically uniform non-equilibrium plasma can be close to each other. However, the interaction of these two kinds of plasma flow with a shock wave can be dramatically different.

More theoretical studies and numerical simulations along with intensive experimental research are needed to understand the phenomena in detailes.

References

1. *I.Adamovich et al*, Studies of Anomalous Shock Wave Propagation and Dispersion in Weakly Ionized Plasmas // 2nd Weakly Ionized Gases Workshop, Proceedings Supplement, April 24-25, 1998, Norfolk, Virginia, USA, p.121-152.
2. *A.Klimov*, Key Experiments in the Field of Plasma Gas Dynamics. Comparison Experimental and Theoretical Results // 2nd Weakly Ionized Gases Workshop, Proceedings Supplement, April 24-25, 1998, Norfolk, Virginia, USA, p.41-64.
3. *K.Khodotaev*, The Plasma Effects un Air Dynamics. The Gas Discharge Theory Model in Aerodynamic Calculations // 2nd Weakly Ionized Gases Workshop, Proceedings Supplement, April 24-25, 1998, Norfolk, Virginia, USA, p309-338.
4. *Yu.Ch.Ganiev et al*, Experimental and Theoretical Study of the Possibility of Reducing Aerodynamic Drag by Exploying Plasma Injection // 2nd Weakly Ionized Gases Workshop, Proceedings Supplement, April 24-25, 1998, Norfolk, Virginia, USA, p.65-92.
5. *Yu.P.Raizer*, Fizika Gasovogo Razryada, Moscow, Nauka, 1988, 592p. (in Russian)
6. *W.Beaulieu, V.A.Bityuin, A.I.Klimov, S.B.Leonov, A.S.Paschina, B.I.Timofeev*, Aerodynamics WT Test of the 1/6 Scale Model of the F-15 Nose Part // This Volume.

ON PHYSICAL-CHEMICAL KINETICS AND STRUCTURE OF SHOCK WAVES PROPAGATING THROUGH IONIC DUSTED PLASMA.

V.Yu.Velikodny, V.A.Bityurin (IVTAN, Moscow), J.T.Lineberry (ERC Inc., Tullahoma, TN,USA).

Abstract. One of the possible explanation of an anomalous propagation of shock waves through non-equilibrium discharge plasma is based on the model of an constricted breakdown penetrating the shock wave. Assuming that average density of the energy input creating either uniform non-equilibrium plasma and strongly non-uniform discharge channel plasma are the same one can realize that plasma local parameters inside of the discharge channel can be very high — the plasma temperature more that 10000K and the initial compression ratio is more that 100/ It is significant that the sound velocity corresponding to such conditions inside of the discharge channel can be higher as compared with this value in balk media for two order of magnitude. Thus, the overheated discharge channel can provide the intensive transport of gasdynamics perturbation through the shock wave front.

Introduction

A number of anomalous phenomena are observed while a shock wave propagates through weakly ionised non-equilibrium plasmas [1]. One of the observed effects of shock wave propagation in such plasma is over kilovolts voltage occurred across the shock wave front even under condition of electron temperature is limited by 20000K. No successful explanation was found up to date (see, for example, [2]). One of proposed in paper [2] hypothesis is the micro particles ejected into the flow by electrode erosion when pulse discharge is initiated. In experimental study [3] it was also observed some amount such particles. A theoretical model of the shock wave propagation through gaseous mixture and plasmas loaded with nano particles and/or (super-) heavy macromolecules has been recently proposed and developed by the authors of this paper (see, for example [4] and the reference list there). In this paper new results obtained with this model applied to three component ionic plasma and with simplified charged particles diffusion model are discussed.

Problem formulation

The object of this study is so called ionic weekly ionised ($\alpha=10^{-6}$-10^{-10}) plasma initially containing only negligible amount of free electrons ($\alpha_e=10^{-12}$-10^{-15} and less). Such a plasma can be created for example when discharge applied to the electronegative gases SF_6, O_2, air and other and the admixture of micro and nano particles occurred due to electrode material erosion or artificially loaded in to the flow. The (nano-) particles concentration considered is in a range of 10^{-7} and less with mass factor $\zeta=10^6$ (ratio of the particle mass to the main carrying gas molecular weight $\zeta=m_{part}/(m_p\cdot\mu_g)$ where m_{part} particle mass, m_p - proton mass and μ_g is molecular weight of carrying gas). When such a three component ionic cold plasma moving with the rather high velocity (Mach number M=2-4 and higher) the significant portion of the flow total energy is stored as the kinetic energy of the particles. This energy can be released in shock wave front resulting in gasdynamics parameter modification of each mixture component. Because of charged components are also involved an electrical field effect can be expected here due to the space charge appearing.

Three component case

The shock wave structure in the three component mixture was analysed on the base of the consistent solution of the Boltzmann-Vlasov and Poisson equations. The solution was obtained with the generalised Mott-Smith method developed elsewhere [6]. It was found that the carrying gas density profile of the shock wave has a multi-scale structure. The fastest changing region sized of several tens of free path and the rather extended relaxation zone sized of several tens thousands free path can be easily resolved. Such a behaviour is caused by the interaction of the nano-particles with the carrying gas. The new interesting feature of the shock wave structure in a three component gases has revealed - the non-monotonic distribution of the partial temperatures in the shock wave front is characterised by the temperature maximum exceeds the equilibrium temperature behind the shock (see Fig.1 and Fig.2). Intermediate scale can also occur due to various non-linear reasons including inter component interaction through electric field. In the case of three-component cold ionic plasma the temperature distribution is characterised by two picks both exceeding the equilibrium temperature.

However even more interesting and extremely important results obtained in this study relate to the electrical field and to the voltage across the shock wave caused by the inter component interaction in the shock wave front.

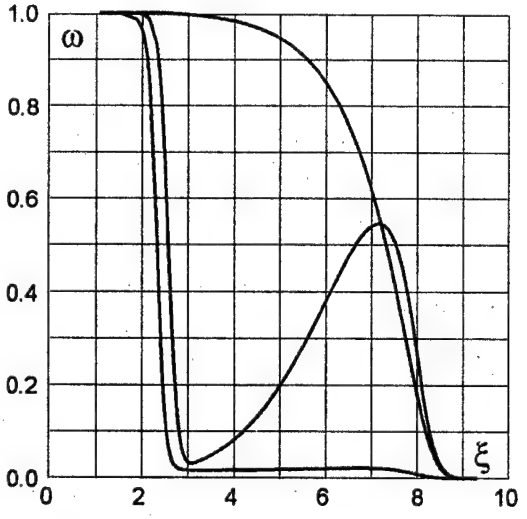

Fig.1. Reduced particle velocity $\omega=\frac{u_i-u_2^0}{u_1^0-u_2^0}$ vs logarithm of reduced distance $\xi=\ln(12+x/\lambda)$. Three component mixture, physical kinetics model case.

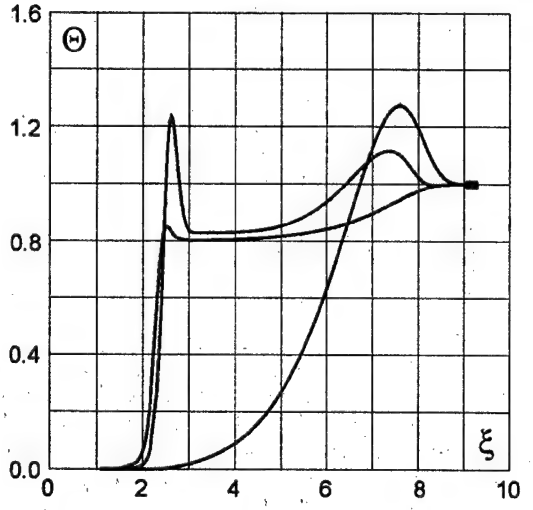

Fig.2. Reduced particle temperature $\Theta=\frac{T_i-T_2^0}{T_1^0-T_2^0}$ vs logarithm of reduced distance $\xi=\ln(12+x/\lambda)$. Three component mixture, physical kinetics model case.

The high density kinetic energy stored in the super-heavy provides the separation of the charged components (heavy and super-heavy) in the shock wave front. This results in a space charge resulting in the (significant) electric field and the latter results in a voltage across the shock wave. Such a polarisation effect is known for case when hot electrons diffusing upstream through the shock wave front create some voltage defined by the electron temperature (see, for example, the classical book by Ya.B.Zel'dovich and Yu.P.Raizer [7]). In the case under consideration the space charge is created not by the difference of thermo diffusivity but by the different «friction» of the difference admixture components in the carrying gas.

New conditions (presence of super heavy components defining «super»-high-energy density — an equivalent «partial» stagnation temperature would be above 10^6K for flow Mach number of 2-6) considered in this paper cause a strong new effects — creation of high electric field strength and, sometimes, high voltage across shock wave front. One of the example of such a case is presented in Fig.3 and Fig.4 for the flow conditions: M=2.5, $\mu_{sh}:\mu_h:\mu_0=2\times10^6:40:1$.

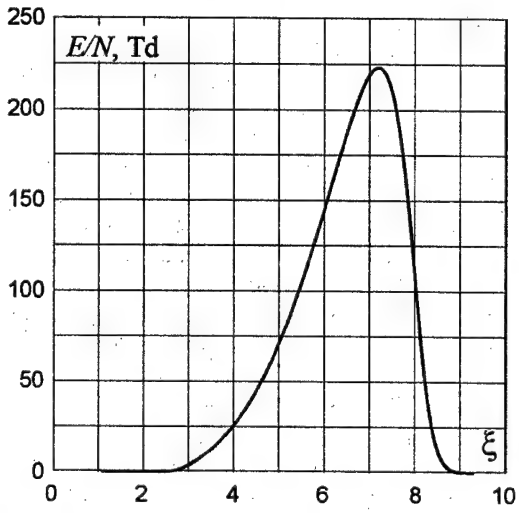

Fig.3. Reduced electrical field [Td] vs logarithm of reduced distance $\xi=\ln(12+x/\lambda)$. Three component mixture, physical kinetics model case.

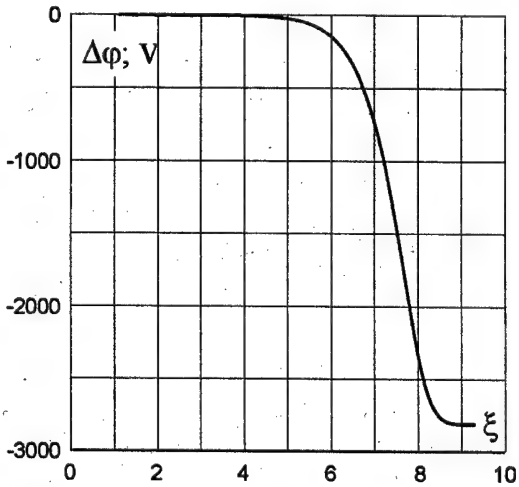

Fig.4. Reduced voltage field [Td] vs logarithm of reduced distance $\xi=\ln(12+x/\lambda)$.. Three component mixture, physical kinetics model case.

It should be noted that in course of this study a great variety of electrical field and voltage has been observed including those are much higher of breakdown level. In the latter one can expect strong non-linear consequences both in gasdynamics and electrodynamics behaviour.

Five component case

In order to assess case when a kind of breakdown phenomena can be expected a simplified particle drift model including the Townsend's ionization process has been developed and implemented into the analysis. Advantages of such a model is the rather wide possibility in mixture composition choice. The simplified model was tested with the above mentioned sophisticated physical kinetic model in three component mixture case.

An example of shock wave propagating through ionic plasma consisting of main gas n_0, heavy (negative) ions n_h, charged super-heavy molecules (clusters, nano-particles) n_{sh}, «light» (main gas) ions n_i, and electrons n_e, are illustrated in Figs.5-8. The others important parameters are: the static pressure before the shock is 10^5H/m^2, the temperature is 300K, a segregated electro-neutrality $Z_{sh}n_{sh}=Z_hn_h$ and $n_e=n_i$ are also assumed; ionization degree $\alpha_p=n_{sh}/n_0=10^{-7}$, $m_{sh}/m_0=10^6$, $\alpha_e=n_e/n_0=10^{-13}$. The most important difference of the five component ionic plasma case from the previous one is an initiation of electron breakdown while electric field strength approach of a critical level of abut 10^6V/m. The ionization process provides the significant amount of free electrons modifying electrical space charge and, consequently, the electric field in the shock wave front.

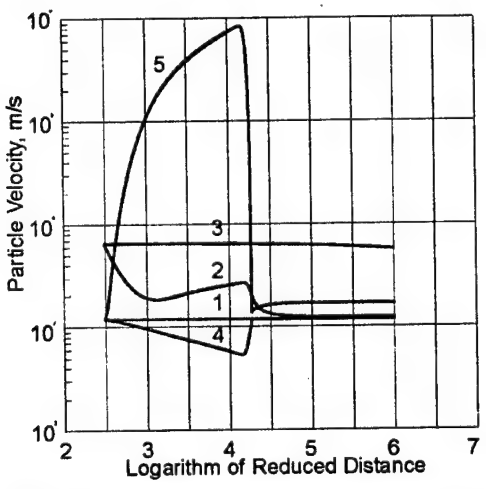

Fig.5. Particle velocity vs logarithm of reduced distance $\xi=\ln(12+x/\lambda)$. Five component mixture, particle drift model case. 1- main carrying gas; 2- heavy ion; 3- super-heavy ion; 4- light ion; 5- electron.

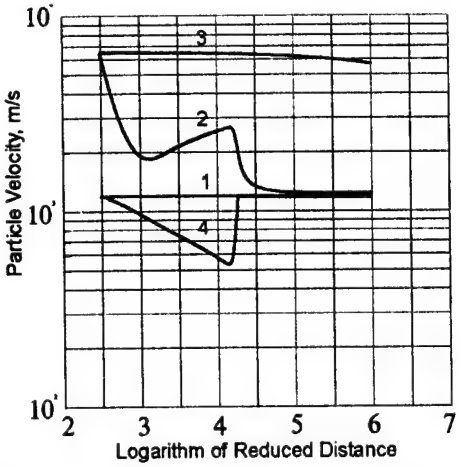

Fig.6. Particle velocity vs logarithm of reduced distance $\xi=\ln(12+x/\lambda)$.. Five component mixture, particle drift model case

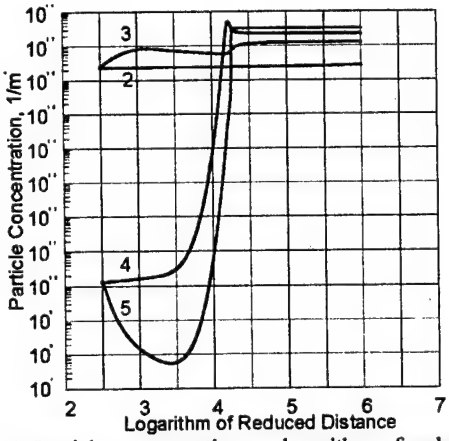

Fig.7. Particle concentration vs logarithm of reduced distance $\xi=\ln(12+x/\lambda)$. Five component mixture, particle drift model case.

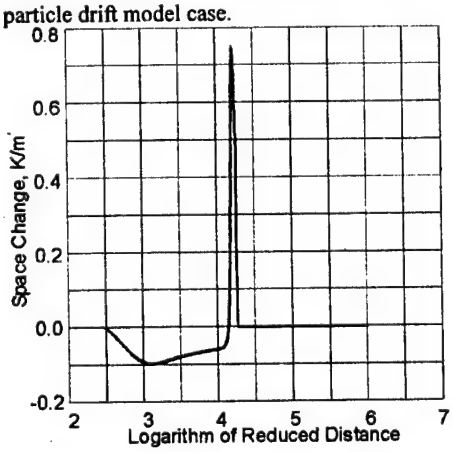

Fig.8. Space Charge vs logarithm of reduced distance $\xi=\ln(12+x/\lambda)$. Five component mixture, particle drift model case.

The particle velocity over the shock wave front shown in Fig.5 and, in enlarged side without electron velocity, in Fig.6. It can been seen that the particle velocity distribution calculated with simplified model are similar those found with more sophisticated kinetics model. Fast ionization starts location with ξ=4.2 (see Fig.5). This results in the fast deceleration of electrons and acceleration of ions the main gas velocity. The electron (light ions concentrations exceed even the initial level of ionization for several times (compare Fig.7).

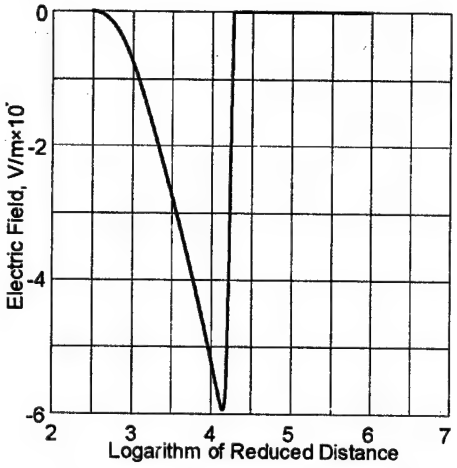

Fig.9. Electrical field [Td] vs logarithm of reduced distance $\xi=\ln(12+x/\lambda)$. Five component mixture, particle drift model case.

Space charge distribution in this region is shown in Fig.8 explaining of the fast reduction of the electric field created by the separation of primary charged particles — the electric field behaviour can be seen in Fig.9. Thus, the new strong electric effects revealed in the dramatic modification of charged particles parameters are found in this study. The main reason of this is the extremely high energy density non-uniformity due to presence of heavy and super-heavy admixture in the gas flow. The level of the electric field strength and the voltage across the shock wave front are found in a qualitatively good agreement with the experimental observations by Klimov et.al. The more sophisticated analysis is in progress now to treat more accurately experimental conditions.

Conclusions

The theoretical model of the shock wave in dusted meekly ionized ionic plasma are developed and tested. The very non-trivial shock wave structure in such a media as revealed.

The strong electrical effects can be observed in a case of ionic dusted plasma which can result in special kind of gas discharge – shock wave initiated discharge.

References

1. *Mishin G.I.,Klimov A.I.,Gridin A.Yu.,* Izmereniya davleniya I plotnosti v udarnykh volnakh v gasorasryadnoy plasme (Pressure and Density Measurnets in Shock waves in Gas Discharge Plasma), Pisma v ZhTF, 1991, vol.17, No.8, pp.84-89 (in Russian) // Soviet Tech.Phys.Letters, 1991,v.17, No.8, pp.413-416.
2. *Adamovich I.V., Subramaniam V.V., Rich J.W., Macheret S.O.* Shock wave propagation in weakly ionized plasmas // Atlanta, GA, AIAA Paper 97-2499, pp.1-18.
3. *Klimov A.I., Gridin A.Yu., Mishin G.I.* Plasma Condensation behind Shock Wave in Non-Equilibrium Discharge and Ball Lightning. // Ball Lightning in Laboratory: Khimiya/ Moscow, 1994, pp.175-183.
4. *Velikodny V.Yu., Bityurin V.A.,* Struktura udarnoy volny v ionnoyi plasme (Shock Wave Structure in an Ionic Plasma), Doklady Rossi'skoi Akademii Nauk, 1998, accepted for publication, (in Russian).
5. *Clemmov P.C., Dougherty J.P.* Electrodynamics of Particles and Plasmas. Redwood City. Addison-Wesley Pub.Comp. 1996, 526p.
6. *A.M.Bashlykov., V.Yu.Velikodnyi,* Struktura udarnoy volny v gasovoy smesi (Shock Wave Structure in a Gaseous Mixture), ZhTF, 1991, vol.61, No8,pp33-42 (in Russian)//Soviet Tech.Phys., 1991, v.36, No.8, pp.865-870.
7. *Zel'dovich Ya.B. and Raizer Yu.P.* Fizika udarnykh voln I vysokotemperaturnykh gidrodinamicheskikh yavlenii (Physics of Shock Waves and High Temperatures Gasdynamics Phenomena). Moscow, 'Nauka' Publishing, 1963, 688p.

BULK VISCOSITY IN NONEQUILIBRIUM MEDIA

Molevich N.E., Nenashev V.E. (Samara State Aerospace University, Russia)

Abstract. The different aspects of the negative second viscosity influence on non-equilibrium media dynamics are considered: (1) the sound amplification and new dispersion characteristics; (2) the heat self-focusing of sound and its anormal reflection on the boundary with non-equilibrium gas; (3) the essential change of nonlinear stationary acoustical structures; (4) the influence of the second viscosity on the hydrodynamic stability of flows and the critical Reynolds number. The second viscosity coefficient in dusty media is obtained. It is shown the possibility of the negative second viscosity existence in such media and, as consequence, the appearance of all above - mentioned effects.

IX. Introduction

It is known that bulk viscosity can be negative in nonequilibrium media. The second viscosity coefficient in nonequilibrium medium (vibrationally-excited gas) was obtained first in [1]. Then the second viscosity reversal in molecular gas is discussed in [2,3]. It is important that $\xi<0$ is possible not only in molecular media with the vibrationally or rotationally excited molecules but also in slightly ionized atomic gases [4,5] and different media with a nonequilibrium heat supply [6,7], e.g., in chemically active mixtures.

In present paper it is considered briefly the gasdynamic properties of nonequilibrium media with $\xi<0$ (part II, III). In part IV it is shown the negative bulk viscosity existence in nonequilibrium dusty gases.

X. Acoustics of nonequilibrium media

First an amplification of sound in the vibrationally-excited gas was predicted in [8,9], an acoustical instability of media with nonequilibrium heat supply – in [10-12]. In [9] it was noted that the sound amplification can be connected with the second viscosity reversal. This connection in general form was obtained in [6,7]

$$\alpha=\frac{\omega^2}{2\rho_0 u_S^3(\omega)}\left[\xi(\omega)+\eta+\chi\left(\frac{1}{c_V}-\frac{1}{c_p}\right)\right], \qquad (1)$$

where α is the acoustic increment (or decrement if $\alpha>0$); ω is the sound frequency; χ, ξ, η — are the coefficients of the thermal conductivity, bulk and shear viscosity; $u_S=(c_pT_0/c_Vm)$ — is the sound speed.

In nonequilibrium media with one relaxation process the form of bulk viscosity coincides with its equilibrium form [13]

$$\xi(\omega)=\frac{\xi_0 c_{V0}^2}{c_{V0}^2+\omega^2\tau^2 c_{V\infty}^2},$$

$$\xi_0=\frac{c_{V\infty}\left(u_\infty^2-u_0^2\right)\tau\rho_0}{c_{V0}},$$

where $u_0=(c_{p0}T_0/c_{V0}m)^{1/2}$, $u_\infty=(c_{p\infty}T_0/c_{V\infty}m)^{1/2}$ are the low-frequency and high-frequency sound speeds. In equilibrium media $u_\infty^2>u_0^2$, $\xi>0$.

In nonequilibrium media the low-frequency specific heats and sound speed depend on the nonequilibrium degrees. For example, in vibrationally-excited gas

$$c_{p0}=c_{p\infty}+c_K+S(\tilde{\tau}+1),$$

$$c_{p0}=c_{p\infty}+c_K+\tilde{\tau}+1),$$

where $S=(E_{K0}-E_{Ke})/T_0$; E_{K0} is the stationary vibrational energy (per molecule); E_{Ke} is its equilibrium meaning; $\tilde{\tau}=\partial\ln\tau/\partial\ln T$.

The typical dependence u_0^2/u_∞^2 on nonequilibrium degree in vibrationally-excited gas is shown in Fig.1. There are four regions of S. In region I $u_0<u_\infty$, $\xi>0$. In region II $u_0>u_\infty$, $\xi>0$. Here the sound wave can be amplified in spectral range $\omega<\omega^*$ (Fig.2). In region III $u_0^2<0$ and low-frequency sound does not propagate. The region IV is the region of acoustic and heat instabilities.

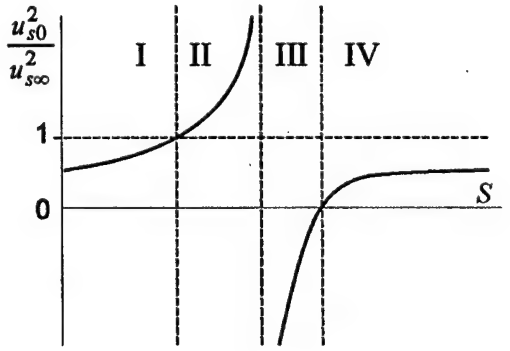

Fig.1.

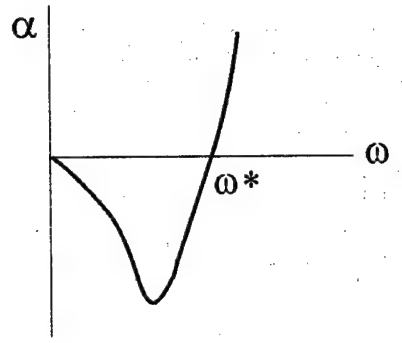

Fig.2.

In cases of media with a few relaxation processes (e.g. in weakly ionized atomic gases the bulk viscosity is formed by processes connected with the relaxation of the electron temperature, ionization degree and Joule heating) the dependencies $\xi(\omega)$, $u_S(\omega)$ are more complicated [4,7], but expression (1) is valid.

In [7] it is shown that the negative second viscosity condition corresponds to the positive feedback between the changes of nonequilibrium states and the gasdynamic disturbances. It leads to the increase of the difference between the compression and rarefaction regions. The nonlinear mechanisms of this instability stabilization (viscosity saturation, spectral energy transfer) are considered in [7,14]. The stationary acoustic structures are essentially depends on the nonequilibrium media properties and the initial spectral composition of the gasdynamic disturbances. As an example the numerical evolution of the step-like disturbance in media with $\xi<0$ is plotted in Fig.3. Taking into account the nonlinear absorption and the integral dispersion (which appear in the third order perturbation theory) leads to the autowave stationary impulse emission. The form, amplitude and speed of impulse depend only on the nonequilibrium media properties ($S,\tau(T)$).

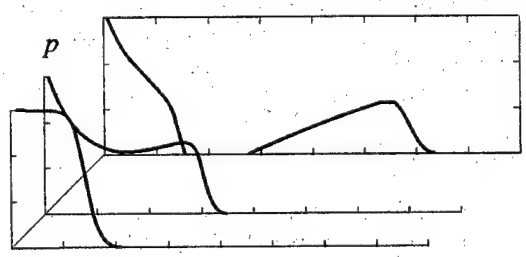

Fig.3

XI. Bulk viscosity influence on the flow stability

In [15,16] it is shown that case $r=\xi/\eta>>1$ leads to the necessity of taking into account the second viscosity influence on the stability both the supersonic and the subsonic flows: the instability threshold increases at $r>0$ and decreases at $r<0$. Such increase of the critical Reynolds number R_{cr} (~9%) was recently observed in circular pipe flow of CO-gas already at small Mach number M=0.1 [17].

In [18] the influence of the relaxation processes on the stability of the compressible flat boundary layer is investigated by asymptotic method. It is found the relaxation correction of the Lees formula (R_{cr}^0)

$$R_{cr}=R_{cr}^0(1+a)\frac{\sqrt{1-M_\infty^2(1-c)^2}}{\sqrt{1-M_0^2(1-c)^2}},$$

where M_0, M_∞ are Mach numbers; c is the phase speed of layer disturbances;

$$a\sim\frac{M_0^4 r}{R_{cr}^o\sqrt{1-M_0^2(1-c)^2}}$$

is the relaxation correction, $|a|\sim 1$ at $|r|\sim 10^3$.

Thus the great relation r leads to the essential influence of the bulk viscosity on the laminar-turbulent transition: the critical Reynolds number decreases at $\xi<0$ and increases at $\xi>0$.

Accordingly to [15] in CO_2, N_2O gases at T~300K the relation $r=2\times10^3$ and at greater temperatures the relation r exceeds considerably this meaning. In the typical laser medium CO_2:N_2:He=1:2:3 (P=1атм., T=300K, $\tau=10^{-5}$c) the second viscosity coefficient $\xi<0$ at the energy supply Q~3MJ/cm^3 and at Q~10MJ/cm^3 the relation $r\approx-10^4$. Note, that such large coefficients of second viscosity including negative ones, are formed not only in vibrationally-excited gas but also in non-isothermal plasma, chemically active mixtures and, also, in dusty gases.

XII. Dusty gases

It is considered the sound propagation in dusty gas, in which the temperature of the dust particles T_p is sustained greater than gas temperature T_g by the external heat source with the power Q. Such source can be, e.g., the light energy absorbed by solid particles of the dust or the electron energy obtained by the dust in collision.

The initial set of equation consist of the mass and impulsive moment conservation

equations for two phases and the energy equations. The last equation have form

$$c_{V\infty}\frac{dT_g}{dt}-\frac{T_g}{\rho_g}\frac{d\rho_g}{dt}=\frac{\rho_p m_0}{\rho_g m_{par}}Q_p-I+\frac{u_g m_0}{\rho_g}f\ ,$$

$$c_{par}\frac{dT_p}{dt}=Q-Q_p-\frac{u_p m_{par}}{\rho_p}\ .$$

Here m_0, m_{par} are the molecular and solid particle masses; c_{par} is the specific heat of particles; ρ_p, ρ_g are the dust and gas phase densities; I is the power of the heat extraction, sustaining the stationary nonequilibrium degree

$$S=\frac{T_{p0}-T_{g0}}{T_{g0}}\ ;$$

$$Q_p=\frac{\rho_p(T_p-T_g)c_{par}}{\tau_T m_{par}}$$

is the rate of heat addition to the gas from dust;

$$f=\frac{\rho_p(u_p-u_g)}{\tau_V}$$

is the rate of work done on the dust by the gas; u_g, u_p are gas and dust velocities; τ_T, τ_V are temperature and velocity relaxation times.

Using this set of equations it was obtained the dispersion relation, the bulk viscosity and sound speed dependencies $\xi(\omega)$, $u_S(\omega)$. In Fig.4 it is plotted the dependence of $r=\xi_0/\eta$ on $\alpha=\rho_{p0}/\rho_{g0}$ in equilibrium dust gas ($S=0$) at Stokes flux law and the particles radius $R_{par}\sim 10^{-6}m$. The relation r is great (hence, the sound absorption is also great) and can be even more for large particles ($\tau_T\sim R_{par}^2$).

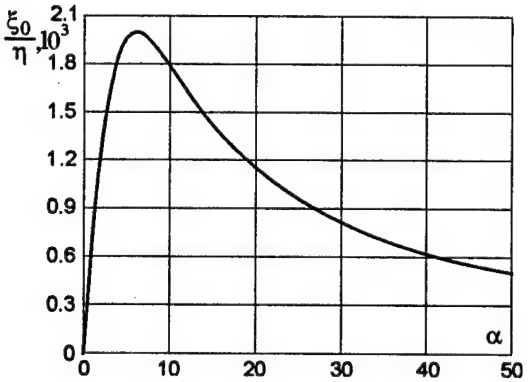

Fig.4

In Fig.5 it is given the dependence $\xi(\omega)$ in nonequilibrium dust gas ($S=1$) at $\alpha=1$ and $\alpha=10$.

At great α the negative viscosity exists in low-frequency spectrum range.

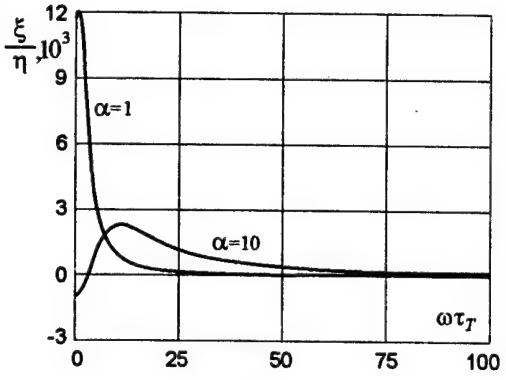

Fig.5

In Fig.6 the dependence u_S^2/u_∞^2 is shown at different S. There is the range of S,α where $u_S(\omega)<0$ and the low-frequency sound can not propagate.

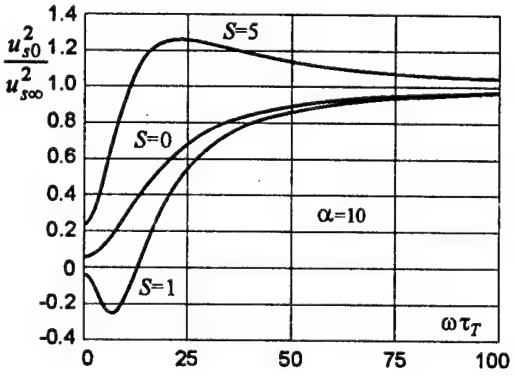

Fig.6.

Thus the dispersion properties of dusty gases can be described by the bulk viscosity formalism. The large meaning of ξ and the possibility of $\xi<0$ leads to the necessity of taking into account gasdynamic effects discussed in part II, III of the present paper.

References

1. *Kogan E.Ya., Moiseev C.C., Molevich N.E., Tur A.V.* // ZTF, 1985, V.55, p.2036.
2. *Osipov A.I., Uvarov A.V.* // Vestnic MSU, Fizika, Astronomy, 1987, V.28, p.52.
3. *Malnev V.N.* // Preprint ITP – 92 , 21E, Kiev, 1992.

4. *Zavershinsky I.P., Kogan E.Ya., Molevich N.E.* // ZETF, 1991, V.100, p.422.
5. *Zavershinsky I.P., Kogan E.Ya., Molevich N.E.* // Acoustic Zh.1992.V.38.p.702.
6. *Molevich N.E., Oraevsky A.N.* // ZETF, 1988, V.94, p.128.
7. *Molevich N.E., Oraevsky A.N.* // Proc. FIAN, 1992, V.222, p.45.
8. *Bauer H.J., Bass H.E.* // Phys. Fluid, 1973, V.16, No.7, p.988.
9. *Kogan E.Ya., Malnev V.N.* // ZTF, 1977, V.47, p.653.
10. *Ingard U.* // Phys.Rev, 1966, V.145, p.41.
11. *Culick F.* // AIAAJ, 1963, V.1, p.1097.
12. *Borisov A.A.* Hydrodynamics investigations, N: ITF, 1976, p.94.
13. *Landau L.P., Lifshits E.M.* // Hydrodynamics, M.: Nauka, 1986.
14. *Zavershinsky I.P., Kogan E.Ya., Molevich N.E.* // Izvestiya VUZov, Pricladnaya nelineinaya dinamica, 1993, V.1, p.87 (in Russian).
15. *Emanuel G.* // Phys.Fluid.sA., 1990, V.2, p.2252.
16. *Kogan E.Ya., Molevich N.E.* // Acoust.Zh., 1995, V.41, p.613.
17. *Nerushev O.A., Novopashin C.A.* // Abst, IV Sibirskiy Sem, 1997, p.76.
18. *Molevich N.E.* // Fluid dynamics, 1999(in print).

ABOUT SOME PECULIARITIES OF STREAMLINE OF BODIES BY FLOWS OF VIBRATION NONEQUILIBRIUM GASES

V.N.Malnev (Taras Shevchenko Kiev University, Kiev, Ukraine),
A.V. Nedospasov (Institute for high temperature physics, Moscow, Russia)

Abstract. Experiments in the hydrodynamics of flows of a weakly ionized plasma reveal the surprising phenomena of the resistance decreasing in streamline. We consider some physical phenomena associated which formation of a long lived nonequilibrium population of vibration levels of symmetric molecules in the process of electron-molecular collisions in a gas discharge. A slow relaxation of vibration energy into the energy of molecular heat motion in the gas flow and on the surface of a streamlined body may result in the peculiarities of the hydrodynamic streamline.

When producing a low ionized plasma in the electric discharge in a gas of symmetric molecules (N_2, O_2) it is possible to form a stationary nonequilibrium population of vibration excited molecules. It is well known that the vibration degrees of freedom are long lived ones and may be easily excited by electrons. For example, the energy of vibration of a nitrogen molecule is equal to 0,29eV and the cross-section of it excitation by electrons has a maximum at the energy about 2eV and approximately coincides with the gas kinetic cross-section $\sigma\approx10^{-15}sm^2$. It means that to excite vibrations of a nitrogen molecule it is enough a few collisions with such electrons. The typical time of relaxation of the vibration energy in the V-T process (transformation of vibration energy into kinetic degrees of freedom) strongly depends on a temperature. In particular, removing the vibration energy requires 10^7 collisions for a vibration excited nitrogen molecule at room temperatures, and 10^4 collisions at a temperature 1500K [1]. This situation manifests itself in the well known hierarchy of relaxation times of degrees of freedom of symmetric diatomic molecules

$$\tau_{kin}<<\tau_v<<\tau\,, \qquad (1)$$

where τ_{kin} is the relaxation time of kinetic (translations and rotations) degrees of freedom, τ_v – is the typical time of V-V processes formation of the vibration temperature T_v, τ corresponds to the most durable time V-T relaxation or transformation of the vibration energy into the energy of kinetic degrees of freedom.

With the help of an external source of energy one can maintain a stationary difference vibration and kinetic temperature T_v-T. We will call such a medium the vibration nonequilibrium gas (VNG). Therefore, at some conditions a neutral component of the weakly ionized low temperature plasma can be treated as VNG.

VNG can be considered as consisting of two subsystems: the subsystem of kinetic degrees of freedom with a temperature T and the subsystem of vibration degrees of freedom with a temperature T_v. The equation which describes a balance of the vibration energy of a molecule can be written in the form

$$\frac{d\varepsilon}{dt}=\frac{\varepsilon_p-\varepsilon}{\tau}+q\,, \qquad (2)$$

where ε_p is the equilibrium energy of molecular vibrations, q is the energy absorbed by the molecular vibrations per unit time. The stationary temperature T_v can be found from the relation $\varepsilon=\varepsilon_0+q\tau$, if we assume that the molecular vibrations are described by the Boltzmann distribution with the temperature T_v. If there is no an external source of energy $q=0$, $T_v=T$.

Further, we assume that in the weakly ionized plasma with a neutral component consisting of symmetric diatomic molecules N_2, O_2 the discharge current provides a stationary regime $T_v>T$ and will discuss the hydrodynamics equations of VNG ignoring a contribution of the plasma charged component into hydrodynamic flow.

A system of the hydrodynamic equations of VNG includes the equation of vibration energy balance (2), the continuity equation and the Navier-Stokes equation (the latter two are in the conventional form). The heat conductivity equation takes into account a "slow" flow of energy from the vibration degrees of freedom and can be written in the form

$$\frac{\partial\vec{v}}{\partial t}+(\vec{v}\nabla)T=$$

$$=\chi\Delta T+\frac{\nu}{2c_p}\left(\frac{\partial v_i}{\partial x_k}+\frac{\partial v_k}{\partial x_i}\right)^2+\frac{\varepsilon-\varepsilon_p}{c_p\tau}\,, \qquad (3)$$

where v is the hydrodynamic velocity, χ is the temperature conductivity coefficient, ν is the kinematic viscosity, c_p is the specific heat of kinetic degrees of freedom at constatnt presure.

For the time of V-T relaxation τ we can use the Landau-Teller formula, which is in a good agreement with experiment in a wide range of temperatures

$$\tau=\frac{\text{const}}{\rho}\exp\left\{\frac{a}{T^{1/3}}\right\} \qquad (4)$$

where ρ is a density of gas, a is a some constant which depends on a frequency of molecular vibrations and a typical length of the intermolecular interactions.

Comparing the system of VNG hydrodynamic equations and the conventional equations of hydrodynamics, we may note that the basin of nonequilibrium energy stored in "slow" vibration degrees of freedom transfers the additional energy into the gas in the processes of V-T relaxation.

When considering the stationary airflow by the incompressible VNG, we must take into account the constant bulk source of heat q/c_p in the heat conductivity equation. Using the known profiles of velocity [2,3] one can take into account the additional heat transfer in the boundary layer and heating of a body by the flow of VNG taking into account the relevant boundary conditions. It is worth noting that along with the bulk V-T processes, deexcitation of molecular vibrations occurs on the surface of the streamlined body. In the later process a part of the vibration quantum of molecules transfers to the surface. The rest part of the quantum transforms in the kinetic energy of the molecule which leaves the surface with a velocity exceeding the velocity of coming molecules. It results in appearance of a macroscopic flow of heat and momentum.

The accommodation coefficient of these processes and probabilities of transition in the vibration spectrum of diatomic molecules were studied in [4-6]. The corresponding results can be used for evaluation of a heat flow from the surface into the gas. We would like to note that this flow does not affect the velocity profile and may be taken into account in the boundary condition for the heat conductivity equation.

The momentum flow from the streamlined surface can also be evaluated with the help of formulas obtained in [4-5]. However, accounting of this flow is more complex problem in the boundary layer theory. The point is that all known velocity profiles obtained at the boundary condition which requires vanishing both the normal and tangential velocity components on the streamlined surface. For example, in the Prandtl equations the pressure gradient normal to the boundary level is assumed to be zero.

The relative value of the momentum flow due to the surface V-T relaxation of vibration excited molecules and charge of the pressure Δp may be roughly estimated with the help of the following formula

$$\frac{\Delta p}{P_0}\approx\alpha\frac{n^*}{n_0}w\frac{\hbar\omega_0}{T} \qquad (6)$$

where n^*/n_0 is the relative density number of vibration excited molecules, w is the probability of the surface relaxation of vibrations, T is the the gas temperatures, α is some constant of the order of one. For example, in [6] we obtained that a probability of relaxation of the first excited vibration level of a nitrogen molecule on the aluminum surface at T=400K happens to be $w=10^{-3}$. The probability of removing the higher excited vibration levels is even larger due to the anharmonicity. This probability increases also when passing from dielectric surfaces to the metal ones. If contents of vibrations excited molecules is of the order of 10%, the relative flow of the momentum into a gas near the surface (6) can be of the same order. We may assume that this momentum flow will result in turbulization of the boundary level and considerable decreasing in the aerodynamic resistance [2] at the lower Reynolds numbers in comparison with streamline by an equilibrium gas. However, a confirmation of this assumption requires a solution of the corresponding hydrodynamic problem.

To our judgement decreasing of the hydrodynamic resistance of bodies in flow of VNG can be connected with two physical effects:

i) additional heating of VNG in the process of the bulk and surface V-T relaxation resulting in decreasing of the gas density;

ii) change of the boundary layer regime associated with the momentum flux from the streamlined surface.

Our calculations show that intensity of the surface V-T relaxation increases when we pass from the surfaces with the lower Debye temperature to ones with the higher. For orientation we give magnitudes of the Debye temperature of some materials (in Kelvin degrees): Ge –250, Al – 400, Si – 650, Be – 1200, diamond – 2000.

In a conclusion we may note one more peculiarity of the hydrodynamics of compessible VNG. It is known that effect of relaxation of slow inner degrees of freedom of a gas (chemical reactions, transfer of energy of vibrations into kinetic degrees of freedom) may be described

with the help of the second or bulk viscosity ξ. In equilibrium media ξ depends on a product of the process frequency and the typical time of relaxation of slow degrees of freedom $\omega\tau$. In VNG the second viscosity depends on the nonequilibrium level T_v-T. At sufficient levels of the external pumping ξ may change sign and become negative. With the help of negative bulk viscosity it is possible to understand application of sound in a gas discharge which observed experimentally [7]. The problem of the bulk viscosity in nonequilibrium media was discussed intensively in [8]. The bulk viscosity of VNG provided that $\omega\tau<<1$ is given by [9]

$$\xi=\rho\tau v_T^2\left(c_k-\frac{1}{3}\frac{a}{T^{1/3}}\frac{q\tau}{T}\right), \qquad (7)$$

Where ρ -is the gas density, v_T – is the heat velocity of molecules, c_k is the vibration specific heat, the time of V-T relation is determined by (5). At sufficient level of the external pumping $q\tau$ the bulk viscosity may be negative. There is no contradiction with a statement of [2] the first viscosity η and the second viscosity ξ must be positively determined.

The point is that a magnitude of the inner friction is associated with the equilibrium kinetic degrees of freedom of molecules and is positive. It may be evaluated in a gas according to the relation

$$\eta=\rho\tau_0 v_T^2>0\ , \qquad (8)$$

where τ_0 is a time of gas collissions. The coefficient ξ in VNG which is called the second viscosity related to the nonequilibrium vibration subsystem and describes the energy flow to the equilibrium subsystem of fast kinetic degrees of freedom. The most simple way to obtain $\xi<0$ in VNG at low temperatures $T<<\hbar\omega_0$, when c_k in (7) is exponentially small and the second viscosity is completely determined by the external pamping.

However the consistent and reliable account of V-T relaxation processes in hydrodynamic flows of VNG due to a complex dependence of the time V-T relaxation on a temperature requires numerical solutions of the streamline problem on the basis of the hydrodynamic equations of VNG.

References

1. *Ya.B.Zeldovich, Yu.P.Raizer*, Physics of shock waves and high temperature hydrodynamic phenomena, Moscow, Fizmatgiz, 1963.
2. *L.D.Landau, Eu.M.Lifshits*, Hydrodynamics, Moscow, Nauka, 1988.
3. *L.G.Loytsyanskii*, Mechanics of liquid and gas, Moscow, , Fizmatgiz,1959.
4. *E.Ya.Kogan, V.N.Malnev*, Accomodation coeffcient of diatomic molecular gas, Zhur. Exp.Theor. Fiz., 1978, v.74, pp.525-532.
5. *E.Ya.Kogan, V.N.Malnev*, Surface relaxation of vibration excited gas, Zhur. Exp.Theor. Fiz., 1978, v.75, pp. 893-897.
6. *E.Ya.Kogan, V.N.Malnev*, Heterogenic relaxation of vibration excited molecules, Ukr.Jour.of Physics, 1983, v.28, pp.374-381.
7. *E.Ya.Kogan, V.N.Malnev*, Propagation of sound in vibration excited gas, Zhur. Techn. Fiz., 1977, v.47, p.653.
8. *N.E.Molevich, A.T.Oraevskii*, The second viscosity in nonequilibrium media, Zhur. Exp.Theor. Fiz, 1988, v. 44,p.128.
9. *V.N.Malnev*, Waves in vibration nonequilivrium media, Preprint ITP-92, 21E, kiev, 1992.

AN ELEMENTARY MODEL OF PHYSICAL-CHEMICAL INTERACTION BETWEEN GAS FLOW AND A WALL

Y.V.Alekseev, and V.A.Bityurin
(Institute of High Temperature of the Russian Academy of Sciences, Moscow, Russia)

Abstract. A model based on physical-chemical background of adsorption and elementary theory of gas phase transport is proposed to assess the influence of interaction of gas molecules with the surface of a solid state body upon mass, momentum and energy fluxes.

The description of adsorption based on the Langmuir' kinetic model assumes that the body surface is uniform and contains a limited number of the adsorption centers N_0 per unit square being equal to the density of surface layers. Let us take into account that the adsorption consists of two stage. The first is a «physical» adsorption caused by a rather week van der Waals' interaction. At the second stage a chemical bind of adsorbat with the surface is formed. The formulation of the kinetic equation of adsorption in terms of absolute reaction rates is based on the calculation of rates of forward and back particle transitions from one equilibrium state to another. These states correspond to minimums of the dependence of Gibbs' potential G upon location of a reaction (distance from surface, see. Fig.1).

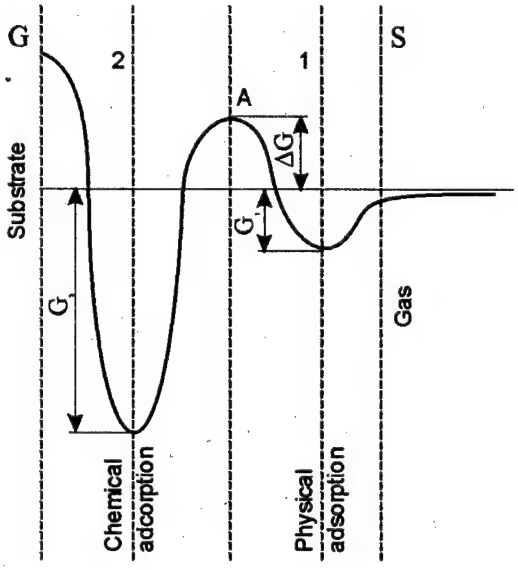

Fig.1.

The particle fluxes corresponding to physical and chemical adsorption, J_1 and J_2 are defined by expressions

$$J_1=J_{1ad}-J_{1des}\ ,\ J_{1ad}=n_s u_s\ ,$$
$$J_{1des}=N_0\nu_1\exp\left\{-\frac{G_1}{kT_1}\right\}a_1\ ,$$
$$J_2=J_{2ad}-J_{2des}\ ,$$
$$J_{2ad}=N_0\nu_1\exp\left\{-\frac{G_1+\Delta G}{kT_1}\right\}a_1\ , \quad (1)$$
$$J_{2des}=N_0\nu_2\exp\left\{-\frac{G_2+\Delta G}{kT_{\text{п}}}\right\}a_2\ ,$$

where the meaning of exponents are clear from the Figure, J_{1ad} is gas flux to the surface (n_s is the number density , u_s is average velocity normal to the surface); J_{1des} is the desorption rate from the first adsorbing layer being proportional to the activity $a_1=\theta_1/(1-\theta_1)$ (θ_1– a fraction of the centers occupied by molecules). The probability of returning of molecule into gas phase is $\nu_1\exp\{-G_1/kT_1\}$, where ν_1 is fluctuation frequency at the equilibrium state, that results in the expression for the life time at the surface as following

$$\tau=\left(\nu_1\exp\left\{-\frac{G_1}{kT_1}\right\}\right)^{-1}\ . \quad (2)$$

The processes, defining values J_{2ad} and J_{2des} has the same nature and for this reason ν_2 is the fluctuation frequency in chemical adsorbed phase, and $a_2=\theta_2/(1-\theta_2)$ is the particle activity in this phase. In the expressions (1) it was assumed that the temperatures of the phase are different: T_s is gas temperature at the surface, T_1 is the temperature at the first adsorbed layer, and T_{sb} is the temperature at the second adsorbed layer. Assuming that the heat conductance of the solid state body is high enough let us guess that T_{sb} is equal to the substrate temperature.

Accompanying the mass transfer the momentum and energy fluxes passing through all phases are provided by particles. Let us consider these processes for the case of gas flow along the surface with velocity v and temperature gradient

$(T_0-T_{sb})/\delta$, where T_0 is gas temperature, T_{sb} is substrate temperature, δ – characteristics size of temperature boundary layer.

In order to define the energy flux it is needed to eliminate the elastic component of fluxes not changing the particle concentration in adsorbed phases in respect to the those in gas phase, or according to Gibbs, not «condensing». Inelastic component of the flux is defined by «condensing» which is greater the stronger interaction of gas molecule with the surface greater and goes to zero when there is no interaction. At the same time «condensing» is defined according to (2) by the particle life time at the surface. Along with increasing of interaction potential G_1 (and, consequently the «condensing») life time τ increases resulting in the growth of energy dissipation in the adsorbing layer.

Thus, the enthalpy fluxes through adsorbed phases are defined by expressions:

$$q_{1H}=\bar{J}_{1ad}\left(c_pT_s-\Delta H_{10}+\frac{mv_s^2}{2}\right)-$$
$$-\bar{J}_{1des}\left(c_{p1}T_1-\Delta H_{10}+\frac{mv_1^2}{2}\right),$$

$$q_{2H}=\bar{J}_{2ad}\left(c_{p1}T_1-\Delta H_{20}+\frac{mv_1^2}{2}\right)- \quad (3)$$
$$-\bar{J}_{2des}\left(c_{p2}T_2-\Delta H_{20}\right)$$

where $\bar{J}_{iad}$ and $\bar{J}_{ides}$ are inelastic states of particle fluxes (their expressions are omitted due to complexity) c_p, c_{p1}, c_{p2} are specific heat capacity per one molecule in gas and adsorbed phase, v_s, v_1 are the tangential velocity in gas phase and in the first adsorbed layer (it assumed that $v_2=0$ because of the strong interaction of adsorbed particles with solid state body there), ΔH_{10} and ΔH_{20} are implicit adsorption heat.

In the case considered of steady state process the particle fluxes are absent: $J_1=J_2=0$, $\bar{J}_1=\bar{J}_2=0$, so that in expressions (3) the condition $\bar{J}_{id}=\bar{J}_{ids}$ is valid and the expressions for the enthalpy fluxes are presented in the following form:

$$q_{1H}=n_su_s\beta_1(H_s-H_1),$$

$$q_{2H}=n_su_s\beta_2(H_1-H_{sb}), \quad (4)$$

$$\beta_1=1-\exp\left\{-\frac{G_1}{kT_1}\right\},$$

$$\beta_2=\exp\left\{-\frac{\Delta G}{kT_1}\right\}\left(1-\exp\left\{-\frac{G_1}{kT_1}\right\}\exp\left\{-\frac{G_1+\Delta G}{kT_{sb}}\right\}\right)$$

The enthalpy flux in gas phase is defined by the expression:

$$q_{2g}=2nu\frac{\lambda}{\delta}(H_0-H_s), \quad (5)$$

where λ is the free length, H_0 is the gas enthalpy outside the boundary layer δ.

Taking into account the continuity the enthalpy fluxes

$$q_{1H}=q_{2H}=q_{gH} \quad (6)$$

and utilizing (4) and (5) one can find H_1 and H_2 and enthalpy flux

$$q_H=n_su_s\frac{H_0-H_{sb}}{\frac{1}{\beta_1}+\frac{1}{\beta_2}+\frac{1}{2\lambda/\delta}}. \quad (7)$$

It is seen from (7) that the enthalpy flux if defined by series resistance of gas phase $(2\lambda/\delta)^{-1}$ and resistance of adsorbed layers $1/\beta_1$ and $1/\beta_2$. The latter according to (4)

$$\beta_2\approx\exp\left\{-\frac{\Delta G_1}{kT_1}\right\}<<\beta_1\cong 1,$$

i.e it is important to take into account the resistance caused by chemical adsorption barrier. The value β_2 depends on the altitude of potential energy barrier ΔH as well as on the change of the entropy at the adsorption ($\Delta S_{ad}<0$):

$$\beta_2=\exp\left\{-\frac{\Delta H}{kT_1}\right\}\cdot\exp\left\{-\frac{|\Delta S_{ad}|}{k}\right\}<<1$$

If $\beta_2<<\lambda/\delta$ then the enthalpy distribution is defined by adsorption resistance. In this case $H_1=H_s=H_0$, i.e. the enthalpy is changed only at the resistance $1/\beta_2$ and the their flux is low:

$$q_H=n_su_s\exp\left\{-\frac{\Delta G}{kT}\right\}(H_0-H_s)$$

In the opposite case the enthalpy is changed only in gas flow ($H_1=H_2=H_{sb}$)

$$q_H=n_su_s\frac{2\lambda}{\delta}(H_0-H_{sb}).$$

The enthalpy distribution found above allows us to define the distributions T and v under condition of self sustained solution of the problem of momentum mv and enthalpy $H=c_pT+\frac{mv^2}{2}$ transport.

It means for the case considered here that two equations (6) for enthalpy flux should be extended by two equations of momentum transport mv. The solution of such a set of four equations provides calculation of T_1, v_1, T_s, v_s. The expression for momentum flux through the adsorbing phases can be derived in simular way along with the fact that momentum is transferred both by elastic and inelastic component of the particle flux J_1 and J_2 :

$$q_{1v}=n_s v_s\left(mv_s-mv_1\right),\ q_{2v}=n_s v_s\beta_2 mv_s\ . \quad (8)$$

The first equation is derived from the gas flux continuity condition at the interface with the first adsorbing face ($q_{1v}=q_{gv}$):

$$n\ v\ \left(mv\ -mv_1\right)=2nu\frac{\lambda}{\delta}\left(mv\ -mv\ \right). \quad (9)$$

In order to derive the second equation it is to be taken into account the fact that molecules with momentum mv_s entered into the first adsorbing layer deviate from initial trajectory due to interaction with substrate. The velocity component decreases to $v_1=v_s\cos\alpha$, α is a average deviation angle during particle migration time τ at the surface. Such a momentum loss leads to decreasing of its flux

$$q_{1v}-q_{2v}=n_s u_s\left(mv_s-mv_1\right)-n_s u_s mv_s\beta_2=$$

$$=n_s u_s mv_s\left(1-\cos\alpha\right). \quad (10)$$

It $\alpha\geq\pi/2$ the loss of the whole momentum occurred, $mv_1=0$, consequently the conditioned gas slip condition is valid at the wall.

To estimate α let us take into account that the local potential energy of interaction (Gibbs potential G_1) is about its mean value G_1 on distances of order of magnetic of the average distance a between atoms on the surface. Molecule moving along the surface deviates on angle $\delta\alpha$ within such an interval. Taking into account that the kinetic energy is significantly greater that δG_1 along the distance a, the deviation angle $\delta\alpha$ can be estimated as following

$$\delta\alpha=\frac{\delta G}{mv_s^2}$$

The sing is defined by the sign of δG. Under assumption that atoms are located chaotically one can obtain a statistical situation, when such interaction actleads to deviation $\pm\delta\alpha$ with equal probability. Such a problem is similar to the problem of one-dimensional Brown notion of particles solved by Smolukhovsky [see [1]). The mathematical expectation of the deviation angle α is $\alpha=\delta\alpha\sqrt{n}$, where n is the number of atoms impact during the particle life at the surface τ, i.e. $n=\tau/\Delta t$, $\Delta t=a/v_s$ is a tree path time. Assuming $\cos\alpha\cong1-\alpha^2/2$ and taking into account (2), one can be find:

$$1-\cos\alpha=\frac{1}{2}\left(\frac{\delta G}{mv_s^2}\right)^2\frac{V_s}{a\cdot\nu_1\exp\left\{-\dfrac{\Delta G}{kT_1}\right\}}\ . \quad (11)$$

The common sokution of (9) and (11) gives:

$$q\ =\frac{n_s u_s mv}{\dfrac{1}{2\alpha/\delta}+\dfrac{1}{\beta_2+(1+\cos\alpha)}}\ ,$$

$$\beta_2\cong\exp\left\{-\frac{\Delta G}{kT_1}\right\}\ . \quad (12)$$

Thus, the momentum flux drops from an initial gas flow value mv_0 till zero at the solid surface (note that the border with gas is the border with the first adsorbing phase) on two series resistance's: in case $(2\lambda/\delta)^{-1}$ and adsorbent $(\beta_2+(1-\cos\theta))^{-1}$. The latter consists of two parallel resistances caused by concurrent processes of momentum loss at the transition from the first adsorbing layer to the second (conductance β_2) and due to friction in the first layer (conductance $(1-\cos\theta)$). For the estimation of the latter the most important value is the non-uniformity δG_1 of the potential depth G_1 along the surface. Assuming further $\delta G\sim0.1G_1$ and utilizing the experimental data on krypton on $\nu_1\exp\left\{-\dfrac{G_1}{kT_1}\right\}$ (G_1=0.1eV, $\tau\cong10^{-10}$s at T_1=2000K) one can obtains $(1-\cos\theta)\sim0.16$. This estimation shows that greater and lower values can be expected. For the lower case the situation with $(1-\cos\theta)<<2\lambda/\delta$ and, probably $(1-\cos\theta)>>\beta_2$) and the friction drag would be defined by momentum change in the adsorbing layer ($mv_s\cong mv_0$), and its value can be small $q_v=n_s u_s V_0\left(1-\cos\alpha\right)$. For the opposite case the skip condition is valid (α_v=1).

Reference

Moelwyn-Hughes, Physical Chemistry, Pergamon Press, London-New York-Paris, 1969, 1408p.

SOME FUTURES OF THE PLASMOID FORMATION WITH REFERENCE TO AERODYNAMICAL PROBLEMS.

Avramenko.R.F., Grishin V.A., Nikolaeva V.I., Paschina A.S. (NIIRP Moscow)

Abstract. The mechanisms of plasmoid formation, having such properties of the macroscopic quantum objects as superfluidity and as superconductivity which are based on the existence of a phone of an electronic Bose – condensate (PEBS) concept are considered. Characteristic PEBS frequency spectrum, appropriated to interaction with a gravitational field of the Earth, is determined. A role of a specified mechanism in formation of a natural plasmoid - fireball - is considered.

Introduction.

Earlier it was obtained [1, 2],that effective parameter change of the flow around the body can be achieved using non-thermal interaction of plasmoid formation with over-running flow. Some scientists consider that plasmoid formations may be of a quantum nature [2,3]. This defines some specific requirements to the formation of plasmoids and their usage in solving the
aerodynamical problems.

Theoretical premises of plasmoid energetical balance.

One of the hypothesis which explains the process of plasmoid forming is based on existence of a phone of an electronic Bose-condensate (PEBS) [3], interaction with it in some conditions can cause the forming of stable plasmoid structures. According to the basic quantum concepts the charge of an electron is an operator. As a basic idea the thesis of noneqvivalence of conductivity currents (amplitude-phase modulations of electron wave function) and currents convection (transfer of charge absolute value) described by Leanar-Vihter potentials is used.

Redistribution of Boze-condensate (BC) electron charge density can first of all be the result of "non-electric" interactions (gravitational, spin, interactions with convectional currents). Presence of such interactions makes up a situation similar to the electron grab by potentional depression. In this case the system has the characters of macroscopic quantum object, characterized by fundamental frequency spectrum which is determined by potential well characteristics (mechanism of interaction with PEBS). In electrical circuits that maintaining plasmoid elements (electrolyte, semiconductors and so on) the main way of interaction with "smeared" BC electrons is the existence of considerable convection currents (for example positive ions). Depending on power and choice of parameters the electric circuit can be the passive PEBS fluctuations receiver or active influence on changes of density and form the macroscopic quantum objects - plasmoid formations with their own specific frequencies spectrum. The similar mechanism is realized in natural plasmoids - fireballs. First results on quantum nature of plasmoid formations is presented in [2,7].

Theoretical and experimental research shows that some frequencies of the PEBS spectrum dependent on gravitational field of the Earth has value close to 50MHz. This frequency range can be seen in cold nonequilibrium plasma specifically in the region of gas discharge of a low pressure [4,5].

When conditions of electro-magnetic and de-Broel conditions are fulfilled the electrical circuit with plasmoid element can be a macroscopic quantum object that has several properties such as superfluidity and superconductivity. This properties take place in condition of existence of critical current (analog the critical Dgozefson current) and critical temperature that correspond to the jump from superconductive to the normal state.The estimate of the critical current and critical temperature give the values I=39.57A and T_k~800...1600K.

This conclusion can be used in aerodynamical research for example in supersonic flow. In this case we have to consider the parameters of the medium (the filling flow) influence on the properties of forming plasmoids. With regard to the non-local nature of quantum interaction the most effect on the aerodynamical parameters of the object will be if specific dimensions of plasmoid will have the values comparable with the dimensions of the object that use the idea of considering the effect of ground pressure (Ucshenkov N.I. 1981).

Experimental research.

The experiments for active and passive electrical circuit were held. As a passive electrical circuit (power level not more then 100Wt) for the modeling conditions of power-exchange in plasmoid formations the variant of non-symmetrical circuit with length about ~λ/2 charged on to the discharger of a special construction for the frequencies about 50MHz which depends on one of the PEBS oscillations spectrum branch, was used.

The experiment showed that general resonance in neighborhood of predicted frequencies take place. It can be associated with two theoretical values of frequency - 47.5 and 49.5MHz. The amplitude of the plasmoid oscillations doesn't depend on pump current and is almost constant. In case when the discharger is not used those frequencies doesn't appear. For selection of plasmoid oscilations the inductive-condencer transmitter of a special construction was used.

In experiments there was an opportunity to take away the power of plasmoid oscilations to the low-resistance active load - kincandescence bulb. Different bulbs were used beginning with little ones type CM-15(~0.5Wt) up to the automobile ones 5..10Wt, 12V.

For the investigation of the active regime the spiral wave conductor (Tesla coil) was used. It was connected to output of the high-frequency generator (power of 63KWt).

Ignition of the discharge from the high-voltage end of the coil with atmosphere pressure leads to the forming of the torch with a delineated structure: bright sentral part and less bright hull. When the oscilation power of the HF generator is not more than 2KWt the length of the torch is about 1..2 length of th coil. Increase of the power leads to the proportional growth of the torch length. Torch has a wave structure with necking and thickening.

The medium state (static pressure, existence of the flows and so on) plays a great role in effecting on characteristics of discharge. For example with an atmospheric pressure the flow out the gas form the hole in the high-voltage electrode leads to the periodical appearance of the plasmoid structures, which look like lightning. Structures form in region non-perturbed by flow in the direction perpendicular to the direction of the flow.

While investigating the flow near the body with Mach numbers (M~1,5..3) there are 2 regimes of the discharge burning depending on pressure of braking. When the pressure is less than 150Torr on the nose part of the model the luminous diffusion ball appears. When the pressure is more than 150Torr the ball decreases till it disappears and the shell appear all around the model. The shell consists of spindle like structures which are oriented along the flow. So there is an critical value of pressure of braking at which the scale of plasmoid formation changes. The similar effect was observed in atmosphere while influencing the torch by the air-flow. Depending on pressure the large-scale "lightning" disappear and are replaced by thread-like structures with specific thickness about 1mm. The critical value of the flow pressure that corresponds to the structure changes is not more than 0.05atm. The growth of the pressure from 1 to 10atm doesn't change the regime of the discharge burning.

Analysis of the facts gives an opportunity to draw an analogy with the superconductors of the first and the second type. Diffusion ball in the flow and the linear "lightning" in slightly disturbed medium can be associated with superconductors of the first type. The specific dimensions of the structures are adjustable to the theoretical estimates for quantum resonators that can be formed by electro-magnetic emission of the spiral wave-conducer on the frequency of 13.5MHz. The harder disturbances of the medium are adjustable to the superconductors of the second type. The small-scaled spindle-like structures can be associated with Abrikosov vortexes. The distribution and orientation of is defined by parameters of the flow for example direction and gradient. The tendency of attaching the threads to disturbances also coordinate with Abrikosov theory [6].

Gas temperature of plasma on the surface of the model is not greater than 120°C. Increasing the temperature of plasma greater than critical value leads to the distraction of super-conducting pares with secretion of binding power.In aerodynamical experiments this moment corresponds to the appearance of bright attachments on the surface of the model. Their existence can cause the destruction of the models' surface.

Such structures differently influence on aerodynamical characteristics of the model in supersonic flow when Mach numbers are about (M~1,5..3) for example on the part of the drag force related to the pressure of the flow on the nose part of the model. In case of diffusion ball the stable decrease of the drag force can be observed (up to 5%). According to the shadow shots existence of the diffusion ball fuzzifies the form of the head shock wave.

For the values of pressure when thread-like structures exist in most experiments the

influence on the aerodynamical characteristics was small. But in some experiments the decrease of drag force up to 50% was fixed. Using the shadow photos we can see that influence from thread-like structures on the head shock wave is local fussing and some times it can be districted. Random nature of the results can be explained by non-optimal characteristics of resonators and some peculiarities of experiments in which the task was to generate the plasmoid formation only before the head shock wave.

Dependence between changes of the drag force and the time especially in time moments of turning-on and turning-off the discharge can be the additional confirmation of the quantum nature of the phenomenon. The effects of dependence drag on time were also observed also in other plasmo-aerodynamical experiments (TsAGI, GosNIAS, NIIRP). This regions show the existence of super-flowing component that was noted by essential amplitude fluctuations (up to 50%) of the drag force function: to the increase after turning-on the discharge (~1sec) and after (!) turning-off the discharge (2..3sec). This periods of time are close to theoretical values of the life-time of plasmoid. And it's very suspicious that this periods can be explained by transient process in electrical circuits of weight data units.

Conclusion.

So it's obvious that for effective influence by plasmoid formation on regime of flow around the body it's necessary to consider its quantum nature. The specific dimension of the plasmoid must be depending on bodies dimensions. The efficiency of influence on the aerodynamical characteristics of the flow around the body depend on energetical parameters of the plasmoid formation. We have also to consider the parameters of the flow that can cause the change of the plasmoid structure - type of the transition "superconductor of the first type - superconductor of the second type". For the determination of the flows influence on the type of transition the special research must be driven.

It's obvious that use of plasmoid structures isn't limited by aerodynamical problems. The fields where the interaction of electric circuits and the plasmoid elements may be: creation of sources of electrical energy using the transformation of the energy from the surroundings, control of the burning process in supersonic region, lessening the noise (while supersonic out-flowing) and so on.In the last example there is an opportunity to transform the energy of noise into the electrical energy.

References

1. *P.F.Avramenko et al.* Izmenenie obtekania tel v slaboionizovannoi plasme (Modification of weakly ionized plasma flow around a body), Scientific Patent, No.007, 1986 (Moscow).
2. Sharovaya molnia v laboratorii (Ball Lightning in Laboratory), 378p., Khimia, Moscow, 1994 (in Russian).
3. *P.F.Avramenko, N.I.Nikolaeva,* Rvantovaya energia elektronnogo Bose-Kondensata v okruzhayutschei srede (Quantum energy of electron Bose-kondensat in ambient media), Khimia, Moscow, 32p., 1991 (in Russian).
4. *V.I.Rakhovski,* Fisitscheskie ocnovy kommutatschii electricheskogo toka v vakuume (Physical background of commutation of electrical current in vacuum), 536p., Nauka, Moscow, 1970 (in Russian).
5. *V.L.Granovskii, L.I.Bykhovskaya,* Zhurnal Experimentalnoi i Teoreticheskoq Fosiki (Jojet Physics JETP), v.16, p.823, 1946.
6. *D.R.Tilly, J.Tilly,* Superfluid and Superconductivity (Russian Translation), Mir, Moscow, 1977.
7. *P.F.Avramenko et al.* Issledovanie plasmennych obrazovanii, iniziituemykh erosionym razryadom (Study of Plasma formation Created by Erosive Discharge), Zhurnal Tekhnicheskoi Fiziki (Jovjet Technical Physics JTP), v.60, No.12, 1990.

OPTIMIZATION OF METHODS OF ENERGY INFLUENCE ON HIGH-SPEED FLOWS

A.L.Kuranov, V.V.Kuchinsky, V.Yu.Sepman, V.S.Sukhomlinov, Yu.A.Tolmachev

Hypersonic System Research Institute of Holding Company "Leninetz",
Laboratory "New Hypersonic Technologies" of St. Petersburg State University,
St. Petersburg, Russia

The physical mechanisms changing the aerodynamic characteristics at energy influence on high-speed flow are divisible into three conventional groups. The most investigated and obvious is thermal mechanism. Dispersion properties of plasma can have a noticeable influence on formation and distribution of shock wave at producing plasma formations about a surface of flight vehicle. The energy action on a flow can be so organized that in neighborhood of streamlined body there will be fields with significant density gradients. The pass through any such non-homogeneity also leads to change of structure of shock wave.

The adding of energy into flow at the use of thermal mechanism of drag reduction can be implemented continuously or pulsewise; in doing so the characteristic frequency of impulses can be much more than the reciprocal of the time for pass of field of heating. At stationary adding of energy the energy release area stretched out maximally along direction of mass velocity is most useful (at fixed integrated power).

At pulsing method of energy supply and fixed power of supply source it is necessary to have more fast energy supply with frequency of the order of the reciprocal of the time of pass of field of heating τ. If the peak power of the source is limited, the optimum is the energy supply that is constant in time. If the peak power is limited and the mean power is given, the organization of extreme short impulses with duration $\Delta t \ll \tau$ is required. Thus, in a series of cases it is expedient to use a pulsed source of energy supply.

However, the received estimations of energetic efficiency of the thermal mechanism show that the power more than 10 MW is required for drag reduction by 10-15% at the real flight vehicles.

On this basis it is necessary to consider also other two mechanisms of influence on shock wave. The received estimations show that the reason of obvious benefit of these mechanisms in comparison with thermal one is that they are essentially non-linear. In other words, insignificant changes of specific parameters of the medium cause noticeable changes of the medium response on perturbations. We suppose that the use of energy for creating the medium (for example, plasma) with specific properties, which exert decisive influence on parameters of shock wave in shock neighborhood area, is very promising.

At application of plasma methods of energy influence on flow the considerable problem is associated with inputting the energy of high density into plasma. We have developed and made in practice the method of increasing the temperature of plasma in a local space site up to tens of thousands degrees. This method gives a hope for making enough effective devices for drag reduction.

NEW TYPE OF SCIENTIFIC SPACE MISSION: SMALL SATELLITES WITH PLASMA THRUSTERS

V.M.Balebanov, R.Z.Sagdeev, G.S.Bisnovatyi-Kogan (Space Research Institute RAS)

Abstract. Small satellites are suggested to use in different space science missions with a total mass 100-700kg, and payload between 25% and 50% respectively. Stationary plasma thrusters of Russian production are supposed to be used for acceleration of satellites after their lunch to the basic orbit, and also for corrections of the orbit. Velocity gain produced by these thrusters may reach about 1km/s/month, what could permit to fulfill any mission inside the Solar system. The resource of the thruster is up to 1 year Possibility of using of Russian conversion rockets for launching of scientific and industrial "low cost" missions are discussed.

Introduction.

Space missions are necessary instrument of the modern science. Astronomical missions are used to extend the range of the observations into different parts of electromagnetic spectrum: infrared, ultraviolet, X-ray and gamma-ray bands, to investigate cosmological microwave background, its fluctuations and spectrum. Space missions investigate interplanetary plasma, comets, and different planets of the Solar System and their satellites. Development of technology and informatics, rapid increase of number of scientific and communication space missions had moved the interest to smaller specialized spacecrafts, designed for deeper and detailed study of few specific problems of largest interest for the moment. Such small missions had made successful X-ray investigations in astronomy since middle of 70-s, when English satellite ARIEL and Dutch one ANS had been launched. Now under successful operation are small X-ray satellites RXTE by USA with unprecedented timing resolution, soon expected a launch of another USA satellite HETE for multi-wavelength observations of cosmic gamma-ray bursts. The programs for development of small science missions are accepted in France on the base of the pointing platform PROTEUS, and in Spain. Small spacecrafts can be part of the telecommunication, navigation and Earth-monitoring space systems.

Modern technology achievements allows to realize light low-cost space vehicles, based on light solar array and electric propulsion engines. One of the most reliable, tested, and high-performance engines is Russian stationary plasma thrusters (SPT). High specific impulse of these engines allows to apply near identical space vehicles to different missions. It allows to realize project of small universal space platform with plasma thruster [1].

Design.

Stationary plasma thruster SPT-70 have operated in space more than 25 years since its first launch in 1971. Its main characteristics are: trust - 20mN; power consumption - 350W; service lifetime is more than 5000 hours; gas (Xe) expenditure - 2mg/s; plasma velocity - 12.5km/s; mass - 1.5kg. Thrusters of SPT-100 type (thrust of about 80mN, specific momentum of about $1500s^{-1}$, with a life time of more than 8000 hours) are currently developed and manufactured in Russia, power processing and control units are provided. Propulsion subsystem is developed and manufactured in USA by a joint Russian-American company, International Space Technology Inc. (ISTI).

Plasma thrusters 14, 20, and 29cm in diameter (Xe based) are the next in the set of Russian thrusters, tested in space. Thrusters SPT-70 and SPT-100 have been flown more than 80 times to correct the orbits of different satellites. The new type of SPT is designed [2] for the spacecrafts with the following characteristics: electrical power is between 300 and 1500W, semiangle of the jet does not exceed 15° (decreasing from 45° in previous sample), thrust efficiency is between 45 and 70 percent (25 and 50 percent in previous sample). The engine has smoothly regulated characteristics, what permits to change by commands either thrust or specific momentum. The engines may provide continuous change in thrust from 10 to 100mN, and in specific momentum from 1100 to $2500s^{-1}$. The schematic design of the spacecraft with two SPT - 100 is presented in Fig.1.

These thrusters may be used in spacecrafts for different functions:

1. to change the orbit of the satellite (acceleration, deceleration, change of an orbit inclination),

2. to use the thruster in a guidance contour of the satellite for the orientation and stabilization of the spacecraft,
3. to perform any orbit corrections.

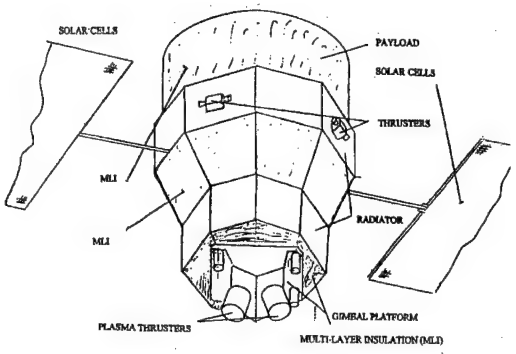

Fig.1.

Possible Scientific Applications.

Small spacecrafts may solve different scientific tasks for direct exploration of the Solar System, as well as for different astronomical observations, not available from the Earth surface. Among them the following may be mentioned:

1. solar activity monitoring from Lagrangian point L_1;
2. Magnetospheric boundaries fine structure study (bow shock, magnetopause, plasmapause, neutral sheet, etc.);
3. Moon investigation and exploration;
4. near Earth asteroid investigation;
5. Earth remote sensing and control;
6. high time and spectral resolution X-ray observations of X-ray sources;
7. investigation of the cosmic microwave background (spectrum and fluctuations);
8. high-precision measurements of low-amplitude star variability and oscillations (stellar seismology, and search of planetary systems and Earth-like planets);

When the spacecraft is in a low circular orbit (e.g. ejected by Shuttle) it can accomplish a number of different missions [3]:

1. to enter a high altitude circular orbit and return to a low orbit;
2. to enter a Lunar satellite orbit;
3. to reach the vicinity of the libration point
4. to reach near Earth asteroids and rendezvous with some of them at a zero velocity;
5. to carry out flights to Venus and Mars;
6. to be used in the interests of telecommunications in near Earth and geostationary orbits;
7. to be used for earth, ocean, and atmosphere observations, or to be used in ecological and navigation systems and so on.

The proposed small space platform with a scientific payload of 25-350 (corresponding to the total spacecraft mass 100-700kg) can be used to investigate space plasmas, solar physics, planets and small bodies of solar system and well as, to solve some applied tasks.

Possible mission scenarios. The low thrust of electric propulsion makes any orbital maneuver dependant on a slowly evolving spiral trajectory before the spacecraft would leave the Earth gravity region. Depending on ΔV requirements the possible missions can be divided in a following way (M_{xe} is given per 100kg of the initial mass of the spacecraft):

— near low Earth orbit (LEO) missions (technology test, free flyers, recoverable payloads - "boomerang" scenario) orbit: 400km to 600-800km (and back), ΔV=1km/s, M_{xe}<10kg; could provide for the tests of new designs (for solar planets etc);

— low orbiting small spacecraft require roughly the same amount of ΔV, M_{xe} in order to reach orbits up to 1000-1500km (without changing the inclination); may provide for the basic LEO orbits for atmospheric and magnetospheric studies; additional capabilities for maneuvers are automatically built in.

— Low orbits with a change of orbital plane (inclination) require a higher mass consumption; to change to an orbit of 51° to 80° (needed for most Earth observations, for example) would require ΔV=4km/s, M_{xe} about 35kg.

— Small spacecraft in plasmasphere with orbits around 10,000-15,000km, ΔV=2-4km/sec, including going to quasi-polar orbits.

— Geostationary orbits: ΔV=4km/s.

— Lunar missions would require a ΔV of >7km/s; and should be placed in a category with initial mass of the order of 150kg or more.

— Spacecraft in solar wind or Earth-Sun libration points: ΔV>8km/s, M_{xe}=60-70kg. Grand orbital maneuvers between bow shock and geotail would require only a modest additional mass of xenon.

— Solar system missions. Earth group planets, comets, asteroids.

Consider the following scenario. A spacecraft with a total mass of 150-300kg is launched from manned near-Earth orbit station (MIR, ALPHA). Than the spacecraft is gradually getting into a required orbit with the help of one or two plasma thrusters of SPT-100 type, having a thrust about 80mN, a specific momentum of about 1500s^{-1}, and a life time of more than 5000 hours. The working gas, Xe (50-115kg), is sufficient to fly to the required region of space, to correct the orbit and stabilize the spacecraft. In this case a total spacecraft velocity increase is 3-7.5km/s.

The SPT, having unique performance and many times proven in space, more than 80 times had flown in space without failures. The large SPT lifetime is confirmed by 8000 hours ground test in Russia, and about 6000 hours ground test in JPL [1].

Fig.2-5 show different examples of SPT application for spacecraft orbit evolution around Earth and Mars (numerical simulations). Fig.6 gives an example of planned scientific missions which should be launched into libration points LI (GEOSTORM for investigation of solar wind plasma), and L2 (RELICT-2 for investigation of microwave background radiation).

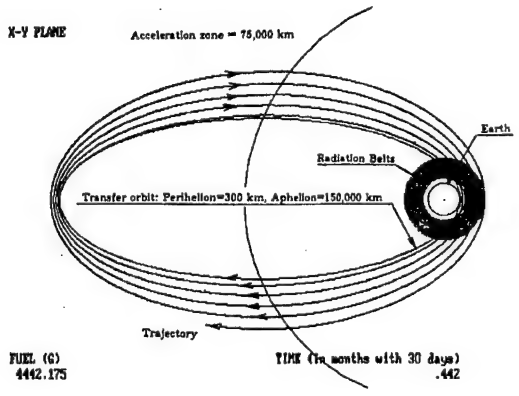

Fig.2.

Evolution from Phobos orbit to 500 km above Mars orbit

Number of loops is 10 times more than displayed.

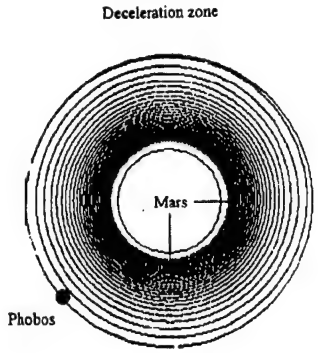

Spacecraft:	
Start total mass (Xe included)	86.5 kg
Electric propulsion system:	
Xe expenditure	0.002 g/s
Plasma velocity	12.5 km/s
Total time required to get to Mars orbit	45 days
Total gas expenditure	7.8 kg

Fig.3.

Evolution from Martian transfer orbit to Deimos orbit

Number of loops is 5 times more than displayed.

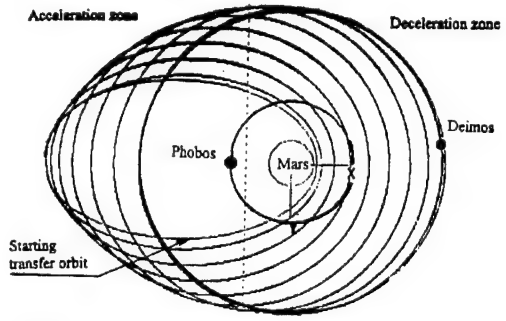

Spacecraft:	
Total mass (Xe included)	100 kg
Electric propulsion system:	
Xe expenditure	0.002 g/s
Plasma velocity	12.5 km/s
Transfer orbit:	
Pericenter (above Martian surface)	500 km
Apocenter (above Martian surface)	35000 km
Total time required to get to Deimos orbit	47 days
Total gas expenditure	8.0 kg

Fig.4.

Evolution from Deimos orbit to Phobos orbit

Number of loops is 5 times more than displayed.

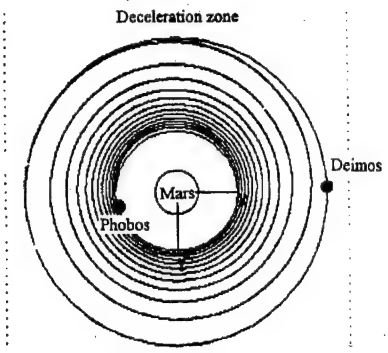

Spacecraft:	
Start total mass (Xe included)	92 kg
Electric propulsion system:	
Xe expenditure	0.002 g/s
Plasma velocity	12.5 km/s
Total time required to get to Phobos	32 days
Total gas expenditure	5.53 kg

Fig.5.

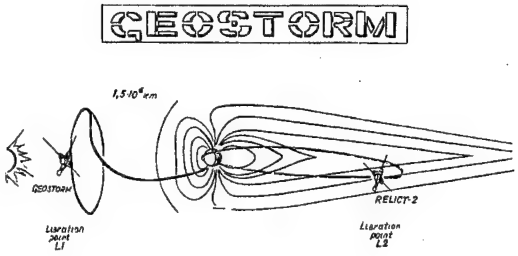

Fig.6.

Rockets.

The low cost launch of the spacecraft is connected with using of ballistic rockets designed for military purposes. Under conversion program these rockets are modernized with a goal to have a possibility of launching a spacecraft to the Earth orbit. For small spacecrafts the rocket SS19 may be used, which is now suggested in two modifications. The first one under name "STRELA" is prepared in NPO "Mashinostroyeniye" has minor modification from the original design. It has 3 stages with launch from the mine, what implies serious restrictions to the size of the spacecraft. It is capable to launch to the height 500-1000km the payload of the mass 1000-800kg. The launch from the cosmodrom Plisetsk permits to reach high latitude orbits. Another modification under name "ROKOT" is designed by the joint Russian-German venture with NPO "Khrunichev Plant" from the Russian side. The modifications here are more substantial, including total reconstruction of the third stage of the rocket, and building of the ground-base design for launching from the surface of the Earth. It permits to launch spacecrafts with maximum size in the plane perpendicular to the rocket axis up to 4 m, almost two times larger than by "STRELA". The mass and orbit height characteristics of these two modifications are almost identical. There is also a possibility to improve substantially mass and orbit height characteristics of "STRELA" by adding a forth stage to the rocket with a powder engine. The powder engine may be used also for rapid crossing of the Earth radiation belts.

For larger spacecraft launch there is a possibility to use a larger conversion missile SS18, which may carry almost 2.5 times larger weight. After reaching a base orbit, using of SPT permits to transform the orbit in order to reach any point of the Solar system [2].

References

1. *V.M.Balebanov et al.* Small Universal Space Platform: Mission Capabilities. Acta Astronautica, **39**, No.1-4, pp.181-188, 1996.
2. *A.I.Morozov et.al.* Plasma Thrusters of New Generation for Small Space Missions. Proc. 1-st Annual International Conference& Exhibition "Small Satellites. New technologies, achievements, problems and prospects for internal cooperation in the New Millenium. 16-20 November 1998. City of Korolyov, Moscow region. VIII.4.
3. *V.M.Balebanov et al.* Small Satellites with Plasma Engines Designed for Research and Applied Problem Solution. Same Proceedings. I.11.

THE METHOD OF INTEGRAL ASSESSMENTS OF MASS-ENERGY CHARACTERISTICS OF SSTO VEHICLE WITH A SCRAMJET

Lebedev P.D. (MAI Moscow.)

The method of forming the conception of airspace crafts(ASC) using G as a main engine was developed. The method is based on the integral analysis. Also the approximate formulas for selection of the basic parameters of engines' acceleration and sub-orbital velocities and for the estimation of their energy-mass characteristics were assumed. The examples of the calculations of simplified scheme of the flight considering the thermal and dynamical restrictions were shown. The basic approaches of constructing the ASC with G on binary kerosene-hydrogen "binary" fuel were analyzed. While analyzing the regeneration and temperature loss is considered and the numeric example of their conceptional estimations in case of launching gravity up to 100t was shown. Use of the R.F.Amramenko, V.I.Nikolaeva, A.I.Klimov, M.B.Pankov and author's results on reducing the aerodynamic drag of the glider and on stabilization of the fuel's combustion by non-traditional electro-physical methods in forming the conception of ASC makes it real to widen the region of hyper-sonic carbon burning in G and as a result increase the relative mass of effective cargo that can be delivered to the orbit by 2..3 times and also reduce the minimal weight and dimensions of ASC.

The author proposes the integral method of the conceptional estimation of energy-mass characteristics of ASC with G as a basic engine that is based on series of calculations in analysis of entire energy-mass exchange with environment by the calculating the drag to the influence of aerodynamical heating and regeneration cooling on the mass characteristics of the whole system. The equation of ASC with G acceleration can be represented as a modification of the K.E.Tsialkovskiy formula considering the impulse loss that depending on aerodynamic drag X and loss of the heat generally depending on friction by part of aerodynamic drag.

$$\ln(m_c/m_0)=\left(V_0^2/2+gH_0\right)\times \frac{1+0.3K_D(X_f/X)(X/R)(1-K_p h_p \eta_p/I_{rc}h_{rc})}{\Delta h_T \eta_T (1-X/R)}$$

The influence of Q_w and X on mass characteristics of ASC can be derived if we substitute the expected values of parameters along the trajectories: $0.41<X_f/X<0.44$; $(0.2<X/R<0.3)$; $(0.5<K_p<0.9)$; $(0.5<\eta_p<0.75)$; $(0.35<\eta_T<0.55)$. Because of heat loss (ΔQ_w) we can expect the mass decrease on the orbit m_0 by about 2..7% as a of aerodynamic drag by 16..23%. (while m_{pn}=4%...7%m_0). This shows the necessity of their consideration even at the step of conceptional research of different projects of ASC with G.

1. Choose of the acceleration trajectory.

Ratio of aerodynamical drag to the thrust X/R for integration system ASC+G And pressure head of flowing air must be bounded by admissible acoustic and heat loads [1]. Considering this restrictments the trajectory of trapezoid-like form by pressure head q_v with non-monoton change of thrust of G was developed. So we can say that inspite of the prevailing influence of inertia on ASC acceleration the change in aerodynamical drag for the given graph of the q_v will cause the necessity of proportional change of engine thrust and so the fuel mass.

2. Choose of the ASC conception.

By the prototype for the numerical modeling the ASC with multi-regime G was taken that was later called TU-2000A. In the numerical model that was used some changes were made but the volume of the glider and the hydrogen tanks stayed the same. The stage of initial acceleration using kerosene and binary fuel mixtures of it with hydrogen up to M=8..10 and so the standard launching gravity was increased by the weight of engine and external tanks.

3 Choose chose of the ASC's engines.

For the acceleration up to M≤5...6 the hydrogen engines with hydrogen steam turbine can be used. A scramjet using kerosene fuel was developed and tested on M about 6,7 with author's participation in MAI. In TsMKB "Souz" and CIAM the flight tests of double-mode scramjet using cryogenic hydrogen fuel were carried out. Tests of scramjet of both types showed the necessity of developing the systems of fuel burning stabilization in sub-sonic flow and control of the flow in the entrance of the input air-duct in zone of "isolator" in combustion chamber - in regions of mixture and combustion and also in neighborhood of pressure shock decrease and in hyper-sonic nozzle.

4. Analysis of the possibilities of electro-physical methods for decreasing of aerodynamical drag, control and stabilization of combustion in sub- and super-sonic flows that can be over-restricted and over-enriched fuel-air mixtures of hydrogen and kerosene was held on model systems in MAI and in TsAGI with help of specialists from several organizations (IVTAN, NIRP, MRTI). The ensuring facts about possibility of generation of local plasmoid formations, streamers and torch discharges that spread along the flow and against it were obtained by this group. Increase of pressure and tempreture caused the increasing of absorption of electrical energy. Use of fuel-air and fuel-argon burners together with HF-discharges localized using Tesla coils in specified zone proved predicted re-influence with mutual stimulating burner-discharge that stayed stable even when the propane-air mixture was over-restricted by 20 times using mixing with argon. Considering the facts from works of R.F.Avramenko, A.I.Klimov and M.B.Pankova on increasing of aerodynamic quality and experiments held by the author on flame and plasma stream we can say that more forces and means of fundamental and practical research in this field of plasmoid and streamer methods of control of the process in engines and coordination on ASC glider and of course on other aircraft objects must be used.

5. Illustration of the possibilities of shown methods. On photograph one of the variants of self-organization of electro-physical objects is shown that were made at MAI on LD-60 system when frequency was about 13,6MHz and the pressure in the camera was from 2 up to 230 kPa. A lot of materials were collected while experiments with Avramenko R.F. and Klimov A.I. that showed the possibility of crossing 300-700mm of silent space or air-flow when active potential not more than 2800V on anode of the GU-23A bulb and not more than 2000v near discharge foot.

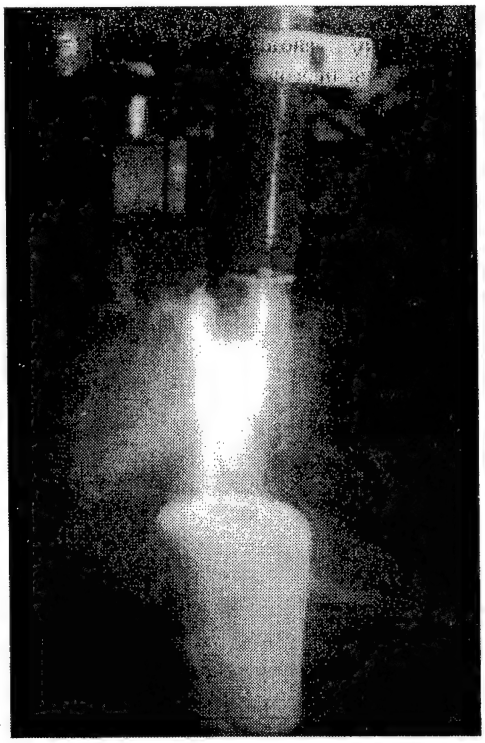

Burning of Propane/Argon in super sonic air flow, stimulated by HF streamer discharge: P_{st}=6kPa, M=2.25, P_{Ar}=150kPa, $P_{C_3H_8}$ =100kPa.

Conclusion.

Methodology of forming the conception of airspace crafts was developed It is based on integral evaluations of energy-mass exchange with whole environment. It is shown that using kerosene as a fuel for G with use of plasma-streamer stimulation of combustion and methods of plasma aerodynamics are useful.

ON APPLICATION OF ELECTROMAGNETIC TECHNOLOGY FOR A DIRECT LAUNCH INTO ORBIT.

M.P.Galanin, A.D.Lebedev, A.P.Lototsky, K.K.Milyaev, V.V.Savitchev, B.A.Uryukov (MAI, Moscow).

Introduction

In spite of the practical stopping of financing of scientific programs on super high speed (~10km/s) acceleration of projectiles all over the world, the possibility of electromagnetic launch of small artificial satellites directly from the Earth still remains in the list of urgent problems of mankind. The necessity to take care of ecology and the optimum usage of a terrestrial surface with the permanent improvement and renovation of artificial satellites, seemingly will force one to be working on this problem in the next 5-7 years.

Such an idea has become already known to mass media (refer to publications [1] in the usual newspaper available to all and in the newspaper [2] of scientific community). Intensive development of methods of electromagnetic acceleration of projectiles has begun in the world in the end 70's. One of the first objectives of the development of such devices was a direct launch of bodies into space [3]. It should be noted that yet the father of cosmonautics G. Oberth did theoretically developed an idea of delivery of cargoes from bases on the Moon to the Earth with the help of magnetic guns [4].

Within the framework of the current state of development of science and technology, there is seen [5,6] only one a possibility of making a high initial pulse sufficient for the direct launch of bodies from Earth into space — the use of an electromagnetic acceleration of either conduction (when the electrical current flows through an object being accelerated) [7-10] type or induction [11-13] type. The first space velocity (8km/s) in an electromagnetic launcher was achieved and exceeded [14] with the help of a conduction accelerator of a railgun type.

The long-term studies directed on the achievement of velocities of projectiles greater than 10km/s in accelerators of conduction type — railguns, have shown that there exist certain physical barriers, which do not allow one to accelerate projectiles up to these velocities. Acceleration of projectiles in a railgun with the help of metallic jumpers (armatures) is preferred compared to acceleration by a plasma armature. The main advantage is in fixation of location where a driving force is applied and stability of the process of acceleration. However, for a railgun at such velocities the subject of a way of formation of a current armature is of a principle character. In case of a metal armature the fundamental physical problem of velocity skin effect isn't solved, though there is a certain hopes to overcome this restriction. The damage of a contact between the armature and rails due to the velocity skin — effect reduces advantages of this way of acceleration, since at velocities of the order 1km/s a spontaneous plasma piston is generated, and it usually turns out to be unstable, particularly at high velocities of motion.

In case of a plasma current armature, the subject of its localisation behind a projectile, which was not solved and can not be solved in laboratories because of impossibility to meet requirements of compactness and super high pressures (acceleration of 5×10^5-10^6g's). Initial investigations, in which the plasma piston was expected to be a compact discharge magnetically pressed to a projectile showed that the discharge breaks down into a number of current structures which easily spread over the barrel length. The high density and highly radiating plasma was capable of absorption of any amount of energy delivered to the channel, which immediately was transferred to walls of a barrel thus destroying electrodes and insulators.

The paper considers some aspects of this problem, there are presented data on some systems of conduction accelerators under development. It should be noted that induction type accelerators, despite more modest achievements in the sense of velocities compared to railguns have chances to be preferable in this field of application. Below we estimate power requirements to the acceleration of projectiles of the mass which is characteristic for launch applications, minimal length of an accelerator, present results of the analysis of processes on sliding contacts which are responsible for negative consequences of the velocity skin — effect, consider the possible cause of the velocity limit in case of the plasma jumper.

The work has been performed under a partial financial support of the Russian Fund for Basic Researches (project No. 97–01-01016).

1. Operating modes of the direct launch system.

Main energy expenditures at the launch of payloads into orbit near Earth take place in the area of dense atmosphere (H≤30-40km) where the

velocity quickly decreases. In a rarefied atmosphere the rate of velocity change is low and is mainly determined by gravity. The presence of two highly different sections of a trajectory allows one to apply sound simplifications to the analysis, which facilitate the evaluation calculations. As a result the initial kinetic energy of a projectile necessary for its delivery to the altitude H can be estimated in the following way (see [15, 16]):

$$E_0 = m\frac{V_0^2}{2} = \frac{g_0 R_0 m}{2}\left(2 - \frac{1}{1+H/R_0}\right)\exp\left(\frac{C_x S p_0}{m g_0 \sin\alpha_0}\right)$$

where m is a mass of projectile; V_0 — initial velocity, g_0 — gravity acceleration on the Earth's surface; R_0 – Earth's radius; S — area of a projectile cross – section; C_x – drag coefficient of projectile; p_0 — atmospheric pressure on the Earth's surface; α_0 — an initial angle of trajectory inclination, which was determined from the condition of delivery of a payload to the orbit of a specified altitude, H at the zero angle of the trajectory inclination. In Fig.1, there is presented the example of evaluation of the muzzle velocity and kinetic energy for a launch of a projectile into a geostationary orbit (the altitude of 36 thousand kilometres). It is seen that with the increase of the payload mass the kinetic energy increases and the velocity decreases. So, in case of a projectile mass of 1 ton at the projectile fineness ratio L=5, the energy required is 60GJ, muzzle velocity – about 11km/s; in case of the 0.1kg mass – 10MJ and 13.5km/s, respectively.

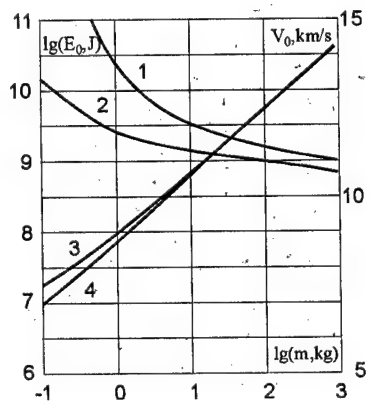

Fig.1. Muzzle velocity (1,2) and kinetic energy (3,4), required for the launch of payloads into geostationary orbit: 1, 3 — $\overline{L}$ =5; 2, 4 — $\overline{L}$ =20.

Today one can consider as a mastered the level of power stored in a single module of the order of 100MJ, which allows one to say about the possibility of a direct launch into space of a payload of the mass not higher than 1kg.

The practical realisation of a direct launch to much extent depends on the length of acceleration up to the initial velocity, i.e. the accelerator length. In the literature one can encounter mentioning of accelerators of many kilometres length [6], which can be located only on slopes of steep mountains. In case of a constant driving force the acceleration length is determined by the acceleration g:

$$L = \frac{V_0 - V_i}{2g}$$

where V_i is the projectile velocity at the input to accelerator. In order to keep integrity of a projectile the acceleration mustn't exceed a certain critical value which is connected with maximum permissible stresses in a projectile design. When a projectile can be approximated by the bulky pig with the driving force exerted to the bottom, then the condition of the limit of the maximum compression stress can be written in the form of $\sigma_{max} = \rho l g < \sigma_*$, where ρ is the material density, l — its length. Let $V_0 >> V_i$, then one can obtain a simple formula for evaluation of the accelerator length:

$$L \geq \frac{E_0}{\sigma_* S}$$

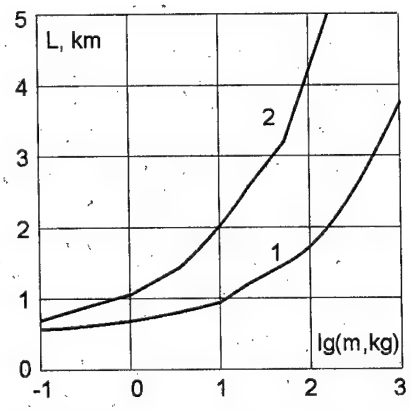

Fig.2. Length of an accelerator required for the launch of payloads into geostationary orbit: 1 — $\overline{L}$ =5; 2 — $\overline{L}$ =20.

In Fig.2 one can find evaluations of the length of accelerators under conditions coinciding with those of Fig.1. It was assumed that the critical stress corresponds to the tensile strength of *Al* ($\sigma_*=10^8 N/m^2$). If one is oriented to the strength of, for instance steel, then the values of the length presented above must be decreased ten times and if the compression strength is taken into

calculations then the length of an accelerator can be further decreased ten times more. The real length of an accelerator can be determined only after the analysis of a stressed state of the projectile structure in the process of acceleration inside a barrel and on exit from it, when the location of exertion of forces changes. For the calculation of the length one should mainly take into account not acceleration allowable by the projectile material but acceleration allowable for equipment which is launched into space. Thus, depending on the design, the length of an accelerator can vary between tens of meters and several kilometres. One should take into account external conditions too.

2. Typical structures of electromagnetic accelerators and the status of works on their investigation.

In Fig.3 one can see the configuration of a typical electromagnetic accelerator of a railgun type. The electric current which creates a magnetic field flows through guides. The interaction between a magnetic field and the current flowing through the armature results in the appearance of the Lorentz force, which pushes the projectile in a positive direction of the axis *OY*. As the armature there can be either a conducting projectile or a plasma piston, which, in turn accelerates the projectile due to usual gas dynamic pressure. Such a configuration was used and is being used in a great number of works both in this country and abroad. Most results relate to it.

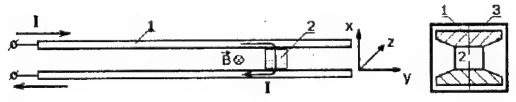

Fig.3. 1- guiding and current carrying rail, 2- armature being accelerated (projectile or plasma piston), 3- mechanical load carrying structure.

However, the problems mentioned in the introduction to this paper first of all refer to this configuration. These are the problem of arrangement of a reliable electric contact in an accelerator with a conducting armature and the problem of the compactness of a plasma piston in case of a plasma armature. In order to overcome the above described difficulties many alternative configurations were proposed.

One of options of such a modification is the use of an armature with rods, which carry the current shown in Fig.4a and the muzzle-fed barrel, the configuration and cross-section of which is presented in Fig.4b [17]. It is distinguished from the simplest design of Fig.3 first of all by the presence of two pairs of current buses located one above another. Along the upper rail the current flows from the beginning of the accelerator to its muzzle where it turns in the opposite direction and flows into the accelerated projectile from the front (relative to the direction of motion) side. In this case certain portion of the current flows also through the trailing part. In more details physical and engineering features of such an accelerator are described in [18,19]. It is assumed that in case of the use of such an accelerator the current can be distributed over a developed periphery of contacts of rods (protruding ends of which are shown in Fig.4a), and the current feed in direction opposite to the direction of motion will considerably decrease the influence of effects of velocity skin effect. The idea of the velocity skin effect is in concentration of the current on the trailing edge of the contact between a rail and conducting projectile being accelerated. The increase of the velocity leads to the increase of the current density in this zone, melting followed by evaporation of armature material.

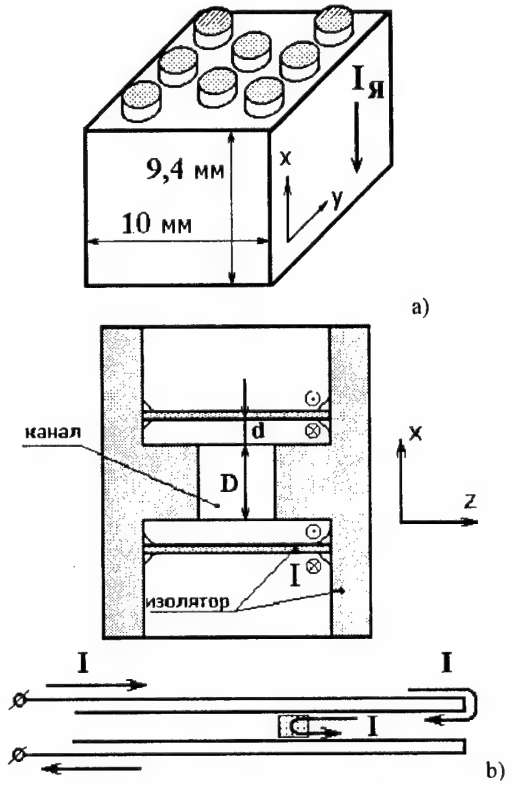

Fig.4. a – the armature with rods; b-configuration and cross-section of a barrel with a muzzle-fed current supply bus. Here D-the barrel calibre, d-thickness of a muzzle fed current bus, which realises mechanical and electrical contacts with the armature.

During this process the metal armature transforms into a plasma one being accompanied with barrel erosion and loss of efficiency of acceleration. The additional engineering advantage of the system is also in the presence of a magnetic pressure on a guiding rail, thus improving the electrical contact with the armature.

There exist different points of view on parameters of such an accelerator: from extremely optimistic [18,20,21] to very restrained [22]. One has been continuing the investigation of such devices. At any case, the distribution of the current flowing into the accelerated projectile is more uniform in this accelerator compared to the classical design railgun [22]. In [19] there is proposed the modification of the muzzle-fed accelerator, the configuration of which is presented in Fig.5. The difference with Fig.4 consists in the presence of a big number of reverse conductors which force the current to be distributed over the entire plane of the contact of the projectile being accelerated.

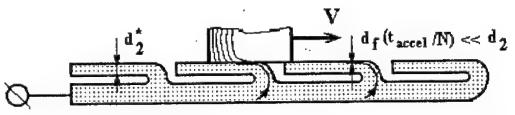

Fig.5. The modified configuration of a muzzle-fed railgun.

The intensive investigation of methods of electromagnetic acceleration of projectiles was initiated all over the world in the end of 70's. Since that 9 symposia on electromagnetic launch technology took place in the USA and 6 in Europe. Until the last year (1998) they were conducted once in two years in turn. In 1998 the decision was undertaken to unite European and American symposia. In 2000 the 10th symposium will take place in the USA. In the USSR, two All-Union Seminars on the subject of electromagnetic launch were conducted in Novosibirsk. Their materials are published in [8, 9]. At the same time intensive studies were carried out in the Institute of High Temperatures of Russian Academy of Sciences (RAS), Institute of Applied Mathematics of RAS, Institute of Hydrodynamics and Institute of Thermal Physics of Siberian branch of RAS, Institute of Electrodynamics of Ukrainian Academy of Sciences, Lubertsy Research and Production Association 'Soyuz", Moscow State University and Baumann University, Troitsk (TRINITI), Physical-Technical Institute of RAS, TsNIIMASH and many other organisations. The well-known processes in our life led to the destruction of co-operation which existed and dramatic decrease of volume of studies. Nevertheless these works are being continued and the evidence of this fact is the list of publications of Russian scientists in various conferences related to the subject of electromagnetic launch. With this paper we would like to draw attention to the problem of a direct launch of projectiles into space with the help of an electromagnetic accelerator and necessity to carry out works on this subject

3. Scaling relationships for a railgun.

After the application of laws of electromagnetism, in [23] the authors obtained scaling expressions for all characteristic operational and engineering parameters of a barrel with a metal armature. It was supposed that main scaling variables are linear dimension $x \leftarrow gx$ and time of acceleration $t \leftarrow \tau t$. Two additional parameters – heat capacity $c_v' = \chi c_v$ and the temperature of construction materials $T \leftarrow \eta T$ allowed one to expand frames of simulation. In connection with the simplicity of the final results let us present some main expressions in Table 1:

Table 1. Scaling relationships for barrel parameters

Parameter	Device under scaling
Barrel calibre, d	gd
Mass accelerated, m	$g\tau^2\chi\eta m$
Projectile position, x	gx
Full length of acceleration of a barrel, s	gs
Acceleration value, a	$g/\tau^2\ a$
Time of acceleration, t	τt
Current magnitude, I	$g(\chi\eta)^{1/2} I$
Joule heating of elements, $A = \int j^2 \rho\, dt$	$g^2\tau\chi\eta A$
Mechanical stresses, S	$\chi\eta/\tau\ S$
Kinetic energy, E_k	$g^3\chi\eta\ E_k$
Electromagnetic efficiency of an accelerator, η_{em}	η_{em}

Source assumptions of such a scaling allow one to perform high reliability predictions of structural versions of accelerators of large scale with the help of corresponding scaling expressions for systems of pulsed power supply and allowing for the use of cheaper construction materials during experimental simulations.

However, for estimation of large accelerators with a plasma armature (PA), which likely will be required for V>10km/s, that is not enough. Electrodynamics of plasma flows in PA has its own characteristic spatial scales, which seems to be compatible to the size of several calibres of 2-5cm of existing laboratory systems.

Nevertheless, during the transition to devices of a larger scale, one can consider PA

accelerators with certain optimism. Fully understandable desire to improve efficiency of an electromagnetic launcher earlier led to the concept of the power supply distributed along the acceleration barrel [24, 25]. Let us explain briefly an idea It follows from the integral electromagnetic equations for an arbitrary current contour of varying inductance that in case of a constant current, I_0, the work done on the contour at its deformation is equal to $A=d\Phi\, I_0$.

At the same time the electromagnetic force of acceleration of a projectile can be obtained from the value of the inductance gradient of a barrel, L' and the current as $dE_k/dx=L'I_0^2/2$. After integration of the latter equation one obtains $\Delta E_k = \frac{1}{2}\Delta A$, which shows that the half of energy being supplied is spent on the development of the magnetic field "supporting" the projectile. In case of proper arrangement of the distributed energy input into the barrel, which is schematically shown in Fig.6, the sequential switching on of sources provides the development of a "travelling" magnetic wave with the field maximum directly behind the projectile. At any moment of the time the total magnetic energy in the barrel doesn't exceed $E_m=kL'\cdot I_0^2\cdot s/(2N)$, where k=2-3, N — number of modules of the power supply.

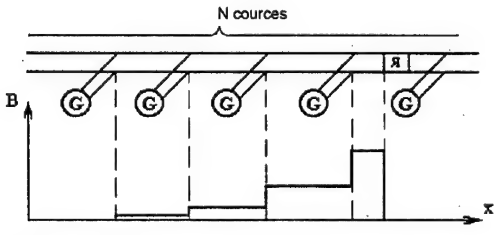

Fig.6. The configuration of a distributed energy (current) input into the railgun barrel and the distribution of the magnetic field, B, over its length.

For the mode of operation of a railgun with PA, another special feature is very important. The maximum voltage on electrodes of an accelerator in case of a sequential switching on of power sources is located in the zone near the projectile being accelerated. At the characteristic longitudinal size of the channel $\Delta x=s/N$ this voltage will be 2-3 times lower. The trailing part of PA, which in a classical railgun shunts the "head" being accelerated, in this case will die out automatically. It is known that in order to achieve a similar effect in laboratory systems of a classical configuration, intensive inventing efforts were undertaken [26]. However this problem is not only unsolved but still is the main obstacle for further increase of muzzle velocity. In connection with this the statement of studies of PA behaviour in laboratory systems of low calibre with a distributed source seems to be extremely important and can lead to the qualitative revision of one of fundamental restrictions in accelerators of projectiles.

4. Processes on sliding contacts.

The most complicated problems during the motion of a projectile in a barrel are observed on sliding contacts between a projectile and rails where friction and electrical current transport take place. The dry friction force, according to evaluations, turns out to be so high that under certain conditions it can completely stop the projectile. However, because of extraction of high thermal energy due to friction the metal contact melts resulting in the appearance of a liquid film, which reduces the friction force so dramatically that it can be neglected in the balance of forces exerted upon the projectile [27,28].

It was obtained in on-site experiments that when velocities of a metal armature were higher than 1.5 km/s, heat extraction in the zone of the contact between the armature and rail leads to heating up and evaporation of the trailing edge of the armature. Evaporation of conducting substance is facilitated by the increase of current density due to the velocity skin effect in the rear part of the projectile. At characteristic for railguns millisecond duration's of current pulses, points of phase transitions in this zone with good accuracy correspond to known threshold values of the integral of the current density $A=\int j^2 dt$ [30]. In simplified models of the process of electromagnetic acceleration [31], there were obtained evaluations of the critical velocity $V_{crit}\approx$ 0,9-1,2km/s, at which the damage of conductivity of the contact of a metal type occurs for various materials of an armature and rail. A two-dimensional model of the current flowing through the armature and rails of infinite dimension in the direction of z-axis was used. The statement of the problem in general is determined by the necessity to have accelerators of a railgun type with more complicated topology of an armature and barrel, in which the value of the critical velocity could be increase two-three times relative to the above mentioned. The effect can be achieved if one will succeed in the decrease of the maximum current density on the contact zone. In case of the success there could be provided the lifetime of the acceleration barrel of the order of 100 cycles, which is required for practical applications.

The consequences of the velocity skin — effect can be eliminated if one would be able to

predict this effect. Still we have no self-consistent analytical models, which describe the distribution of the magnetic field and electric current density over the sliding contact. Some attempts to obtain them are described in works [28,32,33]. However, there are mainly developed the numerical methods of calculation [31,32,34-36] because of the complicated character of processes under investigation.

As an example let us present the data [35, 20] on the value of critical velocity, i.e. velocity of the start of evaporation of the armature for various combinations of materials of a rail and armature. These data are presented in Table 2 for characteristic values of currents and geometric characteristics of the accelerator of a railgun type of a traditional configuration.

Table 2. Critical velocity, V_{cr} m/s, for various materials of a rail and armature

No.	Rail	Armature	V_{cr} m/s
1	Steel	*Al*	667
2	*Cu*	*Al*	685
3	*Ni - Cr*	*Al*	1006
4	*C*	Steel	2160

From values of the critical velocity for different contact pairs one can see the main principle of overcoming the influence of the velocity skin effect on the work of the electromagnetic accelerator: the critical velocity can be increased on account of a sharp difference of electric conductivity of materials of an armature and rail. The data of works [35,20] confirm the conclusion on the possibility to delay the crisis of the contact with the help of the increase of resistivity of both an electrode and armature. From the point of view of the convenience of practical realisation in [33] authors make a conclusion that the most acceptable pair can be copper electrode (rail) /graphite armature. It should also be noted that the critical velocity can be changed by varying armature geometry, preliminary acceleration and other parameters as well as usage of laminated materials [35, 36].

At the same time, the use of low conductivity materials can develop both design and physical obstacles. So, for instance, the necessary length of a contact area under certain conditions must considerably exceed transversal dimensions of the barrel thus resulting in its jamming during acceleration. Another problem can be the increase of the friction force because of graphite doesn't form a liquid film, which in case of a metal contact reduces this force practically to zero. And finally there can arise the problem of the breakdown of the gap between electrodes due to high voltage drop on electrodes because of the use of highly Ohmic materials. Thus, specific experiments must be carried out, which will allow one to test this method to overcome the contact crisis. In Fig.7 the experimentally obtained [37] time dependence of the projectile velocity in the railgun barrel with graphite rails, which demonstrates the possibility to achieve high launch velocities.

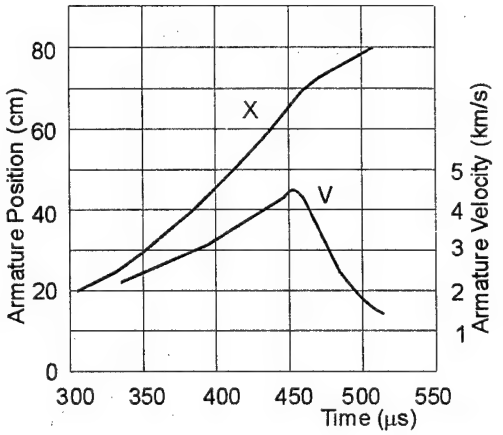

Fig.7. Velocity vs time in a railgun with aluminium armature and graphite layer (experiment).

5. The effect of secondary discharges on operation of an accelerator.

On reaching the critical velocity, the plasma jumper appears behind the projectile and velocity decreases below the predicted one. In case of the plasma armature, there is also observed the disagreement between the predicted and real velocity. The reasons for such a disagreement, generally speaking, are not clear since the plasma jumper must act on the projectile with the same force as the metal armature does. It was only noticed in experiments that the disagreement decreases if the plasma jumper is compact in distinction from one expanded along the barrel length [7]. In [38] there is proposed the calculational model of the effect of a secondary discharge on operation of an accelerator, which is based upon the analysis of properties of the discharge, which appears due to the breakdown of the gap between electrodes near the front edge of the gas "accompanying" the projectile at its entry into the barrel of an accelerator, namely – explosion products flowing out of the preaccelerator. After its appearance, the plasma jumper quickly overtakes the armature, since its mass is much lower than the projectile one. In Fig.8 the comparison between prediction and

experiment taken from [29] is shown. It is seen that the theory can predict well the level of velocity attained by the projectile in the presence of the plasma jumper. The theoretical model of the periodical breakdown of the gap between electrodes allows one to explain the discrepancy between predicted and real projectile velocity in the accelerator in the presence of the secondary plasma jumpers

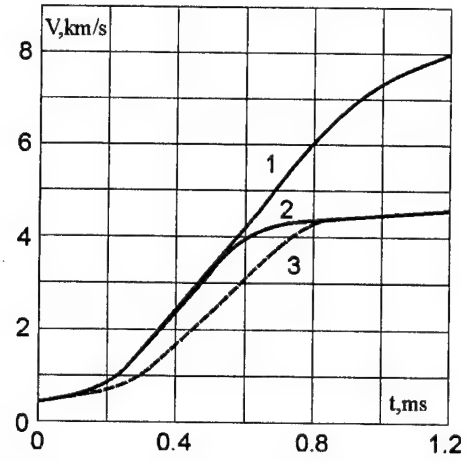

Fig.8. Projectile velocity: 1- prediction in the absence of a plasma jumper; 2-prediction taking into account the plasma jumper; 3- experiment [29].

6. Mathematical simulations of phenomena taking place during electromagnetic acceleration of projectiles.

Electromagnetic acceleration of projectiles is an example of a physical process, the course of which is accompanied by quite a number of various phenomena. First of all these are electromagnetic fields and their propagation in conducting and non-conducting sub-areas of the accelerator. Electric currents lead to heat extraction, i.e. to heat transfer phenomena. The presence of locations with higher current density results in melting followed by evaporation of material of a rail or armature. The appearance of vapour from the conducting material gives the possibility for a breakdown and initiation of electric arc, i.e. creation of plasma. Plasma can exist from the very beginning when the armature is of plasma or combined nature. The projectile motion along the barrel of an accelerator is accompanied by friction and heat extraction followed by the development of a liquid film on the contact surface. The motion of a projectile, as a rule, takes place in air and is accompanied with gas dynamics effects as in case of any projectile. The external power supply system and the necessity to match it are a noticeable part of the statement of a simulation problem. The mathematical simulation of the acceleration in full extent is practically impossible (today). Nevertheless various components allow for corresponding mathematical description.

Three-dimensional description of electromagnetic fields in electromagnetic accelerators is of principle importance. These fields are three-dimensional due to laws of electromagnetism and can be described by two-dimensional models only very approximately, often with the loss of qualitative features of the process. In [39,40] mathematical models are presented, which allow one to calculate three-dimensional unsteady electromagnetic fields in an accelerator of a railgun type. There were constructed models which are uniform in different sub-areas with sharply different electric conductivity: conductor or insulator.

Works [35,36] concern two-dimensional calculations. Despite their knowingly qualitative character, for the case of a classical design railgun one succeeded in determination of the point of the "crisis of electrical contact", the place of which corresponds to experimental data. One should note the study of the influence of points of singularity of the solution on accelerator parameters, which was carried out in [36]. There is a lot of such points in the railgun. These are first of all various angles and joints of different materials leading to singularities of solutions.

In [39,41] examples of self-consistent mathematical description of external electrical circuits, through which the railgun is fed, and outer conducting jacket are presented. As the mathematical modelling shows, it possible in principle to develop such an accelerator, the outer jacket of which will provide the pressing of guides to the projectile thus providing better operation of an electric contact.

In [19,22] the attempt of mathematical simulation of the muzzle-fed accelerator is undertaken, in which the structure of a magnetic field and power supply is much more complicated than in case of a classical accelerator. In particular, there is shown the principle necessity of a spatially three — dimensional description of electromagnetic fields for calculation of forces applied to the projectiles. Let us present some characteristic patterns of the solution. Fig.9 explains the picture of current flow in the accelerator in case of the armature shown in Fig.4. The armature consists of 8 current conducting rods (there is shown the cross — section which passes through three end ones), the space between them is filled with dielectric.

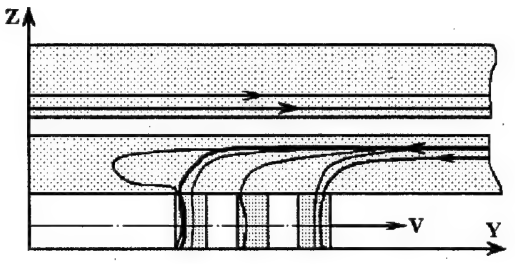

Fig.9. The flow of current in a muzzle-fed railgun.

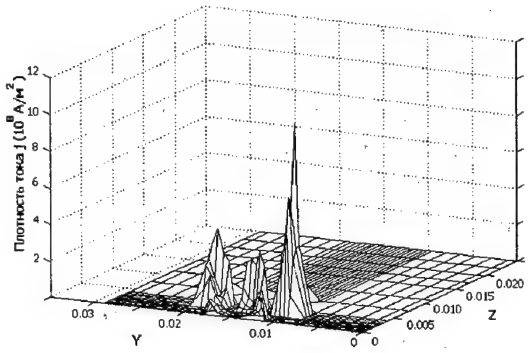

Fig.10. Current density distribution.

The numerical simulation has shown that the current flows on inner surfaces of a current loop formed by the slot between the direct and reverse current buses. As a result, in order to close the circuit through the armature, the current must flow from the inner surface of this loop onto the contact surface of the reverse current bus-rail turned toward the acceleration barrel. The flow takes place on both lateral surfaces of a current bus and by diffusion through the bus. The flow is considerable three — dimensional. The flow of current on the surface leads to the appearance of a considerable portion of the current not in the front, but in the rear part of the armature (relative to direction of motion). The typical distribution of a longitudinal (along rods) component of the current density in the cross-section x=const, which lies near the plane of symmetry x=0 is presented in Fig.10. This picture already shows that the bigger part of the current is carried by the first (relative to the barrel and direction of motion) pair of rods.

The work carried out in [19,22] is one of the first attempts in Russia to develop a numerical three dimensional model of a railgun accelerator of projectiles with a metal sliding contacts, where both electromagnetic and thermal processes, up to phase transitions, are taken into account. The model accounts for specific character of both barrel and armature design and specifical effects of electromagnetism connected with high (about 1km/s) velocity of motion and rate of armature heating up.

References

1. From the magnetic gun into cosmos // Obshaya gazeta, 1998, No.42(272), p.8 (in Russian).
2. *N.Pilyugin, V.Lyshevskyi,* The gun cosmonautics begins // Poisk, 1998, No.1-2, p.11. (in Russian).
3. *R.S.Hawke, A.L.Brooks, C.M.Fowler, D.R.Peterson,* Electromagnetic Railgun Launchers: Direct Launch Feasibility // AIAA Journal, 1982, v.20, No.7, pp. 978-985.
4. *B.V Raushenbakh,* German Oberth, p.334, in B.V.Raushenbakh "Passion ", M., Agrapth, 1997, 432p. (in Russian).
5. *S.Morton, J.Gut,* An Investigative Review of EML Technology for the Swiss Perspective // IV European Symposium on Electromagnetic Launch Technology, Germany, 1993, paper No.1901.
6. *L.Deschamps, P.Glaser,* Prospects Offered by Electromagnetic Launchers for Launching Payloads into Orbit //– Space Technology, V.11, No.1, 1991, pp.45 – 53.
7. *A.D.Lebedev, B.A.Uryukov.* Pulsed boosters of high pressure plasma. // SD AS USSR, Novosybirsk, 1990, 290 p. (in Russian).
8. Materials of I All — union seminar on high current arc discharge in magnetic field (Novosybirsk, 10-13 April 1990), *M.F.Zhukov* (red.), Novosybirsk, Heat Physics Inst. SD AS USSR, 1990, 350p. (in Russian).
9. Materials of II All — union seminar on high current arc discharge in magnetic field (Novosybirsk, 4-6 December 1991), *V.E.Nakoryakov* (red.), Novosybirsk, Heat Physics Inst. SD AS USSR, 1992, 367p. (in Russian).
10. *L.A.Artcymovitch et al.* The electromagnetic acceleration of plasma cluster // GETP, 1957, v. 33, No.1, p.3–8. (in Russian).
11. *H.Weh, J.Jacquelin, F.Moisson,* Coilgun. Concepts // IV European Symposium on Electromagnetic Launch Technology, Germany, 1993, paper No.701.
12. *R.Malifert, P.Moisson, B.Hoftman, M.Loffler,* Coilgun. Energy Coupling and Current Feeding // IV European Symposium on Electromagnetic Launch Technology, Germany, 1993, paper No.702.
13. *M.Loffler,* Coilgun. Velocity Limits // IV European Symposium on Electromagnetic Launch Technology, Germany, 1993, paper No.704.
14. *N.Kawashima, A.Yamori,* Improvement of High Velocity and Stable Railgun (HYPAC) in ISAS. // 5th Europ. Symposium on EML Technology, Toulouse, April 10-13 1995, Proc. Conf. Report N 57.
15. *A.D.Lebedev, C.C.Milyaev, B.A.Uryukov,* Minimization of Energy of Electromagnetic Launch System // IVth European Symposium on EMLT, Celle. Germany. 1993.
16. *N.F.Krasnov,* Rocket aerodynamics". Nauka, Moscow 1968, 310 p. (in Russian).

17. *O.V.Fatyanov, V.E.Ostashev, E.F.Lebedev, F.V.Ulyanov.* Electromagnetic desksides of railgun // Preprint of IVTAN №3-357, RAS, Moscow, 1993, -28p. (in Russian).
18. *Yu.A.Kareev, A.P.Lototsky, Yu.A.Halimullin,* Metal Projectile Acceleration in Muzzle-Fed Railgun // 6th European Symposium on EML Technolodgy (The Hague, 25-28 May 1997). Proceedings, p.314-321.
19. *A.P.Lototsky, Yu.A.Kareev, A.A.Nikolashin, Yu.A.Halimullin, E.P.Polulyah, M.P.Galanin, S.S.Khramtsovsky,* Recent Muzzle-Fed Railgun Experiment on Metal Armature for Arcless Acceleration // IEEE Trans. On Magn., 1999, in press.
20. *Yu.A.Kareev, R.M.Zayatdinov.* Transition Conditions for Solid Armature in Railguns with Muzzle Current Feed. // IEEE Transaction on Magnetics, Vol.31, No.1, pp.180-182, January 1995.
21. *Yu.A.Kareev, A.P.Lototsky, Yu.A.Halimullin.* Metal Projectile Acceleration in Muzzle-Fed Railgun. // Proceeding of 6th European Symposium on Electromagnetic Launch Technology. The Hague, Netherlands, May 25-28, 1997, pp.314-321.
22. *M.P.Galanin, A.P.Lototsky, Yu.P.Popov, S.S.Khramtsovsky,* Numerical simulation of spatially three-dimensional phenomena during electromagnetic acceleration of conducting projectiles // Matematicheskoye modelirovaniye, 1999, in press. (in Russian).
23. *M.Koops, A.Schoolderman.* On scaling relation for hypervelocity launch processes. // 6th Europ. Symposium on EML Technology. Hague, 25-27 May, 1997. Proceeding, TNO-PLM, DELFT, Netherlands, p.124-132
24. *R.Marshall,* The Impact Distributing Railgun Energy Stores on Rail Design. // 5th Europ. Symposium on EML technology, Toulouse, April 10-13, Proc. Conf. Report No.8.
25. *N.N.Grabchak, M.K.Krylov, A.D.Lebedev, A. P.Lototsky.* Investigation of an accelerator with a metal projectile and power feed distributed over the barrel length. // In [9], p.104-118. (in Russian).
26. *E.M.Drobyshevsky, S.I.Rogov, B.G.Zhukov, R.O.Kurakin, V.M.Sokolov.* Experiments on Simple Railgun with the Compacter Plasma Armature // IEEE Trans.Magnetics, v.31, No.1, p.295-298.
27. *M.P.Galanin, A.D.Lebedev, V.V.Savichev, B.A.Uryukov.* The Analysis of Contact Surface Melting Processes at Solid Armature Launching. // VIth European Symposium on EMLT, Hague. Holland. 1997.
28. *B.A.Uryukov, A.D.Lebedev, K.K.Milyaev.* The influence of processes on contact surfaces on dynamics of acceleration of a metal armature. In [9], p.33 – 71. (Russian).
29. *V.B.Zheleznyi, A.D.Lebedev, A.V. Plekhanov.* Impacts on dynamics of acceleration of an armature in an electromaagnetic launcher. // In [9]. p.16-32. (Russian).
30. *G.A.Knoepfel.* Ultrahigh pulsed magnetic fields. Moscow, Mir, 1972. 392pp. (Russian).
31. V.P.Bazilevsky, R.M.Zayatdinov, Yu.A.Kareev. The crisis of electric conductivity of a high speed metal contact // In [9]. p.285-303. (Russian).
32. *A.P.Glinov, N.M.Kolyadin, et al.* The investigation of the crisis of a metal contact in an electromagnetic launcher with the transition to electric arc closure. // In [9], p.315–339. (Russian).
33. *B.Uryukov, V.Chemeris,* The Basic Principle of a Choice of Materials for Contact Pair in the Electrodynamic Accelerator, // 12-th International Pulsed Power Conference, USA, June 1999.
34. *I.S.Glushkov, Yu.A.Kareev and al.* Investigation of Techniques to Increase Armature Transition Velocity. // IEEE Transactions on Magnetics, V.33, No.1, 1997, pp.549 – 553.
35. *M.P.Galanin, A.V.Plekhanov, V.V.Savichev,* Investigation of behaviour of a metal contact during electromagnetic acceleration of conducting projectiles // TVT, 1996, т.34, No.2, p.293-298. (Russian).
36. *M.P.Galanin, V.V.Savichev,* Singularities of an electromagnetic field and their effects at simulation of an electric contact in an electromagnetic accelerator of a railgun type // TVT, 1997, т.35, No.4, p.517-523. (Russian).
37. *Yu.A. Kareev, L.G.Kotova, A.T.Kuharenko, Yu.A.Halimullin,* Investigation of the Metal Contact Crisis in Railguns with Resistive Rails // 5th European Symposium on EML Technology (Toulouse, 5-10 May 1995). Proceedings, Report N 22.
38. *B.Uryukov, V.Chemeris,* Secondary Discharges and their Influence on Work of Accelerator // 12-th International Pulsed Power Conference, USA, June 1999.
39. *M.P.Galanin, Yu.P.Popov,* Quasistationary electromagnetic fields in nonhomogeneous media. Mathematical simulation // M., Nauka, Physmatlyt, 1995, 320p. (Russian).
40. *M.P.Galanin, V.P.Ygnatko, Yu.P.Popov, S.S.Khramtsovskyi* Spatially three – dimensional calculations of conducting armatures electromagnetic launch // JTP, 1995, v.65, No.6, p.9-20. (Russian).
41. *M.P.Galanin, A.V.Plekhanov, Yu.P.Popov, S.S.Khramtsovskyi,* On influence of external conducting shield parameters to armature launch in electromagnetic accelerator // JTP, 1996, v.66, No.10, p.198-206. (Russian).

EXPERIENCE IN DEVELOPMENT OF MHD-DEVICES FOR SPACE APPLICATIONS

I.V.Vitkovsky, I.R.Kirillov (NIIEFA, St-Petersburg)

Abstract. The purpose of this paper is to show briefly to an interested reader the variety and ways of solving the scientific and technological problems arising during development and manufacturing of MHD devices.

Introduction

Since the end of the fifties D.V.Efremov Institute has been engaged in research and development of MHD-devices with liquid metal for space nuclear power installations (SNPI), technological and research facilities. These devices include electromagnetic pumps (EMP) and MHD brakes.

Originally the research and development were aimed at studying a large number of MHD devices varieties. These works enabled to determine the most prospective (from the viewpoint of space application) types of MHD devices - direct current conduction and cylindrical linear induction ones, and to direct efforts to development of theory, design and manufacturing methods.

Numerous papers, reviews, monographs, reprints, reports and technological documentation contain the results of these works. We mention some of them accessible for readers in the chronological order [1-4].

Direct current conduction EMP with straight ducts

The following circumstances had the decisive influence on the choice of these pumps: first, design simplicity and, secondly, the fact that these pumps are supplied with low voltage direct current which can be easily produced in SNPI by thermoelectric generator or thermoionic converter. This enables to obtain a highly reliable power supply source.

3-D solution [2] contains the most complete information about the character of electric fields distribution in MHD ducts of these pumps. In this paper there are expressions for integral characteristics taking into account both longitudinal and transverse end effects at the finite values of magnetic Reynolds number, walls conductivity, velocity profile and real distribution of magnetic field in the duct zone.

The obtained expression for integral characteristics of MHD ducts was used in development of the calculation methods and in designing of the d. c. conduction machines.

The most typical (distinctive) parameters on which specific loads, mass and energy factors of the machine depend substantially are the duct height, its characteristic ratio and pole extension. In this connection at the beginning of calculation it is of practical importance to determine the field of these parameters variation that results in substantial reduction of the calculated variants and enables to estimate the influence of these parameters change on the machine characteristics. As the first approximation it is expedient to consider only electromagnetic characteristics ignoring hydraulic and excitation losses. These simplify calculated dependencies and their analysis to a considerable extent and enable to estimate the boundary values and the character of changing consumed power, efficiency, current and voltage exactly enough.

The obtained theoretical results, correctness of the adopted design and technological approaches were checked in testing a number of machines. Machines with useful power of several kW, with independent or series excitation and with "armature" reaction compensation in different ways were tested. The carried out tests of the industrial MHD machines showed their high reliability and good energy and mass factors. The experiments demonstrated both good qualitative and quantitative fit of the experimental and theoretical results.

Induction MHD machines

The principles of the induction EMP designing lie in the choice of the optimum specific loads (linear current load, excitation winding current density, metal mean flow rate) which provide for satisfactory relationship of three main parameters: efficiency, power factor and pump mass.

In the linear MHD machines (flat and cylindrical ones) the longitudinal end effect influences substantially on its characteristics, especially for the machines with low number of the excitation winding poles. Under "end" effect the whole complex of phenomena in the primary and secondary circuits of the machine associated with the final length of the inductor and the duct in the longitudinal direction is usually meant.

The basic results of the induction MHD machines theory are given in [1, 3, 5 - 7]. Here we mention the most interesting practical results obtained by employees of our Institute. They include, for example, the studies of direct and zero sequence current and voltage, inductive resistance of the winding, as a result of which it was found that EMP inductive resistance could be calculated with an error not higher than 10% according to the formulas for classic electric machines.

Great attention was paid to the studies of longitudinal end effect in the cylindrical and flat MHD ducts. First the 1-D code was developed for the cylindrical MHD machine. It was shown that EMP integral characteristics were the functions of magnetic Reynolds number, slip, pole number and relative length of the magnetic structure extension. This extension length influences the retarding force and additional joule losses caused by liquid metal entering/exiting into the sharply changing magnetic field region. While the pole number increases the characteristics become closer to the ideal ones - maximum values of efficiency in the pumping and generating modes increase while the transition region of electromagnetic braking, which lies between these modes, gets narrow. Various ways of the longitudinal end effect compensation were studied, the expressions for compensation currents, which together with the ideal non-conducting plates beyond the active zone, give the ideal duct characteristics were obtained.

Integral characteristics of the flat MHD duct with thin lateral walls of arbitrary conductivity were obtained as well. Introduction of the thin wall concept enabled us to solve problem only for the duct region taking the longitudinal and transverse end effects into account simultaneously. In addition to the above mentioned parameters the integral characteristics depend now on the relative duct width and on the ratio of the product of conductivity and width of the wall and of the liquid metal region. It was shown that the influence of the longitudinal end effect in the flat duct of infinite width differs from the cylindrical one. In order to obtain ideal machine characteristics at zero conductivity beyond the active zone for the flat machine it is enough to specify the difference of compensation currents, while for the cylindrical machine one needs to specify them individually.

It was shown that in the presence of the conducting duct walls MHD machine characteristics depend in a complex way on magnetic Reynolds number of the liquid metal and the duct walls. Parameters, where taking of the walls influence into account with the use of equivalent Reynolds number results in an error less than 10%, were determined.

The obtained calculated dependencies were checked experimentally and became the base for the development of the up-to-date design code for the induction EMP.

To achieve the high efficiency of MHD machines one has to design their ducts with minimum hydraulic losses. In co-operation with the department of water energy use in Leningrad State Technical University (M.I.Kalinin Leningrad Polytechnic Institute) we studied hydraulic characteristics of a number of ducts with different geometry. Because of the peculiarity of the MHD machines flow ducts their calculated coefficients of hydraulic resistance differ from the experimental ones considerably. Therefore it is expedient to test the MHD machine ducts on models with hydraulic resistance coefficient determined experimentally in the region of Reynolds numbers where the machine will operate.

Based on the theoretical and experimental studies Efremov Institute designed and manufactured cylindrical linear induction pumps for space application. Some of them were used in spacecrafts, the others were tested at the test facilities and now they are ready to be used in SNPI of new generation.

MHD brakes

In parallel with the EMP, development and manufacturing of MHD devices for regulation and control of the liquid metal flow rates [4] were carried out in Efremov Institute. The principle of MHD brakes operation lies in the moving current conducting medium deceleration by magnetic field. Using of MHD brakes enables to regulate flow rate inertialessly according to any specified law and to stabilise the flow rate value.

It was established during research that in the region of micro flow rates (flow rates in the range from the thousandths up to several cm^3/sec) it was possible to provide for automatic stabilisation of the working medium flow rate at considerable changes of pressure with the use of MHD brakes. Stabilisation is achieved by changing of the performance curve slope of MHD device containing EMP and MHD brake connected in series.

In order to explain this the operation of MHD dosing device in the opened hydraulic system with changing counterpressure at its outlet and containing conduction EMP and

MHD brake connected in series is considered below. In the range of the above-mentioned flow rate values even at minimum possible dimensions of the cross-section in the EMP duct the flow velocity is such that its performance (flow rate-pressure) characteristic is almost parallel to X-axis while the slope of the brake characteristic may be any one. During feeding of liquid metal only by a single pump a small change of hydraulic resistance or counterpressure at the system's outlet results in substantial changes in the flow rate value. During feeding of liquid metal by device containing the pump and the brake and having a "steep" performance characteristic the same oscillations cause a considerably smaller change of the flow rate.

So, the substantial stabilisation of the liquid metal flow rate is achieved by a series connection of the pump and the brake with some increase in energy consumption necessary for excitation of magnetic field and compensation of pressure losses in the brake.

Attention should be paid also to the following fact typical for MHD devices operating in the micro flow rates range. It turns out that the best energy and mass factors in the power supply source - MHD device system are achieved in the case when helical duct devices are used. They can be supplied directly from the board power supply sources consuming currents from several units up to tens of amperes.

The small flow rate values in the systems with helical duct MHD devices determine their typical parameters and the corresponding method for calculation of the developed or consumed pressure. As a rule, the duct height and width change in the range of 0.5-5 mm and 1-10 mm respectively. Liquid metal velocity in the duct is 0.5-200 mm/sec, ratio of the average radius to the duct height is more than ten. The laminar flow mode and magnetic Reynolds number values lower than unity correspond to the above-said parameters. Furthermore the magnetic field can be considered to be the plane-parallel one and electrodynamic effects can be considered to be prevailing over the hydrodynamic ones at the sufficient degree of accuracy. This allows using inductionless one-dimensional electrodynamic approximation in calculation of the main characteristics of such devices.

MHD devices test

Ground tests of MHD devices for space application are almost similar to the tests of the analogous devices for industrial applications. Additional peculiarities are connected with the vibration, climatic, thermocyclic tests and so on. The direct "life time" tests require considerable time expenses, that is not always desirable and possible due to many reasons. Therefore, the desire to decrease the test duration by carrying out of the accelerated tests at increased temperatures of the working medium can be understood easily. However, choosing a temperature value it is necessary to take the following circumstances into account: at first, the possible change of the thermal ageing laws for different materials, and, secondly, arising of new thermal destruction processes, for example, mutual diffusion of materials, thermal emission, electric erosion and so on.

Materials used in MHD devices manufacturing

The ducts are manufactured of the same materials, which are used in other SNPI parts where liquid metal is flowing.

During operation the duct material is exposed to the complex chemical and physical influence of the melted metals and alloys, and, as a result, it corrodes and is destroyed gradually in time. Corrosion rate depends on composition and characteristics of the working medium, presence of aggressive inclusions and impurities, liquid metal flow velocity and temperature. These data are established during the experiments, and stainless steel resistance in the alkali and other metals was studied sufficiently by now. In particular, at liquid metal velocities up to 8-10 m/sec, at the temperature up to 550°C and oxygen content in liquid metal up to (7-8) $\times 10^{-3}$% the corrosion rate does not exceed 0.0025 mm/year, strength and ductility characteristics of the stainless steels do not change practically. Increasing of oxygen content in liquid metal results in embrittlement of the steels, presence of carbon (oil vapours) leads to carburization of the material surface layer and loss of ductility.

So, minimum thickness of MHD machine duct walls for the purpose of energy losses decreasing should be weighted against the requirements of reliable duct exploitation during all necessary service time.

Magnetic structures of conduction EMP and MHD brakes are made either of steel 10 or of electrical-sheet steel 10864 (Armko). These materials have good magnetic characteristics, they are easily treated and are nickel-plated, chromium-plated or blued, if necessary.

The hot-rolled and cold-rolled electrical-sheet steels are used in the magnetic structures

of the induction pumps. Insulation coating for the hot-rolled steels is formed by oxidising method. The cold-rolled steels have good industrial insulation coating.

As the magnet wires the heat resistant wires type 700 or 700CK are used. The current conductor in the heat resistant wire 700 is made of the copper-chrome-niobium alloy (alloy 204 or 204A) and is protected from oxidation by galvanic layers of iron and nickel. The wire insulation is made of two layers of the quartz fibre, it is glued up and impregnated with organic-silicate compound and then it is coated by silicone lacquer.

The peculiarity of the heat resistant wire 700CK is the impregnation of the quartz fibre with the glass ceramics composite.

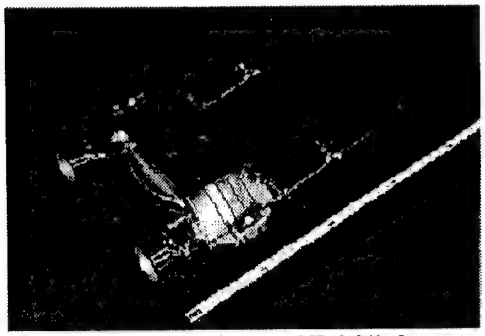

Electromagnetic pump NP-0.2/1×2

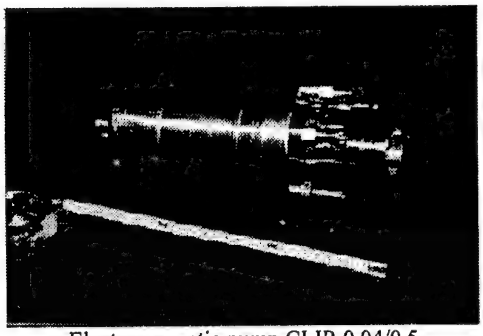

Electromagnetic pump CLIP-0.04/0.5

Mica ceramics is used as the body insulation. The main advantages of such insulation compared to the usually used one, for example to the mica glass insulation, are the following ones. In the initial state the insulation has characteristics similar to those of the dense paper. After pressing and thermal treatment of the insulation it's characteristics become close to those of the vacuum-tight ceramics. This enables to make a new product in the end, using the usual method of MHD device windings manufacturing. The windings with mica ceramics insulation do not release thermodestruction products almost, and, in addition, the insulation is a reliable protection (shielding) against electroerosion and thermoemission phenomena of the current conducting components of the winding.

Developed, studied and used designs, materials and technologies provide for these devices service life time more than ten thousand hours at liquid metal temperatures up to 600°C and neutron fluence up to $10^{19}/cm^2$.

As an example the main parameters of some EMPs for SNPI, developed in Efremov Institute and passed through the complete cycle of tests are presented below.

Parameter	Units	Pump type	
		NP-0.2/1×2	CLIP-0.04/0.5
Pumped metal	-	NaK (78%K)	NaK (78%K)
Temperature	°C	600	200-550
Consumed power	W	310	120
Voltage	V	0.22	19
Supply current, (value)	(A)	d.c., (1400)	a.c., 3 phase 50 Hz, (7)
Flow rate	dm^3/sec	1.4	0.7
Developed pressure	10^5Pa	0.2	0.04
Number of ducts	-	2	1
Mass	kg	12	7

Basing on the results of research and development, we think that a.c. EMPs are the most prospective ones for the new generation of SNPI.

References

1. *Baranov G.A., Glukhikh V.A., Kirillov I.R.* Theory and design of the induction MHD-machines with liquid metal working substance. M.: Atomizdat. 1968 (In Russian).
2. *Lavrentiev I.V.* MHD processes in the ducts at the finite magnetic Reynolds numbers. Ph. D. Thesis. L.: M.I.Kalinin Leningrad Polytechnical Institute (In Russian).
3. Glukhikh V.A., Tananaev A.V., Kirillov I.R. Magnetic hydrodynamics in nuclear power industry. M.: Energoatomizdat. 1987 (In Russian).
4. Gelfgat U.M., Gorbunov L.A., Vitkovsky I.V. Magnetic hydrodynamic braking and control of liquid metal flows. Riga.: Zinatne. 1989 (In Russian).
5. Vol'dek A.I. Induction magnetohydrodynamic machines with liquid metal working substance. L.: Energy. 1970 (In Russian).
6. Lielpeter Ya.Ya. Liquid metal induction MHD machines. Riga.: Zinatne. 1968 (In Russian).
7. Okhremenko N.M. Principles of theory and design of the linear induction pumps for liquid metals. M.: Atomizdat. 1968 (In Russian).

SPACE AND AEROSPACE CONVEYER 2000 AND A SYSTEM FOR DESIGN CONCEPT ANALYSIS

Kurkin I.I. (MAI, Moscow).

Introduction

The system of project-game analyzes was developed and is now improved in MAI. This system is considered as a part(appendix) of a fundamental research (MHD technologies, plasmodynamical and thermoshield tools and devices, plasma engines of flight vehicles, microbaloon forms of hydrogen fuel storage). The system is used for coordination of the leading specialists interaction and for training the specialists in new strategical fields. Project-game system is based on the extended experience of international and native project-constructive elaborations and interaction logic of specialists of different spheres and levels including chief constructors, leading specialists and even engineers. Project-game system was developed during several years. It was edited, corrected and refined using the results of the projects , such as: system of Mars nuclear rocket stages, hybrid power-motion devices, super-heavy flight vehicels and so on.

Conceptions - Aero-space conveyor operations.

(Use of the system in fundamental research - MHD technologies, plasmodynamical and thermoshield tools and devices.) The development of the key steps, that will become the organizing basis of the conveyer (cyclical) operations, is considered. Flight vehicles of the conveyer will provide the strategical priorities in different levels(altitudes) and harmonics. Blocs with thermal memory (BTM) that which are at the same time the elements of thermal shield of the vehicle will control the flight. BTM will provide the effects of conveyer operations management, the required temperatures, altitudes and velocity of the flight will be maintained, temperature shock and aerodynamical loads will decrease. Depending on the different types of engines installed variants of steps in conveyer operation cycles - interaction - support - capture - launch were analyzed. Operation cycles are presented in the form of project-game schemes.

Interrelation scheme - variants aero-space vehicles in scenarios.

Notations:
A - first step of aero-space vehicles(ASV) and cargos launching by traditional twostage scheme;
B - return of ASV or back transportation of cargos;
C - reuse of ASV, cargo interception;
D - the stage of rebounding pull through harmonics;
D1 - rebounding pull through all harmonics;
D2 - inspection problem;
D3 - work of the combined engines;
1-17 - regions of flight tasks and regions of computer program tuning.

While returning of the vehicles the planing trajectories with rebounding are considered. In this case the decrease of the vehicles surface temperature will be provided, for while repeated altitude growth most part of the heat will transmit into space. The predicted intervals of braking are 3000-4000sec.

The research results for further expert analysis are given in a table form
(Table in Fig.1)

Notations:

1 - conceptions, first stage, second stage;
2 - engine combination;
3 - specific engine thrust;
4 - regions of the track from earth to the orbit;
5 - velocities and altitudes of flight;
6 - time per track regions;
7 - track regions trajectories length;
8 - weight of a vehicle on different track regions;
9 - engine thrust per track regions;
10 - requirements;
11 - comments;

Different types of engines and their combinations for single-stage and two stage ASVs which can be launched from traveling and stable launching systems are analyzed. For the combinations of NRE (nuclear rocket engine) the best combinations were derived. Criterion for the best was the weight of the useful cargo that can be carried. Nuclear rocket engine was a standard. NRE can't be used on ASV in nearest future because of ecological restrictments.

Схема связей

Варианты аэро-космических аппаратов по сценариям

Транспортные аэро-космические системы.

Картограмма согласований. Вектор приоритетов

Наземный старт

Ячейка проектной памяти

		Код аппарата		Код ДУ	
1	Концепция	1-ая ступень		2ая ступень	
2	Варианты ДУ	[illegible]	[illegible]	[illegible]	
3	[illegible]	P_{M1}	P_{M2}	P_{Y1}	
4	Участки трассы [illegible]	0-5-1	1-2	3	6-4-7
5	[illegible]	[illegible]	высота	высота	интервал высот
6	[illegible]	E_2		E_3	E_7
7	[illegible]	L_2		L_3	L_7
8	Масса (т)	стартовая-конечная		[illegible]	[illegible]
9	Тяга (н)	[illegible]		интервал	интервал
10	Требования	[illegible]		[illegible]	
11	[illegible]	[illegible]		[illegible]	

1	1 ступень		2 ступень	
2	ТРД	ПВРД	ТРД	
3	450	3000	450	
4	0-5-1	1-2	3	6-4-7
5	0-600 м/с	37 км	65 км	85-156
6	0.43		0.526	0.96
7	0.086		0.184	0.955
8	450 — 305		81.6	[illegible]
9	$4.2 \cdot 10^3$ $1.35 \cdot 10^6$ $1.31 \cdot 10^6$		$1.12 \cdot 10^6 - 3.16 \cdot 10^5$	$4 \cdot 10^3 - 1 \cdot 10^3$
10	$1.35 \cdot 10^6$ Н 374 [illegible] 26.2 т		$1.12 \cdot 10^6$ Н 4.2 т	
11	нет нет нет		нет да нет	

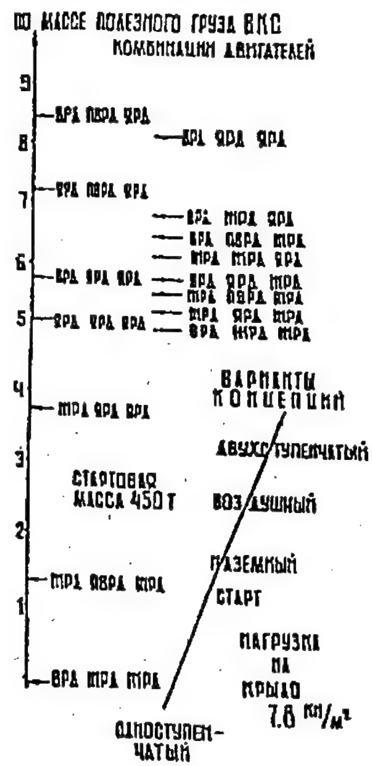

Fig.1.

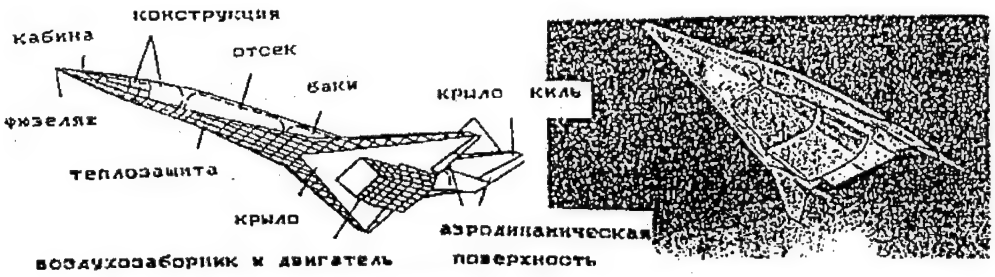

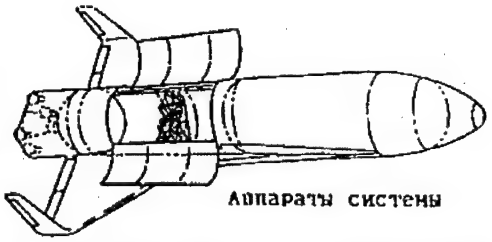

Аппараты системы
аэрокосмического перехватывания

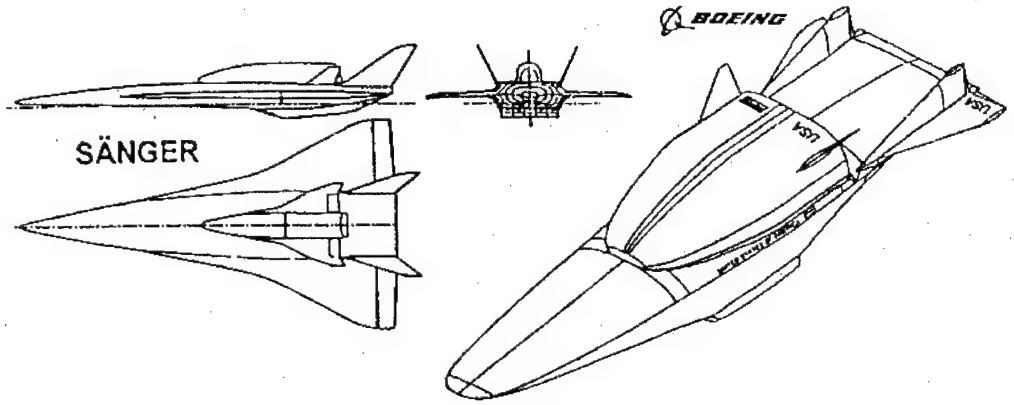

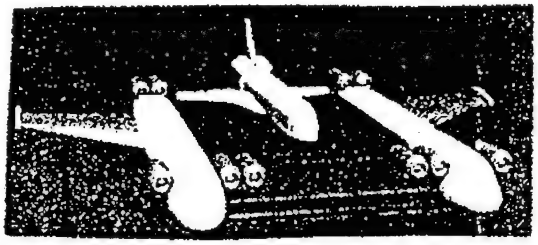

Fig.2.

Схема связей
Зоны транспортных операций по сценариям

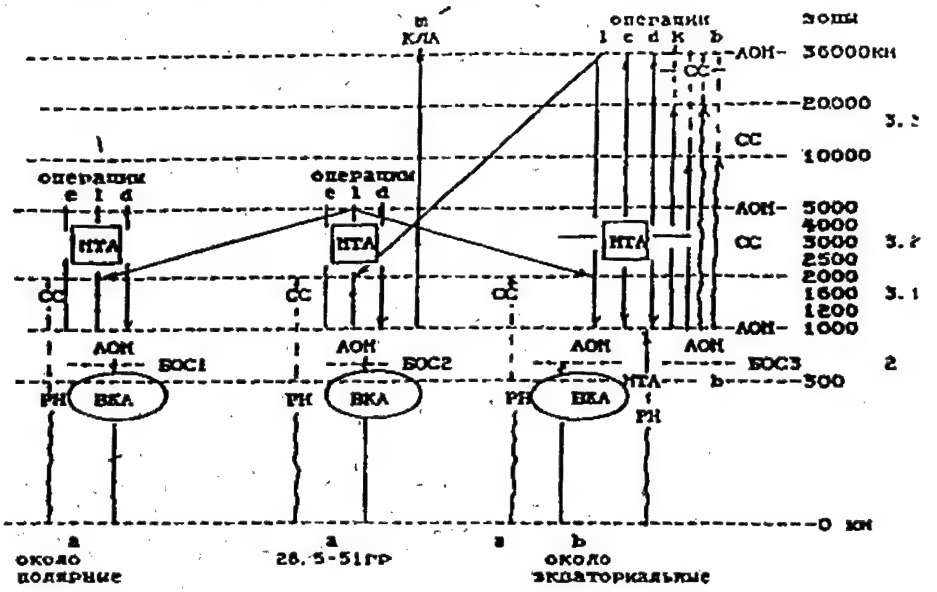

Информационное поле – Варианты массового обслуживания спутников

опорная орбита 300 км рабочая 36000км				b*				c*			
высота промежуточной орбиты			км	3000	10000	20000	27000	3000	10000	20000	27000
стартовая масса РБ-ЖРД			кг	1575	2630	3500	3870	3050	5130	6950	7770
характ.скорость до Нпр МТА-ОМУ			м/с	1196	2667	3474	3743	1197	2687	3550	3855
масса РТ РБ-ЖРД			кг	499	1505	2340	2689	968	2942	4673	5393
хар. скорость с Нпр ЭРД			м/с	3833	1904	824	389	3834	1904	823	389
масса рабочего тела ЭРД	1000		кг	325	178	81	39	645	353	161	78
	2000			178	93	41	19.7	354	185	82	39
	3000			123	63	28	13.0	243	125	55	26
N, кВт	P, Н	$P_{уд.}$ сек	$m_{к}$	кг	1000				2000			
6	0.44	1000	$m_{кр}$	кг				573	876	876	1432	1528
			t	сут				9.9	164	164	41	20
	0.34	2000	$m_{кр}$	кг	413	511	570	595	1211	1211	1524	1573
			t	сут	118	61	27	13	233	233	54	26
	0.26	3000	$m_{кр}$	кг	476	545	586	603			1555	1588
			t	сут	164	84	37	176			74	35
5	0.37	1000	$m_{кр}$	кг			585	633	936	1272	1492	1588
			t	сут			24.7	11.9	197	108	49	24
	0.25	2000	$m_{кр}$	кг	473	571	630	655	1271	1465	1584	1633
			t	сут	141	74	33	16	279	146	65	31
	0.21	3000	$m_{кр}$	кг	536	605	646	663		1534	1615	1648
			t	сут	197	101	44	21		200	88	42
3	0.22	1000	$m_{кр}$	кг		598	710	758		1397	1617	1713
			t	сут		91	41	19.8		180	82	39
	0.17	2000	$m_{кр}$	кг	598	696	755	780		1590	1709	1758
			t	сут	236	123	54	26		244	108	51
	0.13	3000	$m_{кр}$	кг	661	730	771	788		1659	1740	1773
			t	сут	328	168	74	35		334	147	70
2	0.15	1000	$m_{кр}$	кг	443	662	774	822		1461	1681	1777
			t	сут	250	136	62	30		270	123	59
	0.11	2000	$m_{кр}$	кг	662	760	819	844		1654	1773	1822
			t	сут	354	184	82	39		365	162	77
	0.085	3000	$m_{кр}$	кг		794	835	852			1804	1837
			t	сут		252	110	53			221	104

Fig.3. Interrelations scheme. Zones of transport operations by scenarios.

Combinations of chemical engines that by their characteristics can be equivalent to combinations using NRE are assumed. Such vehicles can become the steps of conveyor:

— Shuttle, Concorde, Sanger, Maks, Hope
— X-30, Hermes, Horus, Cargus
— Pegasus rocket, NWHAL (Non-Winger Horizontal Air-Launch) rocket, WHAL (Winger Horizontal Air-Launch) rocket, Entry Vehicles
— The Eureca Platform, ITV(Inter-orbit Transport Vehicle), OMV(Orbital Maneuver Vehicle), Hybrid reuseable ASV with solar-nuclear engine.

Objects of conveyor will be maintained by rocket and aero vehicles (see Fig2). Special cargo delivery to the strategical conveyor steps (by the harmonics) will be realized by rocket and aero vehicles of different countries. Rocket carriers: Zenit, Proton, Arian, Titan, Atlas, Delta, H2, CZ-2E, CZ-3E.

Aero carriers: From the altitude less than 12km – airplane like An-225 "Mria", Boeing-747; From the altitude less than 5km - thermoplane; From sea surface - hydroplane.

Conceptions - Space conveyor operations. (Part of fundamental research - plasma engines of satellites and flying vehicles, microbaloon forms of hydrogen fuel storage) Accompanying, transport and powerray problems are specified. Several-vehicle systems of space assimilation and combined nuclear powerengine blocks using microsphere fuel are analyzed. This blocks can be stored in outer space in cut-off state and by command the are turned-on into functioning state. Thermal power of nuclear reactor can be used only for producing electric energy. Compensation of internal energy loss will be realized using solar contour. Duty regimes are organized using stored energy. Nuclear shield is also used as a thermo storage.

Notations:

BOS1, BOS2, BOS3 - Base orbital Stations;
SS - satellite-Systems;
RC - rocket carriers;
a,b,d,e,k,l,m - variants of transport operations;
1 - zones of usable rocket carriers and reusable ASVs use;
2 - region for preferable use of VOM in zones of base orbital stations (BOS);
3 - region for preferable use of reusable TTV; region of passing delivery and system-satellites removal from their orbits (using TTV and VOM)
3.1 - zone of SS self removal from base orbital stations and from low altitude orbits (300-2000 km); passing delivery and removal of SS from high altitude orbits (1000-2000km) using TTV and VOM;
3.2-3.3 - zones of other base orbital stations support; passing delivery and removal of SS (rocket carriers, TTV and VOM are used); orbits of 2000-5000km and 5000-36000km altitude; self delivery of SS from intermediate orbits 1000-2000 km to the work orbits 36000km.

Base orbital Stations.

Main distribution of satellites is realized using supporting BKA from the three BOS:
BOS on the near polar orbit,
BOS on the near equatorial orbit,
"Alpha"-station.
Polar BOS and "Alfa"-station are technically supported by .. from regions of Russia and USA.
Equatorial BOS is supported from launching systems in France, Japan and China.
The aim of BOS - co-ordination of TTV, ASV and other carriers flights.
Space, shuttle, and transcontinental opportunities of aero-space systems, base orbital stations and satellites by zones and regions are analyzed.
Zones: altitudes 300-36000km.
Regions: near-polar, inclined 28-51 dgr, near equatorial.

Space transorbital transport vehicles(TTV)

Variant 1. Reusable TTV, consists of: nuclear power Station (NPS like SP-100), electrical rocket engines (ERE, working substance Xe). Launching gravity 20540kg. Electrical power of NPS 100-400kWt; specifics gravity 25-50kg/kWt; specifics thrust impulse ERE 1000,2000,3000sec; efficience 0.36-0.62.

Variant 2. Hybrid reusable TTV with solar-nuclear power station (SNPS) and ERE. Solar power station(SPS) is used for operations near space base station (the high radiation security and accuracy of object orientation is required). NPS is used while intensive transorbital operations with sufficient distance from the base objects. Electrical power NPS 300kWt; Electrical power of SPS 25kWt. specifics gravity SPS 51kg/kWt.

Vehicle for orbital maneuvering(VOM).

Variant 1: VOM for use near base station. Launch gravity 810-15000kg; whole engine thrust 4-80 kH; specifics impulse of thrust 320-410 sec.

Variant 2: Hybrid VOM. Chemical engines and also solar ERE are installed. Launching gravity 2000-10000kg. Power of SPS 6kWt; specifics gravity 63kg/kWt. Working substance of ERE -Xe.

Satellites.

Variant 1: System-satellites(SS), gravity - 500, 1000, 2000, 3000kg, using solar power station which has power of 2, 3, 5, 6kWt, specifics gravity SPS 63kg/kWt.

Variant 2: Hybrid system-satellites(HSS). They use solar ... Launching of HSS will be made using rocket-carriers, TTV, VOM, ASV till the intermediate orbits; then the inboard solar ... will be used.

a,b,d,e,k,l,m - variants of transport operations.

Operations of type a. Forming the base orbital station, batch delivery and self-transportation of satellites. There will be ASVs with different purposes: delivery of satellites, TTV and VOM; system equipment of spacecrafts, rescue and probing operations; cleaning up the space by utilization of large-scale fragments in zones of active transport operations. Some satellites are transported from BOS to their orbits 500, 1000, 2000km using solar ERE.

Operations of type b. Forming the TTV and combined usage of TTV/VOM While this operations the ASV, the spacecrafts like Space Shuttle, rocket carriers like "Proton KM", "Titan-4","Arian-5" are used. The TTVs and VOM are delivered to the low altitude orbits. Nuclear TTVs are delivered to the orbit on the altitude of 1000km where they are prepared for the independent operations. Some VOM are used for the delivery of PL to the intermediate orbits at the 10000, 20000,27000 km altitudes. PL independently come out to the orbit at the altitude of 36000km.

Operations of type d. Nuclear reuseable TTV can be used for the delivery of VOM to the altitude of 5000-36000 km. When TTv comes up to the defined region, VOM separates for solving the independent tasks: distribution of new SS to their orbits, getting old satellites from the orbits, their batch transporting. TTV solves other tasks in some other regions till the time of the arrival to the region of the meeting with VOM. After returning of the TTV to the base orbit 1000 km, VOM provides the delivery of the SS batch to the BOS. Then the preparation for the next transport operation cycle begins.

Operations of type e. Realizing the commands from space analytical center TTVs combine the tasks of the removal and delivery of satellites to the 2000-20000km and 36000 km orbits.

Operations of type k. Combining the functions of TTVs and VOM TTVs combine the tasks of the removal and delivery of satellites to the 2000, 3000, 5000km orbits while the delivery of A.. to the orbits at the altitudes of 10000 and 20000 km is realised. TTV gets back to the base orbit of 1000km. A VOM independently gets to the 36000km orbit.

Operations of type l. Combination of TTV functions, reorienatation to the technical support of other BOSs. TTVs realizes: shuttle transport operations at the orbits of 5000-36000km; passing operations (removal-delivery of satellites) on the orbits of 1200, 1400, 1600, 1800 and 2000km. While coming back to the altitude of 2000km delivery of cargos to the other BOSs is realized. Next transport operation cycles to the other BOSs are prepared.

Operations of type m. After finishing of transport operation cycles near Earth TTVs are prepared for the research flight to the other planets. On the Earth the preparations of new TTVs and A.. for next transport operation cycles are driven

SPHERICAL SHOCK WAVES IN AIR AND IN THE CARBON DIOXIDE NON-SELF-SUSTAINED DISCHARGE

A.V.Filippov, A.F.Pal' (Troitsk Institute for Innovation and Fusion Research, Troitsk, Moscow reg.)

Abstract. Results are presented from the study of spherical shock waves (SWs) in air and in a low-temperature plasma of a non-self-sustained discharge in carbon dioxide by using the laser schlieren technique. In order to reconstruct the density jump at the front of a spherical SW, a new calibration procedure and a new method for calculating the signal from the laser schlieren system are used. This method is used to study the interaction of a spherical SW with a plasma of non-self-sustained discharge (NSSD) in carbon dioxide (electronegative gas with dissociative electron attachment). It is found that (i) the decrease in the density jump at the front of a spherical SW after it has entered the heated region of an NSSD exceeds the value predicted by the one-dimensional refraction of the SW by a thermal wall and (ii) the decrease in the density jump with increasing the SW radius for a fixed temperature turns out to be greater than that predicted by the asymptotic law for SW attenuation (in the recombination regime, the SW is attenuated stronger than in the attachment regime). It is established that, in the recombination regime of an isobaric NSSD, SWs are damped, whereas, in the attachment regime, they are weakly amplified. This provides a qualitative explanation of the observed effects of SW propagation in an NSSD in CO_2.

1. Introduction

In recent years, many papers have been devoted to the interaction of shock waves (SW) with a nonequilibrium low-temperature plasma. This problem attracts interest primarily due to the fact that SWs are spontaneously generated in various gas-discharge devices [1–4] and affect the operation of the devices. In addition, interest in the problem at hand is related to the fact that, in experiments on the interaction of SWs with a low-temperature plasma, a number of unexplained phenomena were observed (see review [5] and the literature cited in [6]).

In this paper, we present the results of studying spherical SWs in air and in a low-temperature plasma of an non-self-sustained discharge (NSSD) in carbon dioxide by using the laser schlieren technique. Previously, we used this technique in [7] to study spherical SWs and observed the amplification of weak SWs in the burning regime of the NSSD in CO_2, when the dissociative attachment is the dominating electron-loss process (for brevity, this NSSD regime will be referred to as an attachment regime and the regime in which electron loss due to recombination dominates will be referred to as a recombination regime). However, the method for calibrating the schlieren transducer that was used in [7] had some drawbacks and the observed amplification of an SW in an NSSD was fairly small; therefore, we carried out a more detailed analysis of both the laser schlieren method and the effect of an NSSD plasma on the SW propagation.

Due to the high sensitivity and high time resolution, the laser schlieren method is widely used to study kinetic processes in shock tubes [8] and plasma objects with a nonuniform gas density distribution [9, 10]. The quantitative processing of the results obtained with this method is well developed for the case in which the laser beam diameter is much less than the characteristic nonuniformity scale length [9, 10]. However, the use of the laser schlieren method to determine the SW parameters under conditions such that the characteristic nonuniformity scale length of the gas density is less than the laser beam diameter meets grave mathematical difficulties (see, e.g., [11,12]) due to the necessity of solving the problem of propagation of laser radiation in a highly nonuniform medium. In order to solve this problem, various physical approaches (e.g., the geometrical-optics approximation) and fairly elaborate numerical methods are used. In this paper, in order to calculate the schlieren-system response to SW propagation across the laser beam, we use the partial-ray method proposed in [13], in which this method was employed to determine the VT-relaxation rate of vibrationally excited molecules.

The calculations have used the experimentally obtained frequency response and the sensitivity of the schlieren transducer, as well as the values of the density jump at the front of a spherical SW. The jump has been reconstructed from the recorded times of the arrival of a spherical SW in air for different propagation distances. The reconstruction has been based on the results of a numerical solution to the problem of a point explosion (PPE) in a gas with taking into account the gas pressure ahead of the SW front and the asymptotic law of the SW propagation. To prove the applicability of the partial-ray method, we compare the measured and calculated values of the amplitude of the schlieren-transducer signal. The developed method for calculating the amplitude of the schlieren-transducer signal is used to reconstruct the density jump at the front of an SW interacting

with the plasma of an NSSD in carbon dioxide (electronegative gas with dissociative electron attachment).

2. Experimental setup

The main results were obtained in a experimental setup similar to that described in [14]. An NSSD sustained by a 120-keV electron beam was ignited between two rectangular electrodes $6\times9cm^2$ in size spaced at a distance of 2.5cm. The discharge boundary was located at a distance of 5 cm from the spark source of an SW. We performed two series of experiments with approximately the same energy deposition. In the first series, the discharge voltage U_d and the electron-beam current density j_b were 13.5kV and $60mA/cm^2$, respectively, and, in the second series, they were 10.0kV and $168mA/cm^2$. In the first series of experiments, we observed oscillations of the discharge current, and, in the second series, oscillations were absent. The presence of the discharge-current oscillations points to the attachment regime of the discharge, whereas, in the second series, the recombination regime of an NSSD occurred (see [7]). The delay time of the SW initiation with respect to the instant of NSSD ignition was varied, which resulted in different values of the gas temperature in the discharge region at the instant of the SW arrival.

In order to generate spherical SWs, we used two spark sources. The density jump at the SW front have been measured by the laser schlieren system. Experiments in CO_2 were carried out for three positions of the schlieren system with respect to the discharge chamber. Correspondingly, the SW traveled through the discharge a distance of 1.1, 3.5, and 5.3cm until it intersected the laser beam (the radius of the front of the spherical SW was r_2=6.1, 8.5, and 10.3cm, respectively).

3. Determination of the density jump at the SW front as a function of the spherical shock wave radius

In the one-dimensional case, both the dependence of the density jump at the SW front on the radius and the motion of SWs in a polytrope gas are determined by the characteristic dynamic length r_0 ([15,16]), which is determined by the expression:

$$r_0=\sqrt[3]{E_0/P_0}\,, \qquad (1)$$

where E_0 is the electric-breakdown energy that is carried away with the SW and P_0 is the initial gas pressure in the breakdown region. Therefore, if we determine the value of this parameter from the dependence of the instant of the SW arrival on the distance the SW has traveled, we can find the dependence of the density jump at the front on the SW radius r_2. Figure 1 presents the experimental and calculated dependencies of the instant of the SW arrival on the distance r_2.

The values of the parameter r_0 are determined by the procedure proposed in [6]. By successive approximations, we determine the value of the parameter r_0 that minimizes the sum of the deviations squared of the experimentally determined times of the SW arrival from those calculated based on the results [16] of the numerical solution of a one-dimensional spherical PPE in a gas with taking into account the pressure ahead of the SW front. The speed of sound in air at room temperature was assumed to be 345m/s [17].

From Fig.1, it is seen that the experimental values of the instant of the SW arrival are described well by the one- dimensional theory. Therefore, in order to determine the density jump at the SW front up to the point $r_2=2r_0$, we used the results of the numerical solution from [16].

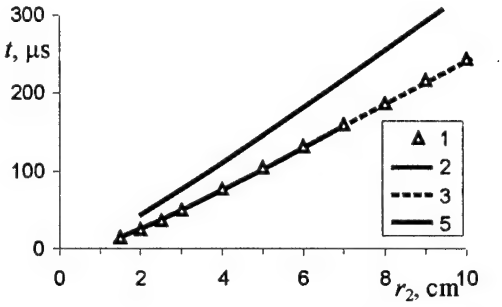

Fig. 1. The time of the SW arrival as a function of the distance. (1) experimental points for the discharge in air (the systematic *error* t_s=13.5ms is subtracted from the experimentally obtained values of the time of the SW arrival), (2) the self-similar Sedov's solution to the PPE with E_0=1.8J, (3) the curve calculated based on the numerical solution [16] to the PPE with taking into account the pressure ahead of the SW front for r_0=2.58cm and E_0=1.8J, (4) the results of calculations by formula (2) for r_0=2.58cm, (5) experimental data for CO_2 discharge, (6) the results of calculations by formula (2) for r_0=1.84cm and γ=1.29.

The motion and parameters of the SW for the distances $r_2\geq1.5r_0$ are described by the asymptotic relationships [16]:

$$\tau=\tau^*+\frac{R_2}{\sqrt{\gamma}}-\frac{\bar{k}_3}{\gamma\sqrt{\alpha}}\sqrt{\ln(R_2/R^*)}\,, \qquad (2)$$

$$\frac{\rho_2}{\rho_1}=1+\frac{2\bar{k}_3}{(\gamma+1)\sqrt{\alpha\gamma}\cdot R_2\sqrt{\ln(R_2/R^*)}}, \qquad (3)$$

$$\frac{P_2}{P_1}=1+\frac{2\gamma\bar{k}_3}{(\gamma+1)\sqrt{\alpha\gamma}\cdot R_2\sqrt{\ln(R_2/R^*)}}, \qquad (4)$$

where $\tau=t/t_0$ is the dimensionless time; $t_0=r_0\sqrt{\gamma}/a_s$ is the characteristic dynamical time; a_s is the adiabatic speed of sound; $R_2=r_2/r_0$ is the dimensionless length; r_1, r_2, P_1, and P_2 are the density and pressure of gas ahead of and behind the SW front, respectively; γ is the adiabatic index; α is the parameter entering the self-similar solution to the problem of a strong explosion in an ideal gas; and $\bar{k}_3$, R^*, and τ^* are certain constants.

According to [16], for γ=1.4, these constants are $\bar{k}_3$=0.322, R^*=0.692, and τ^*=–0.22. The parameter α was calculated by approximating expressions from [16]. Figure 1 presents asymptotic dependencies (2) for $r_2\geq 2r_0$ with r_0 as determined above. From Fig.1, it is seen that formula (2) describes the experiment well. Therefore, in order to determine the pressure and density jump at the SW front for $r_2\geq 2r_0$, we used the asymptotic formulas (4) and (3), respectively.

4. Calculation of the schlieren-transducer signal by the partial-ray method

In the geometrical-optics approximation, the angle δ of the partial-ray deflection is determined by the expression:

$$\delta=2\delta_1=2\sqrt{2(1-n_0/n_1)+\mathrm{ctg}^2\alpha_1}-\mathrm{ctg}\alpha_1, \qquad (5)$$

where n_0 and n_1 are the refraction indexes of gas ahead of and behind the SW front, respectively, and α_1 is the angle of incidence of the partial laser ray on the SW front. The angle of incidence is the following function of time:

$$\alpha_1=\arcsin(1-(Ma_st-y')/r_2), \qquad (6)$$

where M is the SW Max number, a_s is the speed of sound, and t is time. The refractive index of the gas is related to the gas density by the Gladstone–Dale relationships n=1+Aρ. We determined the Gladstone–Dale constants for the gases used from the refractive indices at the wave length of the *He–Ne* laser under normal conditions [18]. Preliminary calculations showed that the deflection angle of the laser beam by the inhomogeneities of the gas density behind the SW front was more than one-hundred times less than the angle of deflection by the SW front, so that the former was not taken into account in subsequent calculations.

Figure 2 presents the values of differences of the maximum and minimum signals from the schlieren transducer, both experimentally obtained and calculated by the procedure discussed above. The figure also shows the maximum signal of the schlieren transducer. Note that the difference of the maximum and minimum values of the calculated signal (in contrast to the maximum value) is almost insensitive to the ±0.1cm shift of the laser-beam axis in any direction about the center of the schlieren transducer. From Fig.2, it is seen that the experimental and calculated values are in good agreement; thus, the partial-ray method for calculating the schlieren-transducer signals can be used to determine the parameters of the SW front.

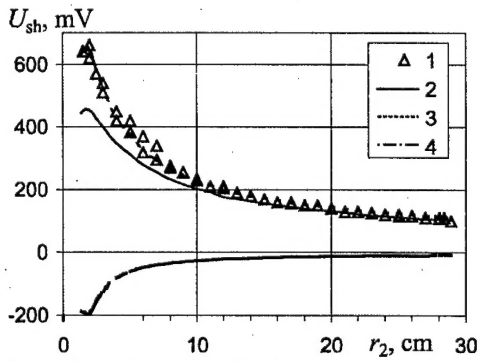

Fig. 2. Experimental and calculated amplitude of the schlieren-transducer signal as functions of the SW radius. (1) experimental values of U_{sh}; (2) calculated values of U_{sh} U_{max}–U_{min}; (3) maximum U_{max} and (4) minimum U_{min} values of the calculated schlieren signal.

5. A spherical shock wave in a plasma of non-self-sustained discharge in CO_2.

Figure 3 presents the values of the density jump at the front of an SW moving in a carbon-dioxide NSSD.

The jump was reconstructed from the experimental values of the schlieren-transducer signal. From Fig.3, it is seen that, for the burning voltage of the discharge U_d =13.5kV and a gas temperature of 400K and higher, the density jump at the SW front r_2/r_1 appears to be higher than for U_d =10.0kV (this effect was reported in [7] as the amplification of a weak SW). Let us discuss this effect.

A comparison of the calculated values of P_2/P_1, r_2/r_1, and τ presented in [19] for $R_2\geq$1.5 and γ=1.3 and 5/3 with those calculated by the asymptotic formulas (2)–(4) shows good

agreement between them. Therefore, we determined the values of the parameter r_0 from three experimentally obtained values of the density jump at the SW front in CO_2 at room temperature (γ=1.29 [17]) for r_2=6.1, 8.5, and 10.3cm by using (3). The corresponding values of r_0 turned out to be 1.84, 1.82, and 1.82, respectively (the dispersion of the values obtained allows us to evaluate the accuracy of determining this quantity). The values of the time of the SW arrival, both experimental and calculated by (2) for τ^*=-0.26, are seen to agree well (Fig.1).

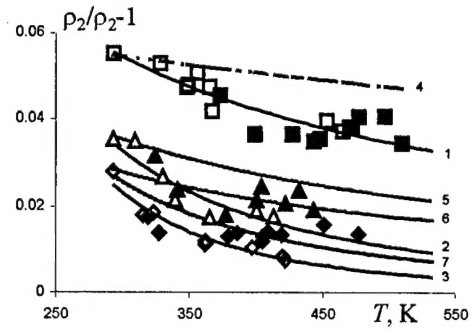

Fig.3. The measured values of the density jump at the SW front in a carbon-dioxide NSSD as a function of the gas temperature for the discharge voltages U_d=10kV (open squares) and U_d=13.5kV (closed squares). Curves 1-3 are drawn through the experimental points for U_d =10kV by the least-squares method for r_2=(1) 6.1, (2) 8.5, and (3) 10.5cm. Curves *4–7* show (4) the results of calculations taking into account refraction of SWs by a thermal wall and using formula (3) for r_2=6.1cm and the results obtained by formula (3) for r_2=(5) 8.5 and (6) 10.3cm (by using the values of the density jump at r_2=6.1 from curve 1) and (7) for r_2=10.3cm (by using the values of the density jump at r_2=8.5cm from curve 2).

Figure 3 shows the values of the density jump at the SW front for r_2=6.1cm in the CO_2 NSSD at different gas temperatures. These values were calculated with taking into account one-dimensional refraction of the SW by a thermal wall [20] at the entrance to the discharge region at r=5.0cm and with the use of (3). Note that the shift of the thermal wall toward the point r=4.0did not lead to a change in the density jump accurate to the fourth decimal place. From Fig.3, it is seen that, as the gas temperature increases, curves *1* and *4* diverge.

Figure 3 also presents the values of the density jump for r_2=8.5 and 10cm, which were calculated by formula (3). By comparing the experimental and calculated data, it can be seen that, in the attachment regime of an NSSD, the experimental values of the density jump are rather close to the calculated ones, whereas in the recombination regime, the experimental values are noticeably smaller than the calculated ones. In [21], it was shown that, in the attachment-instability domain of the NSSD in CO_2, acoustic perturbations (including weak SWs) should increase. In the discharge discussed in [21], the heating process was isochoric, whereas under the conditions of our experiments, it was almost isobaric. Therefore, we will consider the behavior of acoustic perturbations in such a discharge.

The growth rates of acoustic and thermal perturbations with the wavenumbers $k \geq 1\text{cm}^{-1}$ in the isochoric and isobaric discharges are presented in Table 1 (ω is the frequency, and χ is the perturbation growth rate). For longitudinal perturbations, the parameter $s=\ln W/\ln N|_{jd=\text{const}}$, and for transverse perturbations, we have $s=\ln W/\ln N|_{E=\text{const}}$, where W is the specific power of gas heating (per unit volume) and N is the gas density. Figure 4 shows the values of s for transverse perturbations in CO_2 NSSD.

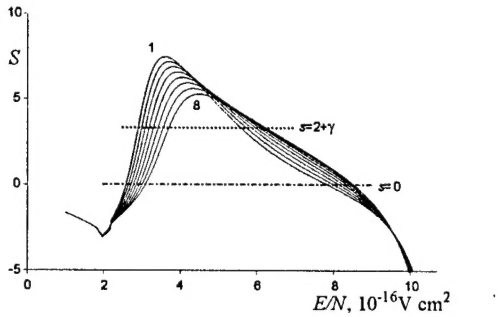

Fig. 4. Parameter s for transverse perturbations versus E/N in CO_2 at atmospheric pressure (N=2.5×10^{19}cm^{-3}). The numbers by the curves are the values of i in expression: j_b=10×2^{i-1} (j_b in μA/cm^2);

Gas heating is characterized by the rate ν_T determined from the expression: $\nu_T=(\gamma-1)W_0/\gamma P_{|t=0}$, where W_0 is the specific power of heating of the unperturbed gas and $P_{|t=0}$ is the gas pressure at the instant when the perturbation occurs. The flow velocity u_0 of the unperturbed gas is determined by the expression $\boldsymbol{u}_0=1/2\nu_T(x\mathbf{e}_x+y\mathbf{e}_y)+\boldsymbol{u}_f$, where the coordinate axes x and y lie in the plane that is parallel to the electrode and perpendicular to the electric-field vector, $\boldsymbol{e}_x$ and $\boldsymbol{e}_y$ are the unit vectors directed along the coordinate axes, and $\boldsymbol{u}_f$ is the gas circulation velocity. If the perturbation wave vector and the velocity vector of the gas motion are oppositely directed, their product is negative.

In Table 1, the growth rates of perturbations for the isobaric discharge are determined accurate to first order in the ratio u_0/a_s.

Table 1. Growth rates of perturbations with the $k>1\text{cm}^{-1}$ in NSSD in plane geometry

Type of discharge	Thermal perturbations		Acoustic perturbations	
	longitudinal	transverse	longitudinal	transverse
Isochoric discharge	$\omega = 0$, $\chi \approx -s\nu_T$	$\omega = 0$, $\chi \approx -s\nu_T$	$\omega \approx \pm ka_s$, $\chi \approx \frac{1}{2} s\nu_T$	$\omega \approx \pm ka_s$, $\chi \approx \frac{1}{2} s\nu_T$
Isobaric discharge	$\omega = 0$, $\chi \approx -(s+1)\nu_T$	$\omega \approx ku_0$, $\chi \approx -(s+1)\nu_T$	$\omega \approx \pm ka_s$, $\chi \approx \frac{1}{2}(s-1-\gamma)\nu_T$	$\omega \approx \pm ka_s + ku_0$, $\chi \approx \frac{1}{2}(s-2-\gamma)\nu_T$

Figure 5 shows (a) the calculated current–voltage characteristics and (b) the contour lines of the current density in an NSSD in CO_2. For the electron and ions swarm parameters and rate constants of main kinetic processes we used the approximate expressions presented in [22].

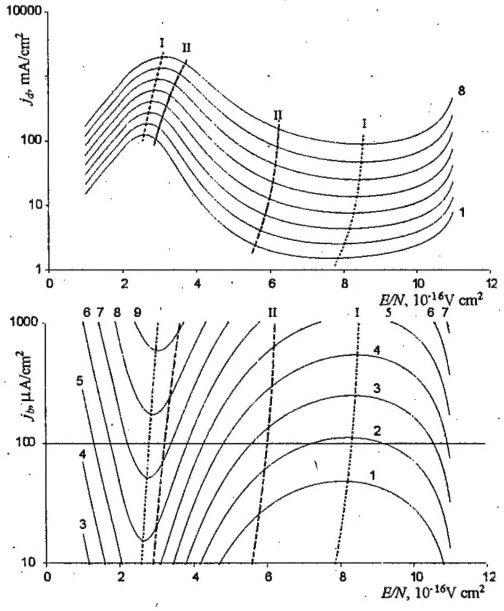

Fig.5. (a) Calculated current–voltage characteristics and (b) contour lines of the current density on the plane $(j_b, E/N)$ for an NSSD in CO_2 at atmospheric pressure. The numbers by the current–voltage characteristics are the values of i in expression: $j_b = 10\times 2^{i-1}$ (j_b in μA/cm^2); lines I and II are the boundaries of the acoustic-instability domains for transverse perturbations in isochoric and isobaric discharges, respectively the numbers by contour lines of the current density are the values of i in expression: $j_d = 10\times 2^{i-1}$ (j_d in mA/cm^2).

Table 2 presents the values of the parameter s for the transverse and longitudinal perturbations in three typical regimes of an NSSD:

(a) when the dissociative attachment dominates over the processes of electron loss (NSSDs in gases of the CO_2 type for $E/N \sim 3\times 10^{-16}$Vcm^2);

(b) when the dominant process of electron loss is recombination and the power of gas heating is close to the energy deposition power (inert gases, as well as gases with fairly fast VT-relaxation);

(c) when recombination dominates the electron loss processes, but only a fraction of the deposited energy is spent on gas heating ($W = \eta_T j_d E$, where η_T is the fraction of the deposited energy that is spent on direct gas heating in an NSSD in N_2, CO, etc.). Note that, for nitrogen, the fraction of the deposited energy spent on direct gas heating is almost inversely proportional to the reduced electric field $\eta_T \approx \eta_{T0} N/E$ [23].

Table 2. The values of the parameter s for various types of perturbations in three typical regimes of an NSSD

Discharge type→	*a*	*b*	*c*
Perturbation type ↓	Diss. attachment dominates	Recom-bination dominates, $\eta_T \approx 1$	Recom-bination dominates, $\eta_T \propto N/E$
Longitudinal perturbations: **k**‖**E**	$s = 1$	$s > 0$ (0.5÷0.8)	$s = 1$ (N_2)
Transverse perturbations: **k**⊥**E**	$s > 0$ (fig. 4)	$s < 0$ (fig. 4)	$s = 0.74$ (N_2)

The boundaries of the domains of the acoustic instability of transverse perturbations in the isochoric (I) and isobaric (II) CO_2 discharges are presented in Figs.5a and 5b. The acoustic-instability domain of the isobaric discharge is seen to be substantially narrower than that of the isochoric discharge.

As is seen from Tables 1 and 2, for all types of NSSDs considered here, longitudinal gas-dynamic perturbations (both acoustic and thermal) in the isobaric regime will be damped. As for transverse perturbations, in the attachment-instability domain of an isobaric NSSD in CO_2 at $E/N > 3\times 10^{-16}$V·cm^2, the quantity $(s-2-\gamma)$becomes positive (Fig.4) and, according to Table 1, transverse acoustic perturbations begin to grow.

In the recombination regime of NSSD, SWs are attenuated. For $E/N \sim 2\times10^{-16}$ V·cm^2, the attenuation coefficient exceeds the amplification coefficient in the domain of the maximum growth rate for $E/N \sim 4\times10^{-16}$ V cm^2. In our experiments, the SW propagated across the electric field; consequently, the gas-density perturbations were transverse. Therefore, we arrive at the following conclusions:

(d) The discrepancy between the values calculated both with taking into account refraction of the SW by a thermal wall and by the asymptotic formula (3) and those obtained in the experiment for r_2 =6.1cm is associated with the SW attenuation in an NSSD, because, at the periphery, the gas is less heated than in the center and the discharge is in the recombination regime even at U_d =13.5kV. An increase in the discrepancy between curves *1* and *4* with increasing *E/N* is due to the fact that the discharge-current density increases with time (see [7]) and, correspondingly, the gas-heating rate ν_T also increases; this leads to an increase in the SW attenuation coefficient.

(i) A strong SW attenuation at r_2=0.5 and 10.3cm in an NSSD for U_d =10kV is due to the fact that, at this voltage, the recombination regime lasts throughout the entire discharge phase [7] and the SW is attenuated, whereas at U_d=13.5kV, after the gas temperature reaches about 400K, the discharge passes over to the attachment regime and the SW begins to grow weakly.

Therefore, for the gas temperature $T \geq 400$K and U_d=13.5kV, the experimental values of the density jump appear to be fairly close to those predicted by the asymptotic law of SW attenuation.

References

1. *A.L.Ipatov, S.N Kabanov., A.A. Korolev, et al.* Pis'ma Zh. Tekh. Fiz., 1984, vol.10, No.3, p.162.
2. *V.G.Grudnitskii, N.A.Popov, and P.I.Sopin.* Teplofiz. Vys. Temp., 1987, vol.25, p.376.
3. *N.G.Basov, E.M.Belenov, V.A.Matsuk, et al.* Dokl. Akad. Nauk SSSR, 1992, vol.327, p.84.
4. *V.V.Stepanov, K.N.Ul'yanov.* Teplofiz. Vys. Temp., 1987, vol.25, p.396.
5. *A.I.Osipov, A.V.Uvarov.* Usp. Fiz. Nauk, 1992, vol.162, No.11, p.1.
6. *S.A.Bystrov, D.A. Mazalov, A.F. Pal', et al.* Plasma Phys. *Rep.*, 1998, vol.23, p.19.
7. *I.V.Kochetov, D.A. Mazalov, A.P. Napartovich, et al.* Plasma Phys. Rep., 1995, vol.21, p.328.
8. *J.H.Kiefer.* Shock Waves in Chemistry. Ed. by A.Lifshitz, New York: Plenum, 1981, p.219.
9. *G.A.Woolsey, S.J.MacGregor, O.Farish.* Proc. R. Soc. London, Ser. A, 1986, vol.405, p.355.
10. *G.G.Yakushev, V.I.Kolpakov, E.N.Zhukova, et al.* Preprint of Inst. of High Temperatures, Acad. Sci. of the USSR, Moscow, 1987, No.5-221.
11. *J. Panda, G. Adamovsky.* Phys. Fluids, 1995, vol.7, p.2271.
12. *S.A.Bystrov, H.Honma, V.I.Ivanov, et al.* Shock Waves, 1998, vol.8, p.183.
13. *J.E.Dove, H.Teitelbaum.* Chem. Phys., 1974, vol.6, p.431.
14. *B.V.Zhuravlev, A.P.Napartovich, A.F. Pal', et al.* Sov. J. Plasma Phys. 1988, vol.14, p.133.
15. *L.I.Sedov.* Metody podobiya i razmernosti v mekhanike (Similarity and Dimensionality Methods in Mechanics), Moscow: Nauka, 1987.
16. *V.P.Korobeinikov.* Zadachi teorii tochechnogo vzryva (Problems of the Theory of Point Explosions), Moscow: Nauka, 1985.
17. *N.B.Vargaftik.* Spravochnik po teplofizicheskim svoistvam gazov i zhidkostei (Handbook of Thermal Properties of Gases and Liquids), Moscow: Fizmatgiz, 1963.
18. Fizicheskie velichiny. Spravochnik (Handbook of Physical Quantities). Ed. by *I.S.Grigor'ev and E.Z.Meilikhov.* Moscow: Energoatomizdat, 1991.
19. *V.P.Korobeinikov, P.I.Chushkin, K.V. Sharovatova.* Gazodinamicheskie funktsii tochechnogo vzryva (Gasdynamic Functions of Point Explosions), Moscow: VTs AN SSSR, 1969.
20. *B.P.Rozhdestvenskii, N.N.Yanenko.* Sistema kva-zilineinykh uravnenii (System of Quasilinear Equations), Moscow: Nauka, 1978.
21. *J.H.Jacob, S.A.Mani.* Appl. Phys. Lett., 1975, vol.26, No.2. P.53.
22. *I.V.Kochetov, D.A.Mazalov, A.F.Pal', A.V. Filippov.* Plasma Physics Reports, Vol.25, No.5, 1999, pp.375–386.
23. *A.A.Deryugin, I.V.Kochetov, A.I.Loboiko, et al.* Sov. J. Plasma Phys. 1988, vol.14, p.200.